Quantifying spatial association between mineral deposits and geology across three African crustal segments of different age, with implication for secular change in mineralization during Earth history.

Tshifhiwa Mabidi

Thesis submitted in fulfilment of the requirements for the degree of
Master of Science

Department of Geological Sciences
University of Cape Town
February, 2006

AEON
AFRICA EARTH OBSERVATORY NETWORK
EARTH STEWAROSHIP THROUGH SCIENCE

Declaration

- I know that plagiarism is wrong. Plagiarism is to use another's work and to pretend that it is one's own.

- Each significant contribution to, and quotation in, this thesis from the work, or works, of other people has been attributed, and has been cited and referenced.

- This thesis is my own work.

- I have not allowed, and will not allow, anyone to copy my work with the intention of passing it off as his/her own work.

Signed by candidate

Abstract

Variations in enrichment of mineralization, expressed in ore deposits, in the continental crust may be one way to test for secular changes in crustal genesis. This study collates and analyses fundamental information about mineral deposits with which to 'fingerprint' the metal endowment of African crust of different age. Three areas of juvenile African crust (e.g. mantle derived over similar lengths of time of ~500 million years, and excluding recycled older crust) of different ages with similar geology are compared. The areas range in age from 0.5 to 3.0 Ga, [e.g. the Zimbabwe Craton (2.5-3.0 Ga), the Birimian Shield (1.8-2.3 Ga), and the Arabian-Nubian Shield (0.5-1.0 Ga)]. The three areas have a total of 2671 mineral deposits, which are divided into six groups according to their geochemical affinities. Using these known deposits, mineral potential maps are created through a data-driven approach, using weights of evidence (WofE). The layers/themes used in WofE are (1) lithology, (2) structures (faults and shear zones), and (3) lithological contacts. The analysis shows that there is strong lithology control on mineralization in all three areas. Archean crust has high predictive values compared to the younger crust. A measure of spatial association (spatial coefficient), based on the WofE approach, is also used to 'fingerprint' the metal endowment in the three selected regions of African crust. The patterns of the mineral deposits distribution within all regions shows that each region has a unique metal endowment, and that there is a greater concentration of mineral deposits in the crust of the Archean Zimbabwe Craton relative to the younger crust of the Birimian and Arabian-Nubian Shields. The analysis of this study therefore quantitatively corroborates studies that suggest older crust is more mineral diverse and more enriched in mineral deposits than younger crust. Thus, secular changes in mineralization or rates of tectonic processes, or both, are implicated, and mineral endowment in the African crust has undergone major evolutionary changes from Archean to Neoproterozoic time.

Keywords: Zimbabwe Craton; Birimian Shield; Arabian-Nubian Shield; Continental crust; Secular change; Mineral deposits; Archean; Paleoproterozoic; Neoproterozoic; Weights-of-Evidence model, Spatial analyses, GIS, Mineral potential maps

Acknowledgements

I would like to express my special thanks to my supervisors Prof. Maarten de Wit and Prof. Christien Thiart, for the guidance, patience, mentorship and motivation that helped me combine my interest in both computing and geology. I am sincerely in debt to them for their guidance and for their continuous support at every stage throughout this study. Prof. Maarten de Wit requires special praise for his belief that it was all possible. He has inspired me to produce nothing less than my best, which was often more than I thought I could do. Maarten and Christien, you are much more than supervisors to me.

This research began with data collection from various sources into a unified GIS database. Part of datasets was taken from GO-GEOID (Gondwana Geoscientific Indexing Database), now housed at AEON, that originated from a PhD thesis of Wendy Wilsher. Digital geological features of Africa used throughout this project were mostly obtained from Council for Geosciences, and De Beers Group in Centurion where I visited and I was lucky to spend some time with Lindsay Urban, Navitha Dukkan and Dr Moctar Doucouré in their GIS Department. I would like to thank them for the time and effort they put into my project. For this I would like to thank Dr Mike de Wit, with whom I also had a valuable discussion. I would also like to thank his group, for making my visit to Centurion not only as productive as possible, but also very pleasant.

I would like to thank Dr Hielke A. Jelsma, whom I visited in De Beers-Geoscience Centre in Johannesburg and Prof. Paul. H.G.M. Dirks for sending me valuable datasets of the Zimbabwe Craton. Nick Lindenberg, the UCT-Geographical Information Systems Manager, is thanked for sharing his expertise, which has greatly improved my work and his valuable time is greatly appreciated. The support from fellow students and staff in the Department of Geological Sciences, notably my fellow AEON companions, Dr. Jacek Stankiewicz, Dr. Justine Tinker, Dr. Daud Jamal, John Decker, and Shaun Moore, are thanked for their support, encouragement and valuable ideas that I have received. I am also grateful for the support and encouragement that I have received from Robert Netshitungulwana, Simon Mabolani, James Mudau and Zibisani Bagai.

Financially, this project would never happen without the generosity of Prof. Maarten de Wit. The National Research Foundation provided financial support during this project. Finally, I would like to express my special thanks to my parents, family, friends and Tshilidzi for their unbelievable support, ultra-patience and endless trust. Not forgetting the Almighty God who always being on my side throughout this study.

TABLE OF CONTENTS

Declaration i

Abstract ii

Acknowledgements iii

Table of Contents iv

List of Figures ix

List of Tables xv

Chapter 1: Introduction **1-1**

1.1 Objectives 1-4

1.2 Definitions of a craton and a shield 1-5

1.3 Definition of mineral potential 1-5

1.4 Methodology 1-6

Chapter 2: Geologic architecture of three different African crustal segments **2-1**

2.1 The Archean Zimbabwe Craton 2-1

2.1.1 Geological Setting 2-4

2.1.2 Tectonic Setting 2-7

2.1.3 Mineralization 2-9

2.2 The Paleoproterozoic Birimian Shield 2-12

2.2.1 Geological Setting 2-12

2.2.2 Tectonic Setting 2-18

2.2.3 Mineralization 2-21

2.3 The Neoproterozoic Arabian-Nubian Shield 2-24

2.3.1 Geological Setting 2-24

2.3.2 Tectonic Setting 2-26

2.3.3 Mineralization 2-29

2.4 Summary of the Mineral Deposits of three regions of African crust of different age 2-31

Chapter 3: Database: acquisition and structure **3-1**

3.1 Spatial Data Input 3-1

3.1.1 Mineral Theme 3-3

3.1.2 Geology Theme.....3-6

3.1.3 Faults Theme 3-10

Chapter 4: Spatial Modelling Methodology **4-1**

4.1 Introduction 4-1

4.2 Knowledge Driven Models 4-1

4.2.1 Boolean logic Model 4-2

4.2.2 Index Overlay / Multicriteria Model 4-3

4.2.3 Fuzzy logic Model 4-4

4.2.4 Disadvantages of Knowledge driven models 4-5

4.3 Data Driven Models 4-5

4.3.1 Weights of Evidence Method.....4-6

4.3.2 Weight of Evidence Modelling 4-7

4.3.3 Conditional Independence.....4-12

4.3.3.1 Chi-square test 4-13

4.3.3.2 Overall or omnibus test 4-14

4.3.3.3 New Omnibus test 4-15

4.3.4 Arc-Spatial Data Modeler 4-15

4.3.5 Implementation of Weights of Evidence Method..... 4-15

4.3.6 Advantages and Disadvantages of Weights of Evidence..... 4-17

4.3.7 Conclusion 4-18

Chapter 5: Spatial Modelling using Weights of Evidence **5-1**

5.1 The Archean Zimbabwe Craton 5-1

5.1.1 Gold deposit 5-1

5.1.1.1 Reclassification of evidential theme patterns 5-1

5.1.1.2 Integration of evidential theme patterns 5-7

5.1.1.3 Validation of results 5-12

5.1.2 CrNiPgeTi deposits.....5-13

5.1.2.1 Reclassification of evidential theme patterns.....5-13

5.1.2.2 Predictive Mineral Potential Maps 5-15

5.1.3 CuZnPbBa deposits 5-17
5.1.3.1 Reclassification of evidential theme patterns 5-17
5.1.3.2 Predictive Mineral Potential Maps 5-19
5.1.4 SnSb deposits.....5-21
5.1.4.1 Reclassification of evidential theme patterns.....5-21
5.1.4.2 Integration of evidential theme patterns.....5-24
5.1.5 Tungsten (W) deposits 5-26
5.1.5.1 Reclassification of evidential theme patterns 5-26
5.1.5.2 Integration of evidential theme patterns 5-28
5.1.6 UThREE deposits 5-30
5.2 The Paleoproterozoic Birimian Shield 5-30
5.2.1 Gold deposit 5-30
5.2.1.1 Reclassification of evidential theme patterns 5-30
5.2.1.2 Integration of evidential theme patterns 5-36
5.2.1.3 Validation of results 5-41
5.2.1.4 Gold (Au) deposits in the Ashanti Belt 5-42
5.2.2 CuZnPbBa deposits 5-47
5.2.2.1 Reclassification of evidential theme patterns 5-47
5.2.2.2 Predictive Mineral Potential Maps 5-47
5.3 The Neoproterozoic Arabian-Nubian Shield 5-50
5.3.1 Gold deposit 5-50
5.3.1.1 Reclassification of evidential theme patterns 5-50
5.3.1.2 Integration of evidential theme patterns 5-53
5.3.2 CuZnPbBa deposits.....5-55
5.3.2.1 Reclassification of evidential theme patterns 5-55
5.3.2.2 Predictive Mineral Potential Maps 5-55
5.5 Discussion 5-58

Chapter 6: Diversity of mineral deposits across the three study regions of African crust **6-1**
6.1 Introduction 6-1
6.2 Spatial coefficients of element groups 6-1

Chapter 7: Testing for secular change of mineralization in African crust **7-1**

7.1 Variations in mineralization across three African crustal segments 7-1

7.2 Towards quantifying secular change in mineralization 7-2

7.3 Discussion 7-5

Chapter 8: Conclusions and Recommendations **8-1**

8.1 Conclusion 8-1

8.2 Recommendation for future work 8-3

References

Appendices

Appendix A1: Glossary

A glossary of terms relating to WofE modelling as described in the thesis.

Appendix A2: Evidential theme patterns for the Zimbabwe Craton

Table 1a: Weights table for proximity to brittle faults (Zimbabwe Craton). The class column is the distance from the faults in metres.

Table 1b. Reclassified weights table of the brittle faults (Zimbabwe Craton).

Table 2a. Weights table for proximity to ductile shears (Zimbabwe Craton).

Table 2b. Reclassified weights table of the ductile shears (Zimbabwe Craton).

Table 3a. Weights table for proximity to combined brittle faults and ductile shears (Zimbabwe Craton).

Table 3b. Reclassified weights table of the combined brittle faults and ductile shears (Zimbabwe Craton).

Table 4a. Unique condition of gold deposit of Model A (brittle faults; Zimbabwe Craton).

Table 4b. Unique condition of gold deposit of Model B (ductile shears; Zimbabwe Craton).

Table 4c. Unique condition of gold deposit of Model C (combined brittle faults and ductile shears; Zimbabwe Craton).

Table 5. Unique condition of the CrNiPgeTi deposit (Zimbabwe Craton).

Table 6. Unique condition of the CuZnPbBa deposit (Zimbabwe Craton).

Table 7. Unique condition of the SnSb deposit (Zimbabwe Craton).

Table 8. Unique condition of the W deposits (Zimbabwe Craton).

Appendix A3: Evidential theme patterns for the Birimian Shield

Table 9a. Weights table for proximity to CGS brittle faults (Birimian Shield). The class column is the distance from the faults in metres.

Table 9b. Reclassified weights table of the CGS brittle faults (Birimian Shield).

Table 10a. Weights table for proximity to De Beers brittle faults (Birimian Shield).

Table 10b. Reclassified weights table of the De Beers brittle faults (Birimian Shield).

Table 11a. Weights table for proximity to merged CGS and De Beers brittle faults (Birimian Shield).

Table 11b: Reclassified weights table of the merged CGS and De Beers brittle faults (Birimian Shield).

Table 12a. Unique condition of gold deposit of Model A (CGS brittle faults; Birimian Shield).

Table 12b. Unique condition of gold deposit of Model B (De Beers; Birimian Shield).

Table 12c. Unique condition of gold deposit of Model C (merged; Birimian Shield).

Table 13a. Weights table for proximity to brittle faults (Ashanti belt, Birimian Shield). Cut-off distance at 1000m.

Table 13b. Reclassified weights table of the brittle faults (Ashanti belt).

Table 13c. Unique condition of the gold deposits (Ashanti belt)

Table 14. Unique condition of CuZnPbBa deposit (Birimian Shield)

Appendix A4: Evidential theme patterns for the Arabian-Nubian Shield

Table 15a. Weights table for proximity to brittle faults (Arabian-Nubian Shield).

Table 15b. Reclassified weights table of the brittle faults (Arabian-Nubian Shield).

Table 15c. Unique condition of gold deposit (Arabian-Nubian Shield).

Table 16. Unique condition of CuZnPbBa deposit (Arabian-Nubian Shield).

List of Figures

Figure 1.1: Location of the three selected African regions analysed in this study. The regions represent 3 distinct 500-million-year time-slices of African crustal growth between the Archean and the end of the Neoproterozoic.

Figure 2.1: Simplified Geology of the Archean Zimbabwe Craton bounded on its sides by younger tectonic domains. Simplified from Jelsma and Thiart (2002) and Jelsma (2003-2004). Insert shows the two countries where the Zimbabwe craton is exposed.

Figure 2.2: Distribution of ductile shears and brittle faults of the Archean Zimbabwe craton (after Jelsma and Dirks, 2002; Jelsma, personal communication, 2004-2005).

Figure 2.3: Distribution of mineral deposits and occurrences of the Archean Zimbabwe craton.

Figure 2.4: Geological sketch map of the West African Craton showing the location of the Leo-man and Reguibat rises, as well as the Baoule Mossi domain (reproduced after Boher et al., 1992), also known as the Birimian Shield, which is the area investigated in this study.

Figure 2.5: Simplified Geology of the Paleoproterozoic Birimian Shield, West Africa, as delineated by its later tectonic margins. Simplified after Milési et al., 1989. Insert highlights the countries of western Africa in which part of the Birimian Shield is exposed.

Figure 2.6: Distribution of brittle faults of the Paleoproterozoic Birimian Shield. Simplified after Milési et al., (1989); Frost-Killian, (2003).

Figure 2.7: Subdivision of the Paleoproterozoic Birmian domain into an (older) eastern subprovince and a (younger) western subprovince divided by the Ouango Fitini Belt (shear zone). Also shown is the distribution of other major rock units in the domain: **1** = Archean cratonic nucleus; **2** = Archean-Proterozoic transition zone; **3** = Paleoproterozoic supracrustal and intrusive rocks with position of volcanic belts; **4** = Pan-African province; **5** = Neoproterozoic/Phanerozoic sedimentary rocks (from Hirdes et al., 1996).

Figure 2.8: Distribution of mineral deposits and occurrences of the Paleoproterozoic Birimian Shield.

Figure 2.9: Simplified Geology of the Neoproterozoic Arabian-Nubian Shield, bounded by tectonic boundaries and unconformities. Simplified after Frost-Killian (2003). Insert shows the countries of northeast Africa in which part of the Arabian-Nubian Shield is exposed.

Figure 2.10: Schematic representations of tectonic structures (major faults and shear zones, undifferentiated) of the Neoproterozoic Arabian-Nubian Shield. Simplified from Frost-Killian (2003).

Figure 2.11: Distribution of mineral deposits and occurrences of the Paleoproterozoic Arabian-Nubian Shield.

Figure 3.1a: Distribution of mineral deposits, based on the most dominant chemical element within each deposit, of the Archean Zimbabwe Craton.

Figure 3.1b: Distribution of mineral deposits, based on the most dominant chemical element within each deposit, of the Paleoproterozoic Birimian Shield.

Figure 3.1c: Distribution of mineral deposits, based on the most dominant chemical element within each deposit, of the Neoproterozoic Arabian-Nubian Shield.

Figure 3.2a: Simplified geology of the Archean Zimbabwe Craton.

Figure 3.2b: Simplified geology of the Paleoproterozoic Birimian Shield.

Figure 3.2c: Simplified geology of the Neoproterozoic Arabian-Nubian Shield.

Figure 3.3a: Distribution of ductile shears of the Archean Zimbabwe craton (Jelsma, personal communication, 2004-2005).

Figure 3.3b: Distribution of brittle faults of the Archean Zimbabwe craton (Jelsma, personal communication, 2004-2005).

Figure 3.3c: Distribution of combined ductile shears and brittle faults of the Archean Zimbabwe craton.

Figure 3.4a: Distribution of brittle faults and shear zones of Paleoproterozoic Birimian Shield (De Beers database, including Milési et al., 1989).

Figure 3.4b: Distribution of brittle faults and shear zones of Paleoproterozoic Birimian Shield (Council for Geoscience-Frost-Killian, 2003).

Figure 3.4c: Distribution of merged brittle faults and shear zones of Paleoproterozoic Birimian Shield.

Figure 3.5: Distribution of brittle faults and shear zones of the Neoproterozoic Arabian-Nubian Shield (Council for Geoscience-Frost-Killian, 2003).

Figure 4.1: Schematic representation of different knowledge driven models. Reproduced from Thiart and de Wit (2000).

Figure 4.2: Flow diagrams of data driven approach. Reproduced from Thiart and de Wit (2000).

Figure 5.1a: Variation of gold contrast versus cumulative buffer distance away from brittle faults.

Figure 5.1b: Percentage of gold deposits (points) versus the total area (percentage) at successive distance away from brittle faults. Note that the number of deposit increases near-linearly with distance away from the faults; there is no sign of any preferred concentration of the deposits away from the faults.

Figure 5.2a: Variation of gold contrast versus buffer distance of the ductile shears. The contrast reaches a maximum at a distance of 5000m, and decreases slightly as the distance away from the ductile shears increases further.

Figure 5.2b: Percentage of gold deposits (points) versus the total area (percentage) at successive distance away from ductile shears. Note a more rapid initial increase in percentage of gold deposits (points) within 30% of the area.

Figure 5.3a: Variation of gold contrast versus buffer distance of the combined brittle faults and ductile shears theme. Note that the contrast reaches a maximum at a distance of about 5000m, and remains near-constant as the distance away from the structures increases.

Figure 5.3b: Percentage of gold deposits (points) versus the total area (percentage) at successive distance away from combined brittle faults and ductile shears.

Figure 5.4a: Model A – Posterior probability map of gold deposits based on reclassified lithologies and brittle faults. [CI = 1].

Figure 5.4b: Model A - Total uncertainty map of gold deposit, expressed in standard deviation units.

Figure 5.5a: Model B – Posterior probability map of gold deposits based on reclassified lithologies and ductile shears. [CI = 0.5].

Figure 5.5b: Model B - Total uncertainty map of gold deposit expressed in standard deviation units.

Figure 5.6a: Model C – Posterior probability map of gold deposits based on reclassified lithologies and combined brittle faults and ductile shears. [CI = 0.63].

Figure 5.6b: Model C - Total uncertainty map of gold deposit expressed in standard deviation units.

Figure 5.7: Model B – Posterior probability map for gold deposit with validation deposits superimposed. The percentage (%) of gold deposits that fall within each unit are indicated in the legend. Note that only 13% of the known gold deposits fall in "no-favourable" areas.

Figure 5.8a: Posterior probability map of CrNiPgeTi deposit model. Note predominant association of this element group with the mafic-ultramafic magmatic deposits of the Great Dyke.

Figure 5.8b: Total uncertainty map of CrNiPgeTi deposit model symbolized in standard deviation units. Also note the high uncertainty associated with the Great Dyke.

Figure 5.9a: Posterior probability map of CuZnPbBa deposit.

Figure 5.9b: Total uncertainty map of CuZnPbBa deposit expressed in one standard deviation units.

Figure 5.10. Variation of contrast of SnSb deposits versus buffer distance away from the granitoid-contacts. Note that the contrast reaches a maximum at a distance of about 8000m.

Figure 5.11a: Posterior probability map of SnSb deposit based on reclassified lithologies and granitoid-contacts. [CI = 0.99].

Figure 5.11b: Total uncertainty map of SnSb deposit expressed in one standard deviation units.

Figure 5.12: Variations of contrast of W deposits versus buffer distance away from the granitoid-contacts. Note that peak contrast value occurs at about 8000m distance.

Figure 5.13a: Posterior probability map of W deposit based on reclassified lithologies and granitoid-contacts. [CI=0.97].

Figure 5.13b: Total uncertainty map of W deposit expressed in one standard deviation units. The uncertainty of the weights of evidence may reflect the fact that only the lithologies theme was used.

Figure 5.14a: Variation of contrast of gold deposits versus buffer distance away from the CGS brittle and ductile faults. Note that the contrast decreases strongly as the distance increases.

Figure 5.14b: Percentage of gold deposits (points) versus the total unit area percentage at successive distances away from the CGS brittle and ductile faults. Note that the number of deposit increases near-linearly with increasing total area.

Figure 5.15a: Variation of contrast of gold deposits versus buffer distance away from the De Beers brittle and ductile faults. The contrast reaches an apparent maximum at a distance of 4000m, and decreases slightly as the distance away from the faults increases.

Figure 5.15b: Percentage of gold deposits (points) versus the total area (percentage) at successive distance away from the De Beers brittle and ductile faults. Note that the number of deposit increases near-linearly with increasing total area.

Figure 5.16a: Variation of gold contrast versus buffer distance away from the merged brittle and ductile faults (CGS + De Beers). The contrast reaches an apparent maximum at a distance of 4000m.

Figure 5.16b: Percentage of gold deposits (points) versus the total unit area percentage at successive distance away from merged brittle and ductile faults. Also, note that the number of deposit increases near-linearly with increasing total area.

Figure 5.17a: Model A – Posterior probability map of gold deposits based on reclassified lithologies and CGS brittle and ductile faults. [CI = 1].

Figure 5.17b: Model A – Total uncertainty map of gold deposits, expressed in standard deviation units.

Figure 5.18a: Model B – Posterior probability map of gold deposits based on reclassified lithologies and De Beers brittle and ductile faults. [CI = 0.96].

Figure 5.18b: Model B – Total uncertainty map of gold deposits, expressed in standard deviation units.

Figure 5.19a: Model C - Posterior probability map of gold deposits based on reclassified lithologies and merged (CGS and De Beers) brittle and ductile faults. [CI=0.96].

Figure 5.19b: Model C – Total uncertainty map of gold deposits, expressed in standard deviation units.

Figure 5.20: Model B –Posterior probability map for gold deposit with validation deposits superimposed. The percentage (%) of gold deposits that fall within each unit are indicated in the legend. 23% of the deposits fall in the "random area. Also note the Ashanti belt in the SE corner of the Birimian Shield (section 5.2.1.4).

Figure 5.21: The geology and faults of the Ashanti Belt, extracted from the simplified geology of the Paleoproterozoic Birimian Shield, West Africa.

Figure 5.22a: Variation of gold contrast versus buffer distance away from the faults. The contrast reaches an apparent maximum at a distance of 4000m, and decreases slightly as the distance away from the faults increases.

Figure 5.22b: Percentage of gold deposits (points) versus the total area (percentage) at successive distance away from the faults. Note that the number of deposit increases near-linearly with increasing total area.

Figure 5.23a: Posterior probability map of gold deposits in the Ashanti belt based on reclassified lithologies and faults. [CI = 0.97].

Figure 5.23b: Total uncertainty map of gold deposits, expressed in standard deviation units. Note that the high uncertainties in favourable areas (zones of highest posterior probability).

Figure 5.24a: Posterior probability map of CuZnPbBa deposit.

Figure 5.24b: Total uncertainty map of CuZnPbBa deposit expressed in one standard deviation units. Note the high uncertainty, which is probably because only one evidential theme is used.

Figure 5.25a: Variation of contrast of gold deposits versus buffer distance away from the faults. Note that the contrast reaches a maximum at about 5000m.

Figure 5.25b: Percentage of gold deposits (Points) versus the total area (percentage) at successive distance away from faults. Note that the number of deposit increases near-linearly with distance away from the faults.

Figure 5.26a: Posterior probability map of gold deposits based on reclassified lithologies and faults. [CI = 0.99].

Figure 5.26b: Total uncertainty map of Gold deposit expressed in standard deviation units.

Figure 5.27a: Posterior probability map of CuZnPbBa deposits. [CI = 1].

Figure 5.27b: Total uncertainty map of CuZnPbBa deposit expressed in standard deviation units.

Figure 6.1: The mineral diversity of selected elements of three areas, as shown by plotting the (natural log, Y-axis) spatial coefficient of the six element groups.

Figure 6.2: Mineral diversity of selected elements in the crust of the three study regions, derived by plotting the (natural log, Y-axis) spatial coefficient ($\ln \rho_{ij}$) of the total sum of six element groups in each region. Each region delineates a unique combination of elements. Confidence interval equals to 2x standard error.

Figure 7.1: Spatial associations between all element groups and three selected regions of African crust.

Figure 7.2: Relative concentration of mineral deposits of all six element groups in the three studied African regions. Five of the six element groups are concentrated to a greater degree in the Zimbabwe craton compared to that of younger crust.

Figure 7.3: Concentration of mineral deposits of six element groups in the cratons (>2.5 Ga) and younger crust (<2.5 Ga) of the Gondwana continents, reproduced from de Wit and Thiart (2005) and Thiart and de Wit (2006). The results are similar to those found in this study on a smaller scale within one continent (e.g. Fig 7.2).

List of Tables

Table 2.1: Summary of the lithostratigraphy, chronostratigraphy and associated granitoids suites of the Archean Zimbabwe Craton. The stratigraphy is based on Wilson et al (1995), with geochronological dates from Taylor et al., 1991; Wilson et al., 1995 and Jelsma et al., 1996.

Table 2.2: Summarized lithostratigraphy and chronostratigraphy of the Birimian Shield (after Bossiére et al. 1996).

Table 2.3: Range of elements used in this study, grouped into 3 geochemical types. Siderophile elements are those which tend to concentrate in metallic iron (native metal state). Chalcophile elements have an affinity for the sulphide phase, while lithophile elements preferentially concentrate in granitoid rocks (modified after Wilsher 1995, Thiart and de Wit, 2006).

Table 3.1: Summary of digital data sets used in this study.

Table 3.2: Total number of mineral deposits of three region of African crust, using the existing GO-GEOID: Gondwana-Geoscientific Indexing Database (Wilsher, 1995), newly added information from CGS: Council for Geoscience (Frost-Killian, 2003) and information from JAES: Journal of African Earth Science (Tadesse et al., 2003).

Table 3.3a: Summary of simplified geology of the Archean Zimbabwe Craton.

Table 3.3b: Summary of simplified geology of the Paleoproterozoic Birimian Shield.

Table 3.3c: Summary of simplified geology of the Neoproterozoic Arabian-Nubian Shield.

Table 5.1: Evidential themes used for spatial modelling of gold deposit.

Table 5.2a: Weights table for golf deposits from WofE applied to lithologic map of Zimbabwe Craton.

Table 5.2b: Reclassified weights table for gold deposits (Zimbabwe Craton).

Table 5.3a: Weights table for CrNiPgeTi deposits from WofE applied to lithologic map of the Zimbabwe Craton

Table 5.3b: Weights table for CrNiPgeTi deposits of lithologic units reclassified into 4 classes (Zimbabwe Craton).

Table 5.4a: Weights table for CuZnPbBa deposits from WofE applied to lithologic map of the Zimbabwe Craton.

Table 5.4b: Reclassified weights table for CuZnPbBa deposits (Zimbabwe Craton)

Table 5.5a: Weights table for SnSb deposits from WofE applied to lithologic map of the Zimbabwe Craton.

Table 5.5b: Reclassified weights table for SnSb deposits (Zimbabwe Craton).

Table 5.6: Cumulative analysis for granitoid-contacts.

Table 5.7a: Weights table for W deposits from WofE applied to lithologic map of the Zimbabwe Craton.

Table 5.7b: Reclassified weights table for W deposits (Zimbabwe Craton).

Table 5.8: Cumulative analysis for granitoid-contacts.

Table 5.9: Evidential themes used for spatial modelling of gold deposit.

Table 5.10a: Weights table for gold deposits from WofE applied to lithologic map of the Birimian Shield.

Table 5.10b: Reclassified weights table for gold deposits (Birimian Shield).

Table 5.11a: Weights table for gold deposits from WofE applied to lithologic map of the Ashanti belt (Birimian Shield).

Table 5.11b: Reclassified weights table for gold deposits (Ashanti belt, Birimian Shield).

Table 5.12a: Weights table for CuZnPbBa deposits from WofE applied to lithologic map of the Birimian Shield.

Table 5.12b: Reclassified weights table for CuZnPbBa deposits (Birimian Shield).

Table 5.13a: Weights table for gold deposits from WofE applied to lithologic map of the Arabian-Nubian Shield.

Table 5.13b: Reclassified weights table for gold deposits (Arabian-Nubian Shield).

Table 5.14a: Weights table for CuZnPbBa deposits from Wofe applied to lithologic map of the Arabian-Nubian Shield.

Table 5.14b: Reclassified weights table for CuZnPbBa deposits (Arabian-Nubian Shield).

Table 6.1: Selected element groups of known mineral deposits ($j_{1\text{-}6}$) from the three studied regions ($i_{1\text{-}3}$).

Table 6.2: Spatial association (ρ_{ij}) between element groups and the three selected regions

Table 6.3: Natural log of the spatial coefficient ($\ln \rho_{ij}$) with the approximate standard error ($s(\ln \rho_{ij})$), below and in brackets of element groups of the three study regions.

Chapter 1

Introduction

Long-term changes in geological and geochemical patterns during the history of the Earth are known as secular changes. There are many types of secular change that have been recorded or suggested to have occurred during Earth's history. Holland and Trendall (1984) review various patterns of secular change during Earth evolution that have been recognized. For example, Thompson et al. (1984) report long-term apparent changes in the chemical composition of the crust and mantle, and conclude that unidirectional variations in Earth processes are the cause for these changes. Other studies have shown that there is an increase in the oxidation state of the atmosphere from the Archean to the Phanerozoic (e.g. Hutchinson, 1992; Groves et al., 2005). Similarly, the heat production of the Earth has decreased steadily over this long period of time (e.g. Pollack, 1997), in turn changing the long-term mantle convection patterns and possibly crustal genesis. Such reported secular changes provide important insight into the long-term evolution of the Earth.

Other secular changes that have been suggested to have occurred during geologic time are less well accepted. For example, it is still not known with certainty if there are significant changes in the chemical make up and thus possibly the formation of continental crust and lithosphere over geologic time. This uncertainty also bears on possible changes in the rates of recycling of continental crust over time and the manner in which mineral deposits are formed (e.g. Barley and Groves, 1992; Hynes, 2001). Many researchers suggest that evolutionary changes of geologic processes are primarily responses to Earth's thermal evolution that, in turn, govern the tectonic, structural and lithostratigraphic environments in which mineral deposits are formed (e.g. Hutchinson, 1992; Herrington et al., 1997).

Variations in enrichment of mineralization in the form of ore deposits in the continental crust may be one way to test for secular variation in formation and recycling of continental crust. Thus, for example, any detected changes in the density of mineral deposits formed during Earth history may relate directly to changes in the genesis and tectonic evolution of the crust. Indeed, de Wit and Thiart (2005) and Thiart and de Wit (2006) have suggested that old continental crust is more enriched in mineral deposits than younger crust, and that this may reflect a secular change in crustal evolution and geodynamic processes.

This project aims to derive fundamental information with which to "fingerprint" the metal endowment in regions of African continental crust of different ages (from Archean to Neoproterozoic) by applying spatial statistics to the known mineral deposits and geology of these areas. This approach allows testing further for secular changes in mineralization during Earth evolution. To realize this, three segments of African crust of different ages are selected, based on the similarity in their geology and crustal genesis: the Neoproterozoic Arabian-Nubian Shield, the Paleoproterozoic Birimian Shield and the Archean Zimbabwe Craton (Figure 1.1), as summarized below:

1. The Arabian-Nubian Shield (0.5-1.0 Ga) is a part of the much larger East African Orogen that extends throughout Eastern Africa (Stern, 1994). It covers several countries, mainly Egypt, Eritrea, Ethiopia, Djibouti, Saudi Arabia, Somalia, Sudan and Yemen. The Arabian-Nubian Shield is recognized as a large region of rapid juvenile crustal growth during the Neoproterozoic.
2. The Birimian Shield (1.8-2.3 Ga) forms a major part of the West African Shield that underlies Ivory Coast, Burkina Faso, Niger, South Mali and West Ghana, Liberia and Mauritania. The West African Shield is recognized as an exceptional large zone of juvenile crustal growth during the Paleoproterozoic.

3. The Zimbabwe craton (2.5-3.0 Ga) of southern Africa is a large Archean crustal block that lies north of the high-grade Limpopo Belt. The craton is mostly exposed in Zimbabwe but extends southwest into Botswana. The Zimbabwe Craton is a region of rapid crustal growth mostly during the NeoArchean.

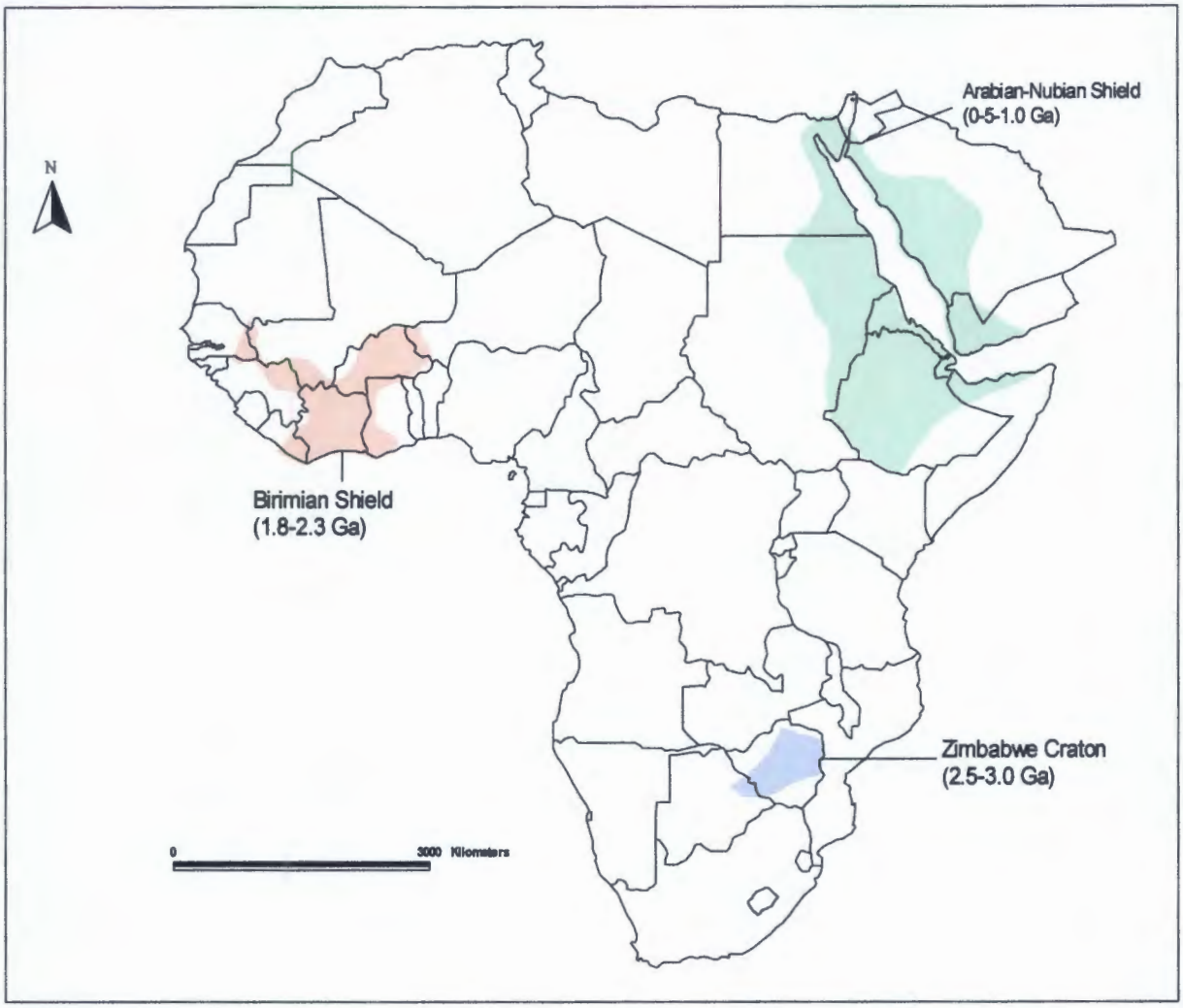

Figure 1.1 Location of the three selected African regions analysed in this study. The regions represent 3 distinct 500-million-year time-slices of African crustal growth between the Archean and the end of the Neoproterozoic.

All three regions (Arabian-Nubian Shield, Birimian Shield and Zimbabwe Craton), formed during approximately the same length of geologic time (e.g. about 500 million years) at different times spanning nearly 2500 million years of Earth history.

All three regions have similar geology, comprising of relatively juvenile granitoid crust interspaced with supracrustal rocks (often referred to as greenstone belts). In addition these 3 regions share similar mineral deposits and tectonic histories that involve major episodes of crustal accretion.

1.1 Objectives

The main objectives of this study are threefold:

1. To upgrade the GO-GEOID (Gondwana-Geoscientific Indexing Database), housed at AEON (Africa Earth Observatory Network). Presently this database holds information on more than 16 000 mineral deposits across Gondwana, including over 6000 deposits in Africa. New data will provide additional information for metallogenic studies. This database forms the basis for the present study of African metallogeny through time.

2. To develop and demonstrate a methodology for quantifying spatial associations between known mineral deposits and geological features as inputs to produce predictive mineral potential maps. No attempt is made in this study to incorporate tonnages and grades of the deposits (e.g. quality of the ores).

3. To determine if there are variations in the total concentration of mineral deposits in crust of different ages, and to test for secular changes in mineralization over a period of 2500 million years of Earth history in Africa, from the Archean to the Neoproterozoic. Mineral diversity patterns detected in those different regions may help to track the evolution of Earth's continental lithosphere.

1.2 Definition of craton and shields

Craton and Shield are two different terms that distinguish continental crust of different age. A craton is defined as a part of the Earth's lithosphere that has attained permanent stability, and has been little deformed for a prolonged period. Cratons are generally restricted to the Archean (e.g. greater in age than 2.5 billion years). Shields are larger areas of post-Archean continental lithosphere that may have cratons embedded within them, and are often partially covered by younger platform sediments (e.g. Bates and Jackson, 1987). Cratons usually have thick lithospheric mantle roots (250-300 km) that exceeds those of younger Shield areas, (100-150 km) (e.g. Fouch et al., 2004).

1.3 Definition of mineral potential

Mineral deposits, whether metalliferous or non-metalliferous, are accumulations or concentrations of one or more useful substances that are for most part sparsely distributed in the Earth's crust (Goossens, 1983). De Wit (2005) defines mineral deposits as natural capital grown out of interactive geological processes that occasionally converge to concentrate useful minerals. The geological processes that lead to the formation of mineral deposits are collectively called mineralization. Mineral potential, as used in this project, is a statistical characteristic attributed to a particular area that describes the probability for the presence of mineral deposits or existence of mineralization. The predictive mineral potential maps generated in this project are based on two factors: favourability and validity. Favourability is determined by integration of geological evidence (rock-age, rock-type, faults etc.) that are considered essential for the formation of a mineral deposit. Validity is determined by how well the predictive models correctly delineate known mineral deposits. These factors are important for assessing the methodologies developed to produce predictive mineral potential maps.

1.4 Methodology

The research methods used in this project combines knowledge of three different disciplines: geology, geographic information system (GIS) and statistics (spatial analysis). All these disciplines are in order to quantify the relationship between geological features and mineral deposits. Such a data-driven approach is based on formulation of a Bayesian probability model (or weights of evidence (WofE) model). The WofE method is a statistical method for combining binary/multiclass of geological evidences to produce mineral potential maps (Bonham-Carter, 1994). This method is applied to all three selected regions.

In summary, this thesis has the following structure:

1. A review of literature pertinent to qualitative and quantitative methods of analysing mineralization (chapter 2).
2. GIS-based spatial data processing: integration of various datasets (geology, faults, minerals) from various sources to one platform; updating the existing GO-GEOID database (chapter 3).
3. Spatial modelling methodology, with a focus on the contrasts between knowledge-driven and data-driven models. (chapter 4).
4. Spatial modelling using WofE method to produce mineral potential maps (chapter 5).
5. Analysing the diversity of mineral deposits across the three African crustal segments to derive metallogenic "fingerprints" of a number of selected chemical element groups (chapter 6).
6. Testing for secular change of mineralization in African crust (chapter 7).
7. In the final chapter 8, results of this project are summarized, conclusions are listed, and recommendations for further studies are suggested.

Chapter 2

Geologic architecture of three different African crustal segments

This chapter outlines the general geology and tectonic evolution of the three African areas of continental crust of different age that are used later for comparative analyses of their respective mineral deposits. The chapter comprises four parts, the first three of which summarise the geology and tectono-stratigraphy of the Archean Zimbabwe Craton, the Paleoproterozoic Birimian Shield and the Neoproterozoic Arabian-Nubian Shield; and the last part is a summary of their respective associated mineral deposits. This framework enables one to relate crustal evolution and metallogenesis over a period of time. The three African regions used in this study range in age from Neoarchean (3.0-2.5 Ga) to Neoproterozoic (0.5-1.0 Ga). The former is often thought to represent a period of rapid growth of continental crust, whilst the later Proterozoic (2.5-0.5 Ga), is believed to characterize a global levelling- out of crustal growth (Condie, 1992, 1994; Windley, 1995). There is, however, considerable controversy about the time-integrated crustal growth, and some believe that there has been steady-state crustal growth and recycling since the Archean (e.g. Fyfe, 1978; Armstrong, 1981, 1991; Bowring et al., 1993; Bowring and Housh, 1995). Results from this thesis may help to resolve some of these crustal genesis debates.

2.1 The Archean Zimbabwe Craton

The Archean Zimbabwe Craton of southern Africa is a large Archean crustal block (2.41 x 10^5 km^2) mostly exposed in Zimbabwe but extending to the southwest into NE Botswana. The craton is bounded on its sides by tectonic boundaries with adjacent younger domains (Figure 2.1): the east-west trending Zambezi domain - thrust faults (2.6-0.5 Ga) in the north; and the Magondi domain (2.0-1.8 Ga) of thrust faults and unconformities in the west. In the south, the Shashe and Limpopo domains (2.6-2.0 Ga) are separated from the Zimbabwe craton by thrust and transcurrent faults.

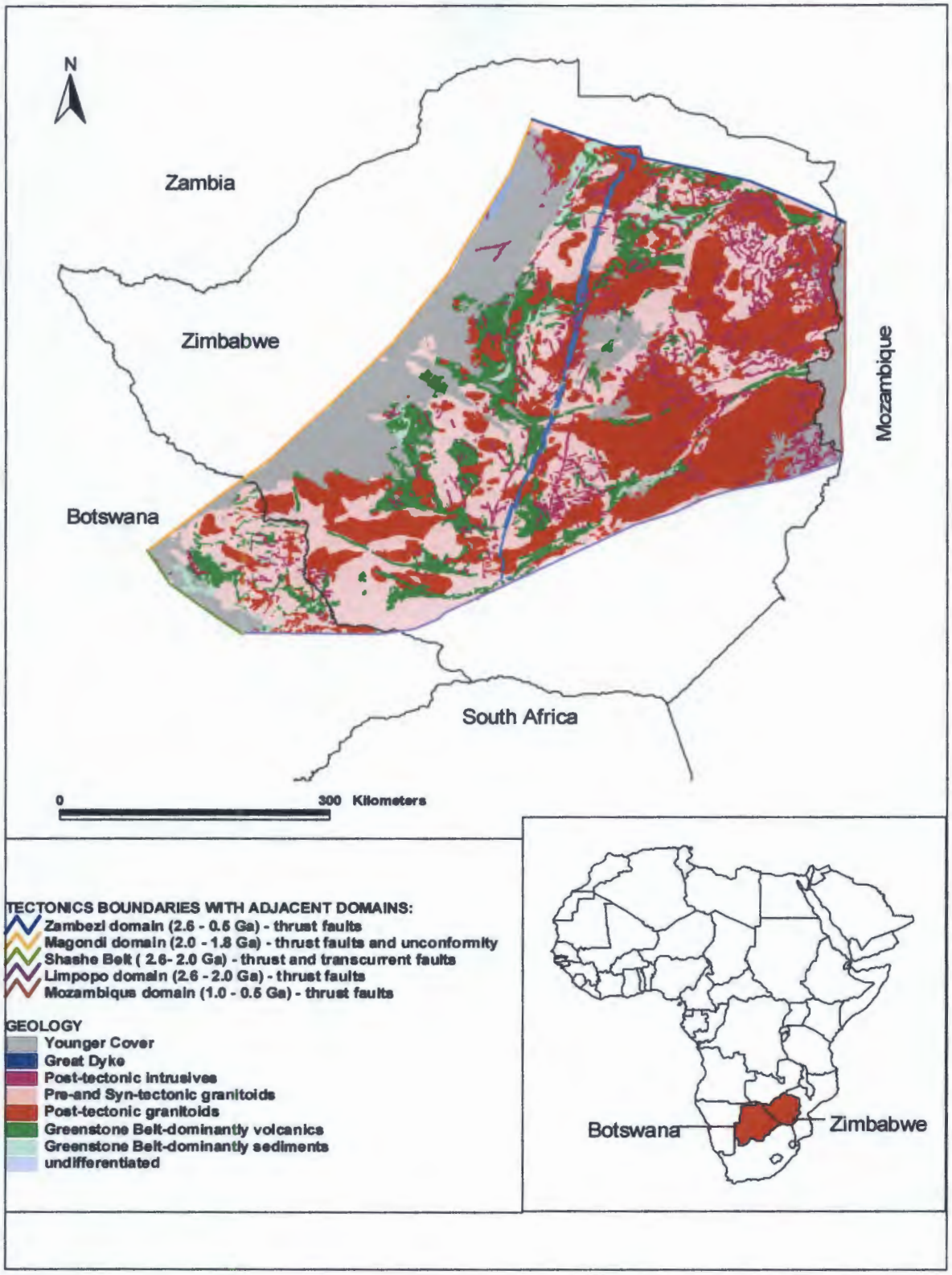

Figure 2.1 Simplified Geology of the Archean Zimbabwe Craton bounded on its sides by younger tectonic domains. Simplified from Jelsma and Thiart (2002) and Jelsma (2003-2004). Insert shows the two countries where the Zimbabwe craton is exposed.

The north-trending Mozambique domain (1.0 – 0.5 Ga) forms the eastern margin of the Zimbabwe Craton (predominantly thrusts).

The Zimbabwe Craton consists of NeoArchean granitoid-gneisses, greenstone belts, intrusive complexes, younger granites, all cut by the ~2.5 Ga Great Dyke, and covered by the Tertiary Kalahari sands in the west. Rocks older than 3.0 Ga make up only a very small domain in the south (The Tokwe Gneiss Complex, Jelsma and Dirks, 2002; Jelsma et al., 2004). Therefore, the craton is predominantly composed of granite-greenstone terrains that were emplaced within ~500 million years between 3.0-2.5 Ga (Wilson et al., 1995; Blenkinsop et al., 1997). The granite-greenstone terrain of Zimbabwe has been used frequently as a type example of Archean tectonism and crust formation (Blenkinsop et al., 1997; Bickle and Nisbet, 1993; Wilson et al., 1995; Jelsma et al., 1996; Dirks and Jelsma, 1998a, 2002). In reality, the Zimbabwe granite-greenstone terrain predominantly represents NeoArchean juvenile continental crust formed in a variety of tectonic settings and metamorphosed through a complex series of structural and magmatic events (e.g. Kusky and Polat, 1999).

Based on previous work, the development of the Archean cratons is viewed in terms of two major episodes each involving volcanism, crustal growth and orogeny (Wilson et al., 1995; de Wit, 1998): NeoArchean (2.5-3.0 Ga) and MesoArchean (3.0-4.0 Ga). Because most of the Zimbabwe craton postdates 3.0 Ga, this study focuses only on crustal evolution and metallogenesis from the NeoArchean (2.5-3.0) onward. The Zimbabwe craton consists of varied granitic and gneisses rocks with widespread greenstone belts mostly ranging in age between 3.0-2.5 Ga. Stabilization of the craton is older than the Great Dyke (~2.5 Ga), because this is a major elongated intrusion of mafic and ultramafic rocks that cuts across the Archean rocks of the Zimbabwe Craton and therefore represents a regional brittle response of the craton at this time (e.g. Mukasa et al., 1998).

2.1.1 Geological Setting

The evolution of Zimbabwe Craton is best explained through a series of crustal growth stages that each added new greenstones and granitoids (Jelsma et al., 1996; Dirks et al., 2002). Each of these stages is represented by the deposition of a volcano-sedimentary sequence on granitoid basement (Wilson et al., 1995). The oldest segment of granitoid crust is the small ~3.5 Ga Tokwe Gneiss Complex, which contains infolded remnants of greenstones that are grouped collectively into the Sebakwian Group (Hofmann et al., 2003; Jelsma et al., 2004). The Tokwe segment has been intruded by NeoArchean granitoids, and there is much dispute about its regional extent. Here we follow Jelsma et al. (2004) and assume that the Tokwe Gneiss Complex is a minor component of the craton. The more widely developed late Archean (3.0-2.6 Ga) greenstones include the Belingwean (2.9 Ga), Lower Bulawayan (2.8 Ga), Upper Bulawayan (2.7 Ga), and Shamvaian (2.65 Ga) Supergroups.

The earliest widespread formation of greenstones, together with associated granitoids suites, is represented by the Lower Greenstone sequences of the Belingwean Group emplaced between 2.9-2.8 Ga. These comprise mafic volcanic sequences in the lower parts that pass upwards into a dominantly bimodal succession with alternating mafic and felsic volcanic rocks. The upper part of the Belingwean Group is a komatiite and mafic volcanic sequence that also incorporates minor sediments (Wilson et al., 1995). An unconformity separates the Upper Belingwean from the base of the Upper Greenstone succession, known as the Lower Bulawayan, that consists of intermediate to felsic volcanic rocks and volcaniclastic sediments. Wilson et al., (1995) indicated that there are a number of granitoid intrusions into the Lower Greenstone successions, some of which may be correlated with felsic volcanism within the Upper Greenstone succession. The Upper Bulawayan includes clastic sediments together with basalts and komatiitic basalts.

The Shamvaian comprises sedimentary associations intercalated with felsic volcanic rocks and is the youngest of the greenstone succession. Subsequent crust formation events added granitoids of the ~2.9 Ga to ~2.8 Ga Chingezi, ~2.7 Ga Sesombi and ~2.6 Ga Chilimanzi suites.

The craton became a stable crustal segment at around 2.5-2.6 Ga (Bickle and Nisbet, 1993; Wilson et al., 1995) following the emplacement of large volumes of crustally derived 2.6 Ga Chilimanzi suite granites (Wilson et al., 1995; Jelsma et al., 1996; Horstwood, 1999; Jelsma and Dirks, 2002), and before the intrusion of the layered igneous complex of the Great Dyke at 2.58 Ga (Mukasa et al., 1998; Oberthür et al., 2002) and its associated satellites dykes and related fracture patterns. Dirks et al. (2002) have shown that the rocks that formed during 2.9 and 2.6 Ga events account for about 90% of all rocks exposed in the Zimbabwe craton. A summarized stratigraphic sequence of the Archean Zimbabwe Craton is given in Table 2.1.

These stages of evolution are believed to be linked to the emplacement of mantle plumes below existing continental crust, causing intracontinental rifting and crustal melting (Dirks and Jelsma, 2002; Bickle et al, 1993; Jelsma et al., 1996; Blenkinsop et al., 1997). This resulted in the formation of an autochthonous stratigraphy that has been correlated across large parts of the craton (Wilson et al., 1995). However, Dirks and Jelsma (1998b; 2002) and Jelsma and Dirks (2000) presented structural data suggesting that tectonic stacking of the stratigraphy has played an important role in the evolution of the greenstone sequences, and that many greenstone sequences are allochthonous and may have been formed in unrelated tectono-magmatic environments (Jelsma and Dirks, 2000; Kusky, 1998; Kusky and Kidd, 1992).

Stratigraphy	Lithologies	Age
Shamvaian Supergroup	Sedimentary rocks with felsic volcanic rocks and Chilimanzi suites (2.6 Ga)	~2.6 Ga
Upper Bulawayan Supergroup	Komatiites and volcanics	~2.7 Ga
	Clastic sediments	NeoArchean
Lower Bulawayan Supergroup	Mafic and felsic volcanics with added granitoids of the Chingezi, 2.9-2.8 Ga;	~2.8 Ga
Belingwean Supergroup	Sesombi, 2.7 Ga; Wedza, 2.6 Ga)	~2.9 Ga
Sebakwian Group	Tokwe Gneiss Complex	MesoArchean ~3.5 Ga

Table 2.1 Summary of the lithostratigraphy, chronostratigraphy and associated granitoids suites of the Archean Zimbabwe Craton. The stratigraphy is based on Wilson et al (1995), with geochronological dates from Taylor et al., 1991; Wilson et al., 1995 and Jelsma et al., 1996.

2.1.2 Tectonic Setting

There is much controversy about the tectonic and magmatic history of the Zimbabwe craton. A number of researchers (Wilson et al., 1995; Kusky and Vearncombe, 1997; Kusky, 1998; Horstwood et al., 1999; Blenkinsop et al., 1997; Dirks and Jelsma, 1998b, Jelsma and Dirks, 2002) have provided various geotectonic interpretations about the crustal growth of Zimbabwe craton, in line with interpretation of Archean craton formations elsewhere in the world (e.g. de Wit and Ashwal, 1997).

Hunter and Stowe (1997) provide a good historical account of the older interpretations. The earlier researchers generally agreed that the evolution of the Zimbabwe Craton induced massive crustal-scale inversions of granitic crust overlaid by mafic greenstone sequences (e.g. Macgregor, 1951). This gravity-driven tectonics was believed responsible for the dome and keel structure that apparently dominated the Zimbabwe craton (Fig. 2.1). This was the classic pattern as first described by Macgregor (1951). With time, as better age-dating techniques became available, new and more plate-tectonic-like models became a more favoured way to explain the geology of the craton (Hunter and Stowe 1997; Hoffmann and Kusky, 2004; Dirks et al., 2002).

Today it is generally agreed that many tectonized granite-greenstone contacts are shear zones with major displacement across them (e.g Kusky and Kidd, 1992; Campbell and Pitfield, 1994; Kusky, 1998; Hoffmann and Kusky, 2004), either as thrusts, normal faults, or strike-slip faults. Deformation is often intense with disruption of the greenstone stratigraphy. Current work on evolutionary models for the Zimbabwe Craton (Jelsma and Dirks, 2000; Dirks et al., 2002) recognises that the stratigraphy of most greenstones belts is cut by a large number of such shear zones that typically parallel compositional layering or cut layering at low angles (Fig 2.2). In turn this suggests that the layer-parallel shear zones are early thrusts that profoundly affected the stratigraphy of the greenstone belts.

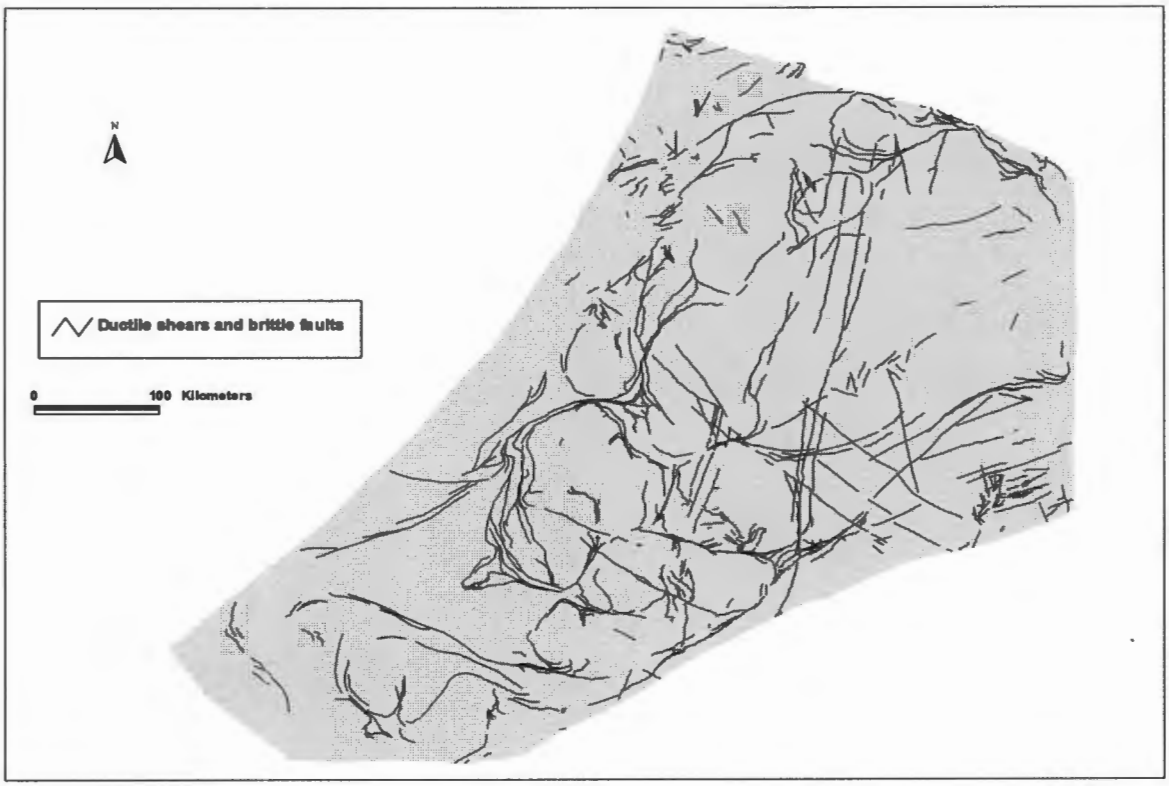

Figure 2.2 Distribution of ductile shears and brittle faults of the Archean Zimbabwe craton (after Jelsma and Dirks, 2002; Jelsma, personal communication, 2004-2005).

The thrusts belts are interpreted to document progressive accretion and crustal thickening through low-angle subduction and/or underplating (Jelsma and Dirks, 2000; Dirks and Jelsma, 2002). This interpretation demonstrated that crustal growth occurred through successive lateral accretion of ***juvenile*** material, along plate margins of progressively growing cratonic nuclei (Dirks et al., 2002; Dirks and Jelsma, 2002). Jelsma and Dirks (2002) described deformational events (D_I-D_{III}) of the Zimbabwe craton from older to younger sequences, whereby the formation of layer-parallel shear zones and recumbent folding was followed by thrusting across generally steeply east-dipping shear zones. The shears, together with outcrop patterns of greenstone sequences, define semi-circular tectonic units (Fig. 2.2) commonly centred on gneisses, and arranged in an overlapping, fish-scale fashion, underlain by the east-dipping thrusts (Jelsma and Dirks, 2000).

Deformational events are represented by an early phase of deformation that produced large recumbent folds, duplex geometries and shear zones bounding low-strain domains. The shear zones of this type form a curvilinear pattern throughout the greenstone-gneiss terrains of the craton, and are related to an early (E-W) trending lineation and an early-verging sense of shear (Dirks and van der Merwe, 1997; Jelsma and Dirks, (2000). The shears in turn envelop structural domains characterized by upright folding (Campbell and Pitfield, 1994). Deformation in the Zimbabwe craton, therefore, is linked to episodic periods of growth of granite-greenstone crust. The important conclusion for this thesis is that most of the craton was created at zones of primary magma formation from the mantle (arcs, mid-ocean-ridges, hotspots), and that most of the rocks are juvenile (e.g. derived direct from the mantle rather than by melting of older rocks). Therefore, this implies that the NeoArchean continental crust of the Zimbabwe craton formed over a period of nearly 500 million years of mantle fractionation. Any associated mineralization is assumed to have a similar juvenile origin.

2.1.3 Mineralization

Mineralization in the Archean greenstone belts are closely related to progressive evolving geotectonic activities. Gold is the most important economic mineral in Archean granite-greenstone terranes throughout the world and Zimbabwe is no different. Jelsma (1993) have shown that with the development of a hydraulic gradient, fluids migrate from contraction shear to structurally-controlled pathways, redistributing and reconcentrating mineralization, particularly gold, into second-order structures. Isotropic lithologies, such as massive volcanogenic and clastic metasediments, generally low in primary gold, react in a brittle manner and form suitable host-rocks for epigenetic and syntectonic mineralization.

NeoArchean granitoid-greenstone terrains are generally richly endowed in Ni, Cu-Zn, Fe and Au mineralization, which directly or indirectly resulted from periods of continental voluminous magmatism, including the emplacement of the most extensive successions of ultramafic lavas or komatiites preserved in Earth history (e.g. Hutchinson, 1992; Herrington et al., 1997). Thus, mineralization in greenstone belts globally is linked to the magmatic and metamorphic processes which affected Archean granite-greenstone terrains during their formation. The associated shear zones provided conduits for massive fluid remobilization and escape from the subcontinental lithospheric mantle, which would have both stabilized the cratonic roots of the cratons, and initiated large-scale granite emplacement into their mid- and upper-crust (e.g. Kusky, 1998; Kusky and Polat, 1999).

Most of the gold deposits appear spatially and structurally associated with deformation zones within, or adjacent to, greenstone belts, or with folds between major deformation zones. The shear zones play an important role in the localisation of mineral deposits such as base metals and gold. Recognition of the tectonic setting of particular lithologic sequences can therefore significantly aid the understanding of regional metallogeny and aid the exploration for mineral deposits. Like all Archean cratons, the Zimbabwe craton is richly endowed in gold (de Wit and Thiart, 2005; Thiart and de Wit, 2006; see Fig. 2.3) and is therefore a good NeoArchean example to analyse in this project.

The craton is also enriched with other deposits, such as Tin (Sn) and Tungsten (W), that are most often related to the heat pulse of granite intrusion and related hydrothermal circulation. Whereas, the primary source of the deposits are most likely magmatic (e.g derived from the granites), secondary enrichments is often in the aureoles around the margins of the granites (Taylor, 1979).

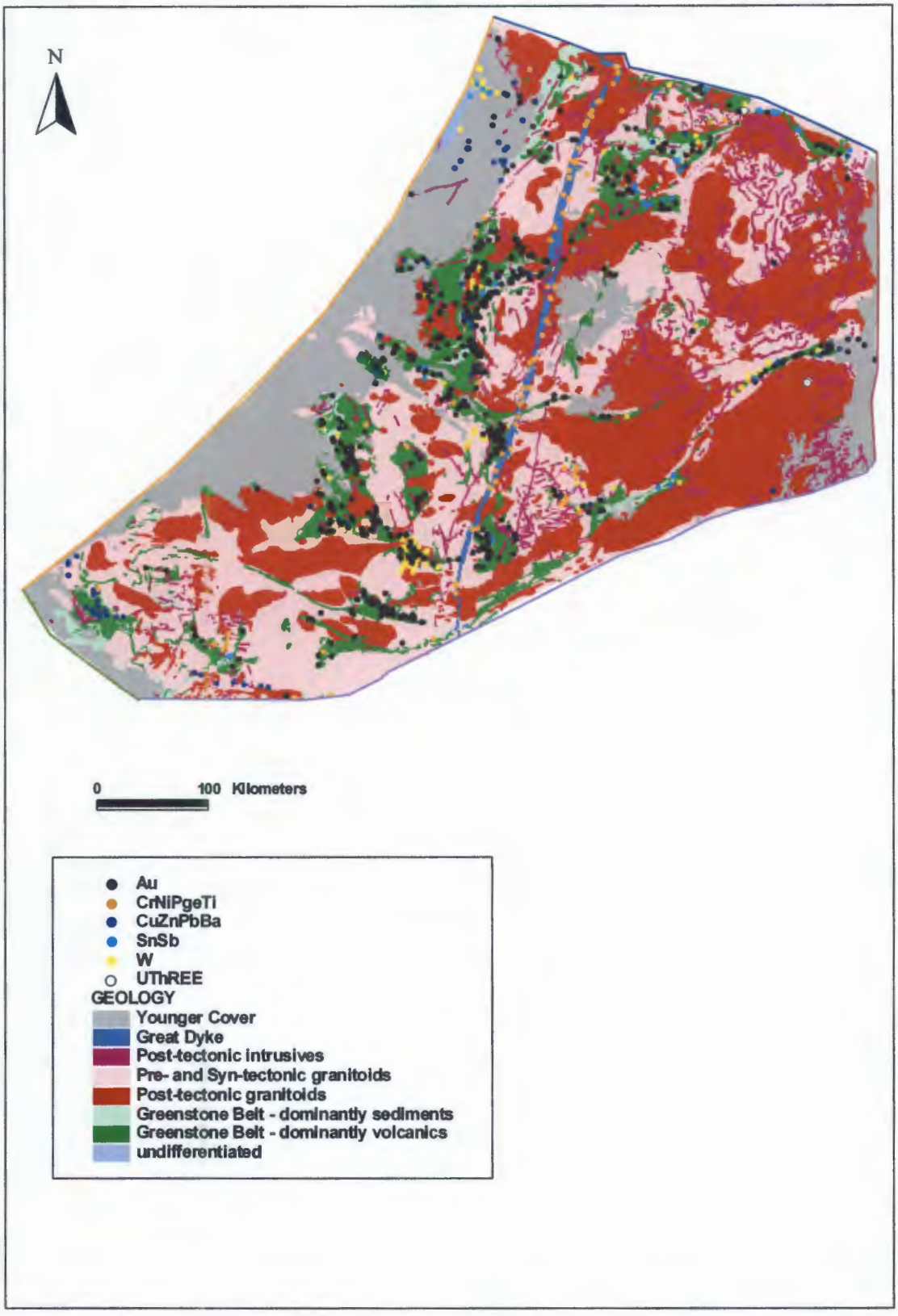

Figure 2.3 Distribution of mineral deposits and occurrences of the Archean Zimbabwe craton.

2.2 The Paleoproterozoic Birimian Shield (West Africa)

The West African Shield is a region that has been stable since ~2.0 Ga and consists of two major basement domains of Archean and Paleoproterozoic age, the Reguibat Rise in the north and the Leo-Man Rise in the south. These two basement domains are separated by Neoproterozoic and Phanerozoic Platform sediments of the Taoudeni basin and are entirely surrounded by Pan African and Hercynian Mauritanides belts (Fig 2.4). The origin and evolution of these regions is the result of complex polycyclic crustal growth and structural evolution. Here, I concentrate on the southern parts of the Shield that comprises two large areas: an Archean craton (the Leo-Man Craton, 3.4-2.5 Ga) making up the western part, and the much larger Paleaoproterozoic Baoulé-Mossi domain (1.8-2.3 Ga) (Abouchami et al., 1990; Triboulet and Feybesse, 1998; Egal et al., 2002) that make up the central and eastern part. The basement in West Africa was deformed during three major orogenic events: Liberian (~2.7 Ga), Eburnean (~2.1 Ga), affecting the Birimian terrains; Abouchami et al., (1990); Liégeois et al., (1991); Boher et al., (1992) and the Pan-African (Liégeois et al., 1994).

2.2.1 Geological Setting

The Paleoproterozoic Baoulé-Mossi domain (8.85×10^5 km^2) is the specific area of study for this thesis, and is known as the type area of the Birimian epoch in Africa (Cahen and Snelling, 1984) and therefore referred to here as the Birimian Shield. The Birimian Shield forms the major part of the southern sector of West Africa, and is also known as the Birimian granite-greenstone terrain. It underlies much of the Ivory Coast, Burkina Faso, SW Niger, S. Mali and W. Ghana (Fig.2.5). The Birimian Shield comprised predominantly juvenile continental crust formed during a period of a major crustal growth between 2.3 and 2.1 Ga that have been affected by the Eburnean orogeny at ~2.0 Ga (Cahen and Snelling, 1984; Abouchami et al., 1990; Boher et al., 1992).

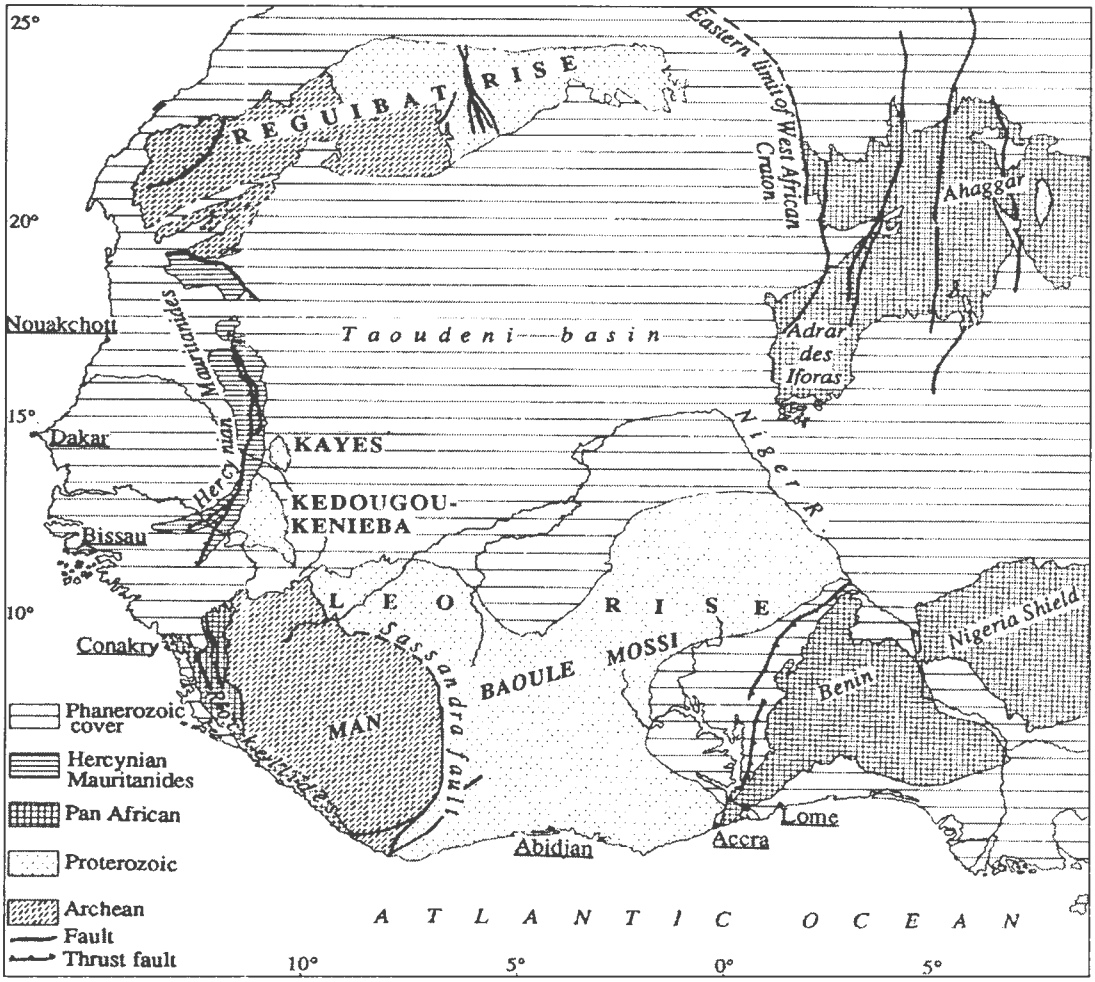

Fig 2.4. Geological sketch map of the West African Craton showing the location of the Leo-man and Reguibat rises, as well as the Baoule Mossi domain (reproduced after Boher et al., 1992), also known as the Birimian Shield, which is the area investigated in this study.

This crust consists of an association of low-grade sedimentary basins, plutono-volcanic belts and granitoid batholiths resembling Archean granite-greenstone terrains (Attoh and Ekwueme, 1997; Hirdes and Davis, 2002). The volcanics and sedimentary strata of these belts are referred to as Birimian (~1.8-2.3 Ga, a period of ~500 million years), which were deformed together with granitoids in the Eburnean orogenic cycle 2.0-2.2 Ga. Thus, the term Eburnean refers to all tectonic, metamorphic and plutonic events affecting the Birimian rocks during the Paleoproterozoic between 2.0-2.2 Ga.

Numerous studies have addressed the geology and tectonic evolution of the Birimian (Paleoproterozoic) terrain (Hirdes et al., 1996). Paleoproterozoic supracrustal rocks are widespread across the shield, and these are distributed in narrow NE-SW trending sedimentary basins and linear and arcuate volcanic belts, both intruded by several generations of granitoids. These belts have a stratigraphy similar to those of Archean greenstone belts, except that komatiites are unreported (e.g. Attoh and Ekwueme, 1997).

The formation of these Paleoproterozoic supracrustal rocks and associated syn-volcanic and syn- to late-kinematic intrusives marks the major Birimian juvenile crust forming event. Geochronology and isotope geochemistry to date indicate that the majority of the rocks formed within a maximum time interval of about 200 million years (2.05-2.27 Ga; Hirdes and Davis, 1998, 2002; Bossiére et al., 1996; Davis et al., 1994; Doumbia et al., 1998; Kouamelan et al., 1997), but rocks as old as 2.3 and as young as as 1.8 are also present. The entire period of **juvenile** crustal growth and stabilization of the Birimian Shield therefore lasted about 500 million years, as is the case for the Zimbabwe craton.

The lithostratigraphic succession of the Paleoproterozoic formations, although previously much debated (Milési et al., 1992; Feybesse and Milési, 1994; Hirdes et al. 1996; and others), is now considered to be well established. Attoh and Ekwueme (1997) stated that many of the Birimian greenstones belts are unconformably overlain by coarse, clastic sedimentary rocks referred to as Tarkwaian. The sequences are therefore separated into the Birimian Supergroup and the Tarkwaian Group (Table 2.2). The Birimian Supergroup has been divided into lower and upper formations. The Lower Birimian comprises of volcano-sedimentary package with intercalated fluvio-deltaic metasediments and the Upper Birimian composed of volcanic-volcanoclastic-clastic package.

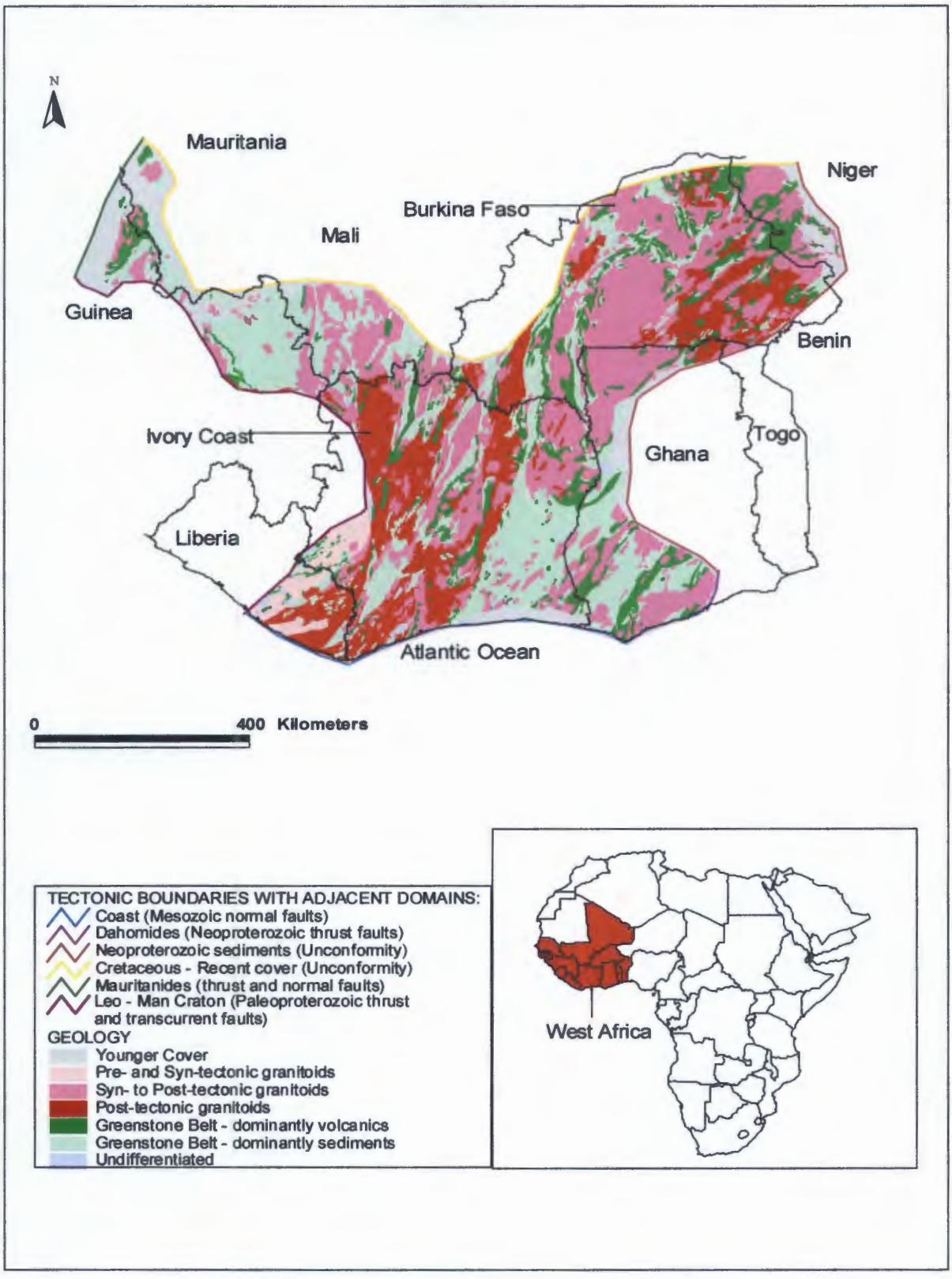

Figure 2.5 Simplified Geology of the Paleoproterozoic Birimian Shield, West Africa, as delineated by its later tectonic margins. Simplified after Milesi et al., 1989. Insert highlights the countries of western Africa in which part of the Birimian Shield is exposed.

The coarse clastic sedimentary sequence of the Tarkwaian Group lies unconformably on the Birimian Formations (Bossiére et al., 1996; Hirdes et al., 1996) and is not considered to be part of the Birimian Supergroup by most research groups. All these rock formations were deformed together and intruded by syn-, late-and post-tectonic granitoids (Hirdes et al., 1992; Pons et al., 1995).

Stratigraphy	**Lithologies**	**Age**
Tarkwaian	Coarse-clastic sedimentary rocks (sandstone, siltsone, shale and conglomerate)	2.0-1.8 Ga
Upper Birimian	Volcanic-volcanoclastic-clastic rocks (basalts and interflow sediments) and syn-tectonic and intrusive granitoids	2.3-2.0 Ga
Lower Birimian	Volcano-sedimentary rocks and fluvio-deltaic metasediments	

Table 2.2 Summarized lithostratigraphy and chronostratigraphy of the Birimian Shield (after Bossiére et al. 1996).

Although early workers believed that the Birimian Shield accumulated in basins developed on Archean crust (e.g. Petters, 1991; Leube et al. 1990), it is now generally accepted that the components of individual supracrustal rocks probably represent juvenile materials generated in a variety of active tectonic settings (e.g. Beziat et al. 2000). Various oceanic accretion models have been proposed for the crustal growth of the West African Shield at ~2.1 Ga as oceanic plateaus (Abouchami et al. 1990), intraoceanic island arc and back-arc basin (Vidal and Alric, 1994).

Condie, (1992) summarizes the Paleoproterozoic crustal evolution of the Birimian Shield as the type of orogeny involving the growth and amalgamation of many juvenile island arcs and slices of oceanic crust or oceanic plateaus into a new continental terrain. The individual terranes were mutually sealed by intervening accretionary wedges, and this process typically gave rise to a wide orogen that contained little or no older crustal material, that therefore represents considerable new and rapid continental crustal growth.

In contrast, Kouamelan et al. (1997) relates the Eburnian orogenesis to major underplating processes under Archean basement especially along the western and north western margins of the Leo-Man Craton. (e.g. western Ivory Coast) which had been possibly thinned during underplating. They suggested that there is a close proximity between the Archean crust and an accretion zone associated with the juvenile Birimian magmatism. This conclusion is supported by some crustal residence ages obtained in the eastern part of the Leo-Man Craton that suggest participation of subordinate Archean crustal component in the Birimian magmatism along the boundary between Leo-Man Archean and Baoulé-Mossi Birimian domains (Boher et al., 1992).

However, most workers agree that the bulk of the Birimian terrains comprise **juvenile** materials, added to the new crust in the Paleoproterozoic between 2.3-1.8 Ga. Therefore, the majority of the Birimian rocks are juvenile in that they were all mantle derived within a short time span at approximately the age of the rocks (Boher et al., 1992; Béziat et al., 2000).

2.2.2 Tectonic Setting

The earliest tectonic features identified in the Birimian rocks resulted from subhorizontal, compressional deformation (Milési et al., 1992; Ledru et al., 1991; Leigeois et al., 1991) and this was followed by subvertical transcurrent deformation (Vidal and Alric, 1994; Pons et al., 1995). Marcoux and Milési, (1993) emphasize that the structures of the Birimian rocks reflects three main Eburnean tectono-metamorphic phases (D_1-D_3). The first phase, (D_1) resulted from a major diachronous collision event, between 2150 and 2100 Ma, and was responsible for thrusting Early Proterozoic formations across Archean basement (Leo-Man Craton) in the west (Feybesse and Milési, 1994) and also thrust faults to the SE in the Ashanti region. The second phase (D_2) gave rise to large SW-NE striking left-lateral shear zones that dominate the regional NE-SW tectonic fabrics of the Birimian Shield (Fig. 2.6), accompanied by emplacement of multiphase granite intrusions (Ledru et al., 1994). The third phase (D_3) was responsible for the north-north-easterly striking right-lateral shear zones, well marked in Burkina Faso.

Petters (1991) considered that D_1 is generally penetrative and coaxial affecting only the Lower Birimian. During D_2 and D_3 the tectonic setting was one of transcurrent movement, in which D_2 (sinistral) and D_3 (dextral) transverse dislocations caused folding and also controlling the emplacement of granitoids. The Paleoproterozoic age of these tectonic events is demonstrated by the associated syntectonic magmatic activity, dated at 2.2-1.9 Ga (Leube et al., 1990; Liégeois et al., 1991; Boher et al., 1992). Metamorphism was mostly restricted to lower greenschist facies (Bossiere et al., 1996; Hirdes et al., 1996; Béziat et al., 2000), except adjacent to some plutons where higher grade contact metamorphic assemblages developed (Bourges et al., 1998; Debat et al., 2003).

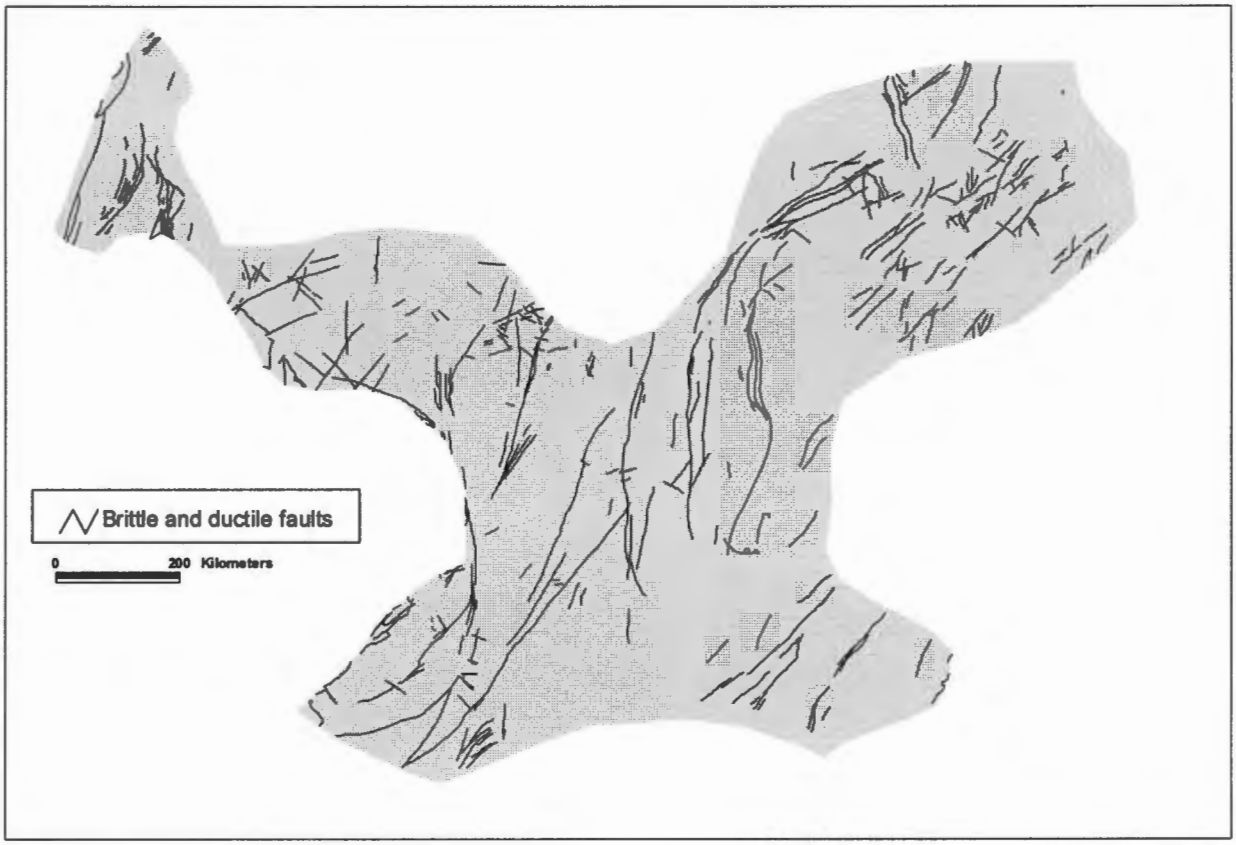

Figure 2.6 Distribution of brittle faults of the Paleoproterozoic Birimian Shield. Simplified after Milési et al., (1989); Frost-Killian, (2003).

Recent isotopic work by Hirdes et al. (1996) reveals that the Paleoproterozoic Birimian Shield in West Africa, which was seen previously interpreted as a single entity, contains two distinct generations of the Birimian terrains (Western and Eastern subprovinces) juxtaposed along the northeast-southwest trending transcurrent shear zone (possibly separated by a regional lineament known as the Ouango-Fetini belt (shear zone) in Ivory Coast, Hirdes and Davis, 2002) (Fig. 2.7).

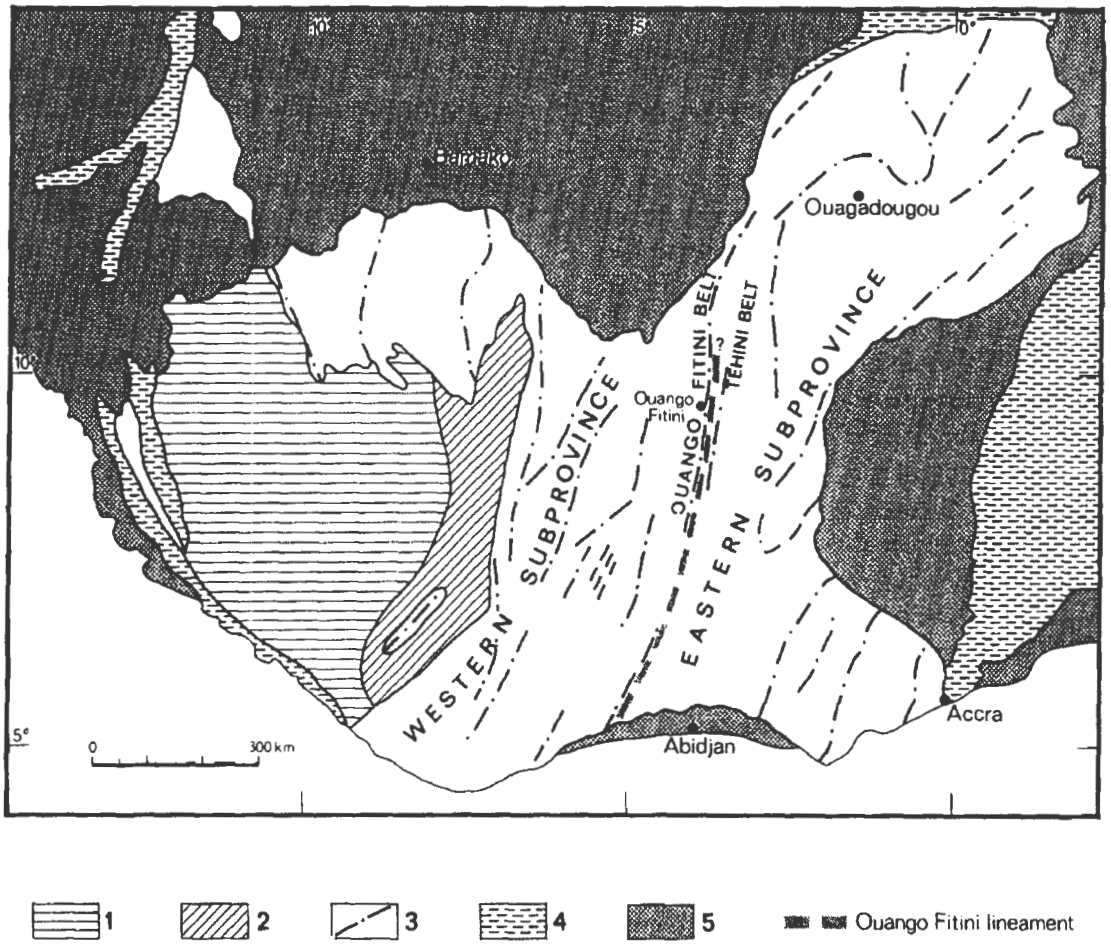

Fig. 2.7 Subdivision of the Paleoproterozoic Birmian domain into an (older) eastern subprovince and a (younger) western subprovince divided by the Ouango Fitini Belt (shear zone). Also shown is the distribution of other major rock units in the domain: **1** = Archean cratonic nucleus; **2** = Archean-Proterozoic transition zone; **3** = Paleoproterozoic supracrustal and intrusive rocks with position of volcanic belts; **4** = Pan-African province; **5** = Neoproterozoic/Phanerozoic sedimentary rocks (from Hirdes et al., 1996).

The geochronology data define a narrow age range difference of ~55 Ma between the eastern and western Birimian subprovinces that is compatible with the age range encountered in most Birimian supracrustal rocks and Eburnean intrusives elsewhere in Ivory Coast and the neighbouring countries Ghana and Mali (Hirdes et al., 1996). The ages that define these differences are single mineral $^{207}Pb/^{206}Pb$ and U-Pb ages on zircon, monanzite, and sphene from magmatic and metamorphic rocks, as well as Rb-Sr whole-rock ages (Kouamelan et al., 1997). The eastern subprovince, located to the east of the central shear zone, covers Ghana, eastern Ivory Coast and Burkina Faso, comprising predominantly ~2185-2150 Ma volcanism and coeval granitoid plutonism.

In contrast, the western subprovince, (central Ivory Coast, western Mali and Guinea) is characterised by younger, 2105 Ma terrains, but the detailed age relationships within these two subprovinces are still controversial.

2.2.3 Mineralization

The Birimian Shield is extensively mineralized with gold deposits, but a greater variety of mineralization occurs in the Birimian greenstone belts (Fig. 2.8) as is characterized in particular by Au, Fe, Zn-Ag, Cu ± Mo ± Au deposits. Numerous studies (Milési et al, 1992; Herrington, 1997) have shown that mineralization seems to be preferentially concentrated in an eastern belt along an arc following the main northeasterly structural trend in Ghana, Ivory Coast and Burkina Faso (e.g. the Ashanti gold fields, Fig. 2.8), and in a northwesterly belt in Mali parallel to the main structural N-S trend of transcurrent shear zone. Milési et al., (1992) consider the lithological, structural and metamorphic controls of the economic gold and base metal mineralization, and recognize three main tectonic contexts:

(1) Pre-orogenic: Pre D_1 mineralization related to early extension zones. Here, stratiform Fe, Cu, Au, and Zn-Ag mineralization took place during the deposition of Lower Birimian and is found preferentially in its upper parts, in settings that were characterized by sedimentary and paleotectonic instability, and associated hydrothermal and tholeiitic volcanic activity. In their model, all the deposits whose main features are mentioned were formed prior to the first tectono-metamorphic phase.

(2) Syn-orogenic: Post-D_1 to syn-D_2 mineralization associated with subsequent deformation. No gold deposits appear to be directly related to the first orogenic phase (D_1), but various types of auriferous mineralization took place in localized extensional or transtensional environments following the D_1 phase.

(3) Late orogenic: A large number of discordant, mesothermal gold deposits were emplaced following peak metamorphism of the orogeny, after the most intense stage of compressive deformation across the shield, which gave way to brittle transcurrent deformation towards the end of the D_2 and D_3 tectono-metamorphic phases. Milési et al. (1992) also distinguish different types of gold deposits in West Africa, including the Ashanti gold province in Ghana, one of the world's greatest gold producers. The Ashanti gold deposits were formed after the Birimian host rocks were deposited, with mineralization overlapping with the intrusion of the granites, regional metamorphism and deformation (Marcoux and Milési, 1993; Oberthür et al., 1998).

In summary, ore formation occurred predominantly during three main episodes of mineralization, and possibly partly in continuum, that show a paragenetic evolution from disseminated auriferous arsenopyrite mineralization, which is particularly well-developed in Ghana (Ashanti-type), to a gold-bearing mesothermal quartz lode mineralization with Cu-Pb-Zn-Ag-Bi which formed ~2.0 Ga (Mumm et al., 1997; Oberthür et al., 1998). Milési et al. (1992) have shown that both episodes of mineralization commonly appear to be restricted to the Lower Birimian unit and along structural contact between the Lower and the Upper Birimian units. The metallogenic history of this three-phase evolution coincides with the Eburnean tectono-thermal events. Therefore, the major pulse of **juvenile** crustal growth ~2.1 Ga in West African Shield was accompanied by significant metallogenic enrichment of mineral deposits apparently structurally controlled and closely associated with major shear zones. Thus, new crust and mineralization were clearly linked to Paleoproterozoic mantle differentiation processes.

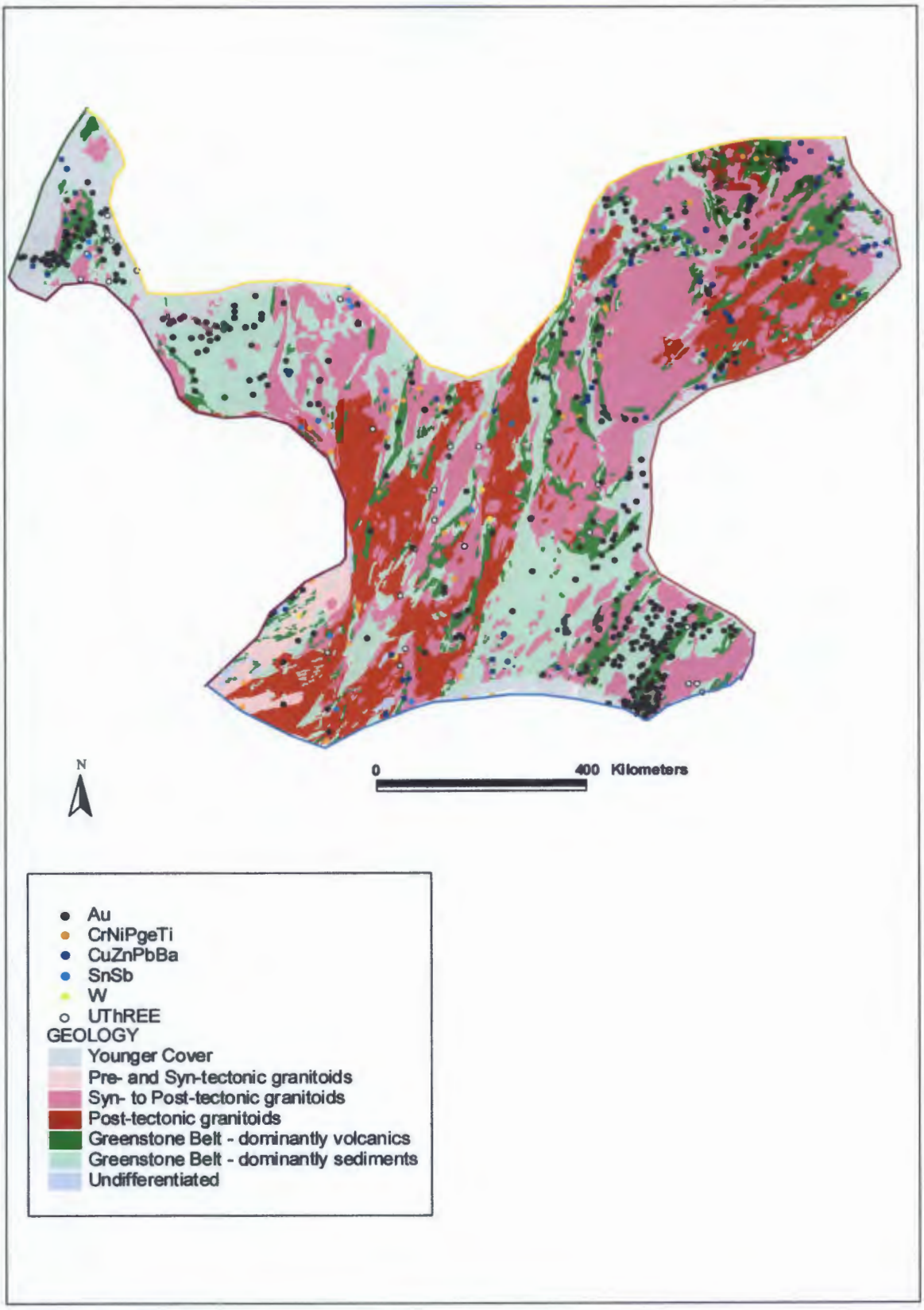

Figure 2.8 Distribution of mineral deposits and occurrences of the Paleoproterozoic Birimian Shield.

2.3 The Neoproterozoic Arabian-Nubian Shield

The Arabian-Nubian Shield (ANS) is a region of ~2.82 x 10^6km^2 composed of Neoproterozoic basement exposed on either side of the Red Sea in W. Arabia and NE Africa, and covers countries such as Egypt, Eritrea, Ethiopia, Saudi Arabia, Somalia, Sudan and Yemen (Fig 2.9). The ANS is bounded on its sides by tectonic boundaries and major unconformities and is the northern extension of East African Orogen (EAO) that stretches from Egypt to Mozambique belt in the south of East Africa (800-650 Ma; Stern, 1994; Shackleton, 1996; Berhe, 1997; Grenne et al., 2003). The Arabian-Nubian Shield and the Mozambique belt form one of the largest orogenic zones in Africa (Berhe, 1997). The EAO represents the closure of the Mozambique Ocean between India and Eastern Africa in Late Neoproterozoic times during the formation of Gondwana (Meert, 2003; de Wit, 2003; Kusky et al., 2003; Ghosh et al., 2004; Kusky, 2004; Stern et al., 2004; Tadesse and Allen, 2004).

2.3.1 Geological Setting

The ANS comprises a collage of juvenile arc terranes and associated ophiolite fragments formed in the Neoproterozoic (Stern, 1994; Johnson and Woldehaimanot, 2003; de Wit, 2003; Meert, 2003 and references therein). This juvenile Neoproterozoic crust of the ANS encompasses a series of volcano-sedimentary terranes of low metamorphic grade located within a number of NE–SW to N–S trending belts (ophiolites and metasediments) and intercalated with moderate-to-high-grade terranes (partly reworked pre-Pan-African crust) (Worku and Schandelmeire, 1996; Grenne et al., 2003). All of these terranes are intruded by voluminous granitoid batholiths, and plutons suites that range from ultramafic to felsic, and record a range of ages from 870–540 Ma (Grenne et al., 2003; Eyal et al., 2004; Johnson and Woldehaimanot, 2003).

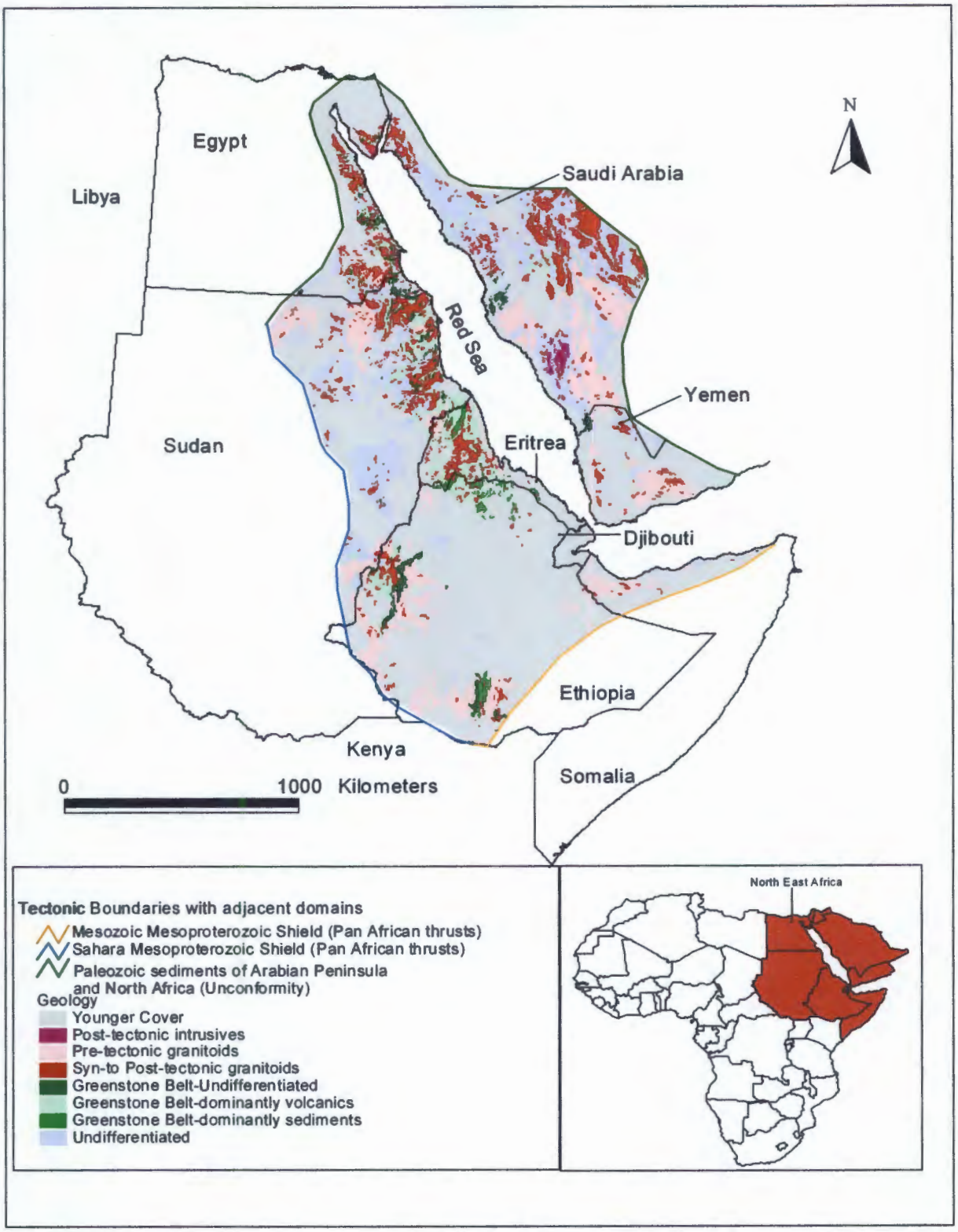

Figure 2.9 Simplified Geology of the Neoproterozoic Arabian-Nubian Shield, bounded by tectonic boundaries and unconformities. Simplified after Frost-Killian (2003). Insert shows the countries of northeast Africa in which part of the Arabian-Nubian Shield is exposed.

A number of the low-grade belts that contain narrow elongate linear zones composed of dismembered mafic–ultramafic complexes and associated marine sediments have been identified as ophiolites sequences representing collisional suture zones (Berhe, 1990; Zimmer et al, 1995; Abdelsalam and Stern, 1996; Stern et al., 2004; Dilek and Ahmed, 2003; Tadesse and Allen, 2005). These ophiolitic belts and associated volcano-sedimentary sequences are considered to be analogues to greenstone belts (Berhe, 1997). Thus, the outcrop patterns of the ANS ophiolites and associated granitoids have been interpreted to comprise Archean-like granite-greenstone terrains. Since the rocks mostly have overlapping ages with their mantle extraction ages, the ANS is a typical **juvenile** region of rapid crustal growth between ~900-500 Ma (Stern, 2002; Stern et al., 2004; Tadesse and Allen, 2005).

2.3.2 Tectonic Setting

Various models have been proposed to explain the crustal evolution of the ANS. Studies by several workers document processes of lateral crustal growth in ANS, involving island arcs, ocean crust and oceanic plateaus, and subsequent ocean closure, amalgamation of the arc complexes and accretion to ancient continental lithospheric basement of the central Sahara (Berhe, 1990; Stern, 1994; Windley et al., 1996, 2003; Stern and Abdelsalam, 1998; Blasband et al., 2000; Eyal, et al., 2004; Genna et al., 2002; Grenne et al., 2003; Meert, 2003). Based on a recent compilation of age and geochemical data, Stern and Abdelsalam, (1998) concluded that most of the juvenile ANS crust formed in intra-oceanic convergent margin settings. Amalgamation of these terranes may have begun as early as 800 Ma and continued to 620 Ma. Blasband et al., (2000) and Eyal et al., (2004) provide a more recent compilation of geochronology and tectonic settings of the ANS, and show that island arcs and oceanic crust formed during the interval of (~950-850 Ma and 850-650 Ma respectively), and were accreted by about 650-600 Ma.

Late strike-slip movements related to a change from compressional to extensional tectonism occurred about 600 Ma, followed until 530 Ma by oblique continent-continent collision between this collage of continental blocks (Grenne et al., 2003).

Grenne et al., (2003) also emphasize that suture zones were formed in response to the terminal collision between East and West Gondwana, with the Arabian-Nubian Shield being squeezed between them (e.g. Berhe, 1990; Stern, 1994; Abdelsalam, 1994; Abdelsalam and Stern, 1996). The sutures were divided into arc-arc sutures (separating arc terrains) that formed between ~800 and 700 Ma, and arc-continent sutures (separating the Arabian-Nubian Shield from large East and West Gondwana fragments) which formed between ~700 and 650 Ma (Kröner et al., 1991; Abdelsalam and Stern, 1996).

Stein, (2003) presents an alternate model of the evolution of the ANS based primarily on geochemical studies of volcanic and plutonic rocks to a major upwelling event in the mantle. He suggests that the formation of the continental crust and its lithospheric mantle is related to the rise of a large Pan-African plume around 900Ma. The plume was responsible for the production of oceanic plateaus and an enriched 'plume mantle' which was overprinted later by the subduction mechanism to produce calc-alkaline magmas and lithospheric mantle material. The idea that juvenile crustal growth may in large part be accomplished by additions from mantle plumes challenges the dominant arc accretion model for continental growth in the Arabian-Nubian Shield, but either way, the crust of the ANS is dominantly juvenile, derived from the mantle at the time of its formation.

Figure 2.10 represents structural trends (brittle faults and shear zones) of the Neoproterozoic Arabian-Nubian Shield. The structural trends in the ANS are related to the terrane amalgamation and suture zones. The displacements along these structures range from large amounts of thrusting to large amounts of strike-slip displacement coupled to the thrusting associated with north-trending shortening and NW-trending transcurrent

displacements (Abdelsalam and Stern, 1996). Yibas (2000), Yihunie and Tesfaye (2002), and Yihunie (2002) have identified five deformational phases (D_0 to D_5) which are genetically associated with the repeated opening and closure of the small ocean (marginal) basins and accompanied granitic magmatism and transpressive shortening between about 900 and 500 Ma. Whereas D_0 and D_1 structures are genetically associated with the closure of the oceanic basins between ~880 and 770-720 Ma, respectively, the D_2-D_4 structures are associated with the subduction of the marginal basin and continued sinistral transpressive collision that occurred between ~670 and 550 Ma. The D_3 structures represent mainly N-S trending shortening zones, whilst D_4 structures are mainly NW-SE trending dextral strike-slip faults. D_5 involves dextral faults that were formed in response to late deformation that gave rise to the NE-SW and ENE-WSW trending faults.

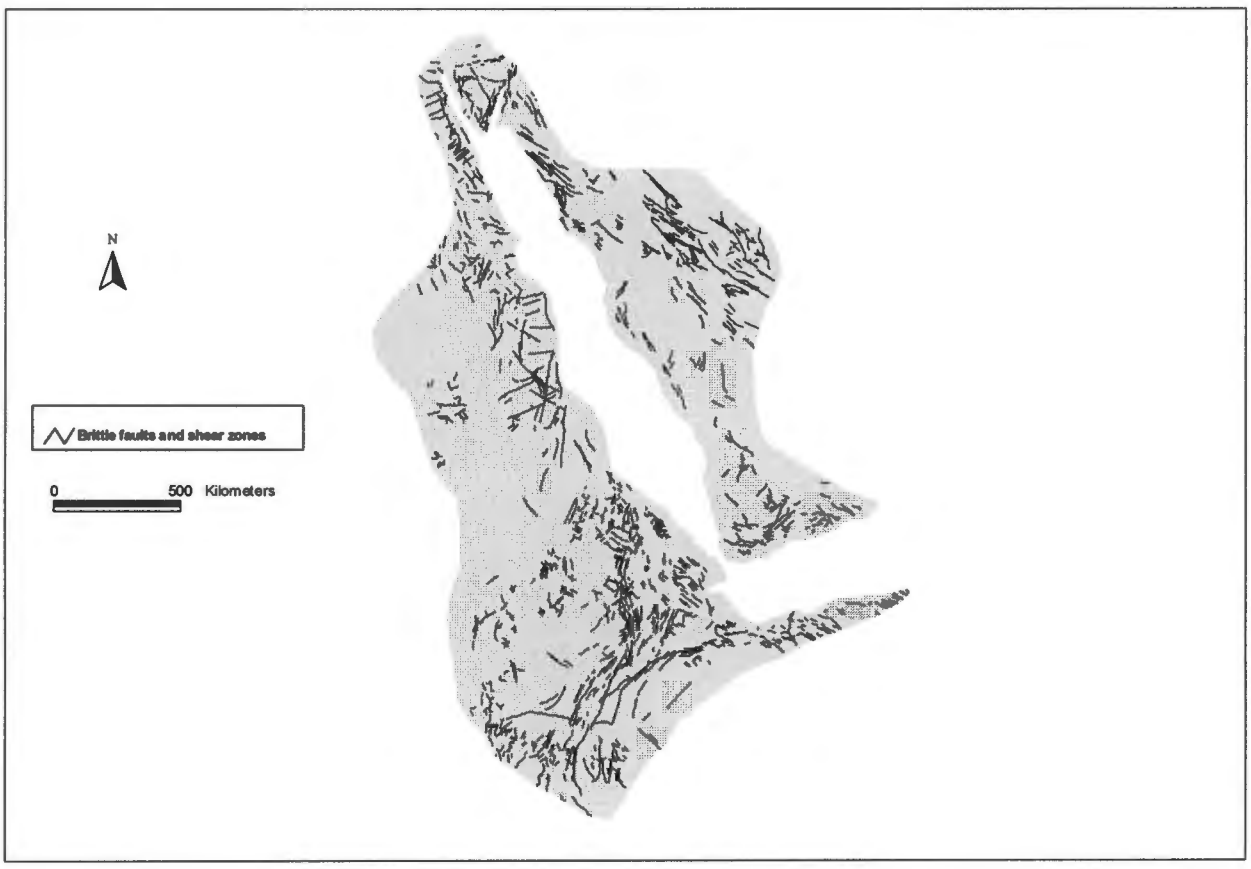

Figure 2.10 Schematic representations of tectonic structures (major faults and shear zones, undifferentiated) of the Neoproterozoic Arabian-Nubian Shield. Simplified from Frost-Killian (2003).

2.3.3 Mineralization

Information on mineralization in the Arabian-Nubian Shield is generally scarce. Although many small occurrences have been discovered over the centuries, only small scale mining activities have developed, usually associated with deposits in major shear zones. Metallogeny within the ANS is also diverse and includes Cu-Ni and Cr mineralization (see Fig. 2.11) associated with the Neoproterozoic ophiolites. Arc-type volcanogenic base and precious metal deposits are associated with formely active plate margins, whilst shear zones hosted mesothermal gold mineralization is related to accretionery and strike-slip tectonics. Sn-W-REE mineralization is associated with post-cratonization alkali granite magmatism (Agar, 1992).

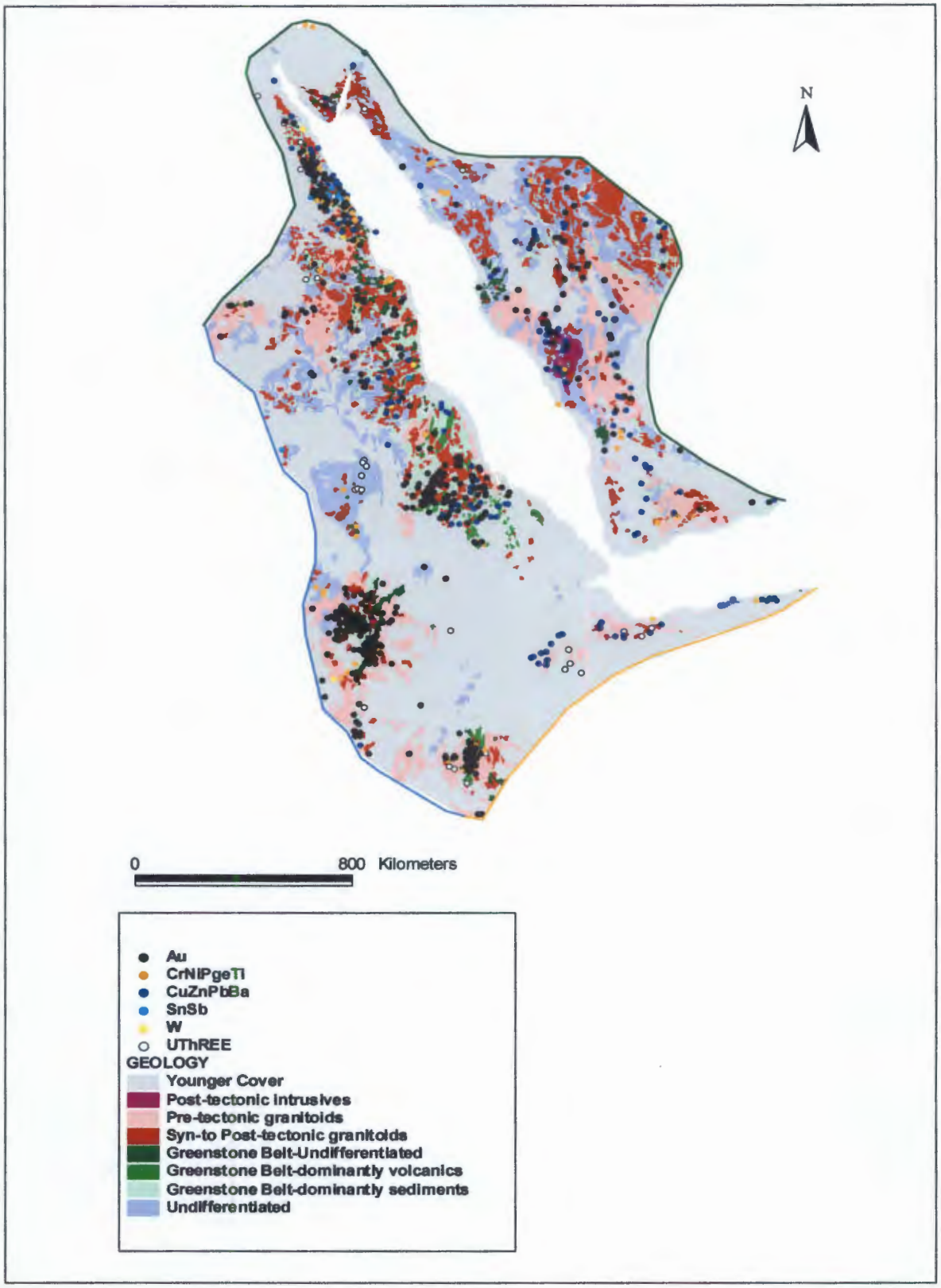

Figure 2.11 Distribution of mineral deposits and occurrences of the Paleoproterozoic Arabian-Nubian Shield. The ANS is 50% younger cover and so caution should be given to the mineral inventory.

2.4 Summary of the mineral deposit of the three regions of African crust of different age

This chapter concludes with a discussion concerning the group of elements selected to fulfill the research aims of this project. Table 2.4 lists these elements together with its geochemical classification into siderophile, chalcophile or lithophile groups. Wilsher (1995), summarized some of these general behavioural characteristics of these elements in relation to both the formation of the Earth, and other further differentiation processes. The elements are chosen to represent a wide range of geochemical behaviour and, in particular, concentration within mineral deposits within continental crust. Much of the information for the element selected has been taken from Wilsher (1995) and Herrington et al., (1997).

Gold and PGE are mostly grouped together because they both behave either as siderophile or chalcophile elements, and are commonly enriched in Archean and Paleoproterozoic rocks. Gold is the most important economic mineral in Archean granite-greenstone terrains (as epithermal/mesothermal deposits, Campbell and Pitfield, 1994; Groves et al., 1995; Herrington et al., 1997) throughout the world. The mineralization is described mostly as epigenetic and the distribution pattern is commonly structurally-controlled and related to regional fractures or shear zones. Herrington et al. (1997), Partington and Williams (2000) suggest that the timing of mineralization in all Archean to Proterozoic gold deposits is late in the tectonic or orogenic events, usually after the main phase of deformation, regional metamorphism and granite intrusion. Platinum Group Element (PGE) mineralization is more related to mafic intrusions (e.g large magmatic intrusions, for example, the Zimbabwe Great Dyke, 2.5 Ga), and ultramafic rocks of ophiolites (e.g. Yubdo dunites in Ethiopia, de Wit and Berg, 1981). The mineralization in the Neoproterozoic Arabian-Nubian Shield also can be considered similar to the Archean granite-greenstone terrain of Zimbabwe.

Symbol	Element/Group	Geochemical Group
Au	Gold	Siderophile
Pt (PGE)	Platinum Group	
Ni	Nickel	Siderophile
Cr	Chromium	Lithophile/Chalcophile
Ti	Titanium	
Cu	Copper	Chalcophile
Pb	Lead	Chalcophile/Siderophile
Zn	Zinc	Chalcophile
Ba	Barium	Lithophile/Chalcophile
Sn	Tin	Siderophile/Chalcophile
Sb	Antimony	Chalcophile
W	Tungsten	Lithophile/Siderophile
U	Uranium	
TH	Thorium	Lithophile
REE	Rare Earth Elements	

Table 2.3 Range of elements used in this study, grouped into 3 geochemical types. Siderophile elements are those which tend to concentrate in metallic iron (native metal state). Chalcophile elements have an affinity for the sulphide phase, while lithophile elements preferentially concentrate in granitoid rocks (modified after Wilsher 1995, Thiart and de Wit, 2006).

Nickel can be either siderophilic or chalcophilic, while Chromium usually behaves as a lithophile in the earth's crust but as a chalcophilic element in the mantle. Nickel and Chromium are both enriched with magnesium in ultramafic rocks. Nickel mineralization often occurs in massive and disseminated sulphides that form when sulphur combines with nickel and other elements (e.g. Cu, Co, PGE) in magmas of mafic or ultramafic composition. Nickel mineralization is essentially restricted to Archean and Paleoproterozoic greenstones, but large rich deposits are also known in the Neoproterozoic East African Orogen exposed in Madagascar (e.g. Rambeloson, 1997).

Copper, zinc, lead and barium are collectively make up important base metals in remobilized sulphide/sulphate minerals. They are highly concentrated in near-surface massive sulphide deposits, often in magmatic arcs, or as as MVT deposits (Mississippi Valley-Type, Sawkins, 1990; Hutchinson, 1992).

Tin, antimony and tungsten are lithophile elements which separate into late phase residual minerals and pegmatites in granitoid terrains as do uranium, thorium, and the rare earth elements which are, grouped together as incompatible lithophilic elements. Although Tungsten also has siderophile characteristics, in this project it is treated as lithophile.

Chapter 3

Database: acquisition and structure

One of the objective of this project is to upgrade the Gondwana-Geoscientific Indexing Database (GO-GEOID), housed at AEON. GO-GEOID combines the geology of the major continental fragments of Gondwana (de Wit et al., 1988), with a mineral database that was constructed subsequently, using open access literature sources (Wilsher et al., 1993; Wilsher, 1995). GO-GEOID is a relational database that contains three layers: the geology of Gondwana, including chronostratigraphy and lithostratigraphy; Gondwana tectonics, in the term of major faults, tectonic lineaments, as well as structural trends of foliation; and the mineral resources of Gondwana. In 1998-1999, in collaboration with the BRGM, the Go-GEOID was updated (Thiart and de Wit, 2000) increasing the database to over 17 000 mineral deposits, of which 8839 are in Africa. For this project, various datasets from other sources were also embedded into GO-GEOID.

3.1 Spatial Data Input

In this study, the same three thematic (evidential) themes/layers are considered in each region: mineral deposits, geology, and tectonic elements (Table 3.1). These themes were assembled into maps in a digital format to be used as evidence in order to create a mineral potential map. The maps of all three African segments were extracted from different sources (Table 3.1), edited (reclassified) and merged into data layers using Database Access, ESRI (Environmental Systems Research Institute) - ArcView GIS 3.3 and ArcGIS 9.0 (ArcGIS-toolbox-spatial adjustment) (www.esri.com).

Data type	Description
GEOLOGY	Reclassified geological maps of: Zimbabwe craton (*Chronostratigraphy interpretations for southern Africa 1: 1 000 000,* Jelsma and Thiart, 2002); Birimian Shield (*West African Gold Deposits: in their lower Proterozoic lithostructural setting, 1: 2 000 000*, Milési et al., 1989) Arabian-Nubian Shield (*International Metallogenic Map of Africa, at a scale of 1:5 000 000,* Frost-Killian, 2003)
FAULTS	All faults and ductile shears evidential themes were compiled from: Zimbabwe craton (Jelsma, 2004-2005, personal communication); Birimian Shield (*West African Gold Deposits: in their lower Proterozoic lithostructural setting, 1: 2 000 000*, Milési et al., 1989) Arabian-Nubian Shield (*International Metallogenic Map of Africa, at a scale of 1:5 000 000,* Frost-Killian, 2003)
MINERAL DEPOSITS	All known mineral deposits compiled in this study were extracted and edited from three different source (i.e. Gondwana-Geoscientific Indexing Database (GO-GEOID, Wilsher, 1995); Council for Geoscience (CGS, Frost-Killian, 2003); and from Journal of African Earth Science (JAES, Tadesse et al., 2003).

Table 3.1 Summary of digital data sets used in this study.

3.1.1 Mineral Theme

The mineral deposits database is based on 15 chemical elements, divided into six groups according to their geochemical affinities (e.g lithophile, chalcophile, siderophile), as well as their relative abundance in the database. The elements were selected to represent the widest possible range of geochemical behaviour for elements within the earth and, in particular, for their concentration within mineral deposits throughout the continental crust. The six element groups, and the total number of deposits in which these groups occur on each of the areas studied (Fig. 3.1) are summarized in Table 3.2.

	Au	CrNiPgeTi	CuZnPbBa	SnSb	W	UThRee	Total Shield
Arabian-Nubian							
GO-GEOID	31	10	23	5	1	30	100
CGS	225	48	126	17	9	15	440
JAES	260	32	33	0	1	2	328
Total used	516	90	182	22	11	47	868
Birimian							
GO-GEOID	205	23	74	16	5	20	343
CGS	236	15	18	5	0	12	286
Total used	441	38	92	21	5	32	629
Zimbabwe							
GO-GEOID	624	105	94	66	275	3	1167
CGS	1	3	3	0	0	0	7
Total used	625	108	97	66	275	3	1174
Total overall	1582	236	371	109	291	82	2671

Table 3.2 Total number of mineral deposits of three region of African crust, using the existing GO-GEOID: Gondwana-Geoscientific Indexing Database (Wilsher, 1995), newly added information from CGS: Council for Geoscience (Frost-Killian, 2003) and information from JAES: Journal of African Earth Science (Tadesse et al., 2003).

The total number of deposits for the three African regions were combined and merged from three different sources (Frost-Killian, 2003; Tadesse et al., 2003; Wilsher, 1995) into one platform. In total there are just over 2600 deposits across the three selected regions of which 1610 were extracted from GO-GEOID and 1061 new deposits were added. The mineral deposits in these three regions are stored in a coded (geographically referenced) form that includes: shape, site-name, country, commodity, host rock-type, status, size, and age of the deposits. The distributions of mineral deposits of each region are shown in Figure 3.1a-c.

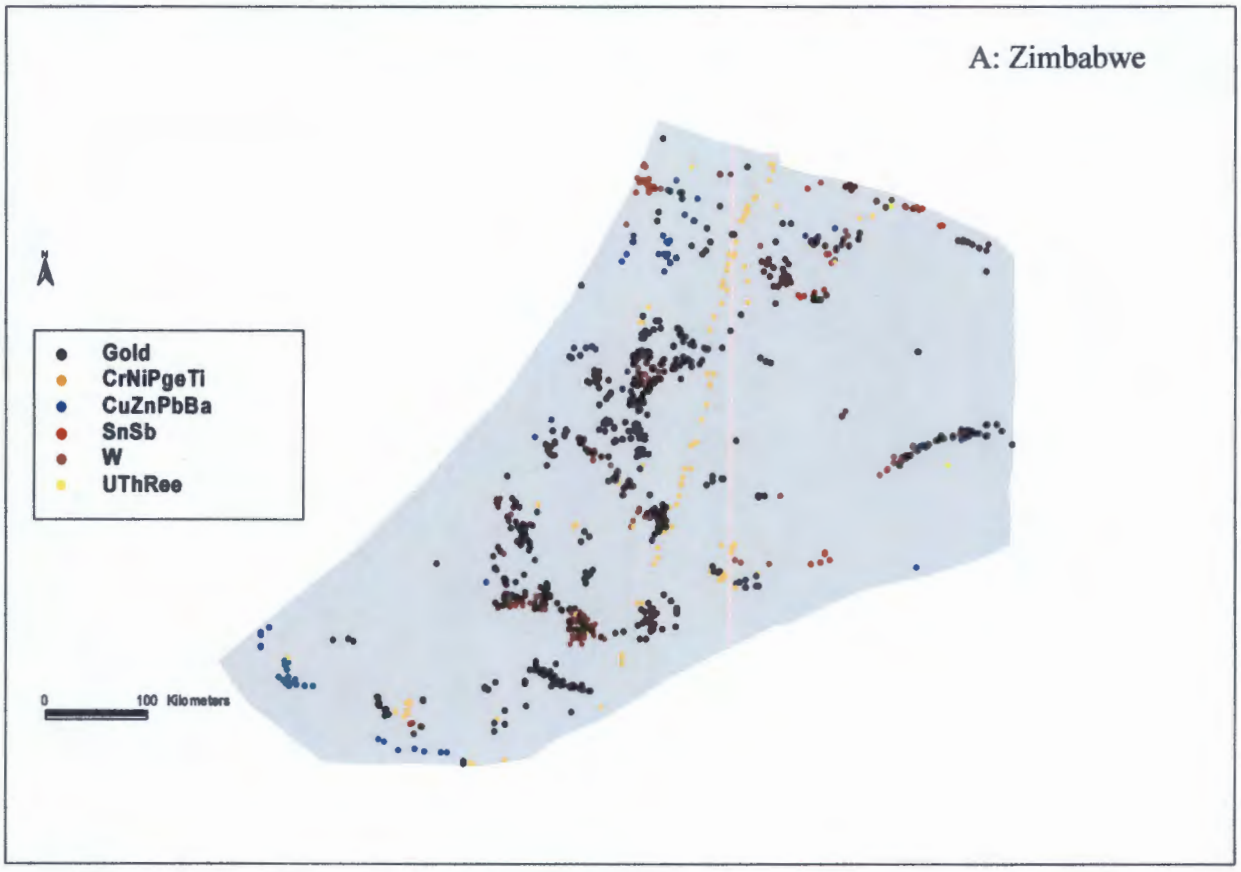

Figure 3.1a: Distribution of mineral deposits, based on the most dominant chemical element within each deposit, of the Archean Zimbabwe Craton.

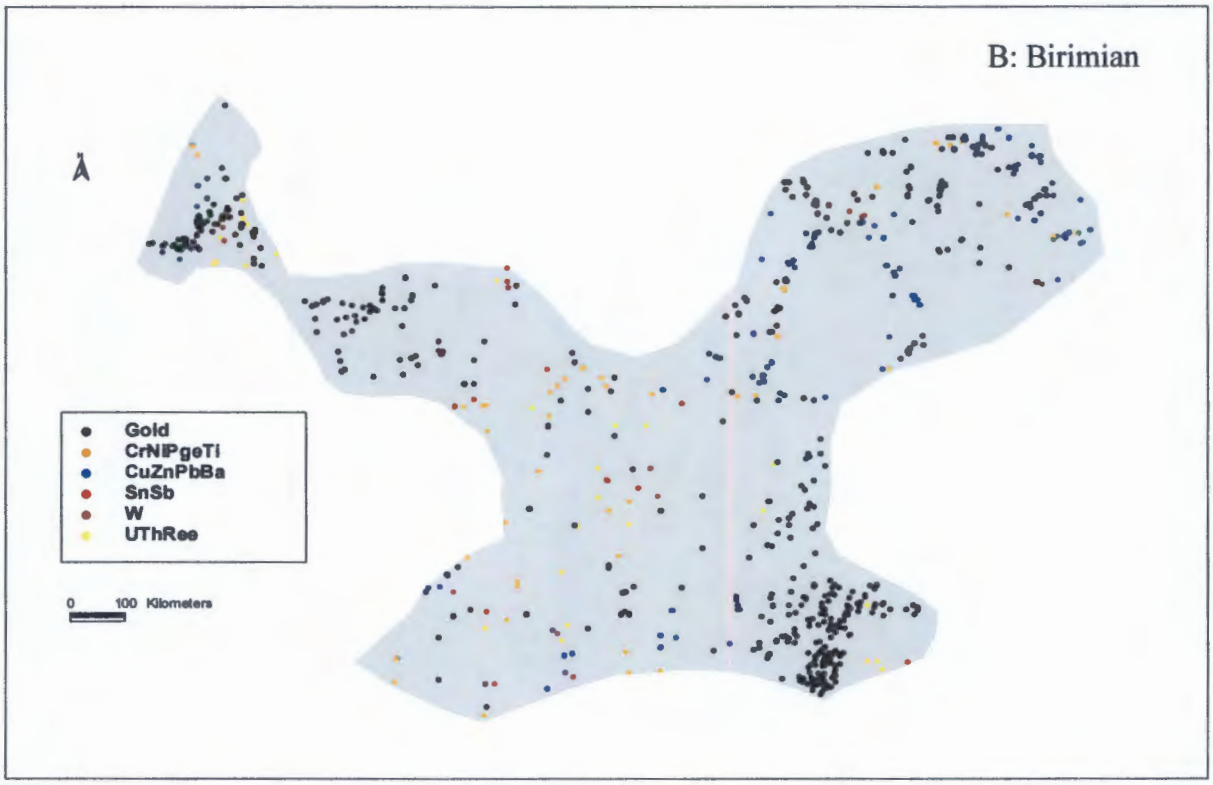

Figure 3.1b: Distribution of mineral deposits, based on the most dominant chemical element within each deposit, of the Paleoproterozoic Birimian Shield.

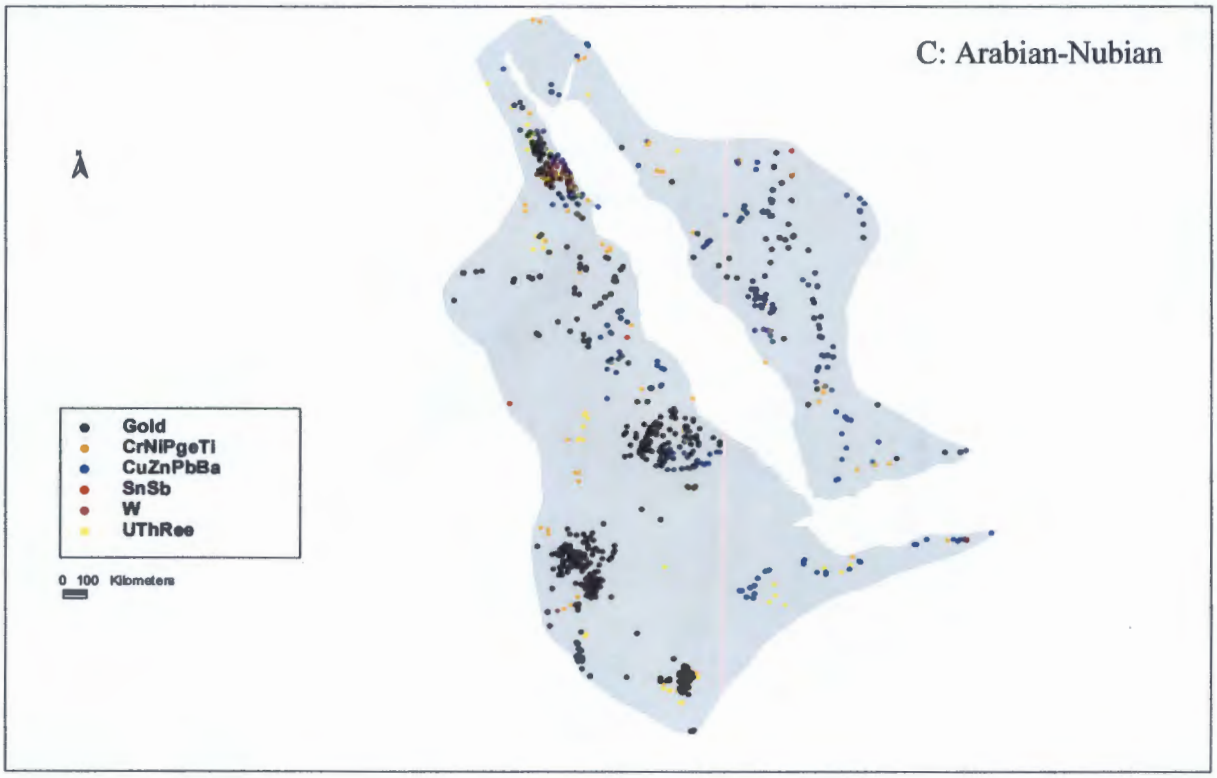

Figure 3.1c: Distribution of mineral deposits, based on the most dominant chemical element within each deposit, of the Neoproterozoic Arabian-Nubian Shield

3.1.2 Geology Theme

Geological data inputs of three African regions were compiled from geologic maps at various scales (Table 3.1): the Birimian Shield (Milési et al., 1989), the Zimbabwe Craton (Jelsma and Thiart, 2002) and the Arabian-Nubian Shield (Frost-Killian, 2003). All maps were simplified and reclassified for the purpose of this study. The geology and the environment of mineral deposit formation are important criteria in attempting to understand the genesis of mineral deposits, since they provide evidence for the source material and inferred conditions for the concentration of elements which form the mineral deposits. The geology maps were edited, adding new information to the existing data and reclassified to simplify their information into rock-types common to each region (Tables 3.3a-c). The simplified geology maps (Fig. 3.2a-c) represent a synthesis of a reclassification of rock-types. The percentage area of each rock-type on each region is also given.

The geological maps, where applicable, were converted and readjusted to geographic coordinates, e.g. original map of the Birimian Shield (Milési et al., 1989) uses UTM (Universal Transverse Mercator projection) coordinates. Projection from one surface to another resulted in slight distortion that was readjusted to the best possible fit. Distortions were adjusted using the Spatial Adjustment tool of Arc-GIS, so that respective contacts from different maps join seamlessly.

Rocktypes	Period - Age	Reclassification of rocktypes
Lamagondi, Karoo and younger unconsolidated sediments	Paleoproterozoic, Paleozoic Cenozoic	Younger Cover
Ultramafic and mafic plutonics	Archean	Great dyke
Ultramafic - mafic intrusives	Archean	Post-tectonic intrusives
Gneisses	Archean	Pre- and Syn-tectonic granitoids
Granitoids	Archean	Post-tectonic granitoids
Metavolcanics	Archean	Greenstone Belt – dominantly volcanics
Metasediments	Archean	Greenstone Belt – dominantly sediments
Granitoids and granitic gneisses	Archean basement	Undifferentiated

Table 3.3a. Summary of simplified geology of the Archean Zimbabwe Craton.

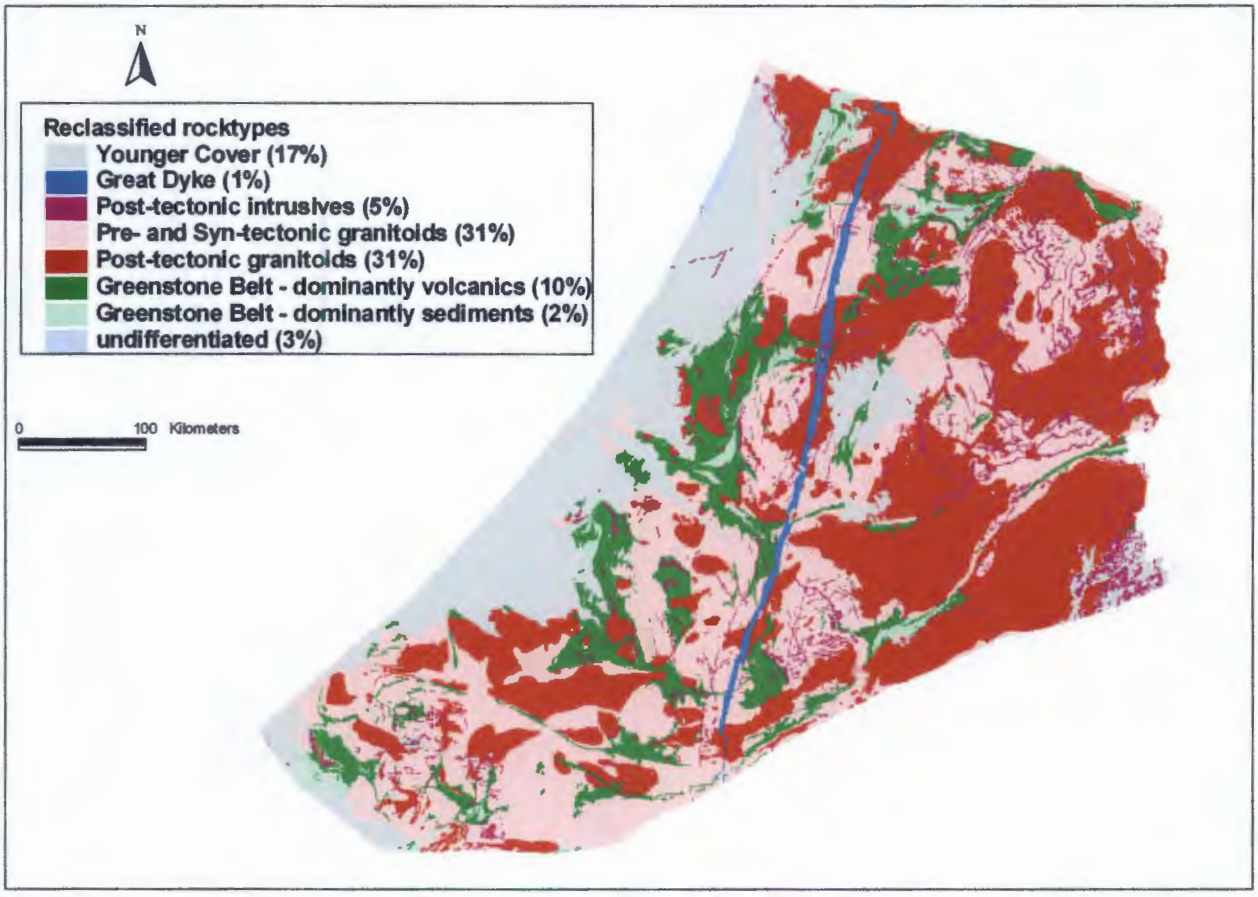

Figure 3.2a. Simplified geology of the Archean Zimbabwe Craton.

Rocktypes	Period - Age	Reclassification of rocktypes
Sediments	Mesozoic – Cenozoic	Younger Cover
Gneisses	Paleoproterozoic	Pre- and Syn-tectonic ganitoids
Granitic gneisses	Paleoproterozoic	Syn- to Post-tectonic granitoids
Granites, granodiorite and other granitoids	Paleoproterozoic	Post-tectonic granitoids
Volcanics	Paleoproterozoic	Greenstone Belt – dominantly volcanics
Volcanoclastic rocks	Paleoproterozoic Neoproterozoic	Greenstone Belt – dominantly sediments
Basement	Paleoproterozoic	Undifferentiated

Table 3.3b. Summary of simplified geology of the Birimian Shield.

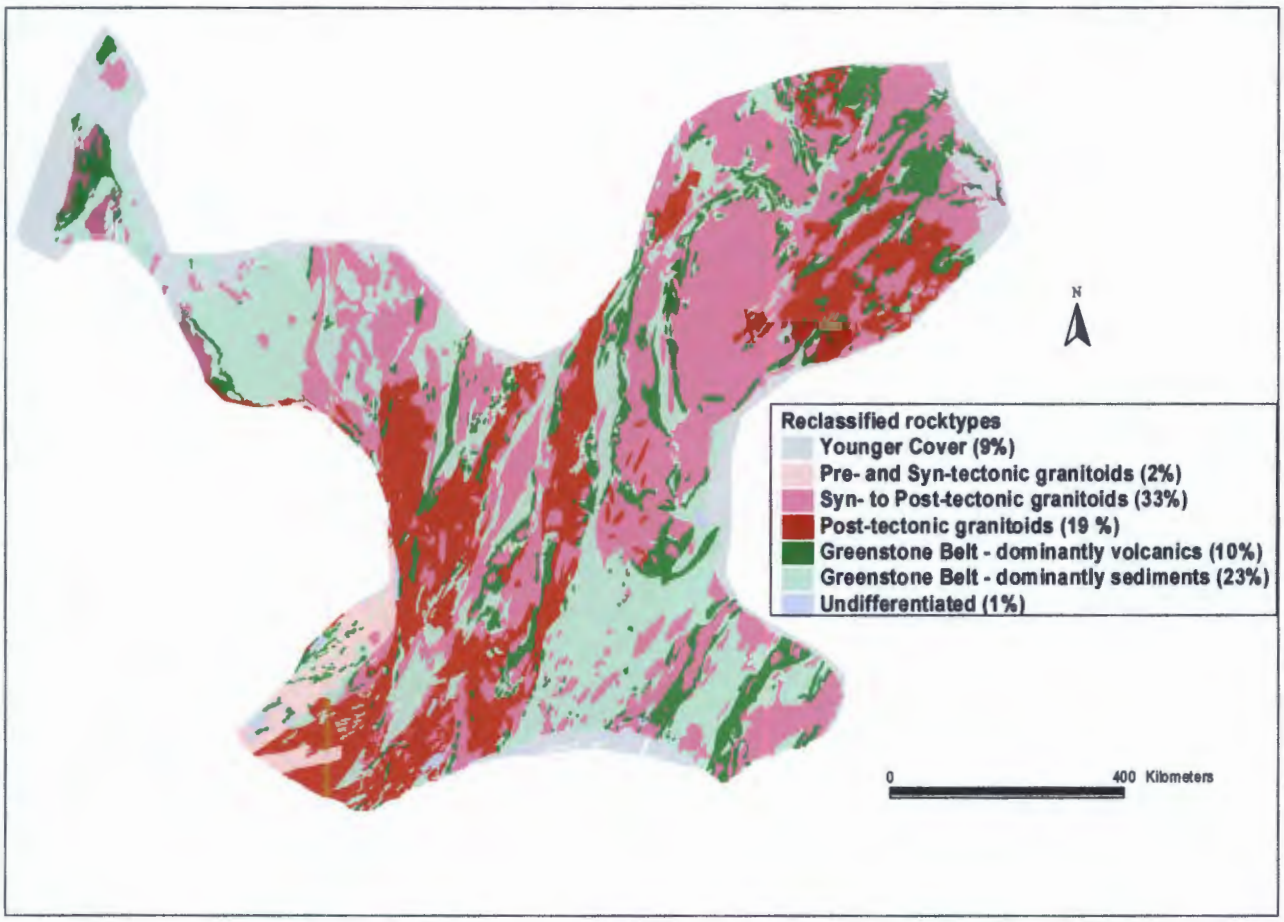

Figure 3.2b. Simplified geology of the Paleoproterozoic Birimian Shield.

Rocktypes	Period -Age	Reclassification of rocktypes
Sediments and Volcanics	Paleozoic – Cenozoic	Younger Cover
Mafic intrusives	Neoproterozoic - Cambrian	Post-tectonic intrusives
Granite-gneiss basement complex mostly covered by sand	Neoproterozoic, Mesoproterozoic, Cambrian	Pre-tectonic granitoids and paragneisses
Granites and granitic gneisses	Neoproterozoic - Cambrian	Syn- to Post-tectonic granitoids
Greenstone Belt	Neoproterozoic - Cambrian	Greenstone Belt - undifferentiated
Mafic – ultramafic metavolcanics with basic compositions	Neoproterozoic - Cambrian	Greenstone Belt - dominantly volcanics
Mafic metasediments	Neoproterozoic - Cambrian	Greenstone Belt - dominantly sediments
Para- and ortho-gneisses	Neo- to Meso-proterozoic	Undifferentiated

Table 3.3c. Summary of simplified geology of the Neoproterozoic Arabian-Nubian Shield.

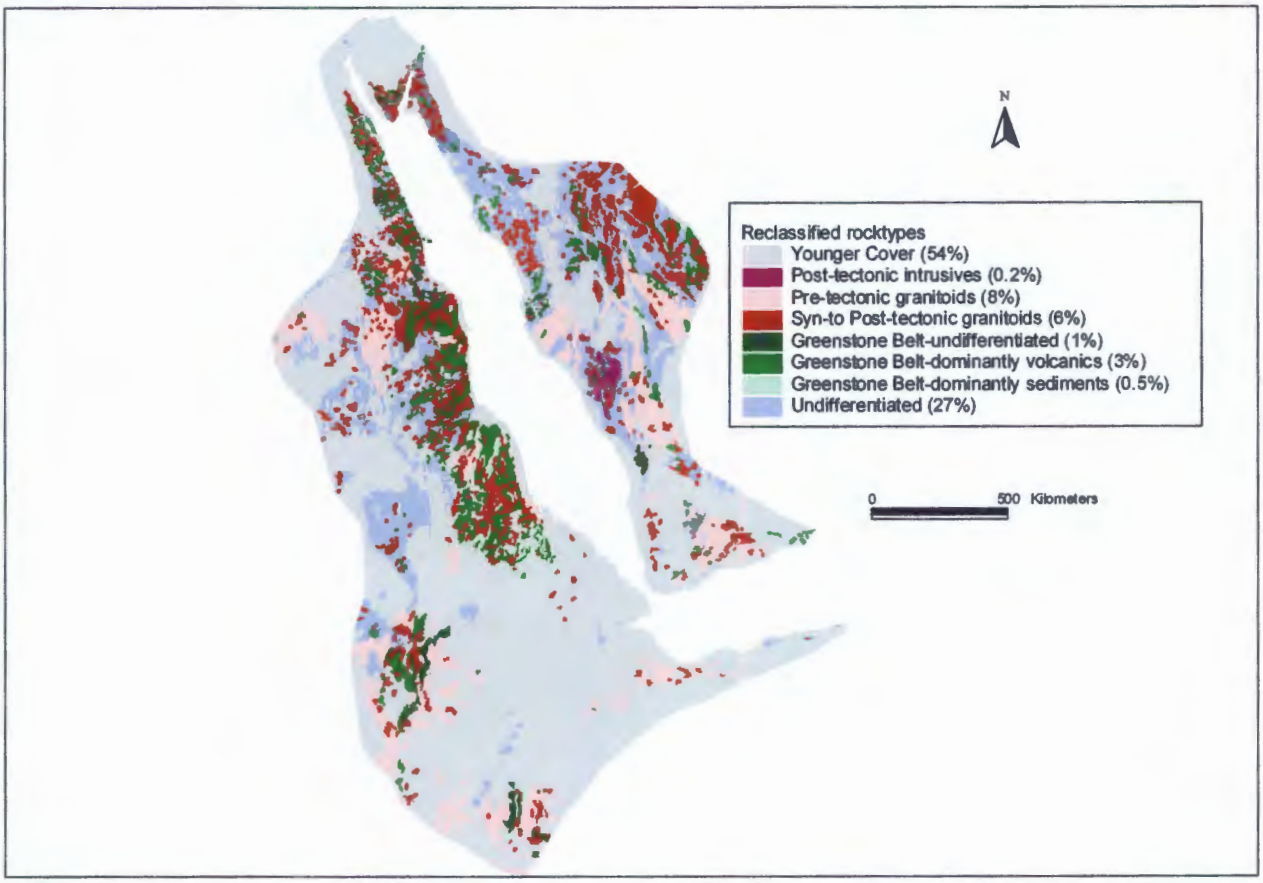

Figure 3.2c. Simplified geology of the Neoproterozoic Arabian-Nubian Shield.

3.1.3 Faults Theme

Structural maps showing major faults and shear zones of the three shields of varying scales, and hence varying accuracies, were compiled from different sources (Table 3.1). All different structural datasets compiled for the three selected areas were selected for spatial data analyses. The structural datasets (brittle faults and ductile shears) are differentiated and combined for each region for the purpose of this study (Figs. 3.3-3.5). It is justified to combine the brittle faults and ductile shears into one tectonic map, since they may merge into shear zones at greater depths (Groves et al., 1995). For the Zimbabwe craton a set of ductile shear zones and brittle faults are differentiated (brittle faults and ductile shears), whereas, the faults and shear zones of the Birimian and Arabian-Nubian Shields are not differentiated (Figs. 3.3-3.5), because such data is not available (lack of structural information and/or poorly exposure). However, from the literature, it is clear that many of the faults are in fact ductile shears (Milési et al., 1989). The structural datasets for all three regions are therefore to be treated separately during spatial modelling.

The faults layers, were converted, readjusted and merged with the geology (e.g. The Birimian Shield – Geological Map; Milési et al., 1989) as before (geology theme). Distortions on a map were adjusted using the Arc-GIS spatial adjustment tool. The distributions of the faults of each region are shown in Figure 3.3-3.5.

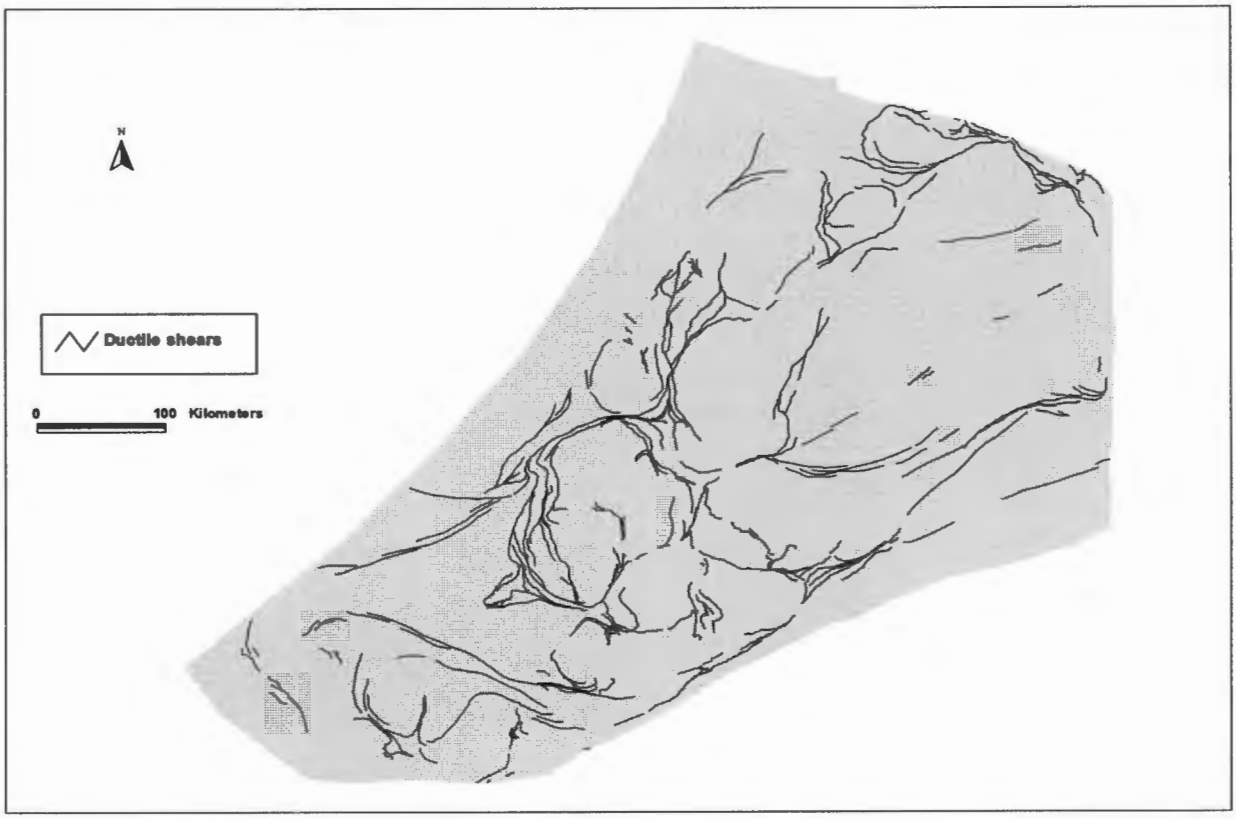

Figure 3.3a: Distribution of ductile shears of the Archean Zimbabwe craton (Jelsma, personal communication, 2004-2005).

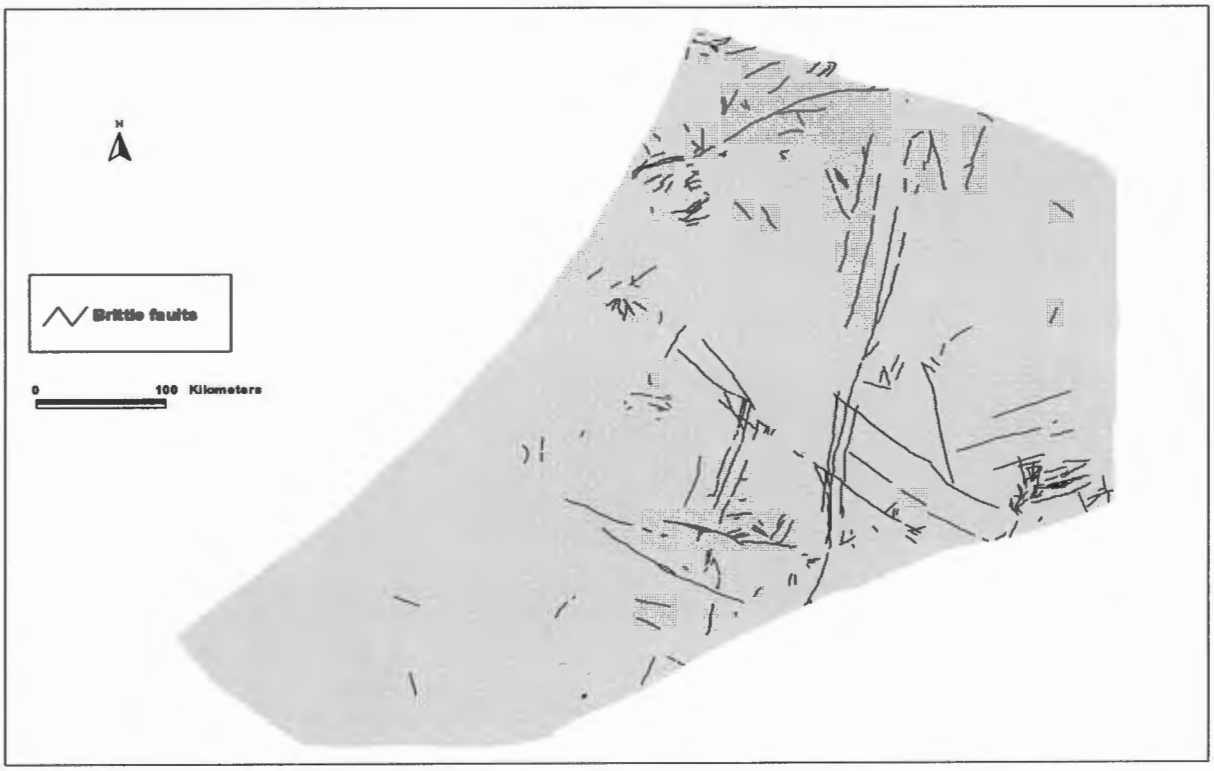

Figure 3.3b: Distribution of brittle faults of the Archean Zimbabwe craton (Jelsma, personal communication, 2004-2005).

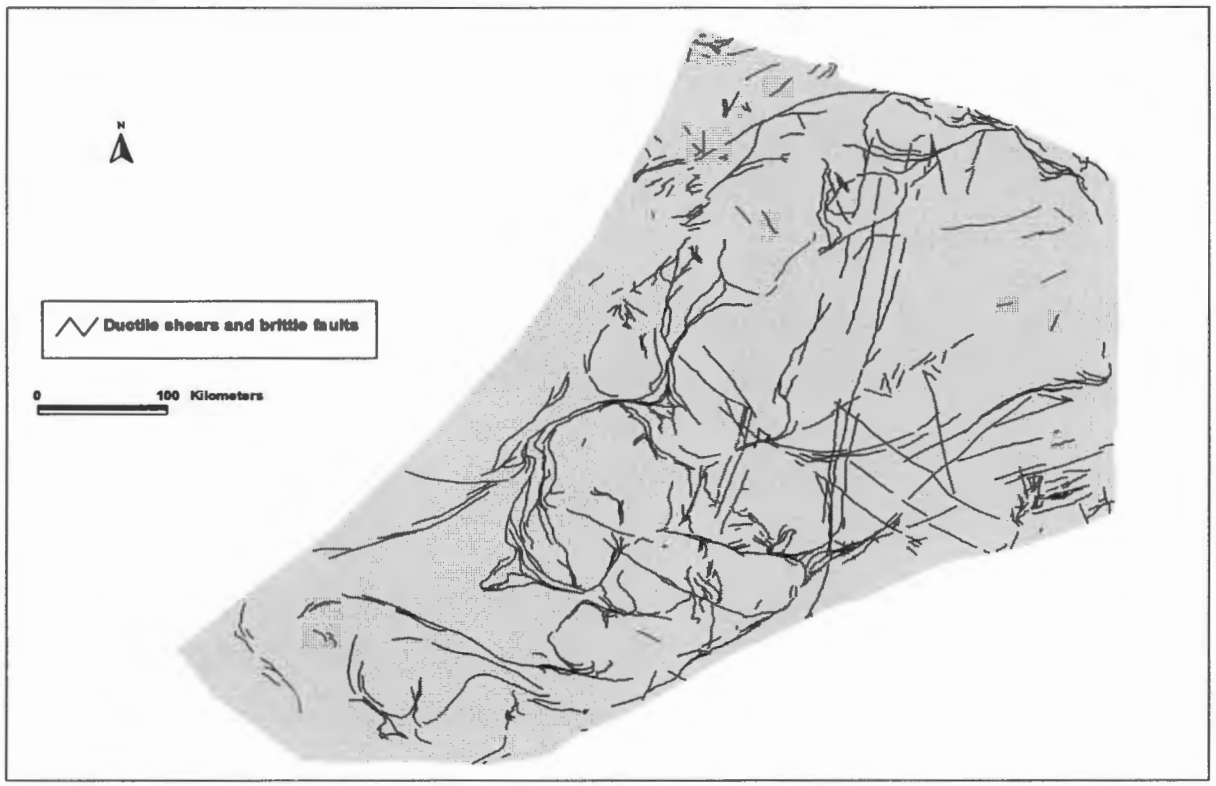

Figure 3.3c: Distribution of combined ductile shears and brittle faults of the Archean Zimbabwe craton.

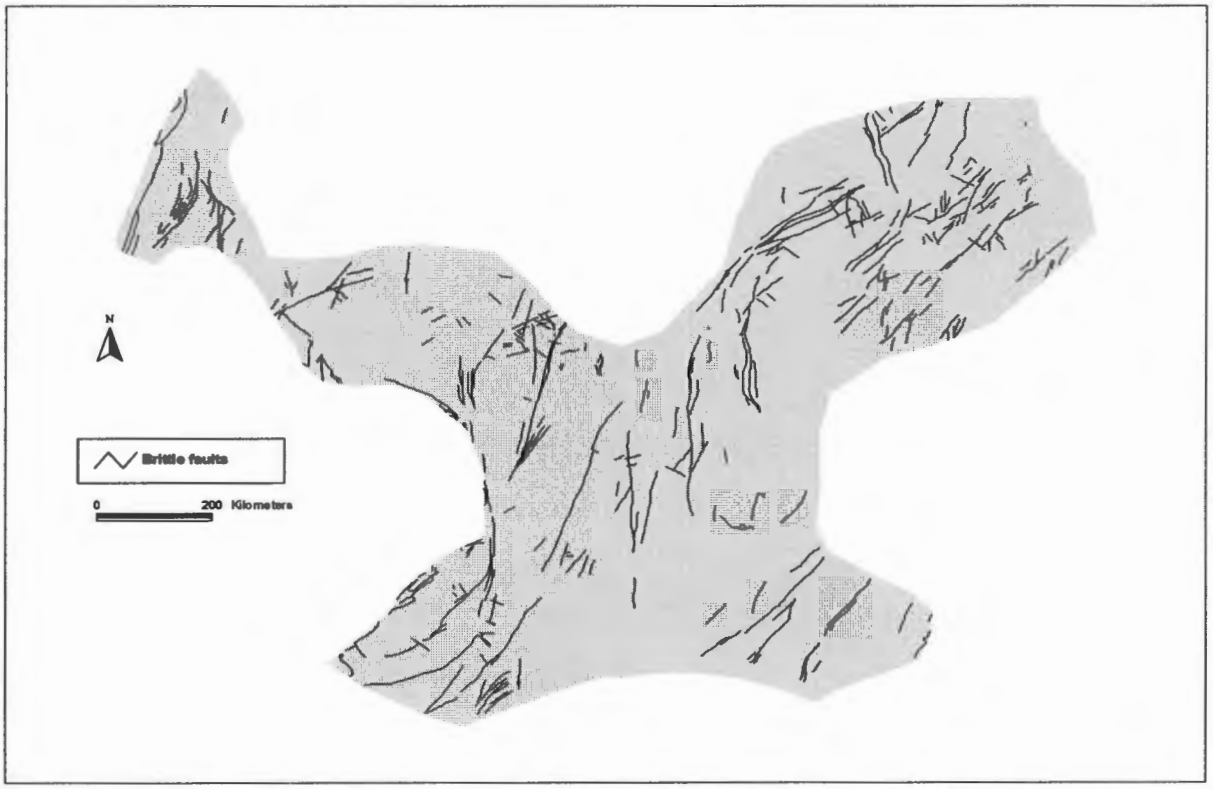

Figure 3.4a: Distribution of brittle faults and shear zones of Paleoproterozoic Birimian Shield (De Beers database, including Milési et al., 1989).

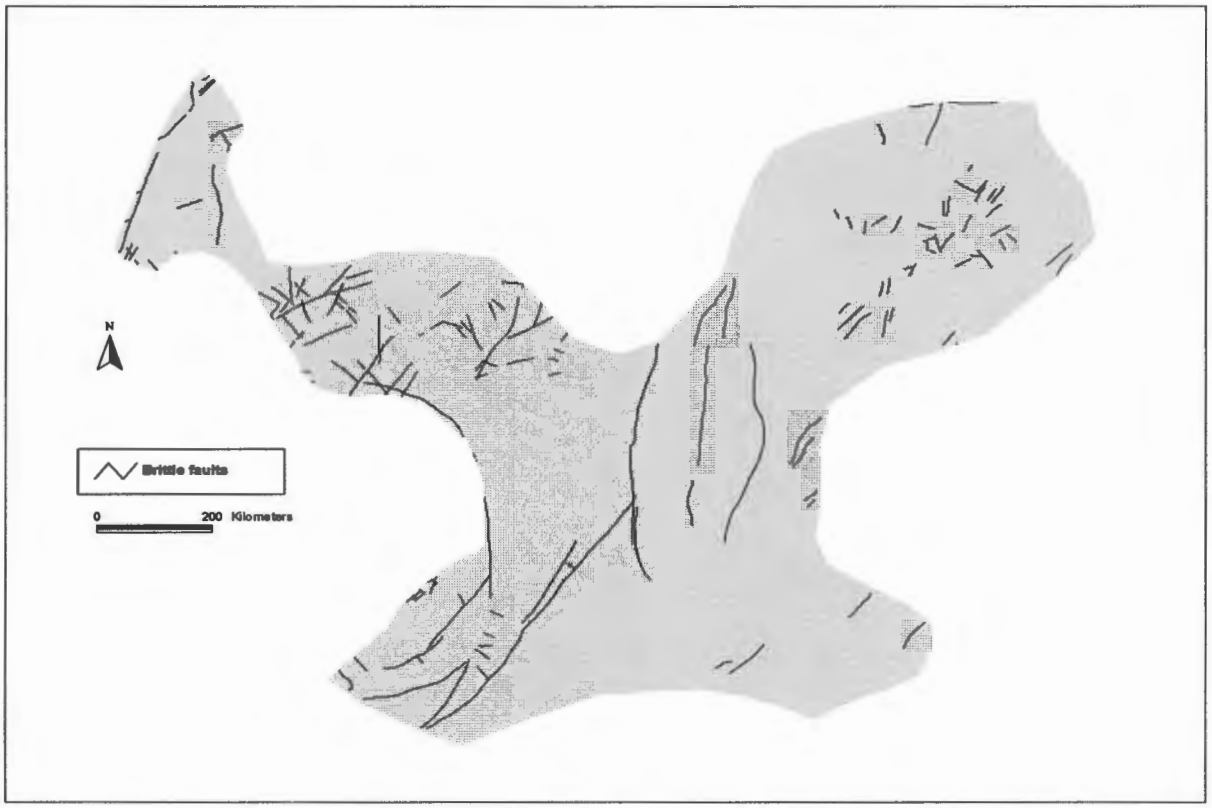

Figure 3.4b: Distribution of brittle faults and shear zones of Paleoproterozoic Birimian Shield (Council for Geoscience-Frost-Killian, 2003).

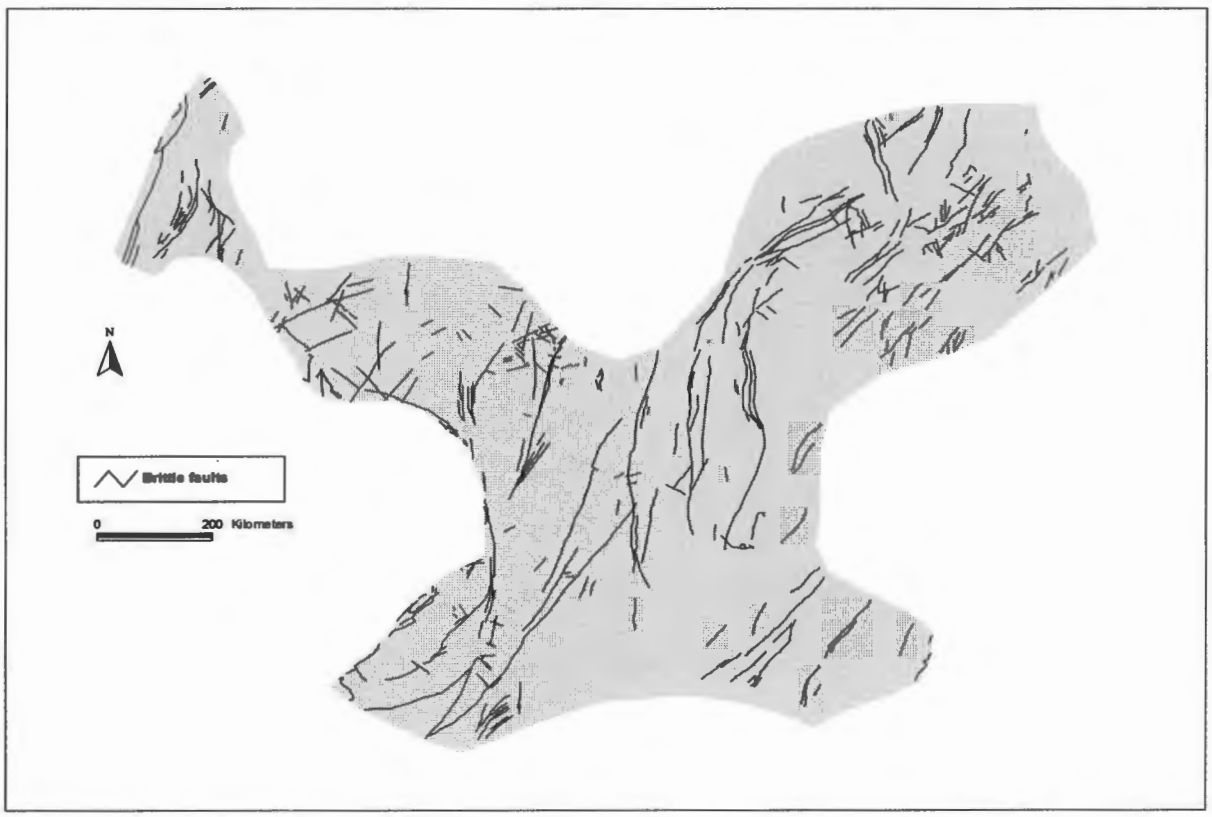

Figure 3.4c: Distribution of merged brittle faults and shear zones of Paleoproterozoic Birimian Shield.

Figure 3.5 Distribution of brittle faults and shear zones of the Neoproterozoic Arabian-Nubian Shield (Council for Geoscience-Frost-Killian, 2003).

Chapter 4

Spatial Modelling Methodology

4.1 Introduction

This chapter reviews literature pertinent to qualitative and quantitative methods of mineral potential mapping. Quantifying spatial association between mineral deposits and geological features using knowledge and data-driven approaches are well described by Bonham-Carter (1994). A knowledge driven approach depends on the "expert" knowledge while data-driven approach depends on the available "known" data.

The purpose of any prediction or spatial analysis method is a process of combining a set of input maps with a function to produce an output map showing the potential of, for example, mineral deposits. Thus,

$$Output\ map = f\ (input\ layers) + \varepsilon$$

where, f = function of combining a set of input maps (evidential layers),

ε = spatial uncertainty of missing data. The function f can be knowledge or data driven.

4.2 Knowledge driven Models

A knowledge driven approach depends entirely on prior knowledge of the experts (e.g. geologist) about the geologic environment in which specific types of mineral deposit are believed to form. Knowledge driven approaches include methods such as Boolean logic (Section 4.2.1), Index overlay (section 4.2.2) and Fuzzy logic (Section 4.2.3). The Wildcat method is another model for mapping mineral potential (Carranza, 2002). The method is developed for areas where no mineral deposits are known, and is only based on geological map data. The Wildcat method is beyond the scope of this study.

4.2.1 Boolean Logic Model

The Boolean logic model involves the logical combination of maps resulting from the application of conditional operators (logical intersection ∩, logical union ∪ and complementation). In this model, all identified spatial factors that are responsible for any mineralization can only have two states; favourable (true or 1) and non favourable (false or 0). The third row (Boolean) of Figure 4.1 illustrates a simple query structure of intersection between three layers (age, rocks and faults). Using a Boolean logic technique, a first order potential map is produced, essentially a "back of the envelope" model.

It is a useful first step in defining mineral potential zones, and combinations are practical and easily applied. The output is either favourable or not favourable.

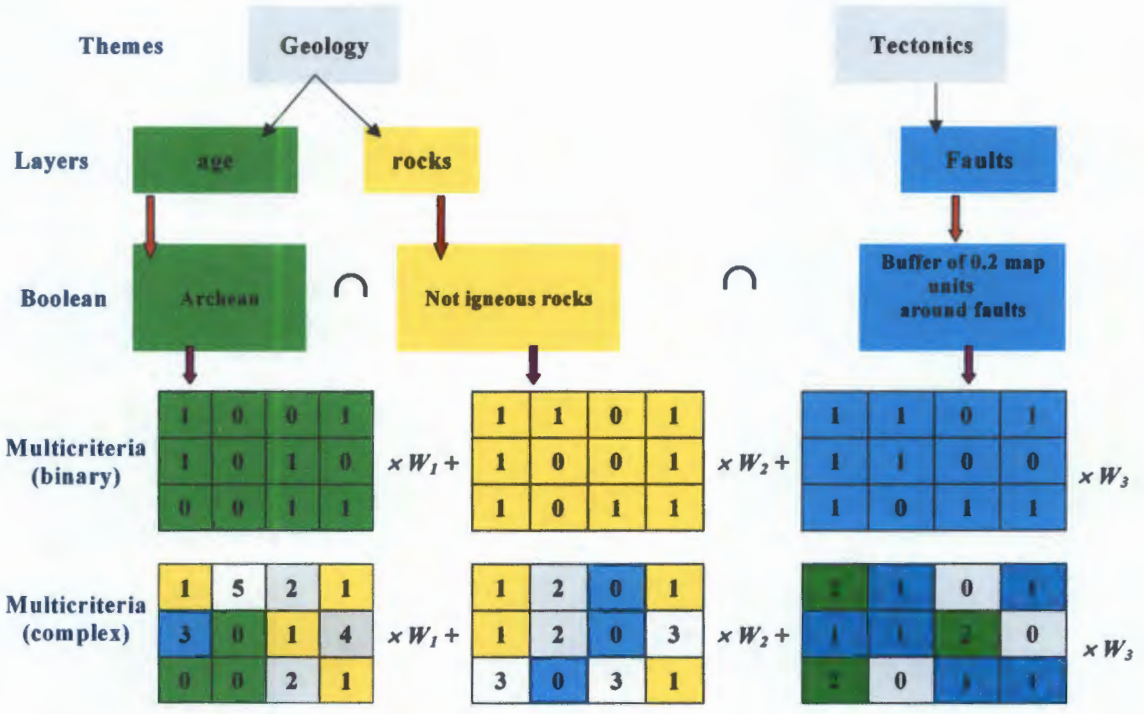

Figure 4.1 Schematic representation of different knowledge driven models. Reproduced from Thiart and de Wit (2000).

4.2.2 Index Overlay / Multicriteria Model

Index overlay models allow for a more flexible combination of maps which is not possible with Boolean logic combination operation alone. Maps are added together in different weighted combinations (Bonham-Carter, 1994). The simplest kind of index weighting is where the input maps are binary and each map carries a single weight (4th row, Fig. 4.1: multicriteria binary). When maps are not binary, multi-class maps (different layers of database) are combined by first assigning a weight to each map and then assigning another (internal) weight to the criteria that constitute the map (Fig. 4.1, 5th row: multicriteria-complex).

Multicriteria (binary) – when binary maps are added together in a weighted combination, each map is simply multiplied by its weight factor, summed over all the maps being combined and normalized by the sum of the weights. The result is a value ranging between 0 and 1. The output score S (for each pixel) is defined as:

$$S = \frac{\sum_{i}^{n} W_i class(MAP_i)}{\sum_{i}^{n} W_i} \qquad (4\text{-}1)$$

where W_i is the weight of the i-th map, class (MAP_i) is either 1 for presence or 0 for absence of the binary condition and n is the number of maps (evidential themes) being combined. The result produces a map showing regions that are ranked according to the score (ranking near 1 is the most favourable and a ranking near 0 is the least favourable).

Multicriteria (complex) – each layer/map is allocated a weight W_i, the so called external weight, as is done in the binary method. The map classes on each input map are now assigned different weights (internal weights). The score in each pixel is defined as:

$$S = \frac{\sum_{i}^{n} S_{ij} W_i}{\sum_{i}^{n} W_i} \qquad (4\text{-}2)$$

S is the weighted score for an area object (cell, pixel), n is the number of maps (evidential themes), W_i is the weight for the i-th input map. S_{ij} is the score for the j-th class of the i-th map, the value j depending on the specified class occurring in a cell. In this approach, layers are represented by an external weight, and any information attached to each layer is given as an internal weight. These weights are setup in a multicriteria matrix (the knowledge of an expert is used to create the multicriteria matrix).

This method is advantageous in that it develops a variety of scenarios through different weight schemes, reflecting differences in opinion amongst experts, and allows the evaluation of sensitivity of the mineral potential maps to such differences. For example, it gives flexibility to an exploration geologist to manipulate weight on different elements or evidence maps through his/her geological knowledge about the terrain in different stages of the analysis. The disadvantage lies in its linear addictive nature where all evidence maps are combined by additive union method to generate the mineral potential maps. The resulting models remain subjective.

4.2.3 Fuzzy logic Model

The fuzzy logic approach is similar to that of multicriteria overlay, but the combination rules are more flexible and improve on the linear additive nature of the model. Fuzzy logic differs from other empirical modelling in that relationships between inputs and outputs can be extracted from the membership functions. Membership of a fuzzy set, is expressed on a continuous scale from 1 (full membership) to 0 (non-membership).

Fuzzy logic relies on the users to assign weights to the input layers based on previously obtained knowledge of the evidential theme. Given two or more maps with fuzzy membership functions for the same datasets, a variety of operators can be employed to combine the membership values together. Five operators, which are found useful for combining the datasets, are fuzzy and, fuzzy or, fuzzy algebraic product, fuzzy algebraic sum and fuzzy gamma operators (Bonham-Carter, 1994; Wright and Bonham-Carter, 1996).

The advantage of fuzzy logic model is that it is a more flexible weighting of maps and map classes than that of multicriteria and its nonlinear combination of maps.

4.2.4 Disadvantage of Knowledge driven models

- The knowledge driven models are subjective.
- The approach is strictly dependent on the expert knowledge to generate the weights needed to create a favourability map or, in the case of fuzzy logic, to create membership functions.

4.3 Data Driven Model

Data driven models essentially use three techniques: weights of evidence, regression analysis, and neural networks. In data driven models, weighting is calculated based on the quantification of relationships (associations) between the evidential layers and known mineral deposits (Fig. 4.2). Thus, the data driven approach rely on data: known mineral deposits are used as a reference set.

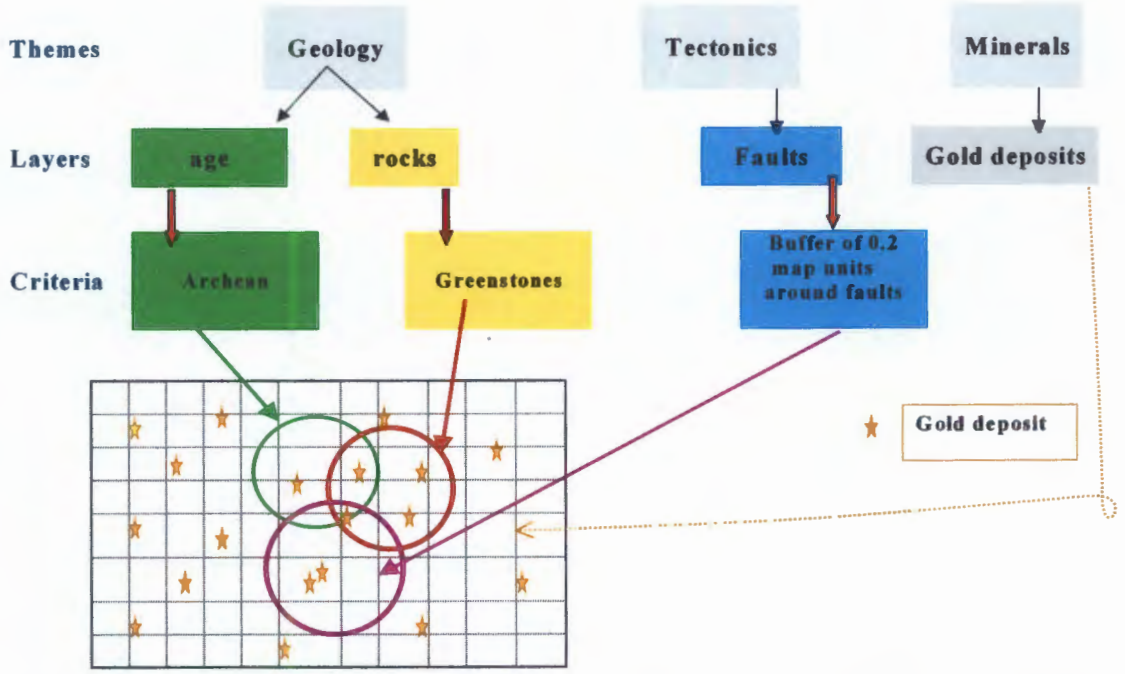

Figure 4.2 Flow diagrams of data driven approach. Reproduced from Thiart and de Wit (2000).

4.3.1 Weights of Evidence (WofE) Method

The WofE model originated in biostatistics (Spiegelhalter, 1986) and was originally developed for prediction of the probability that a new patient would be diagnosed to have a disease based on presence or absence of a set of symptoms. During the late 80's, a number of authors applied WofE to geological data (e.g. Bonham-Carter et al., 1988, 1989; Agterberg et al., 1990, 1993). Recently several workers applied WofE to mineral potential mapping, such as:

- Carrranza and Hale (2000; 2002), to search for areas likely to contain gold and porphyry copper deposits in Baguio District, Philippines;
- Thiart and de Wit (2000), to study gold and tin models of Africa;

- Scott (2000), to identify mineral potential in Yarrol, Queensland;
- Asadi and Hale (2001), to predict gold and base metal mineralization in Iran;
- Raines (1999) and Mihalasky (2001), to examine epithermal gold in Nevada, USA;
- Boleneus et al. (2002), to study epithermal gold in Washington, USA; and
- Billa et al. (2004), to analyse gold-rich epithermal and porphyry systems in the central Andes.

There have also been a variety of published applications of the method to other problems, such as analysis of the distribution of archaeology sites in the landscape in California (Hansen, 2000) and assessment of flowing wells in the greater Toronto area (Cheng, 2004).

Boleneus et al. (2002) states that the process used in WofE modelling essentially is a quantitative version of the inspection method of overlaying several different map themes to identify areas where mineralization may be present. The larger the number and magnitude of appropriate overlapping anomalies in data maps such as geochemistry, geology, and others, the greater the better the quantification that mineralization may be present.

4.3.2 Weights of evidence Modelling

A WofE model uses a probability framework based on set theory that uses Bayes Rule to combine evidence (Bonham-Carter, 1994). Known mineral deposits are used as reference set of training points (e.g either present or absent: see Fig. 4.2). Each training point occupies a small unit area known as cell or pixel. The cell in which the deposit occurs is represented by value 1 (present) or 0 (absent).

The ratio of the total number of present pixels to the ratio of the total number of cells (present and absent) in the map is known as prior probability (observed probability). Using the known mineral deposits in the area, the prior probability of a deposit is:

$$P(D) = \frac{N(D)}{N(T)} \tag{4-3}$$

where $P(D)$ is the prior (initial) probability, $N(D)$ is the total number of known deposit, and $N(T)$ is the total number of pixels / cells in the study area. The prior probability of mineral deposit occurrence is modified (updated) by other sources of information (evidential themes), resulting in a posterior probability. Some evidence will cause the posterior probability to increase (likelihood of mineral deposit will increase), and some evidence will cause it to decrease (Bonham-Carter, 1994). The posterior probability of a deposit given the presence of evidential theme B, ($P(D \mid B)$), is:

$$\begin{aligned} P(D \mid B) &= \frac{P(D \cap B)}{P(B)} \\ &= \frac{P(D \cap B)}{P(B)} \frac{P(D)}{P(D)} \\ &= P(D) \frac{P(B \mid D)}{P(B)} \end{aligned} \tag{4-4}$$

Thus the conditional (posterior) probability of deposit, given the presence of a pattern, is the prior probability of the deposit multiplied by the factor $P(B \mid D) / P(B)$. A similar expression can be derived for the posterior probability of a deposit occurring given the absence of the pattern $\overline{B}$:

$$P(D \mid \overline{B}) = P(D) \frac{P(\overline{B} \mid D)}{P(\overline{B})} \tag{4-5}$$

Similar expressions can be derived for the absence of a deposit given the presence of pattern B. Thus:

$$P(\overline{D} \mid B) = \frac{P(\overline{D} \cap B)}{P(B)} \frac{P(\overline{D})}{P(\overline{D})}$$

$$= P(\overline{D}) \frac{P(B \mid \overline{D})}{P(B)} \tag{4-6}$$

and similarly the probability of the absence of a deposit given the absence of pattern B:

$$P(\overline{D} \mid \overline{B}) = P(\overline{D}) \frac{P(\overline{B} \mid \overline{D})}{P(\overline{B})} \tag{4-7}$$

These posterior probabilities can be expressed in the odds formulation. Odds are defined as a ratio of the probability that an event will occur to the probability that it will not occur, e.g. $\frac{p}{1-p}$. Thus, the odds of a deposit D given the presence of B is:

$$O(D \mid B) = \frac{P(D \mid B)}{P(\overline{D} \mid B)}$$

$$= P(D) \frac{P(B \mid D)}{P(B)} \frac{P(B)}{P(B \mid \overline{D}) P(\overline{D})} \text{ (from 4-4 and 4-6)}$$

$$= O(D) \frac{P(B \mid D)}{P(B \mid \overline{D})} \tag{4-8}$$

$O(D)$ is the prior odds of D and $P(B \mid D) / P(B \mid \overline{D})$ is known as the sufficiency ratio LS. The odds of D given B absent is:

$$O(D \mid \overline{B}) = \frac{P(D \mid \overline{B})}{P(\overline{D} \mid \overline{B})}$$

$$= P(D) \frac{P(\overline{B} \mid D)}{P(\overline{B})} \frac{P(\overline{B})}{P(\overline{B} \mid \overline{D}) P(\overline{D})} \text{ (from 4-5 and 4-7)}$$

$$= O(D) \frac{P(\overline{B} \mid D)}{P(\overline{B} \mid \overline{D})} \tag{4-9}$$

$P(\overline{B} \mid D)/P(\overline{B} \mid \overline{D})$ is called the necessity ratio LN. LS and LN are likelihood ratios. Taking the natural logs both sides of Eq. 4-8 and 4-9:

$$\log O(D \mid B) = \log O(D) + \log \frac{P(B \mid D)}{P(B \mid \overline{D})}$$

$$= \log O(D) + W^{+} \tag{4-10}$$

and

$$\log O(D \mid \overline{B}) = \log O(D) + \log \frac{P(\overline{B} \mid D)}{P(\overline{B} \mid \overline{D})}$$

$$= \log O(D) + W^{-} \tag{4-11}$$

where the positive weight of evidence is defined as the natural log of LS:

$$W^{+} = \log \frac{P(B \mid D)}{P(B \mid \overline{D})} \tag{4-12}$$

and the negative weight of evidence as the natural log of LN:

$$W^{-} = \log \frac{P(\overline{B} \mid D)}{P(\overline{B} \mid \overline{D})} \tag{4-13}$$

The estimates of uncertainty in weights and contrast are also valuable for helping to decide about reclassifying (and simplifying) the evidential themes. If the total number of training points is large, the variances of the weights are approximately given by the expression (Bonham-Carter, 1994):

$$s^2(W^{+}) = \frac{1}{N(B \cap D)} + \frac{1}{N(B \cap \overline{D})} \tag{4-14}$$

and

$$s^2(W^{-}) = \frac{1}{N(\overline{B} \cap D)} + \frac{1}{N(\overline{B} \cap \overline{D})} \tag{4-15}$$

where $N(B \cap D)$ is the number of pixels where pattern B and the deposit occurs simultaneously; $N(B \cap \overline{D})$ is the number of pixels of pattern B that contain no deposit; and $N(\overline{B} \cap \overline{D})$ is the total number of pixels that contain neither pattern B or any deposits.

The weights provide a measure of spatial association between the points and the evidential theme. Weights are calculated for each class of the evidential theme. A positive value of the weight indicates that there are more points in that class than would occur due to chance; conversely a negative value indicates fewer points occur than expected. A value near zero indicates that the training points are distributed randomly with respect to that class. These weights give unitless measures of spatial association between mineral occurrences and test domain. The difference between the weights is known as the contrast, C_w:

$$C_w = W^+ - W^- \tag{4-16}$$

The contrast is an overall measure of spatial association between the training points and the evidential theme, combining the effects of the two weights. The standard deviation of C, is calculated as:

$$s(C) = \sqrt{s^2(W^+) + s^2(W^-)} \tag{4-17}$$

Another guide to the interpretation of the contrast value comes from the estimates of the uncertainty of the weights and contrast by calculating the studentized contrast ($C/s(C)$) (Bonham-Carter, 1994). The studentized contrast is a measure of the certainty with which the contrast is known, and is also useful for choosing the cut-off distance because it shows the contrast relative to the uncertainty due to the weights.

If more than two patterns are used, the weights are calculated from each map independently and then combined into a single equation. The general expression for the log posterior odds can be defined as:

$$\log O(D \mid B^k{}_1 \cap B^k{}_2 \cap \ldots B^k{}_n) = \log(D) + \sum_{i=1}^{n} W_i^k \tag{4-18}$$

where the superscript k is positive (+) or negative (-) if the predictor pattern is present or absent, respectively. The calculation of the posterior odds is easy to follow because adding weights together is similar to the intuitive approach for combining evidence based on common sense. By making an assumption of conditional independence (section 4.3.3) evidential themes can be used to update the prior logit (log of the odds) to obtain the posterior logit. The advantage of using the loglinear model over the ordinary probability expression is that weights are easier to interpret than probability factors.

This method can be extended to evidential themes that are multiclass. It is better to use multiclass evidential themes than using a binary one, as they reflect the real picture of favourable or unfavourable evidence with more precision, whilst no information is lost.

4.3.3 Conditional Independence

In the WofE model one of the assumption is that the evidential themes must be conditional independent (CI) with respect to known mineral deposits. Conditional Independence between two spatial patterns are defined as:

$$P(B_1 \cap B_2 \mid D) = P(B_1 \mid D)P(B_2 \mid D) \qquad (4\text{-}19)$$

If the assumption of CI is violated, the posterior probability will be either over-or under-estimated (Bonham-Carter, 1994; Wright and Bonham-Carter, 1996). In practice, this assumption is commonly violated to some degree, particularly if a large number of input maps are being used. The CI value can be checked using statistical tests to show how serious the violation is, and the user has to decide whether to discard or combine some layers.

Three kinds of tests have been proposed to test for CI: (1) Chi-square test for independence (χ^2 test) (Agterberg et al., 1990), (2) the overall or omnibus test (OT) (Bonham-Carter, 1994) and (3) the new omnibus test (NOT) (Agterberg and Cheng, 2002; Thiart et al., 2005).

4.3.3.1 Chi-square test

Chi-square is a statistical test used to determine the probability of obtaining the observed results by chance, under a specific hypothesis. This method considers all possible pairwise comparisons of evidential themes. A contingency table is used for each pair to characterize the degree of association between evidential patterns, using only the location of known points (Agterberg et al., 1990). However in the case where it is only applied between two layers at a time, the number of deposits falling in each cell is the observed value (O), and it is compared with the expected value (E). The expected values are determined by multiplying marginal frequencies (row and column) and dividing by the total number of observed deposits (Bonham-Carter, 1994). Thus:

$$\chi_{ij}^{\ 2} = \frac{(O_{ij} - E_{ij})^2}{E_{ij}} \tag{4-20}$$

where i and j indicate the corresponding row or column of the contingency table. χ^2 value is sometimes referred to as the degree of similarity and is effectively a measure of the degree of goodness of fit of association between the corresponding datasets. The disadvantage of the χ^2 test is that it only tests for conditional independence between two or more layers at a time. Furthermore the expected number in a cell (i, j) must be greater than 5.

4.3.3.2 Overall or omnibus test (OT)

The (OT) is the ratio of the observed number of known deposits $N(D)$ to the predicted number of deposits (Bonham-Carter, 1994). Thus,

$$OT = \frac{N(D)}{N(D)_{calc}} \tag{4-21}$$

where the predicted number, $N(D)_{calc}$ of deposits point is:

$$N\{D\}_{calc} = \sum_{k=1}^{m} P_K * N\{A\}_k \tag{4-22}$$

where P_k is the posterior probabilities for the *k-th* unique condition, $N\{A\}_k$ is the area in unit cells for the *k-th* unique condition (collection of grid cells in which the combination of the evidential themes occurs in the output map), and k = 1, 2..., m. The number of predicted mineral deposits ($N(D)_{calc}$) is usually larger than the observed number of mineral deposits (Bonham-Carter, 1994).

If the predicted number of occurrences is larger than the number of observed mineral deposits, then the assumption of conditional independence is seriously violated. Thus, when OT is less than one, the condition of independence is violated. No statistical guideline is available to decide when a value <1 is significant. A general guideline is that, if OT >0.85, the conditional dependence is not of concern (Bonh am-Carter, 1994). If OT <0.85 some themes should be rejected or combined. Thiart et al. (2005) noted that the problem with OT tests is that the threshold of 0.85 is empirical and arbitrary.

4.3.3.3 New Omnibus test (NOT)

Agterberg and Cheng (2002) derived a new omnibus test (NOT) using the expectation and variance of the predicted number of deposits $N(D)_{calc}$. This new omnibus CI test value is therefore defined as:

$$NOT = \frac{N(D)_{calc} - N(D)}{s[N(D)_{calc}]} \tag{4-23}$$

where, $s[N(D)_{calc}]$ represent the estimation standard deviation of variance of the predicted deposits. The *NOT* provides a statistical basis for deciding whether the ratio in the omnibus test is too small compared to tabled normal distribution. The advantage of this test is that it is no longer 'back of the envelope', and that degrees of freedom are not involved.

4.3.4 Arc Spatial Data Modeler for weights of evidence

The WofE model is implemented in Arc-SDM (Kemp et al., 2001) an extension that is freely available for use with ArcView GIS 3.3. It is a useful modeler for data-driven (weights of evidence, logistic regression analysis and neural networks) and knowledge-driven (Fuzzy logic) approach. The Arc-SDM approach is not a 'black box' computer operation, with input data fed into it at one end and a prediction map coming out at the other end (Raines and Bonham-Carter, 2004). Instead, a series of subjective decisions are required that strongly dependent on an understanding of the characteristics of the mineral deposits and their exploration guidelines, augmented by statistical analysis of the spatial associations between known mineral sites and the GIS data layers (evidential themes).

4.3.5 Implementation of Weight of Evidence

Before the modelling process can start, the researcher needs to:

1. Define the study area (geographic extent) and subsequently all other evidential themes used are "clipped" to the study area grid.

2. The Arc-SDM extension program calculates a suggested unit area based on the size of the study area and the number of points available (prior probability). It is advantageous for the user to make the unit cell as small as possible.
3. Each map is treated as multi-class (categorical) or binary to determine the optimum reclassification scheme. WofE calculations are used for this optimization process, either using a cumulative form for the maps with higher measurement level, or a non-cumulative form for the categorical maps. The categorical form is used where data occurs in unrelated and mutually exclusive categories.
4. The basic procedure for calculating cumulative weights is to digitally establish a series of buffers around lines/polygons (such as faults or favourable lithology) of the evidential theme being tested in order to calculate weights and contrast values for each buffer band. The buffer band with the maximum contrast value is the optimal band or defines the extent of the buffer area of the evidential theme. Therefore, maximum contrast usually provides the cut-off distance for the buffer zone at which the spatial association of the resulting binary pattern is optimal.
5. After all the evidence themes are reclassified (to optimize the spatial association between the known mineral occurrences and the evidence) the evidence can be combined together, to produce an output map of posterior probabilities showing the relative favourability.
6. The combination of input maps assumes that the maps are conditionally independent (CI) of one another with respect to the reference points. When conditional independence (CI) is violated, one remedy is that evidential themes are combined or rejected based on expert's knowledge.
7. Recalculate posterior probabilities to produce a final predictive map.

8. Optionally, it is also possible to calculate the effects of uncertainty in the weights, and uncertainty due to missing information, and to produce an uncertainty map.

4.3.6 Advantages and Disadvantages of Weights of Evidence

Advantages:

- WofE provides a quantitative method for integrating multiple sources of evidences.
- It avoids subjective choice of evidences and subjective estimation of weights for evidences compared with other methods.
- Generalizing the evidential class can reveal insight into spatial data association.
- The only assumption is the one of conditional independence.
- It is possible to include expert opinion in the analysis and it can be implemented straightforward within a GIS.
- It is possible to consider uncertainties due to the variances of the weights.
- It is possible to extent the process to other areas outside the training area by assuming that the same conditions will apply to this extended area and using the known weights of the training area.

Disadvantages:

- Requires training points and evidential themes; otherwise the quantified spatial association can be statistically non-significant.
- It is sensitive to the number of deposits and the size of the study area.
- It does not take deposit size or grade into account.
- With the use of binary pattern some useful information in the continuous evidences may be lost after data conversion.

- It assumes that the maps are conditionally independent of one another with respect to the response variable. However, sometimes violation of the CI assumption will results in maps with "inflated" posterior probability whilst the ranking of the pixels will still be the same.

4.3.7 Conclusion

This chapter has summarized statistical models in which map weighting is controlled either subjectively (knowledge driven) or is determined from measured associations (data-driven). It is apparent in the literature that the field of spatial statistical modelling methods is a growing and changing field and numerous studies are using several different techniques of modelling in order to discover the most appropriate model for the area of interest.

This study is restricted to a data driven approach, namely, weights of evidence (WofE) modelling.

Chapter 5

Spatial Modelling using Weights of Evidence

This chapter presents the results of WofE modelling on the mineral deposit data of the three selected regions of African crust discussed in chapter 2 and 3. Three evidential themes are tested to evaluate the mineral potential of the areas, namely: (1) lithology (rocktypes), (2) structures (brittle faults and ductile shears), and (3) lithologic contacts (contacts between different rocktypes) for some mineral groups. In each region, a pixel/cell size of 1×1 km^2 is used in the analysis. The mineral deposits datasets are based on the 6 element groups as outlined in Chapter 3 (Table 3.2).

5.1 The Archean Zimbabwe Craton

5.1.1 Gold deposits

The total training area is 240 544 km^2, and the unit area equal to 1 km^2. In the training area the total number of gold deposits is 625. The total number of gold deposits is divided randomly into two subsets: a subset of 501 (80%) of the 625 known gold deposits is used to generate the posterior probability map. The other subset of 124 deposits (about 20%) of the 625 known gold deposits is used to validate the probabilistic model. The prior probability is 0.0021.

5.1.1.1 Reclassification of evidential theme patterns

The evidential themes used for creating posterior probability map of gold are given in Table 5.1. The themes are divided into three spatial association models with common geology: Model A – brittle faults, Model B – ductile shears, and Model C – combined faults and shears. Three models were considered because the brittle faults and ductile shears were compiled from different sources and are treated separately (see Chapter 3).

Model	Theme 1	Theme 2
Model A	Geology	Brittle faults
Model B	Geology	Ductile shears
Model C (A and B)	Geology	Combined faults and shears

Table 5.1 Evidential themes used for spatial modelling of gold deposit.

An evidential theme of the simplified geology map (Fig. 3.2a) is reclassified into lithological units based on the calculated positive weights and negative weights of evidence (Table 5.2a). Based on the contrast values, the lithologic units are reclassified into four classes: (1) very favourable, (2) favourable, (3) random and (4) negative association classes (Table 5.2b). The greenstone belt-dominantly volcanics unit shows the highest positive association (C_w=2.76), and captures 321 of the known gold deposits (very favourable). The greenstone belt-dominantly sediments also show a positive association with 35 known deposits (favourable), but the W^+ and contrast values (C_w=1.22) are lower than the greenstone belt-dominantly volcanics. This might be expected because gold deposits are known to occur preferentially within the volcanic rocks of greenstone belts (e.g. Vinyu et al., 1996; Herrington et al., 1997). The third class is random, whilst the fourth class contains negative contrast values, missing data and zero mineral points.

The structures (brittle faults and ductile shears) used for the spatial modelling of gold deposits are discussed below under Model A, Model B and Model C (Table 5.1).

CLASS	S_VALUE	AREA_SQ_KM	NO_POINTS	WPLUS	S_WPLUS	WMINUS	S_WMINUS	CONTRAST	S_CONTRAST	STUD_CNT	
2	Greenstone Belt - dominantly volcanics	24923	321	1.8269	0.0562	-0.9318	0.0756	2.7587	0.0942	29.2835	1
6	Greenstone Belt - dominantly sediments	5224	35	1.1671	0.1696	-0.0510	0.0466	1.2181	0.1759	6.9250	2
9	No data	466	1	0.0240	1.0011	0.0000	0.0450	0.0240	1.0021	0.0240	
5	Post-tectonic intrusives	13133	23	0.1796	0.2087	0.0096	0.0460	0.1892	0.2137	0.8854	3
3	Pre- and Syn-tectonic granitoids	74378	62	-0.9229	0.1271	0.2442	0.0481	-1.1671	0.1358	-8.5917	
1	Younger Cover	41727	18	-1.5821	0.2358	0.1573	0.0458	-1.7394	0.2402	-7.2425	
4	Post-tectonic granitoids	73630	35	-1.4850	0.1691	0.3001	0.0466	-1.7851	0.1754	-10.1778	4
7	Great Dyke	2850	1	-1.7887	1.0002	0.0101	0.0450	-1.7988	1.0012	-1.7967	
8	undifferentiated	406	0								
-99	Missing Data	3807	5								
		240544	501								

Table 5.2a. Weights table for gold deposits from WofE applied to lithologic map of the Zimbabwe Craton. Glossary in appendix A2

CLASS	DESCRIPTION	AREA_SQ_KM	NO_POINTS	WPLUS	S_WPLUS	WMINUS	S_WMINUS	CONTRAST	S_CONTRAST	STUD_CNT
1	Very favourable	24923	321	1.8269	0.0562	-0.9318	0.0756	2.7587	0.0942	29.2835
2	Favourable	5224	35	1.1671	0.1696	-0.0510	0.0466	1.2181	0.1759	6.9250
3	Random	13599	24	-0.1719	0.2043	0.0096	0.0461	-0.1815	0.2094	-0.8665
4	Negative association	196798	121	-1.2481	0.0929	1.4195	0.0515	-2.6675	0.1062	-25.1158

Table 5.2b. Reclassified weights table for gold deposits (Zimbabwe Craton)

- **Model A: Brittle faults**

The WofE method is applied to the faults (Model A) in order to find the buffer distances that maximize the spatial association between the gold deposits and the faults. It is clear from Figure 5.1a that as the buffer area increases the contrast value decreases. The contrast value is also very small (<0.24), thus no spatial association between brittle faults and gold deposits. This is also illustrated in figure 5.1b as the area increases the percentage of gold deposits increases proportional with the area.

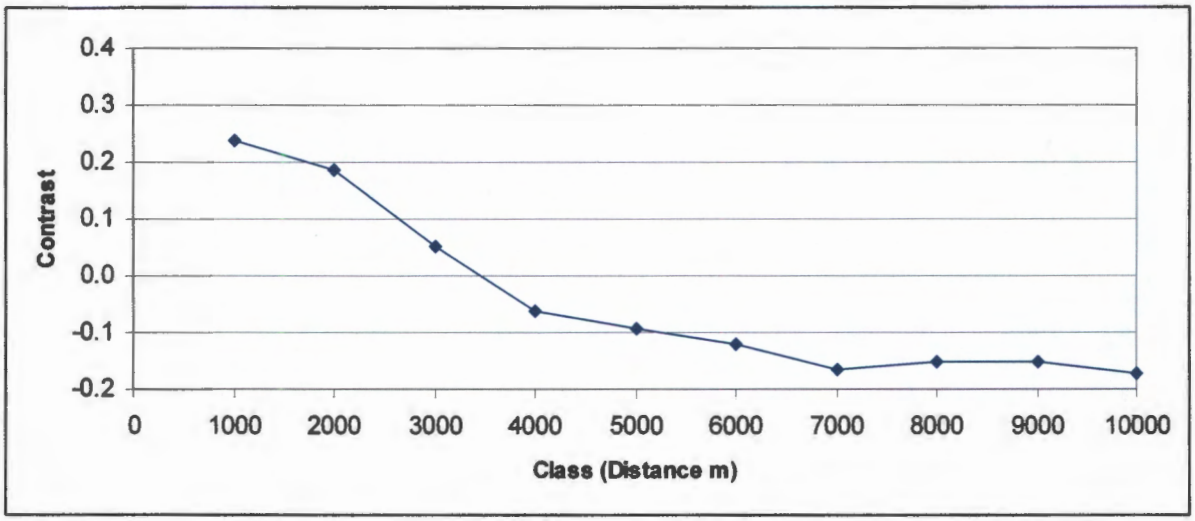

Figure 5.1a: Variation of gold contrast versus cumulative buffer distance away from brittle faults.

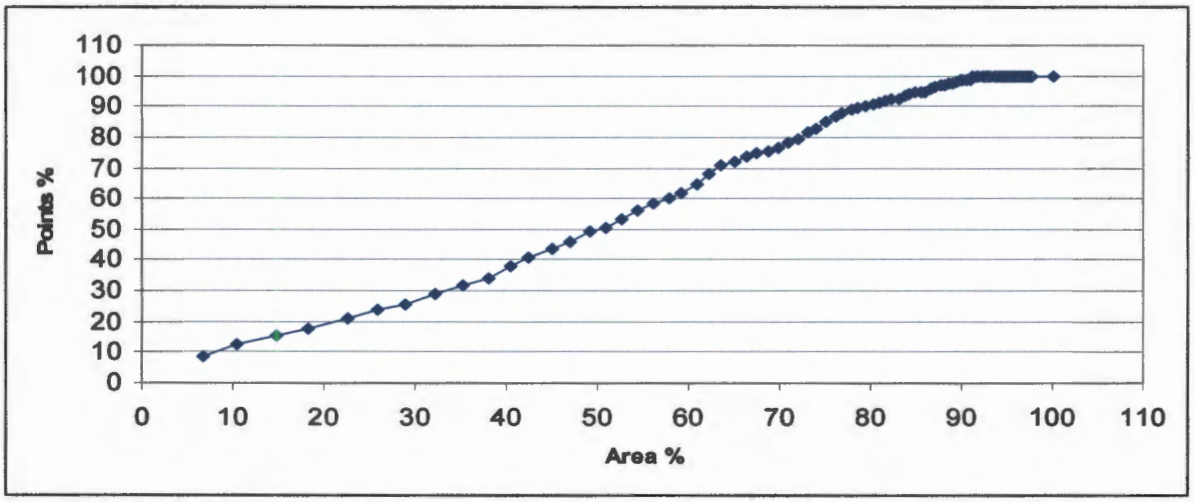

Figure 5.1b: Percentage of gold deposits (points) versus the total area (percentage) at successive distance away from brittle faults. Note that the number of deposit increases near-linearly with distance away from the faults; there is no sign of any preferred concentration of the deposits away from the faults.

- **Model B: Ductile shears**

Variations of contrast for buffer distances from the ductile shears (Model B) show a more positive spatial association to the mineral deposits than model A as illustrated in Figure. 5.2a. The contrast values is high (>2.0 and the studentized contrast value is extremely high). The contrast value is maximized at a distance of 5 km. Figure 5.2b confirm this findings where most points (89%) are captured within 32% of the total area.

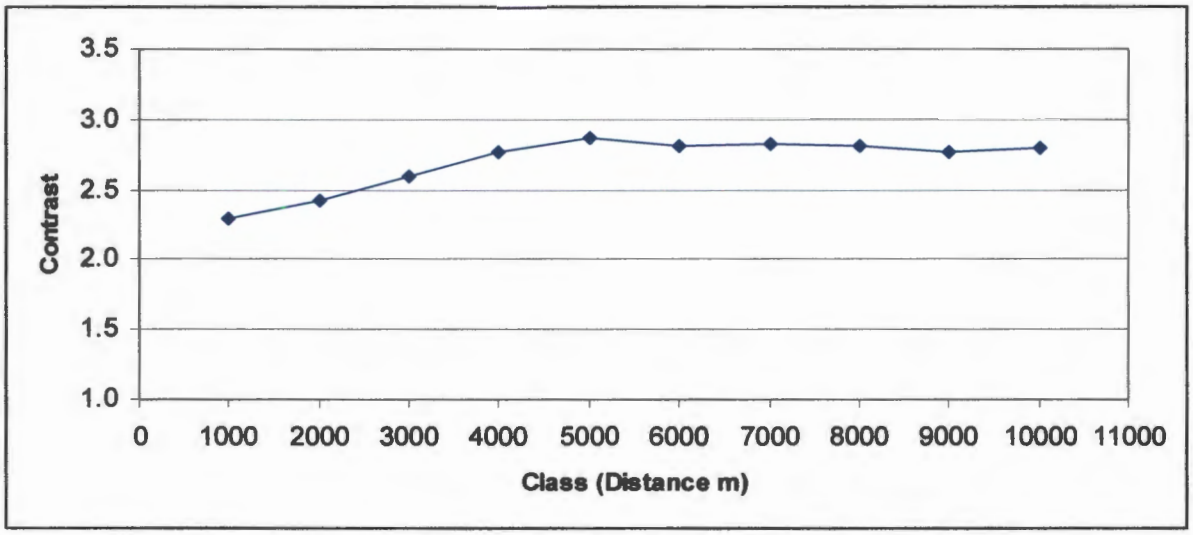

Figure 5.2a: Variation of gold contrast versus buffer distance of the ductile shears. The contrast reaches a maximum at a distance of 5000m, and decreases slightly as the distance away from the ductile shears increases further.

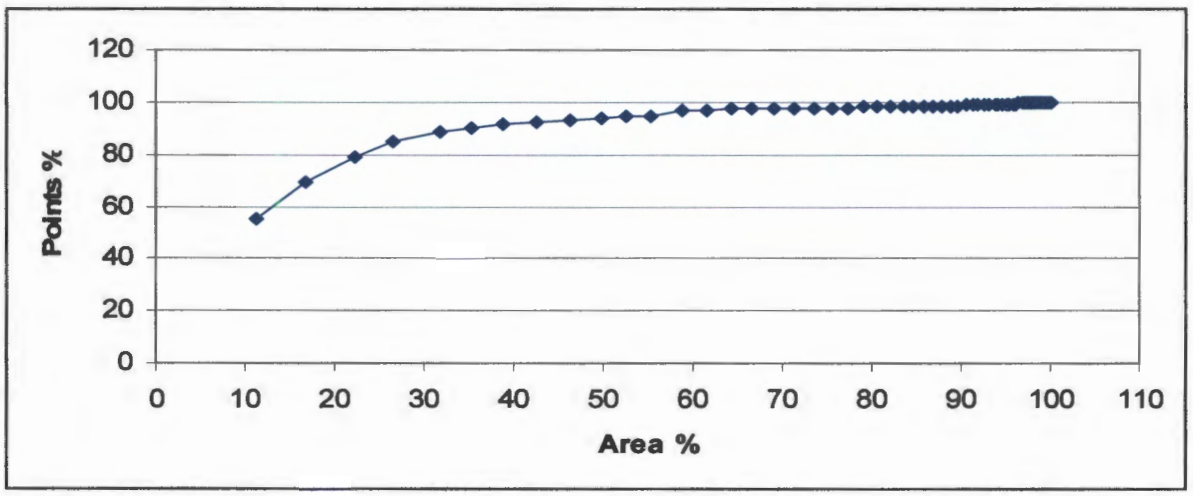

Figure 5.2b: Percentage of gold deposits (points) versus the total area (percentage) at successive distance away from ductile shears. Note a more rapid initial increase in percentage of gold deposits (points) within 30% of the area.

- **Model C: Combined faults and shears**

The combined faults and shears (Model C) shows a similar result as those for Model B. The contrast values is high (>2.0) and is maximized at a distance of 5 km (Fig. 5.3a). Figure 5.3b confirms the findings where most points (92%) are captured within 47% of the total area.

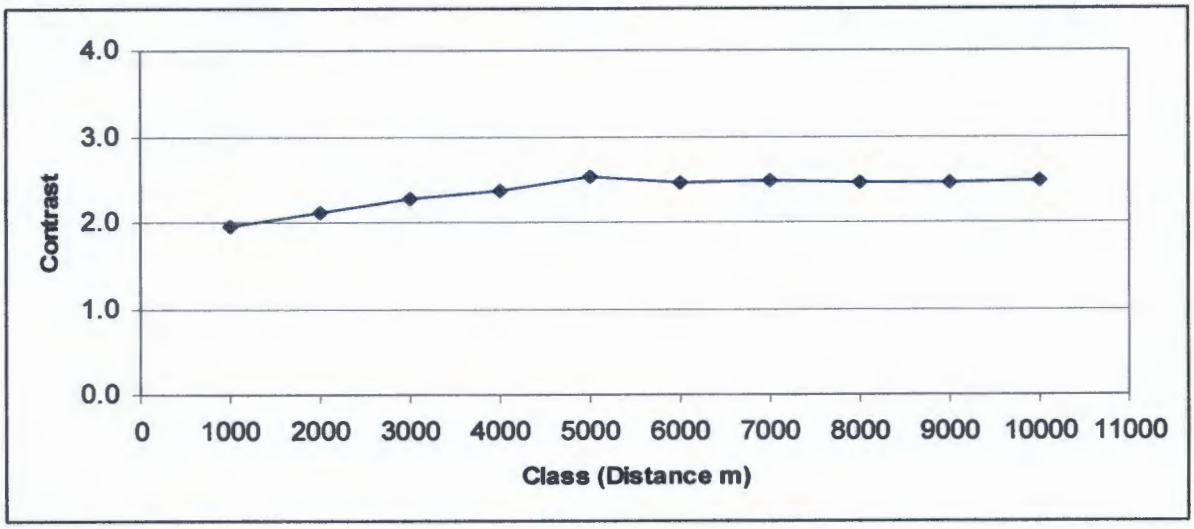

Figure 5.3a: Variation of gold contrast versus buffer distance of the combined brittle faults and ductile shears theme. Note that the contrast reaches a maximum at a distance of about 5000 m, and remains near-constant as the distance away from the structures increases.

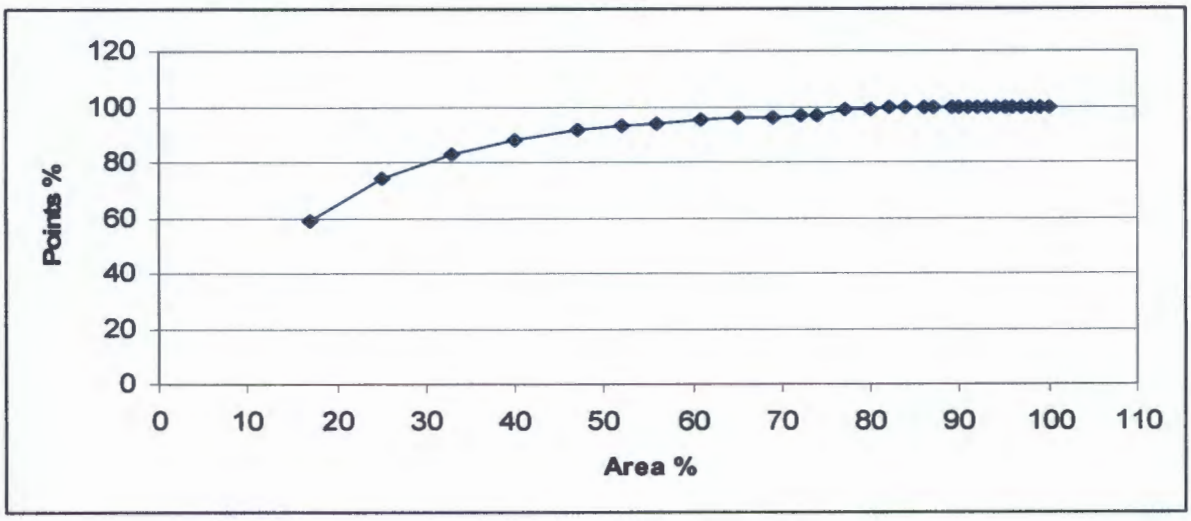

Figure 5.3b: Percentage of gold deposits (points) versus the total area (percentage) at successive distance away from combined brittle faults and ductile shears.

In conclusion, there is no obvious spatial association between the gold deposits and brittle faults (model A). The spatial association of model B and C shows similar results, indicating a maximum distance (cut-off value) of 5 km. Therefore, 5 km is applied uniformly over models A, B, and C. Thus, all structural maps are reclassified into binary maps: buffer distance < 5000m from faults and buffer > 5000m from fault (Appendix A2).

5.1.1.2 Integration of evidential theme patterns

In the WofE analyses, one of the assumptions is that evidential themes must be conditionally independent of each other. To check for CI, the "overall test" is used (section 4.3.3.2). Model A shows a conditional independence of 1, whilst for Model B and Model C the conditional independence is 0.5 and 0.63, respectively. Although Model B and C violate the assumption of CI, the evidential themes are not rejected, as the resulted posterior probability is "inflated" but the rankings of the cell are the same (Appendix A2). Rejecting an evidential theme pattern or combining themes is statistically correct, but in this case is considered inappropriate. The evidential theme patterns pertain to real geological features that are responsible for gold distribution in the area.

Posterior probability maps are generated for all three models (Figs. 5.4a-5.6a). The favourability maps are symbolized by 6 breaks from lowest (blue) to highest (red) probability. Uncertainty maps of the posterior probability, based on one standard deviation, are presented as Figure 5.4b-5.6b. Uncertainty maps show regions where the favourability estimates are relatively uncertain, due to the effects of uncertainty in the weights, and/or uncertainty due to missing information. Note that the patterns in all three maps are very similar. The resulted posterior probability of model B and C are higher than model A. This "inflated" posterior probability is probably due to the violation of CI.

The uncertainty in model B and C (Fig. 5.5b and 5.6b) is greater than model A (Fig. 5.4b). The edge effect (western border of the craton) is much less in model B and C than model A. Also note that the uncertainty in model B and C increases more or less by "1" standard deviation. This is probably due to the posterior probability that is "inflated" (violation of CI). The validity study is based on model B.

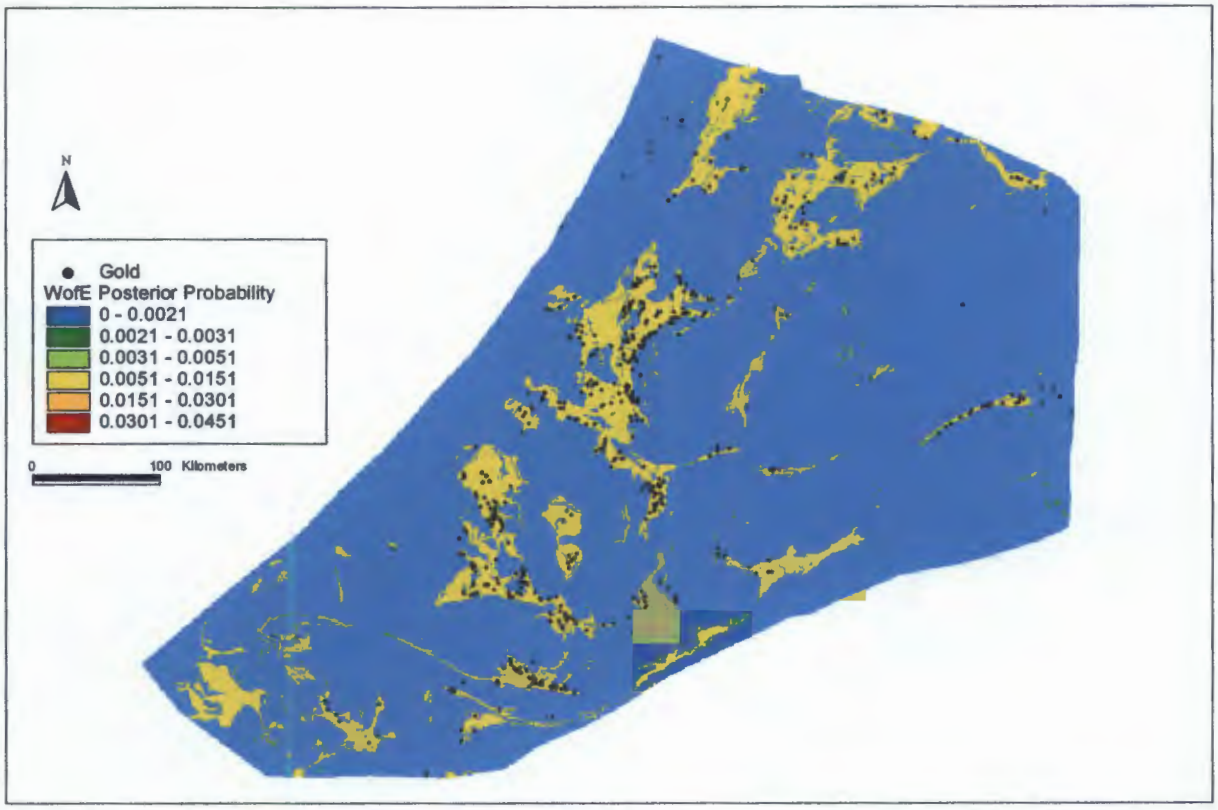

Figure 5.4a: Model A – Posterior probability map of gold deposits based on reclassified lithologies and brittle faults. [CI = 1]

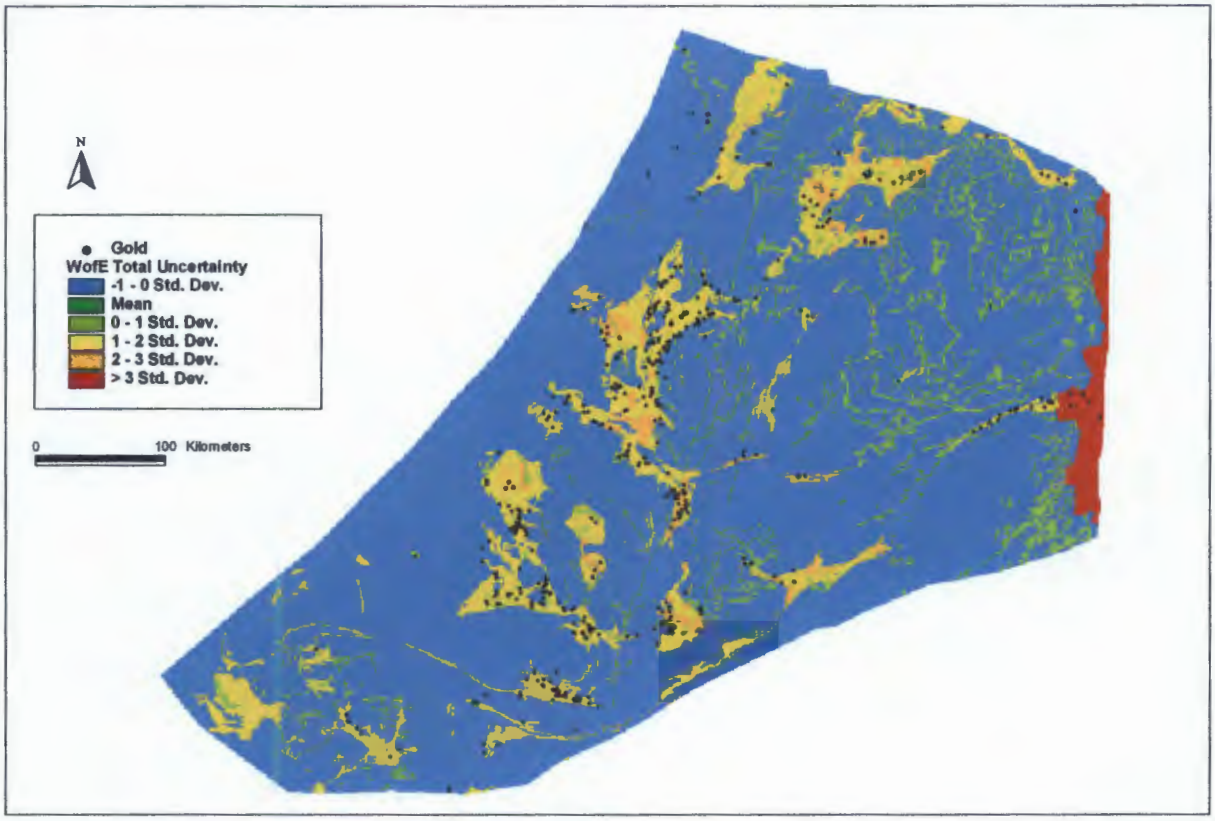

Figure 5.4b: Model A - Total uncertainty map of gold deposit, expressed in standard deviation units.

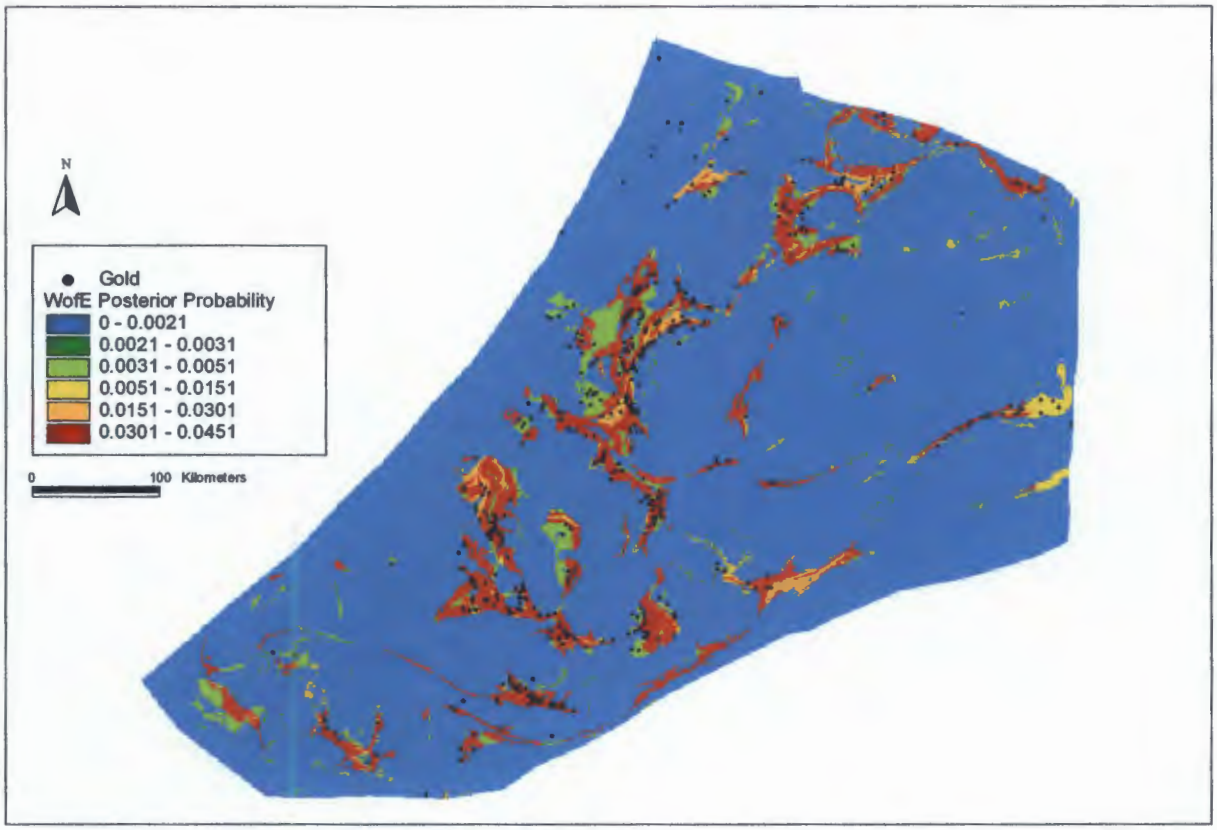

Figure 5.5a: Model B – Posterior probability map of gold deposits based on reclassified lithologies and ductile shears. [CI = 0.5]

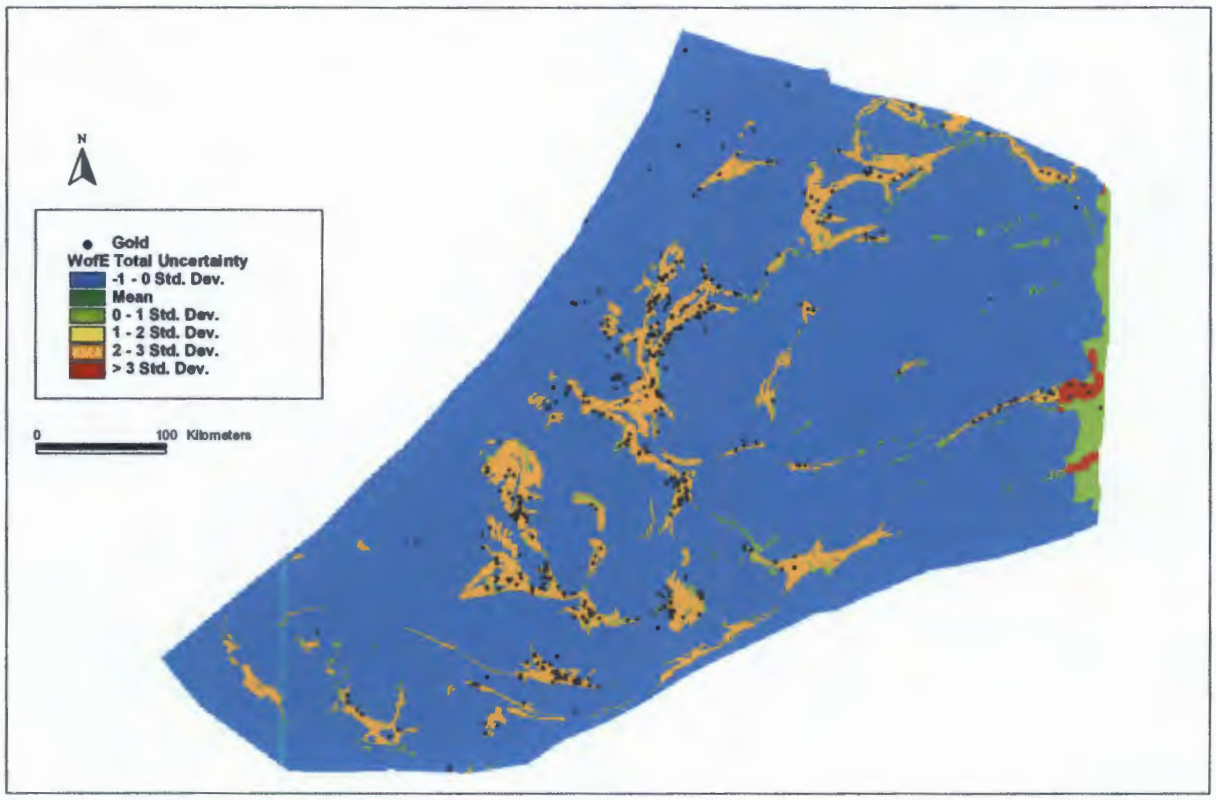

Figure 5.5b: Model B - Total uncertainty map of gold deposit expressed in standard deviation units.

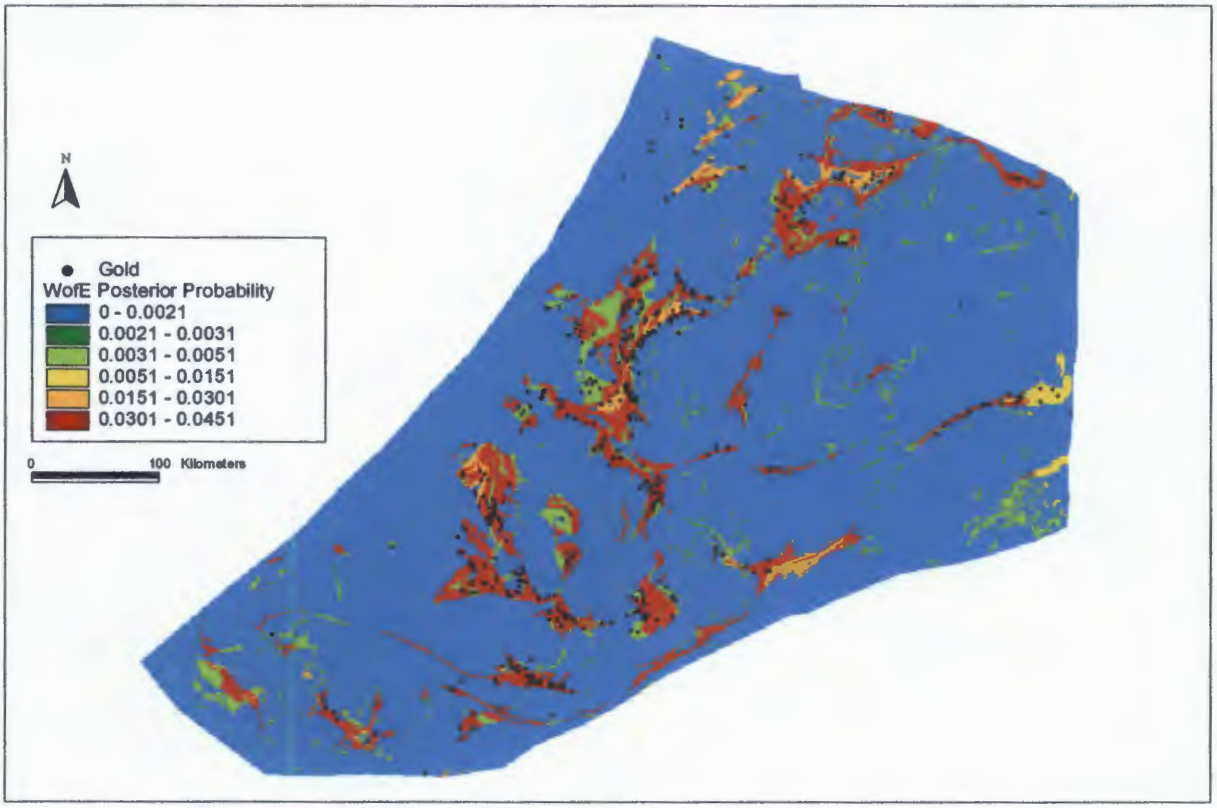

Figure 5.6a: Model C – Posterior probability map of gold deposits based on reclassified lithologies and combined brittle faults and ductile shears. [CI = 0.63]

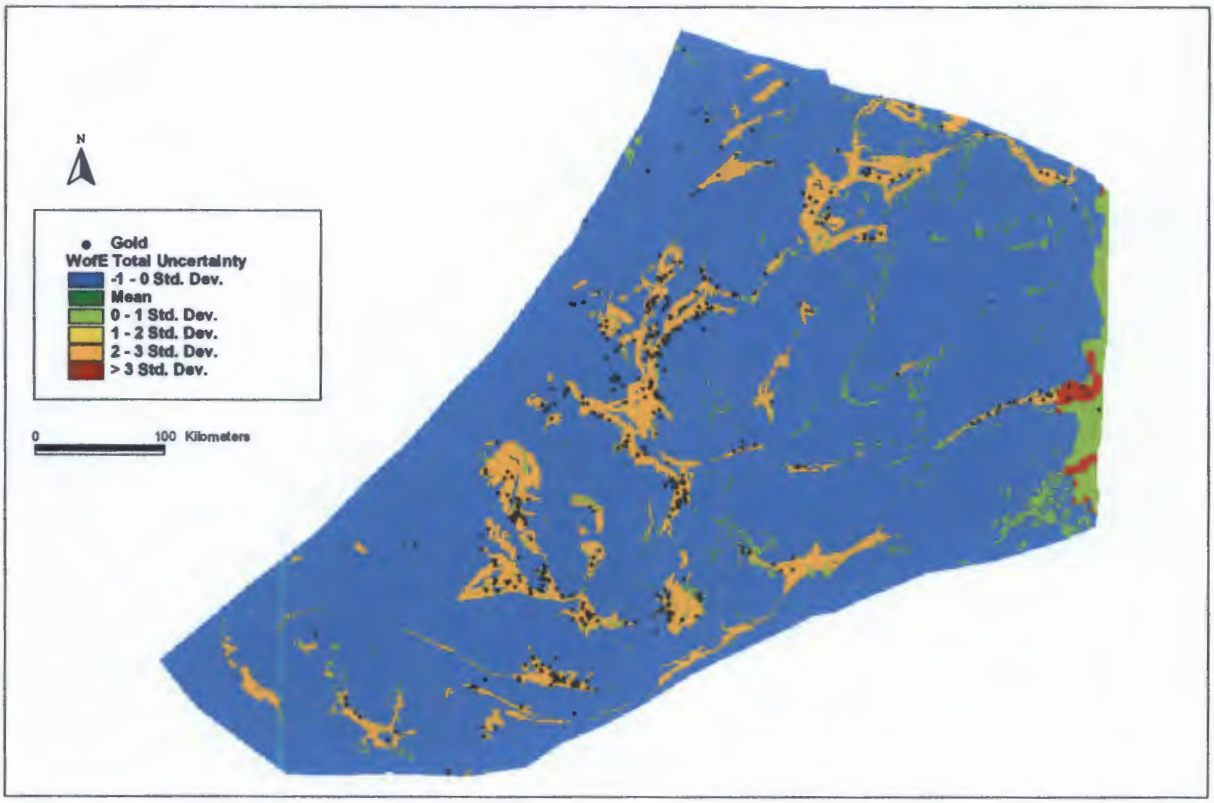

Figure 5.6b: Model C - Total uncertainty map of gold deposit expressed in standard deviation units.

5.1.1.3 Validation of results

The mineral potential map of model B is validated against a random set (124) of mineral deposits not used to generate the probabilistic model (Fig 5.7). In the resulting map, 54% of the validation deposits fall in most favourable area for gold. Only 13% of the deposits fall in the random area (blue < prior probability). The results, therefore, empirically validate the potential map.

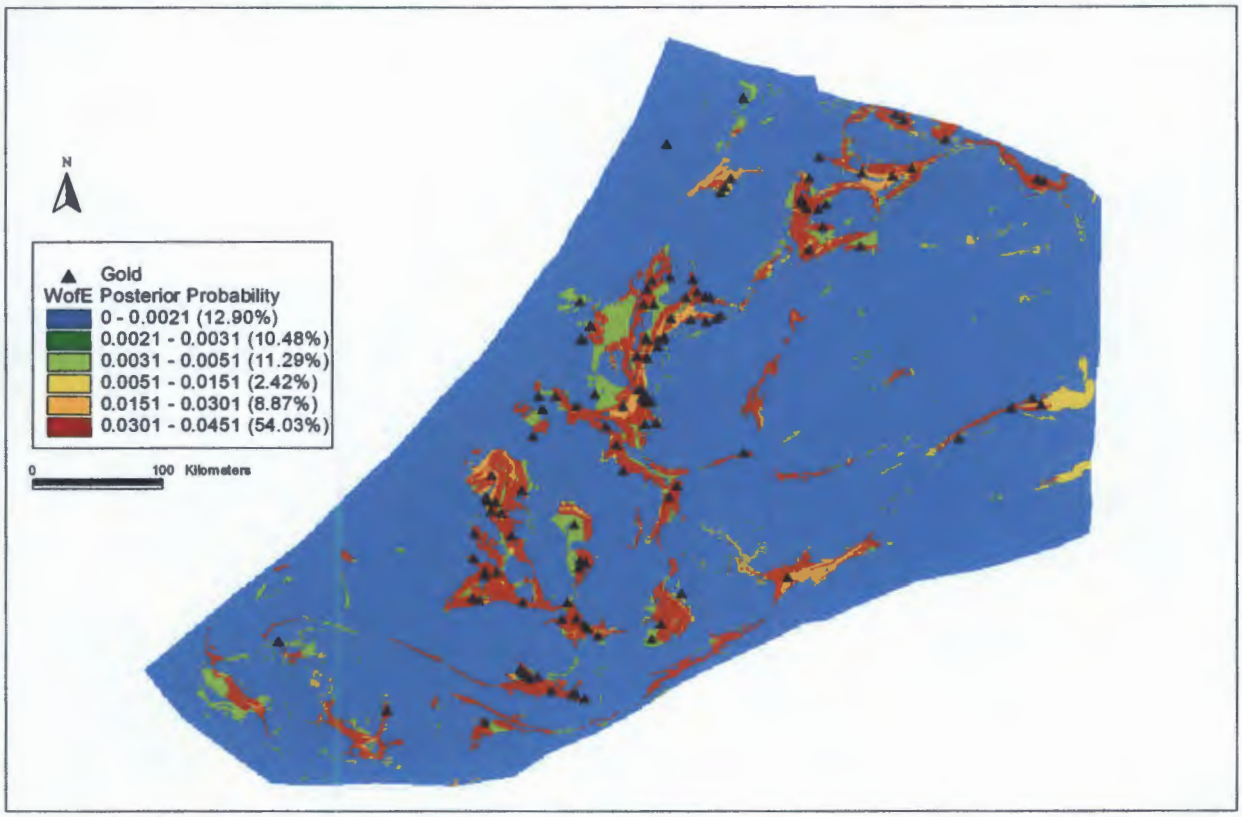

Figure 5.7: Model B – Posterior probability map for gold deposit with validation deposits superimposed. The percentage (%) of gold deposits that fall within each unit are indicated in the legend. Note that only 13% of the known gold deposits fall in "no-favourable" areas.

5.1.2 CrNiPGETi

In the training area, only 108 CrNiPgeTi deposits are present, with the prior probability equals to 0.00044. The number of CrNiPgeTi deposits in the training area is too small to be divided into two subsets to facilitate validation.

5.1.2.1 Reclassification of evidential theme patterns

The simplified geology map is reclassified into lithological units in order to calculate the positive weights and negative weights of evidence (Table 5.3a). Based on contrast values of weights, the lithologic units were reclassified into four classes (Table 5.3b): very favourable (1), favourable (2), random (3), negative association (4). The Great Dyke unit show the highest positive association capturing 38 deposits in a relatively small area in comparison with other classes. The unit with no data is grouped with the Great Dyke into a single class, because this unit contains only 1 deposit in a very small area. The greenstone belt-dominantly volcanic unit contains 26 deposits in a large area and the contrast value is therefore lower than the very favourable group. The third class is random, and the fourth class contains classes with negative contrast values as well as those containing missing data or zero mineral points.

The brittle faults and ductile shears show no spatial association with the CrNiPgeTi deposits (and are not shown here). Intuitively this might be expected because CrNiPgeTi deposits are generally associated with magmatic intrusions (e.g. Hutchinson, 1992; Herrington et al., 1997). The lithology, therefore, provides a better spatial association with mineralization than distance from or along particular faults or shears in the region. Thus, brittle faults and ductile shears results are not used as a predictive theme because they lacked geological significance and the contrast value are not definitive.

CLASS	S_VALUE	AREA_SQ_KM	NO_POINTS	WPLUS	S_WPLUS	WMINUS	S_WMINUS	CONTRAST	S_CONTRAST	STUD_CNT	
7	Great Dyke	2850	38	3.3881	0.1633	-0.4217	0.1195	3.8097	0.2024	18.8238	1
9	No data	466	1	1.5501	1.0011	-0.0073	0.0967	1.5574	1.0057	1.5485	
2	Greenstone Belt - dominantly volcanics	24923	26	0.8277	0.1962	-0.1642	0.1105	0.9920	0.2252	4.4053	2
6	Greenstone Belt - dominantly sediments	5224	4	0.5182	0.5002	-0.0154	0.0981	0.5336	0.5097	1.0468	
5	Post-tectonic intrusives	13133	8	0.2893	0.3537	-0.0199	0.1000	0.3092	0.3675	0.8412	3
3	Pre- and Syn-tectonic granitoids	74378	21	-0.4800	0.2182	0.1610	0.1072	-0.6410	0.2432	-2.6359	
4	Post-tectonic granitoids	73630	9	-1.3173	0.3334	0.2857	0.1005	-1.6030	0.3482	-4.6040	
1	Younger Cover	41727	1	-2.9468	1.0000	0.1847	0.0967	-3.1315	1.0047	-3.1169	4
8	undifferentiated	406	0								
-99	Missing Data	3807	0								
		240544	108								

Table 5.3a. Weights table for CrNiPgeTi deposits from WofE applied to lithologic map of the Zimbabwe Craton

CLASS	DESCRIPTION	AREA_SQ_KM	NO_POINTS	WPLUS	S_WPLUS	WMINUS	S_WMINUS	CONTRAST	S_CONTRAST	STUD_CNT
1	Very favourable	3316	39	3.3881	0.1633	-0.4217	0.1195	3.8097	0.2024	18.8238
2	Favourable	24923	26	0.8277	0.1962	-0.1642	0.1105	0.9920	0.2252	4.4053
3	Random	93141	33	-0.2529	0.1741	0.1354	0.1155	-0.3883	0.2089	-1.8583
4	Negative association	119164	10	-1.6610	0.3162	0.5712	0.1011	-2.2322	0.3320	-6.7236

Table 5.3b. Weights table for CrNiPgeTi deposits of lithologic units reclassified into 4 classes (Zimbabwe Craton)

5.1.2.2 Predictive mineral potential maps

A final posterior probability map is based on the lithology theme alone (Figure 5.8a). All areas that show posterior probabilities greater than the prior probability (0.0004) are favourable, whereas values less than the prior probability are relatively unfavourable. The posterior probability map is symbolized by 4 breaks from lowest (blue) to highest (red) probability. An uncertainty map based on one standard deviation is presented as Figure 5.8b, showing six standard deviation breaks from lowest (blue) to highest (red) uncertainty. It is interesting to note that the Great Dyke (area with highest probability) also shows the highest uncertainty, probably because only one evidential theme is used in this analysis. Also note the edge effect in Figure 5.8b, similar to that of Figure 5.4b.

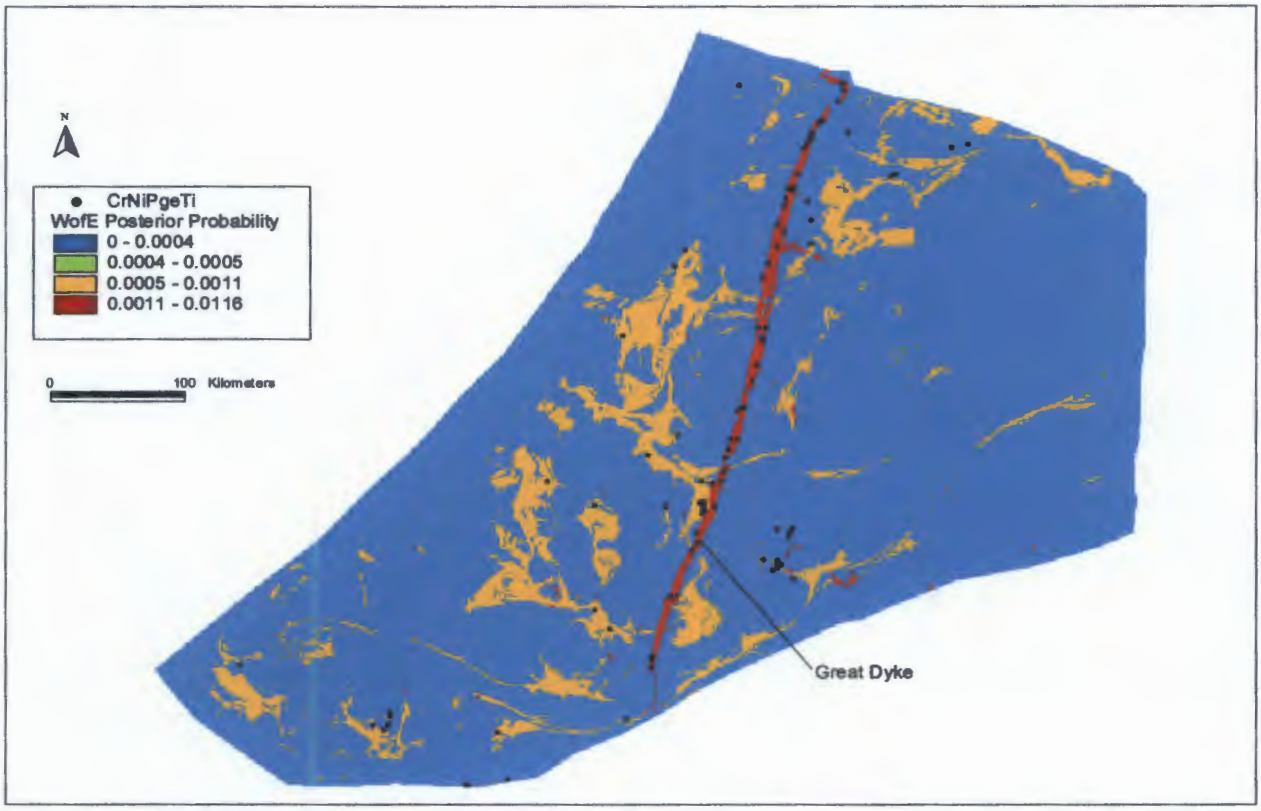

Figure 5.8a: Posterior probability map of CrNiPgeTi deposit model. Note predominant association of this element group with the mafic-ultramafic magmatic deposits of the Great Dyke.

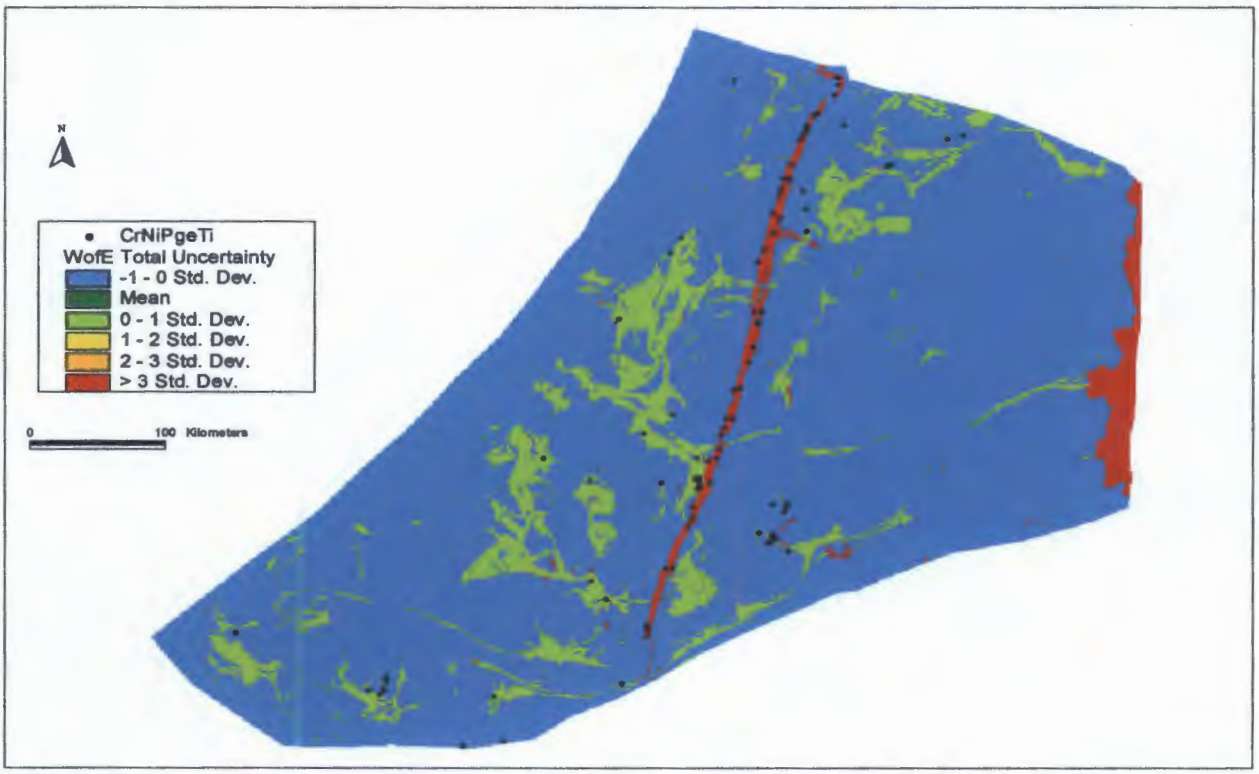

Figure 5.8b: Total uncertainty map of CrNiPgeTi deposit model symbolized in standard deviation units. Also note the high uncertainty associated with the Great Dyke.

5.1.3 CuZnPbBa

In the training area the total number of CuZnPbBa deposits is 97, and the prior probability equals 0.0004.

5.1.3.1 Reclassification of evidential theme patterns

The simplified geological map is reclassified into lithological units to calculate the weights of evidence (Table 5.4a). Based on the contrast value, numbers of points and weights values, the lithological units are reclassified into four classes (Table 5.4b). These classes show that the greenstone belt-dominantly volcanic unit shows the highest positive association capturing 33 known CuZnPbBa deposits. The post-tectonic intrusives unit also show positive association with 14 deposits but the contrast value is lower than for the greenstone belt-dominantly volcanics. The third class is random, and the fourth class consists of all classes with negative contrast values, as well as those containing no mineral points.

The CuZnPbBa mineral deposits show a negative spatial association with ductile or brittle faults. Thus, brittle faults and ductile shears are not used as evidential themes. Therefore, the lithology theme is the strongest (and only) predictor theme. Expert knowledge (de Wit, personal communication) suggests CuZnPbBa mineralization has an association with one of the following processes: plutonic, hydrothermal, volcanic or sedimentary. This broadly covers the entire spectrum of base-metal deposit types, which in turn implies that such mineralization is not confined to one particular tectonic domain.

CLASS	S_VALUE	AREA_SQ_KM	NO_POINTS	WPLUS	S_WPLUS	WMINUS	S_WMINUS	CONTRAST	S_CONTRAST	STUD_CNT	
2	Greenstone Belt - dominantly volcanics	24923	33	1.1947	0.1742	-0.3156	0.1270	1.5103	0.2156	7.0057	1
5	Post-tectonic intrusives	13133	14	0.9777	0.2674	-0.1024	0.1111	1.0801	0.2896	3.7298	2
1	Younger Cover	41727	20	0.1777	0.2237	-0.0425	0.1155	0.2202	0.2517	0.8749	
6	Greenstone Belt - dominantly sediments	5224	2	-0.0471	0.7072	0.0010	0.1037	-0.0481	0.7148	-0.0673	3
7	Great Dyke	2850	1	-0.1343	1.0002	0.0015	0.1032	-0.1358	1.0055	-0.1351	
3	Pre- and Syn-tectonic granitoids	74378	17	-0.5630	0.2426	0.1801	0.1133	-0.7431	0.2677	-2.7759	
4	Post-tectonic granitoids	73630	8	-1.3068	0.3536	0.2847	0.1072	-1.5915	0.3695	-4.3075	
8	undifferentiated	406	0								4
9	No data	466	0								
-99	Missing Data	3807	2								
		240544	97								

Table 5.4a. Weights table for CuZnPbBa deposits from WofE applied to lithologic map of the Zimbabwe Craton

CLASS	DESCRIPTION	AREA_SQ_KM	NO_POINTS	WPLUS	S_WPLUS	WMINUS	S_WMINUS	CONTRAST	S_CONTRAST	STUD_CNT
1	Very favourable	24923	33	1.1947	0.1742	-0.3156	0.1270	1.5103	0.2156	7.0057
2	Favourable	13133	14	0.9777	0.2674	-0.1024	0.1111	1.0801	0.2896	3.7298
3	Random	49801	23	0.1406	0.2086	-0.0410	0.1179	0.1816	0.2396	0.7582
4	Negative association	152687	27	-0.8714	0.2000	0.6863	0.1196	-1.5577	0.2330	-6.6844

Table 5.4b. Reclassified weights table for CuZnPbBa deposits (Zimbabwe Craton)

5.1.3.2 Predictive mineral potential maps

The posterior probability map is based only on the lithology theme. The posterior probabilities are classified by 4 breaks from lowest (blue) to highest (red) probability (Fig. 5.9a). A total uncertainty map of CuZnPbBa deposit model is presented in Figure 5.9b. It is noted that the probability of the base metal deposits in the NW part of the craton are probably mostly related to the fact that this mineralization occurs in Paleoproterozoic carbonates, a lithology not-identified in this study of the Lomagondi belt rocks which are Mesoproterozoic in age (Master, 1990).

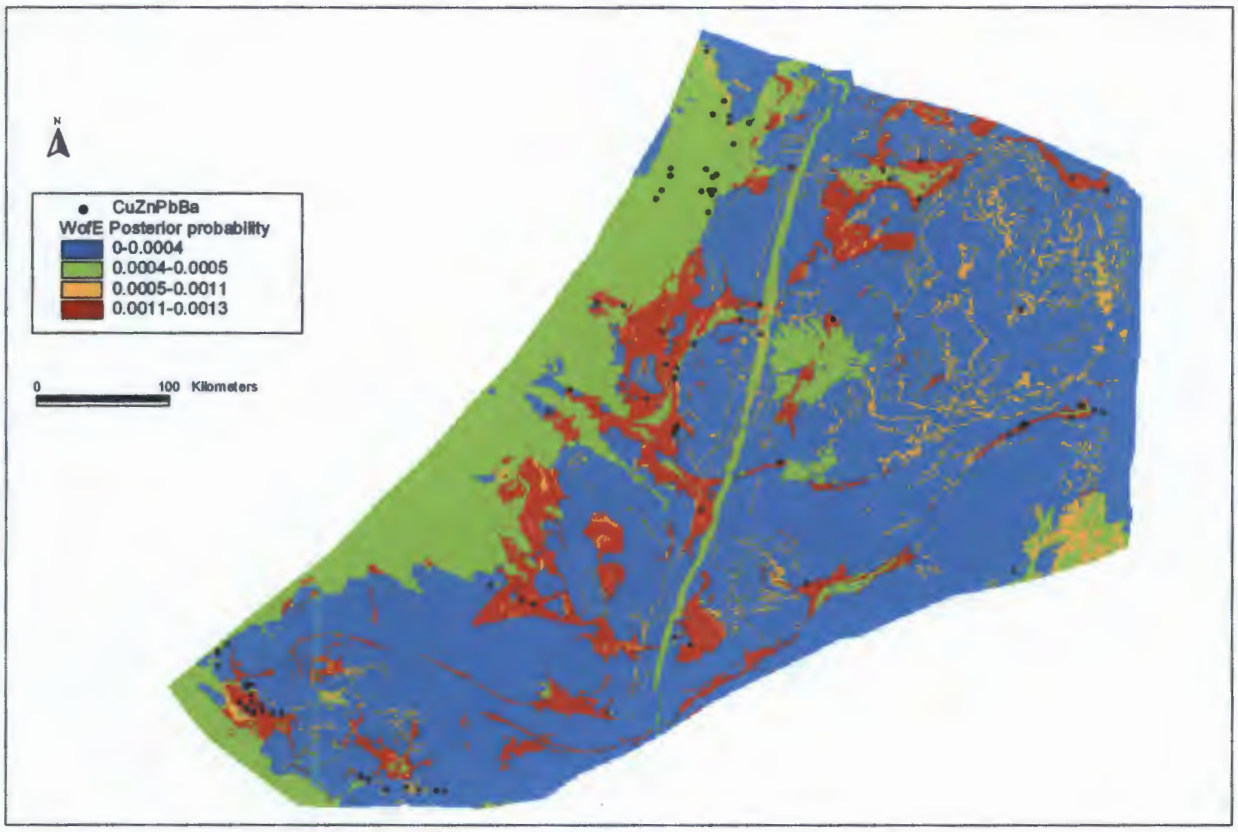

Figure 5.9a: Posterior probability map of CuZnPbBa deposit.

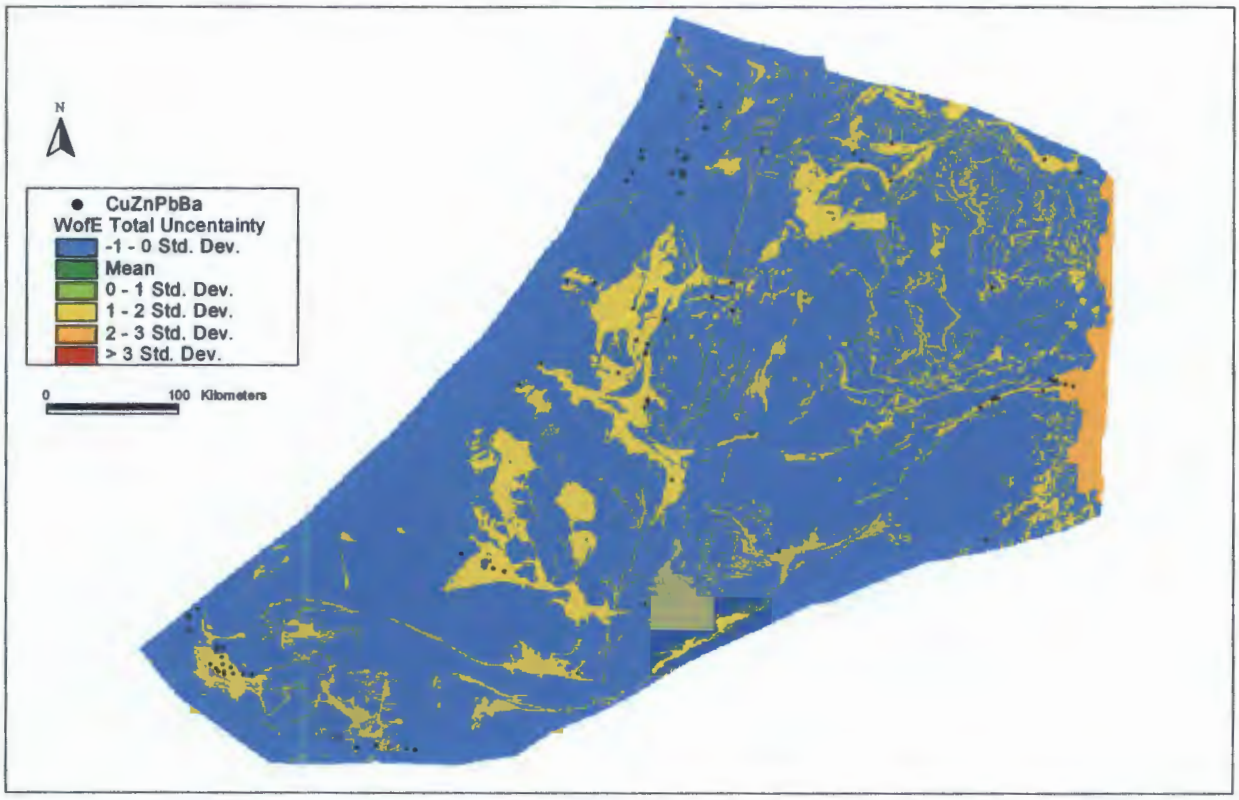

Figure 5.9b: Total uncertainty map of CuZnPbBa deposit expressed in one standard deviation units.

5.1.4 SnSb deposit model

Only 66 known SnSb deposits are present in the Zimbabwe craton, and prior probability is 0.0003.

A new third evidential theme is created based on the possible occurrence of tin mineralization close to the igneous contacts of granitoids (pre-and syn-tectonic granitoids; post-tectonic granitoids). SnSb mineralization is most often found in close association with granitoid rocks (primarily in veins or as replacement deposits, sometimes disseminated or concentrated as stockwork deposits (e.g. Taylor, 1979)). Therefore, it may be expected that during the emplacement of the granitoids, SnSb mineralization was concentrated and distributed close to the contacts between the greenstone belts and the granitoids.

5.1.4.1 Reclassification of evidential theme patterns

Two evidential themes are used to create a prediction map for SnSb deposits, the lithology and the granitoid-contacts maps. First, the simplified lithologic map is reclassified into lithological units to calculate the weights of evidence (Table 5.5a). Based on contrast values, number of points, area and weight values, the lithological units is reclassified into 4 classes (Table 5.5b). From the given tables, the greenstone belt-dominantly volcanic unit shows a positive association with 45 deposits. The greenstone belt-dominantly sediments unit also shows a positive spatial association, with 3 deposits, but with a lower contrast value than shown with the volcanics. The third class is random, and the fourth class consists of all the classes with negative contrast values as well as those containing zero mineral points.

CLASS	S_VALUE	AREA_SQ_KM	NO_POINTS	WPLUS	S_WPLUS	WMINUS	S_WMINUS	CONTRAST	S_CONTRAST	STUD_CNT	
2	Greenstone Belt - dominantly volcanics	24923	45	1.8697	0.1492	-1.0341	0.2182	2.9038	0.2644	10.9841	1
6	Greenstone Belt - dominantly sediments	5224	3	0.7229	0.5775	-0.0242	0.1260	0.7472	0.5911	1.2640	2
5	Post-tectonic intrusives	13133	5	0.3117	0.4473	-0.0217	0.1281	0.3334	0.4653	0.7166	3
1	Younger Cover	41727	6	-0.6622	0.4083	0.0986	0.1291	-0.7608	0.4282	-1.7768	
3	Pre- and Syn-tectonic granitoids	74378	7	-1.0861	0.3780	0.2651	0.1302	-1.3512	0.3998	-3.3800	4
4	Post-tectonic granitoids	73630	0								
7	Great Dyke	2850	0								
8	undifferentiated	406	0								
9	No data	466	0								
-99	Missing Data	3807	0								
		240544	66								

Table 5.5a. Weights table for SnSb deposits from WofE applied to lithologic map of the Zimbabwe Craton

CLASS	DESCRIPTION	AREA_SQ_KM	NO_POINTS	WPLUS	S_WPLUS	WMINUS	S_WMINUS	CONTRAST	S_CONTRAST	STUD_CNT
1	Very favourable	24923	45	1.8697	0.1492	-1.0341	0.2182	2.9038	0.2644	10.9841
2	Favourable	5224	3	0.7229	0.5775	-0.0242	0.1260	0.7472	0.5911	1.2640
3	Random	54860	11	-0.3297	0.3015	0.0813	0.1349	-0.4110	0.3303	-1.2442
4	Negative association	155537	7	-1.7991	0.3780	0.9125	0.1302	-2.7116	0.3998	-6.7828

Table 5.5b Reclassified weights table for SnSb deposits (Zimbabwe Craton)

The second evidential theme is a granitoid-contacts theme. First, a series of buffer zones, each arbitrarily chozen with a 1000m width, were constructed around the granitoid contacts before performing the analysis. The WofE process is run through the buffer distances in order to maximize the spatial association between the SnSb deposits and granitoid-contacts (Fig. 5.10)

The cumulative results (Table 5.6; Fig 5.10) show that contrast values are maximized at a distance of 8000m away from the granitoid-contacts capturing 60 of the 66 deposits. The studentized contrast at 8 km is 2.08. Therefore, it may be concluded that the buffered pattern of granitoid-contacts is probably a good predictive theme, confirming that SnSb deposits form close to granitoid-contacts.

CLASS	AREA_SQ_KM	NO_POINTS	WPLUS	S_WPLUS	WMINUS	S_WMINUS	CONTRAST	S_CONTRAST	STUD_CNT
1000	89173	26	0.0608	0.1961	-0.0376	0.1581	0.0984	0.2520	0.3906
2000	118505	37	0.1292	0.1644	-0.1438	0.1857	0.2731	0.2480	1.1009
3000	142590	44	0.1175	0.1508	-0.2003	0.2132	0.3178	0.2611	1.2168
4000	157662	50	0.1449	0.1414	-0.3517	0.2500	0.4965	0.2873	1.7285
5000	171791	52	0.0982	0.1387	-0.2983	0.2673	0.3965	0.3011	1.3168
6000	180340	55	0.1058	0.1349	-0.4067	0.3015	0.5125	0.3303	1.5514
7000	187107	55	0.0689	0.1349	-0.2874	0.3015	0.3563	0.3303	1.0788
8000	193493	60	0.1224	0.1291	-0.7664	0.4083	0.8888	0.4282	2.0755
9000	198787	60	0.0954	0.1291	-0.6470	0.4083	0.7424	0.4282	1.7337
10000	203184	60	0.0735	0.1291	-0.5357	0.4083	0.6092	0.4282	1.4227

Table 5.6 Cumulative analysis for granitoid-contacts.

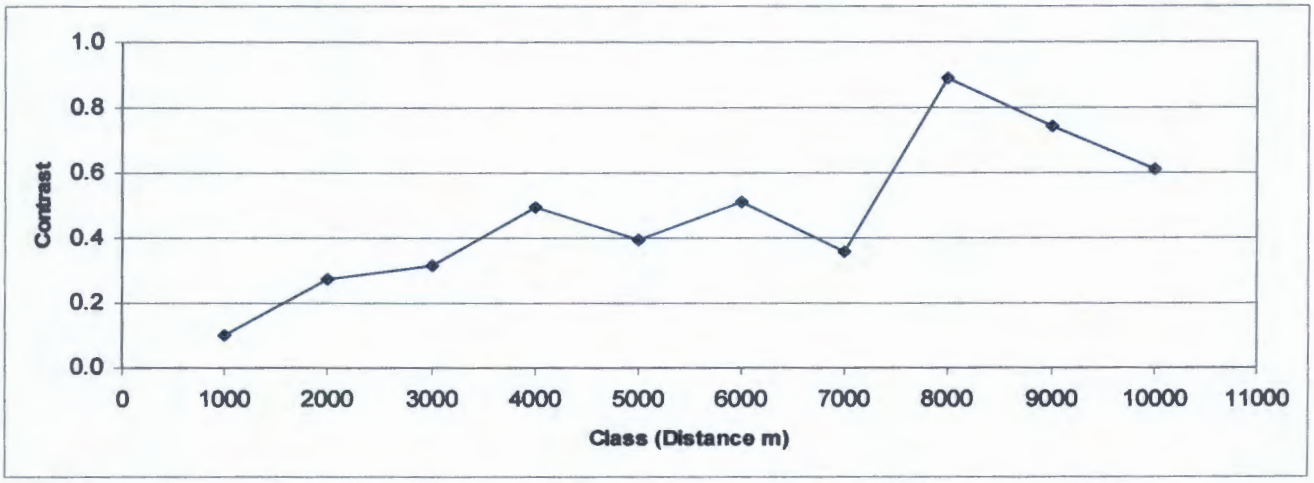

Figure 5.10. Variation of contrast of SnSb deposits versus buffer distance away from the granitoid-contacts. Note that the contrast reaches a maximum at a distance of about 8000m.

Based on the optimum buffer distance of 8km, the granitoids-contact theme is reclassified into binary pattern (near contact <8000m, and away contacts >8000m).

5.1.4.2 Integration of evidential theme patterns

The evidential themes (lithology and binary granitoid-contacts) are combined to produce SnSb potential map. Conditional independence is 0.99. A final posterior probability map is shown in Figure 5.11a. The posterior probabilities are classified by 4 breaks showing favourable (highest posterior probability) and unfavourable areas (lowest posterior probability). The SnSb mineralization is concentrated and distributed close to the contacts between the greenstone belts and the granitoids. A total uncertainty map of SnSb deposit is presented in one standard deviation unit (Figure 5.11b).

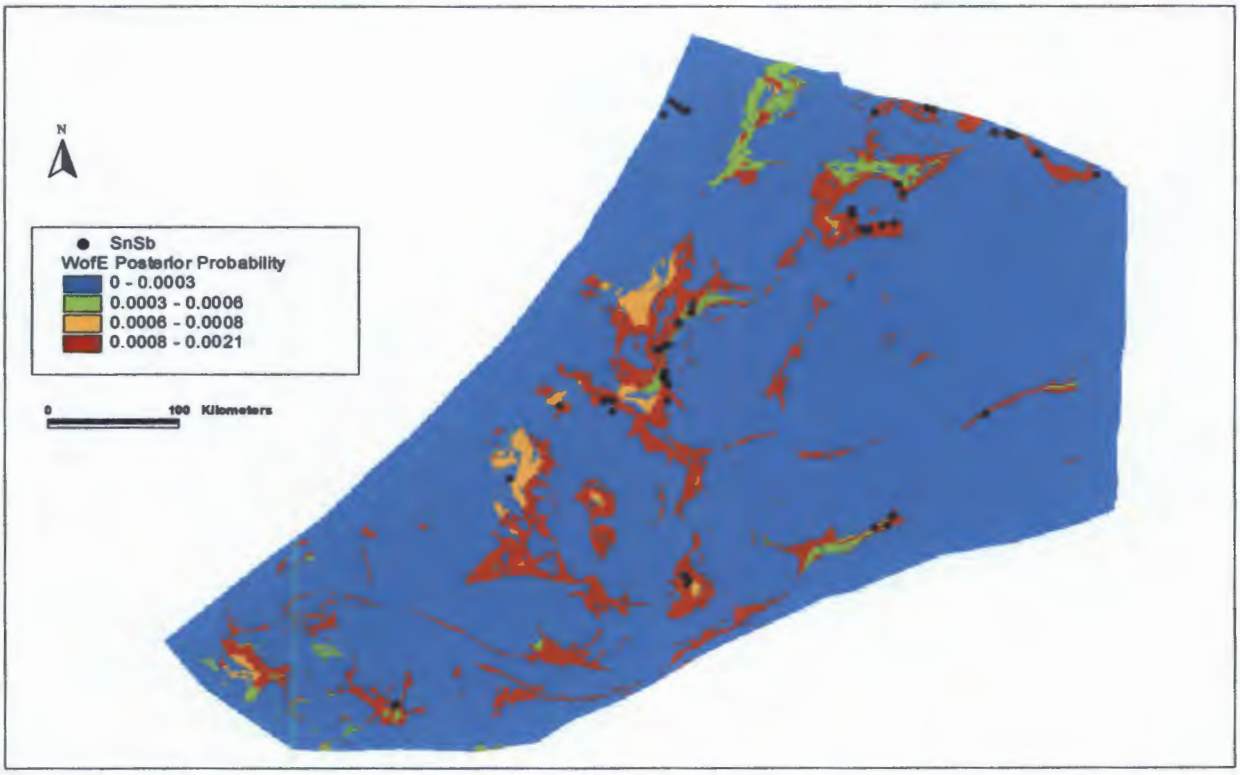

Figure 5.11a: Posterior probability map of SnSb deposit based on reclassified lithologies and granitoid-contacts. [CI = 0.99].

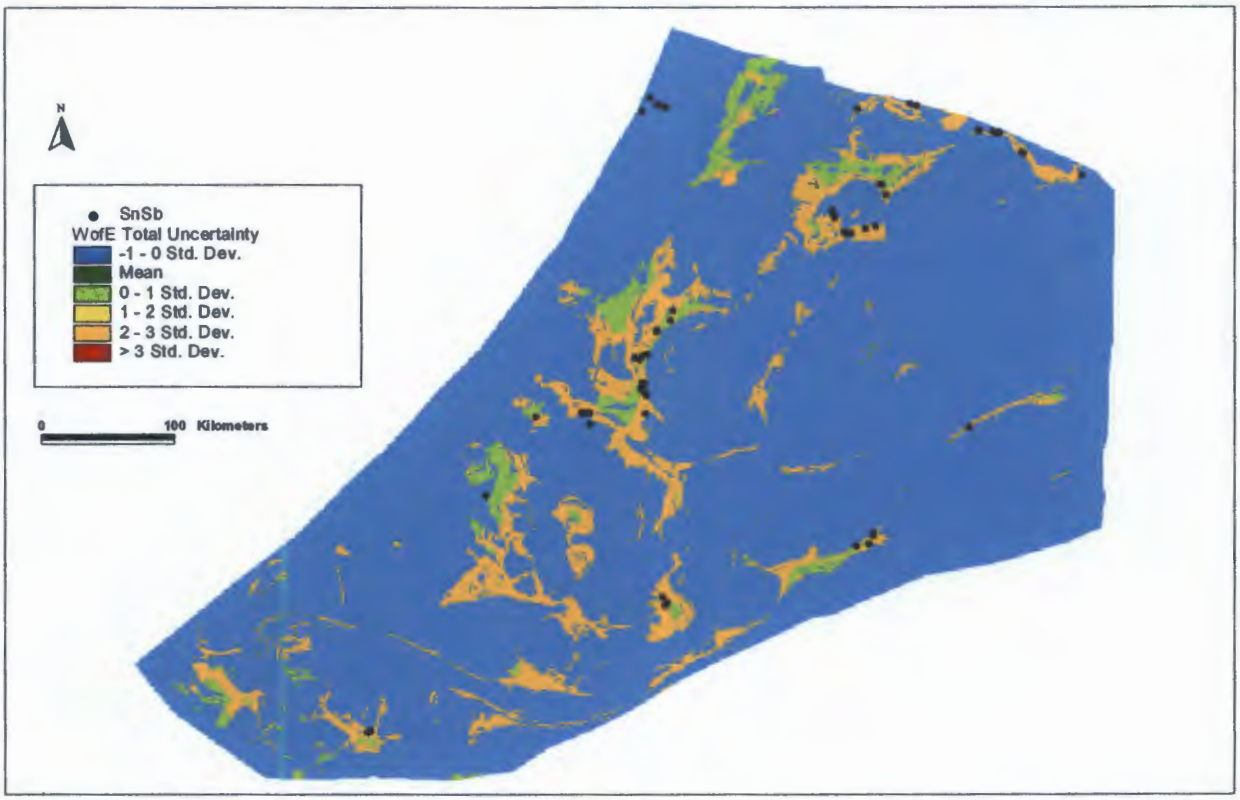

Figure 5.11b: Total uncertainty map of SnSb deposit expressed in one standard deviation units.

5.1.5 W

In the training area the total number of tungsten (W) is 275 deposits, and the prior probability is equals to 0.0011.

Tungsten (W) deposits may be formed similarly to SnSb deposits. A similar evidential theme is created based on the granitoids-contacts. Previous studies have explained that it is evident, that SnSb and W deposits are often found in association with granitoids rocks, primarily in vein type (hydrothermal) deposits (e.g. Dixon, 1979).

5.1.5.1 Reclassification of evidential theme patterns

Two evidential themes are used to create a prediction map for W deposits. The simplified geology map is reclassified into lithological units in order to calculate the weights of evidence (Table 5.7a). Based on contrast values of weights, the lithologic units were reclassified into four classes: very favourable, favourable, random, and negative association classes (Table 5.7b). The greenstone belt-dominantly volcanics unit show the highest positive association (highest contrast value) with 163 deposits. The unit with no data is grouped together with greenstone belt-dominantly volcanics (very favourable class), because this unit contains only 5 deposit with positive contrast value in a very small area. The third class is random, and the fourth class contains classes with negative contrast values as well as those containing no mineral points.

The evidential theme of granitoid-contacts shows a positive spatial association with the deposits. Results of analysis (Table 5.8; Fig. 5.12) show that the maximum contrast values form at an optimal distance of 8000m. The area encompasses 246 of 275 W deposits. Therefore, based on the optimum buffer distance the granitoid-contact map is reclassified into a binary map as was done for the SnSb deposits (near contacts < 8000m, and away contacts > 8000m).

CLASS	S_VALUE	AREA_SQ_KM	NO_POINTS	WPLUS	S_WPLUS	WMINUS	S_WMINUS	CONTRAST	S_CONTRAST	STUD_CNT	
2	Greenstone Belt - dominantly volcanics	24923	163	1.7335	0.0786	-0.7877	0.0945	2.5212	0.1229	20.5114	1
9	No data	466	5	2.2328	0.4496	-0.0164	0.0609	2.2492	0.4537	4.9571	
8	undifferentiated	406	1	0.7529	1.0012	-0.0019	0.0604	0.7548	1.0031	0.7525	
5	Post-tectonic intrusives	13133	19	0.2198	0.2296	-0.0145	0.0625	0.2343	0.2379	0.9847	2
6	Greenstone Belt - dominantly sediments	5224	6	-0.0113	0.4085	0.0003	0.0610	-0.0116	0.4130	-0.0281	
1	Younger Cover	41727	24	-0.7035	0.2042	0.1027	0.0632	-0.8062	0.2137	-3.7721	
4	Post-tectonic granitoids	73630	31	-1.0156	0.1796	0.2533	0.0641	-1.2689	0.1907	-6.6530	
3	Pre- and Syn-tectonic granitoids	74378	26	-1.2017	0.1962	0.2782	0.0634	-1.4799	0.2061	-7.1788	3
7	Great Dyke	2850	0								
-99	Missing Data	3807	0								
		240544	275								

Table 5.7a. Weights table for W deposits from WofE applied to lithologic map of the Zimbabwe Craton

CLASS	DESCRIPTION	AREA_SQ_KM	NO_POINTS	WPLUS	S_WPLUS	WMINUS	S_WMINUS	CONTRAST	S_CONTRAST	STUD_CNT
1	Favourable	25389	168	1.7453	0.0774	-0.8312	0.0967	2.5765	0.1239	20.8005
2	Random	18763	26	0.1766	0.1963	-0.0168	0.0634	0.1934	0.2062	0.9376
3	Negative association	192585	81	-1.0167	0.1111	1.3336	0.0720	-2.3503	0.1324	-17.7522

Table 5.7b. Reclassified weights table for W deposits (Zimbabwe Craton)

CLASS	AREA_SQ_KM	NO_POINTS	WPLUS	S_WPLUS	WMINUS	S_WMINUS	CONTRAST	S_CONTRAST	STUD_CNT
1000	89173	114	0.1119	0.0937	-0.0723	0.0789	0.1842	0.1225	1.5037
2000	118505	145	0.0680	0.0831	-0.0708	0.0878	0.1387	0.1209	1.1480
3000	142590	188	0.1428	0.0730	-0.2527	0.1073	0.3955	0.1297	3.0485
4000	157662	209	0.1482	0.0692	-0.3620	0.1231	0.5102	0.1413	3.6116
5000	171791	224	0.1317	0.0669	-0.4330	0.1401	0.5646	0.1552	3.6376
6000	180340	233	0.1225	0.0656	-0.4944	0.1544	0.6169	0.1677	3.6783
7000	187107	239	0.1110	0.0647	-0.5293	0.1667	0.6404	0.1788	3.5806
8000	193493	246	0.1064	0.0638	-0.6183	0.1858	0.7247	0.1964	3.6898
9000	198787	246	0.0793	0.0638	-0.4989	0.1858	0.5782	0.1964	2.9439
10000	203184	248	0.0655	0.0635	-0.4591	0.1925	0.5246	0.2027	2.5875

Table 5.8. Cumulative analysis for granitoid-contacts.

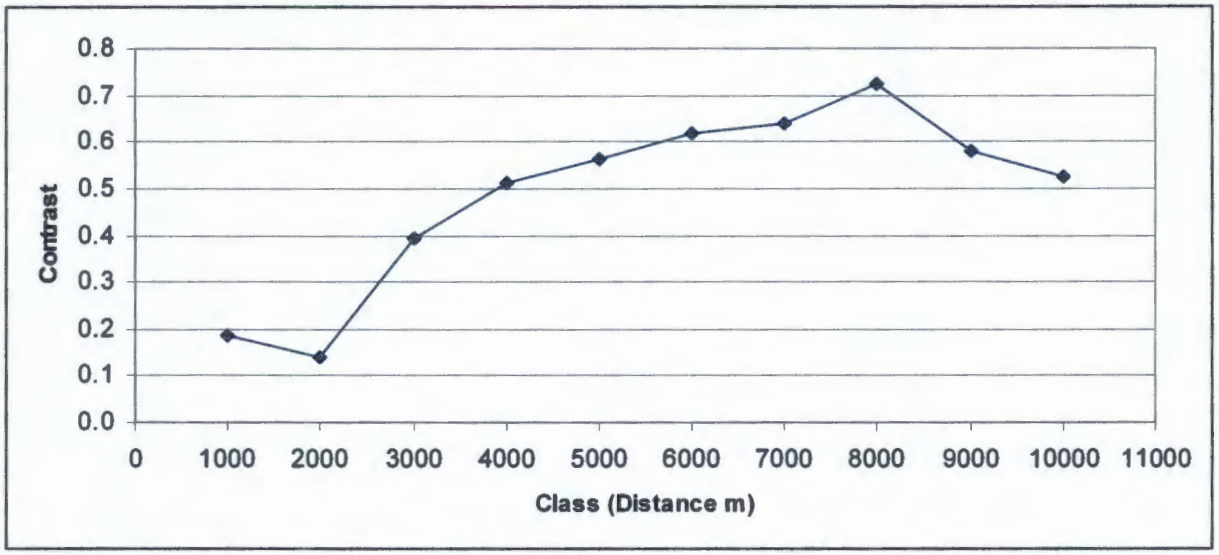

Figure 5.12. Variations of contrast of W deposits versus buffer distance away from the granitoid-contacts. Note that peak contrast value occurs at about 8000m distance.

5.1.5.2 Integration of evidential theme patterns

The two evidential themes (lithology and binary granitoid-contacts) are combined to produce W potential map. Conditional independence equals 0.97. A final posterior probability map is shown in Figure 5.13a. The posterior probabilities are classified by 4 breaks from lowest (blue) to highest (red) posterior probability, displaying similar pattern to SnSb, except that the post-tectonic intrusives for tungsten (W) show a random spatial association. This may be probably due to the ranking of posterior probabilities. A total uncertainty map of W deposit model is presented in Figure 5.13b, displaying uncertainty due to effects of weights of evidence.

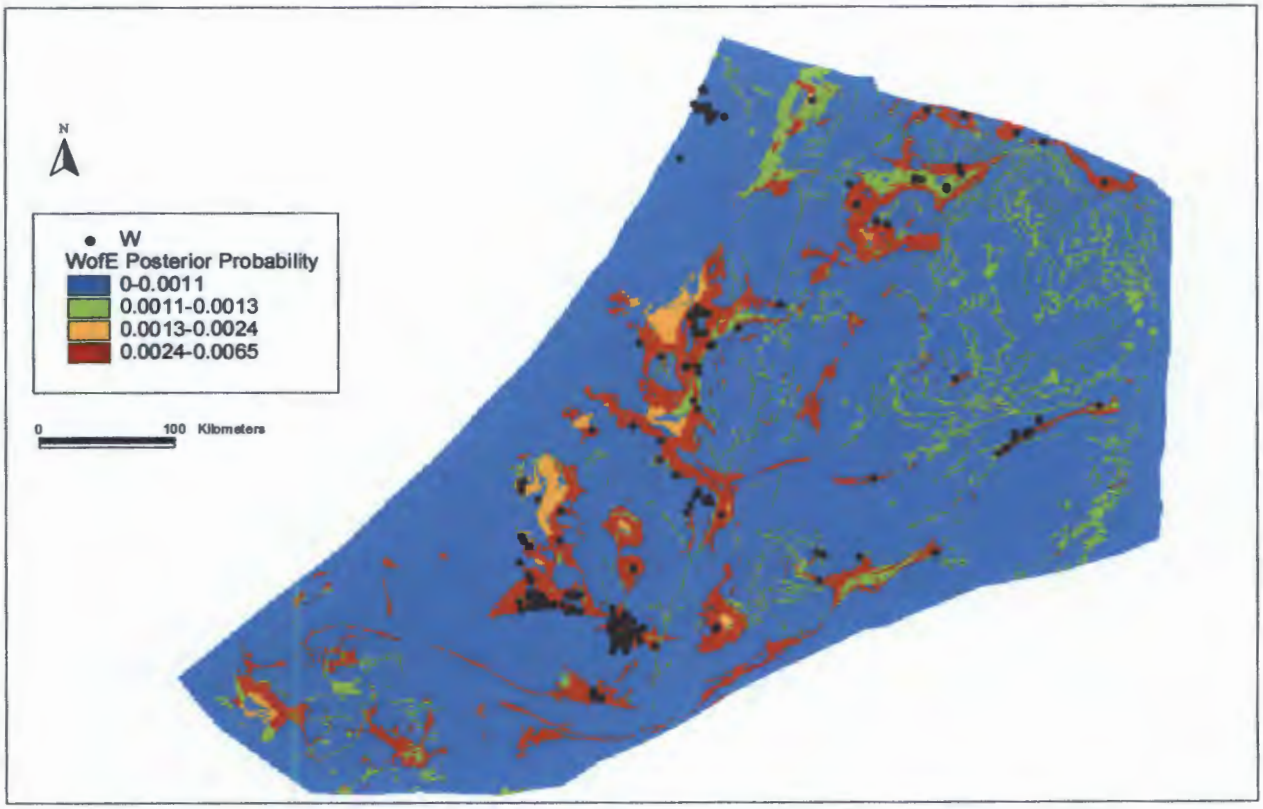

Figure 5.13a: Posterior probability map of W deposit based on reclassified lithologies and granitoid-contacts. [CI = 0.97].

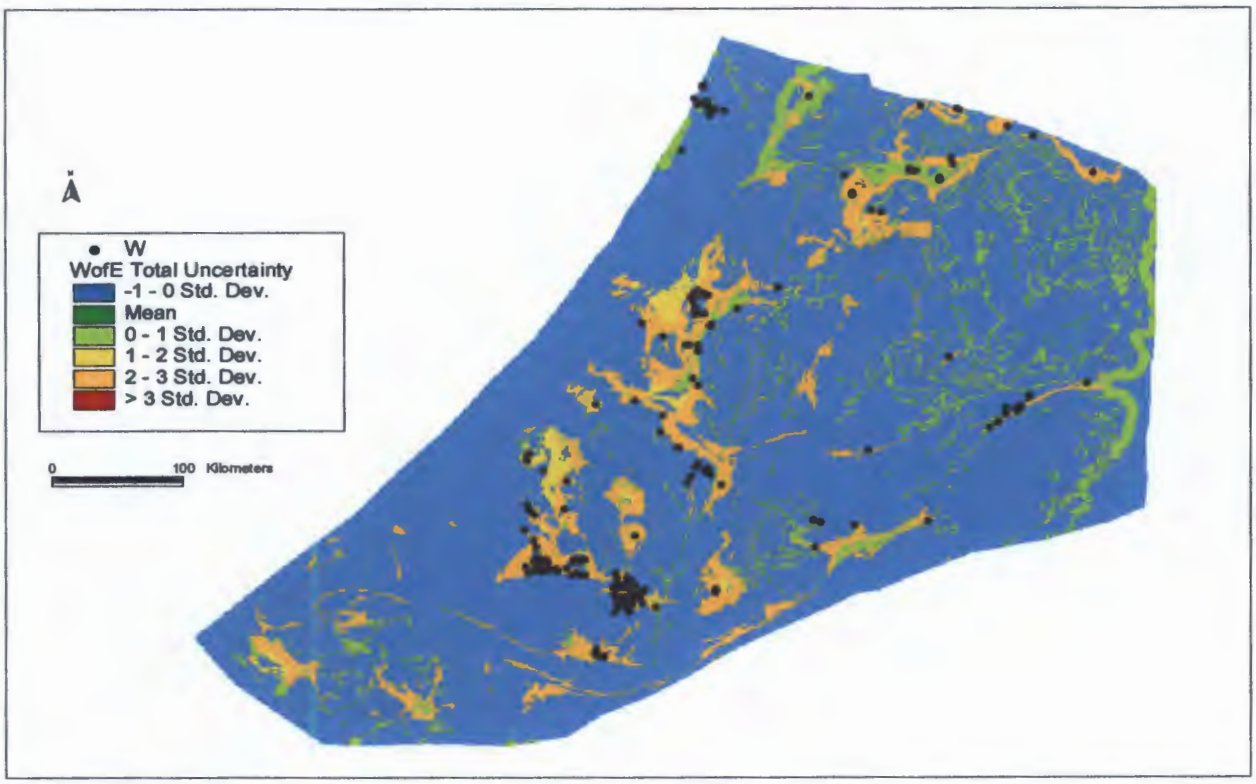

Figure 5.13b: Total uncertainty map of W deposit expressed in one standard deviation units. The uncertainty of the weights of evidence may reflect the fact that only the lithologies theme was used.

5.1.6 UThREE deposit model

Because the WofE method is very sensitive to the number of known deposits. The element group encompassing uranium, thorium, and rare earth elements are not analysed further because of the low number of deposits in the dataset of Zimbabwe. The relatively small numbers of mineral deposits in the study areas would result in large uncertainties in the weights, and the quantified association would be non-definitive.

5.2 The Paleoproterozoic Birimian Shield

The evidential themes used for the Birimian Shield include its simplified geology and faults. The total training area is 884 648 km^2 and the unit area equal 1 km^2. For reliable analysis to be applied, WofE requires a significant number of training points per unit area. The mineral deposits of CrNiPgeTi (38), SnSb (21) and W (5) and UThREE (32) are therefore not analysed in this region, because the total number of mineral deposits are too low relative to the size of the region.

5.2.1 Gold deposit

The total training area is 884 648 km^2, and the unit area equal to 1 km^2. In the training area the total number of known gold deposits is 441. This total number of gold deposits is divided randomly into two subsets. A subset of 353 (80%) of the 441 known gold deposits are used to generate posterior probability map, and the remaining subset of 88 (20%) of the 441 gold deposits is used to validate the probabilistic models. The prior probability is 0.0004.

5.2.1.1 Reclassification of evidential theme patterns

The geological themes used for creating a prediction map for gold are given in Table 5.9. The themes are divided into three spatial association models with common geology: Model A - Brittle and ductile faults (CGS), Model B - Brittle and ductile faults (De Beers) and

Model C - Merged brittle and ductile faults (CGS + De Beers). Three models were considered because the brittle faults and ductile shears are compiled from different sources (see Chapter 3). Unlike for Zimbabwe Craton, the Birimian Shield brittle faults and ductile shears are undifferentiated.

Model	Theme 1	Theme 2
Model A	Geology	Brittle and ductile faults (CGS)
Model B	Geology	Brittle and ductile faults (De Beers)
Model C	Geology	Merged faults (CGS + De Beers)

Table 5.9. Evidential themes used for spatial modelling of gold deposit.

The evidential theme of the simplified geology map (Fig. 3.2b) is reclassified into lithological units to calculate the weights of evidence; the results are shown in Table 5.10a. Based on the contrast value, the numbers of points, area and weights values, the lithologic units are reclassified into four classes. The greenstone belt-dominantly volcanics unit shows a positive association (C_w=1.6) with 125 known gold deposits (very favourable). The greenstone belt-dominantly sediments also show a slight positive association, with 135 known deposits (favourable) across a relatively large area. This could be expected because gold deposits occur more frequently in igneous-related rocks within the greenstone belt (e.g. Herrington et al., 1997). The third class is random, and the fourth class contains classes with negative contrast values as well as those containing undifferentiated data and zero mineral points. The new weights for the reclassified map are given in Table 5.10b.

The evidential themes (brittle faults and ductile shears) used for spatial modelling of gold deposits are discussed below under Model A, Model B, and Model C (Table 5.9).

CLASS	S_VALUE	AREA_SQ_KM	NO_POINTS	WPLUS	S_WPLUS	WMINUS	S_WMINUS	CONTRAST	S_CONTRAST	STUD_CNT	
2	Greenstone Belt - dominantly volcanics	86864	125	1.2822	0.0895	-0.3362	0.0665	1.6184	0.1115	14.5116	1
3	Greenstone Belt - dominantly sediments	228406	135	0.3915	0.0861	-0.1844	0.0681	0.5759	0.1097	5.2477	2
1	Younger Cover	78741	22	-0.3581	0.2132	0.0292	0.0551	-0.3873	0.2202	-1.7585	3
4	Syn- to Post-tectonic granitoids	295485	60	-0.6773	0.1291	0.2228	0.0586	-0.9001	0.1418	-6.3474	
5	Pre- and Syn-tectonic granitoids	21275	2	-1.4475	0.7071	0.0188	0.0535	-1.4663	0.7092	-2.0677	
6	Post-tectonic granitoids	164365	7	-2.2394	0.3780	0.1871	0.0539	-2.4265	0.3818	-6.3555	4
7	Undifferentiated	3126	0								
-99	Missing Data	6386	2								
		884648	353								

Table 5.10a. Weights table for gold deposits from WofE applied to lithologic map of the Birimian Shield

CLASS	DESCRIPTION	AREA_SQ_KM	NO_POINTS	WPLUS	S_WPLUS	WMINUS	S_WMINUS	CONTRAST	S_CONTRAST	STUD_CNT
1	Very favourable	86864	125	1.2822	0.0895	-0.3362	0.0665	1.6184	0.1115	14.5116
2	Favourable	228406	135	0.3915	0.0861	-0.1844	0.0681	0.5759	0.1097	5.2477
3	Random	395501	84	-0.6324	0.1091	0.3250	0.0612	-0.9574	0.1251	-7.6520
4	Negative association	173877	9	-2.2394	0.3780	0.1871	0.0539	-2.4265	0.3818	-6.3555

Table 5.10b. Reclassified weights table for gold deposits (Birimian Shield)

- **Model A: CGS faults**

The WofE method is applied to the CGS brittle and ductile faults (Model A) in order to find the buffer distance that maximize the spatial association between gold deposits and the faults. It is clear from Figure 5.14a that as the buffer area increase the contrast value decreases. The contrast values are also very small (<0.7), showing no spatial association between brittle faults and gold deposits. This is also illustrated in figure 5.14b where the plotted percentage of gold deposits (points) against percentage of area, increases proportional with the area.

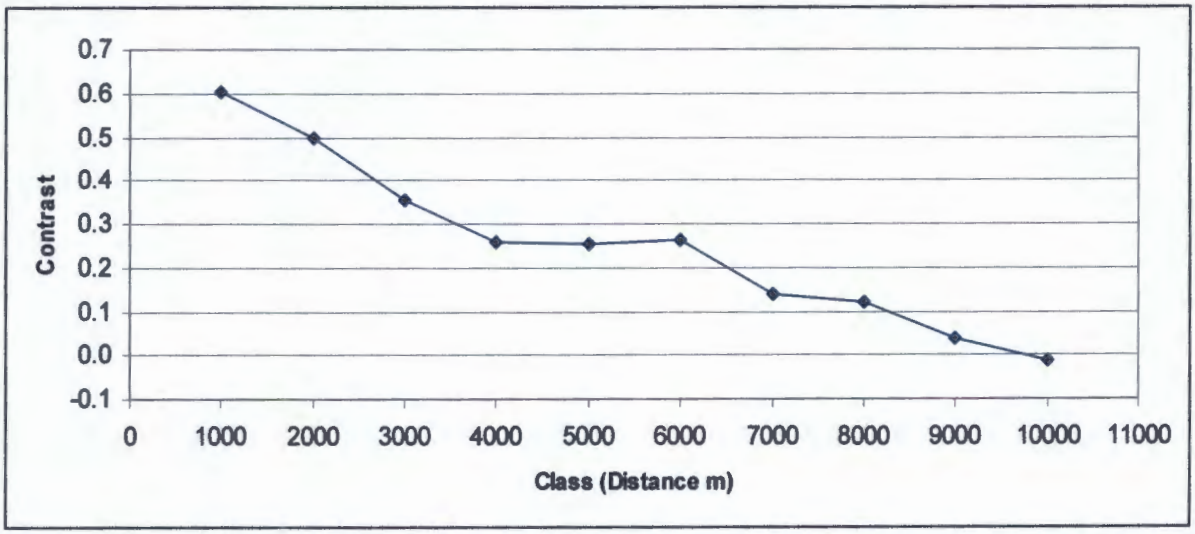

Figure 5.14a: Variation of contrast of gold deposits versus buffer distance away from the CGS brittle and ductile faults. Note that the contrast decreases strongly as the distance increases.

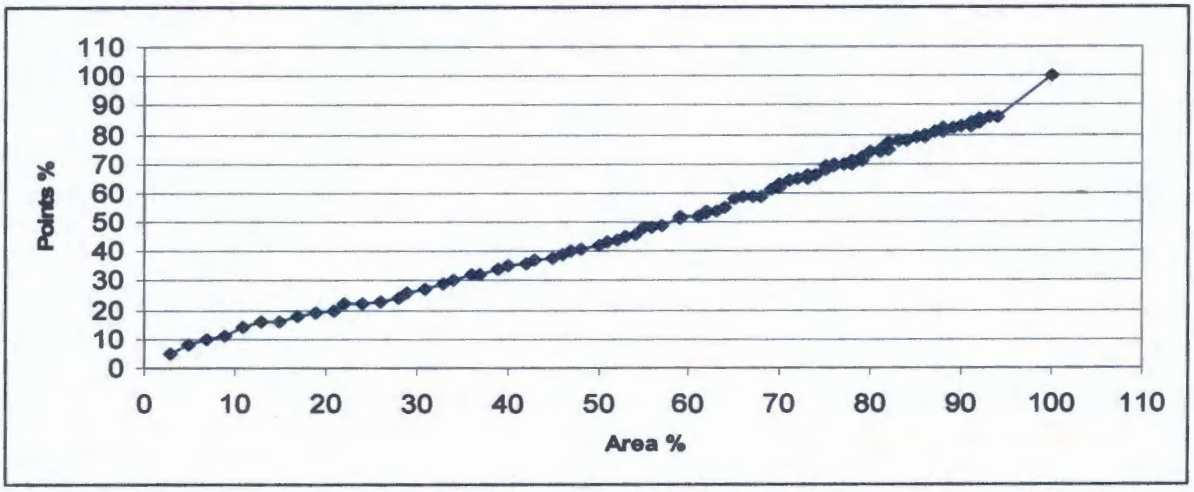

Figure 5.14b: Percentage of gold deposits (points) versus the total unit area percentage at successive distances away from the CGS brittle and ductile faults. Note that the number of deposit increases proportional with increasing total area.

- **Model B: De Beers faults**

The De Beers brittle and ductile faults (model B) show a higher contrast value than Model A with gold deposits for the first 4 km (Fig. 5.15a). No clear cut-off value is evident from figure 5.15a, therefore in order to standardize optimal distance, it was decided to use the same cut-off value of 5000m based on the more robust analyses of the ductile shears of the Zimbabwe Craton. Figure 5.15b. indicate that the percentage of gold deposits (points) increases near-linearly with increasing total area confirming no spatial association.

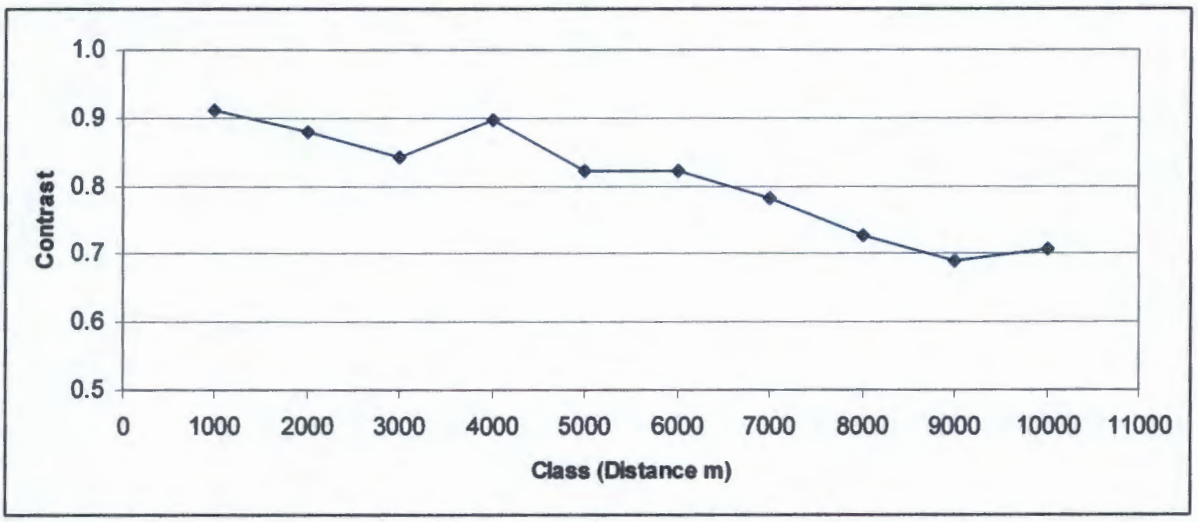

Figure 5.15a: Variation of contrast of gold deposits versus buffer distance away from the De Beers brittle and ductile faults. The contrast reaches an apparent maximum at a distance of 4000m, and decreases slightly as the distance away from the faults increases.

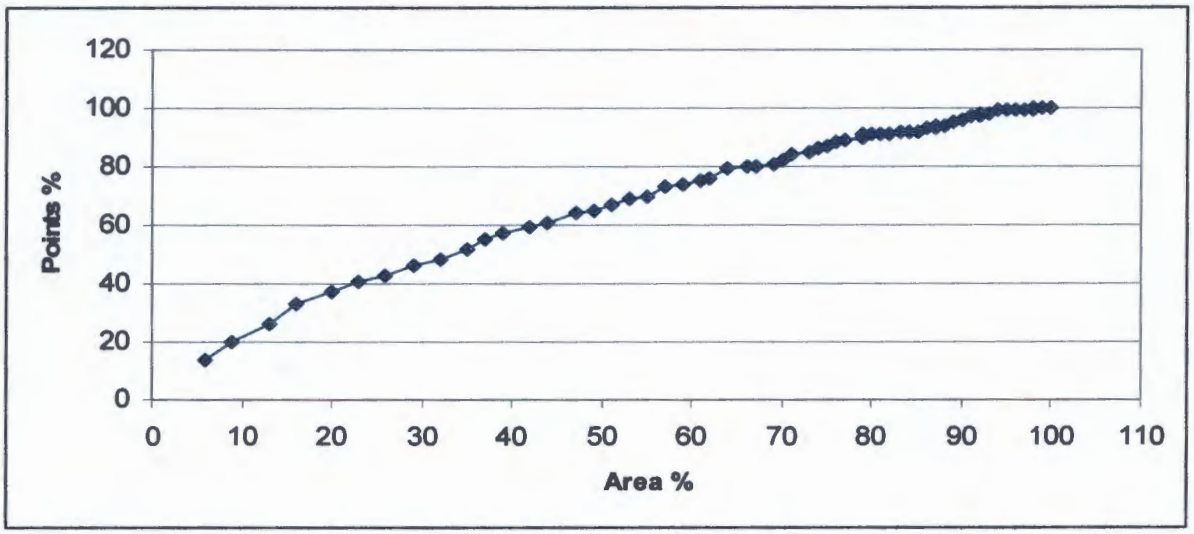

Figure 5.15b: Percentage of gold deposits (points) versus the total area (percentage) at successive distance away from the De Beers brittle and ductile faults. Note that the number of deposit increases near-linearly with increasing total area.

- **Model C: Merged CGS and De Beers faults**

The merged brittle and ductile faults (Model C) show a similar result as those for Model B. The contrast values are very low (<1.0). No clear cut-off value is evident from Figure 5.16a, therefore in order to standardize optimal distance, the same cut-off value of 5000m is applied based on the analyses of the ductile shears of the Zimbabwe Craton. Figure 5.16b. indicate that the percentage of gold deposits (points) increases near-linearly with increasing total area.

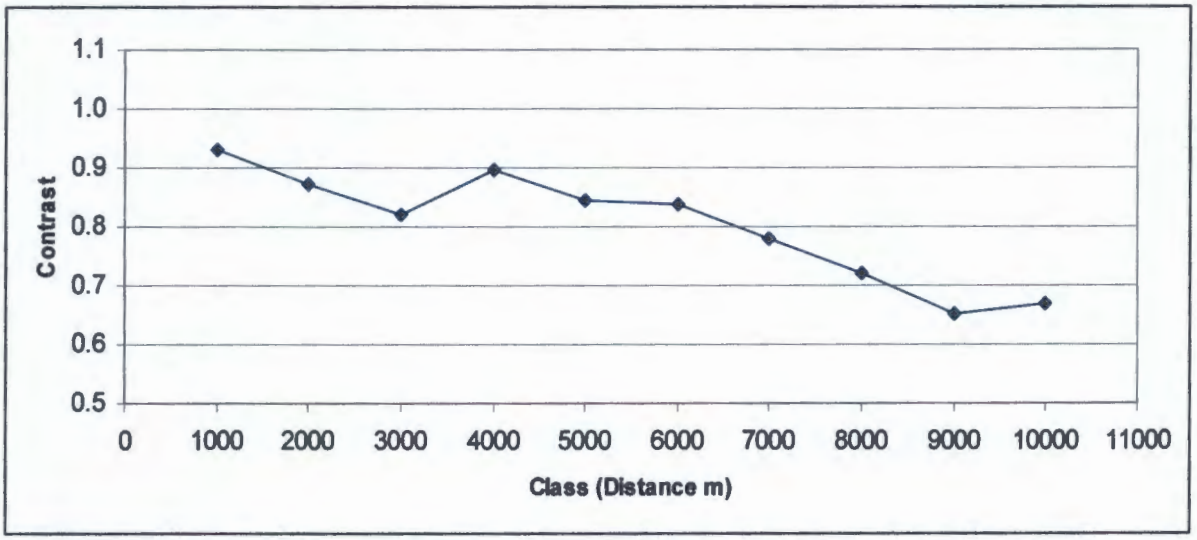

Figure 5.16a: Variation of gold contrast versus buffer distance away from the merged brittle and ductile faults (CGS + De Beers). The contrast reaches an apparent maximum at a distance of 4000m.

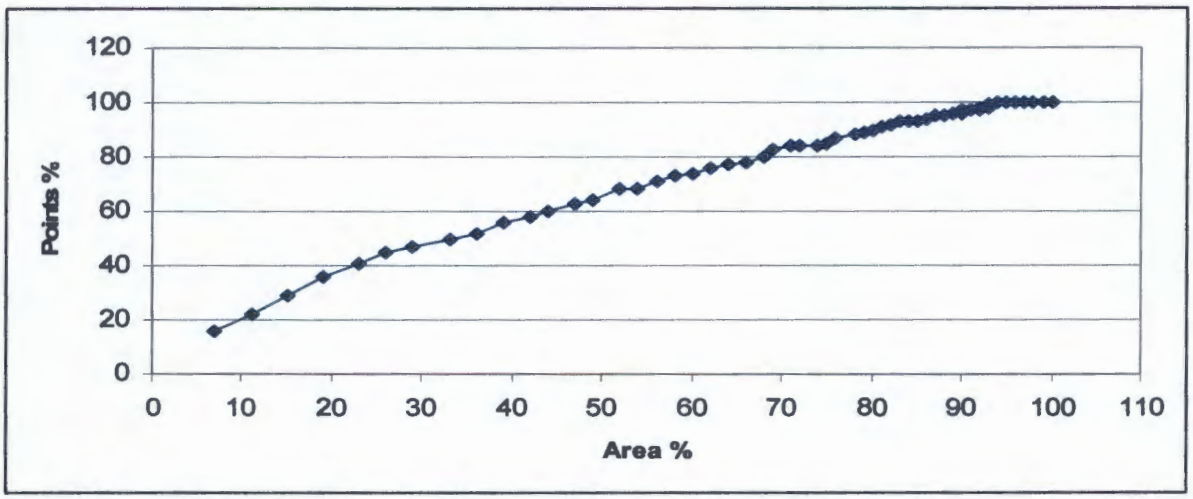

Figure 5.16b: Percentage of gold deposits (points) versus the total unit area percentage at successive distance away from merged brittle and ductile faults. Also, note that the number of deposit increases near-linearly with increasing total area.

The WofE analysis indicates that the gold deposits have low spatial association with the brittle and ductile faults (Fig. 5.14-5.16). It is likely that not all shear zones and faults have been mapped to the same degree as it is the case for the Zimbabwe Craton, because the outcrop in this relatively flat region of Africa is poor and often covered by thick laterites (Burke, 1996). Thus, there is no obvious spatial association between the gold deposits and brittle faults (model A-C). The spatial association of model B and C shows similar results, indicating a maximum distance (cut-off value) of 4 km. Based on the results of the Zimbabwe Craton cut-off distance is applied at 5 km uniformly over model A, B, and C. Thus, all structural maps are reclassified into binary maps: buffer distance < 5000m from faults and buffer > 5000m from fault (Appendix A3).

5.2.1.2 Integration of evidential theme patterns

The evidential themes patterns (lithological units, binary brittle faults or ductile shears) were combined to produce mineral potential map (Fig. 5.17-5.19). All models show conditional independence of the evidential themes, the CI is 1, 0.96, and 0.96 respectively. The posterior probability maps are symbolized by 5 breaks from lowest (blue) to highest (red) probability (Fig. 5.17a-5.19a). The posterior probabilities of model A show low spatial association, whereas model B and C have a slight better association with the deposits and the geology. The posterior probability maps of model B and C have increased, although the "patterns" in all models are similar.

The uncertainty maps of the posterior probability, based on one standard deviation breaks, are presented in Figure 5.17b-5.19b, showing regions where the favourability estimates are relatively uncertain. The uncertainty map of model A shows an edge effect in the south (towards the ocean). The higher uncertainty in models B and C are associated with higher posterior probabilities.

Similar to the gold mineralization of the Zimbabwe Craton, the posterior probability maps are also driven strongly by the lithologic theme (e.g. lithologies have strong predictive areal association with gold deposits). It is possible, therefore, that brittle and ductile faults are not as important as host for gold mineralization in the Birimian Shield (e.g Paleoproterozoic), as is the case for the Zimbabwe Craton (Archean).

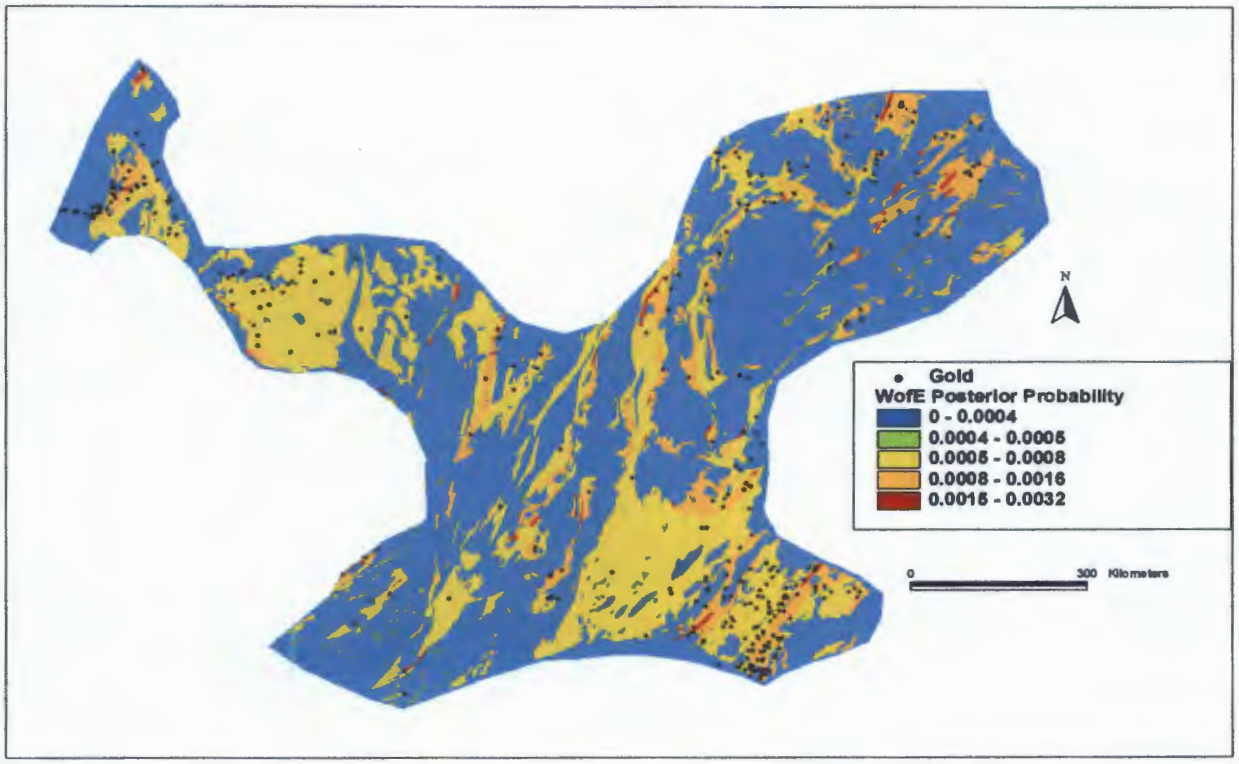

Figure 5.17a: Model A – Posterior probability map of gold deposits based on reclassified lithologies and CGS brittle and ductile faults. [CI = 1].

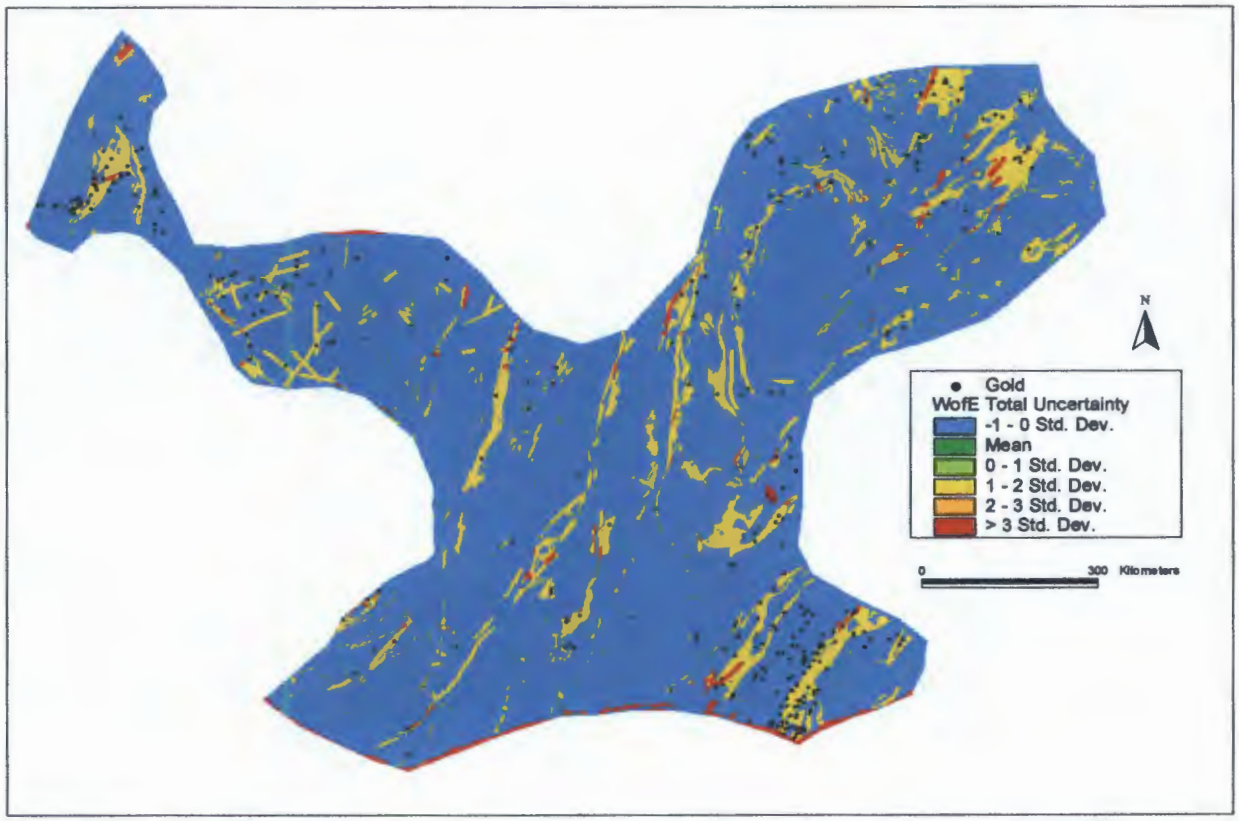

Figure 5.17b: Model A – Total uncertainty map of gold deposits, expressed in standard deviation units.

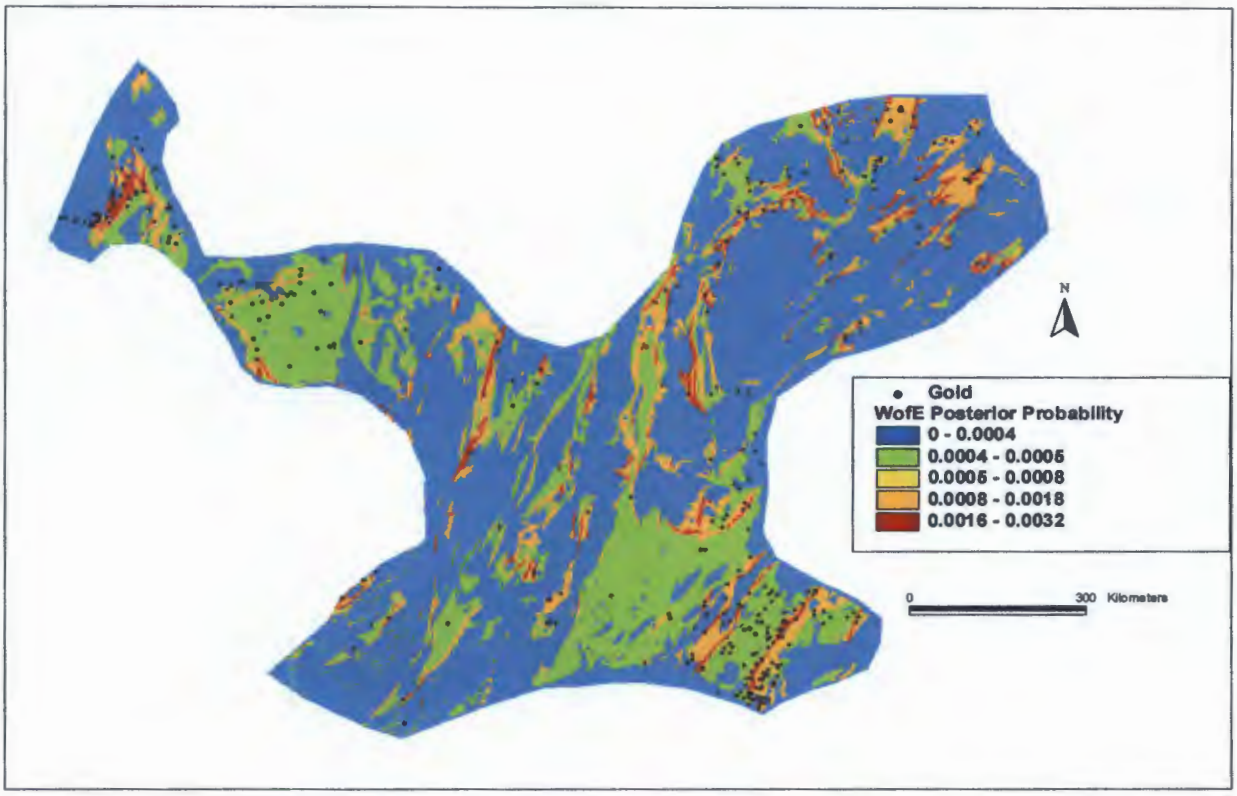

Figure 5.18a: Model B – Posterior probability map of gold deposits based on reclassified lithologies and De Beers brittle and ductile faults. [CI = 0.96].

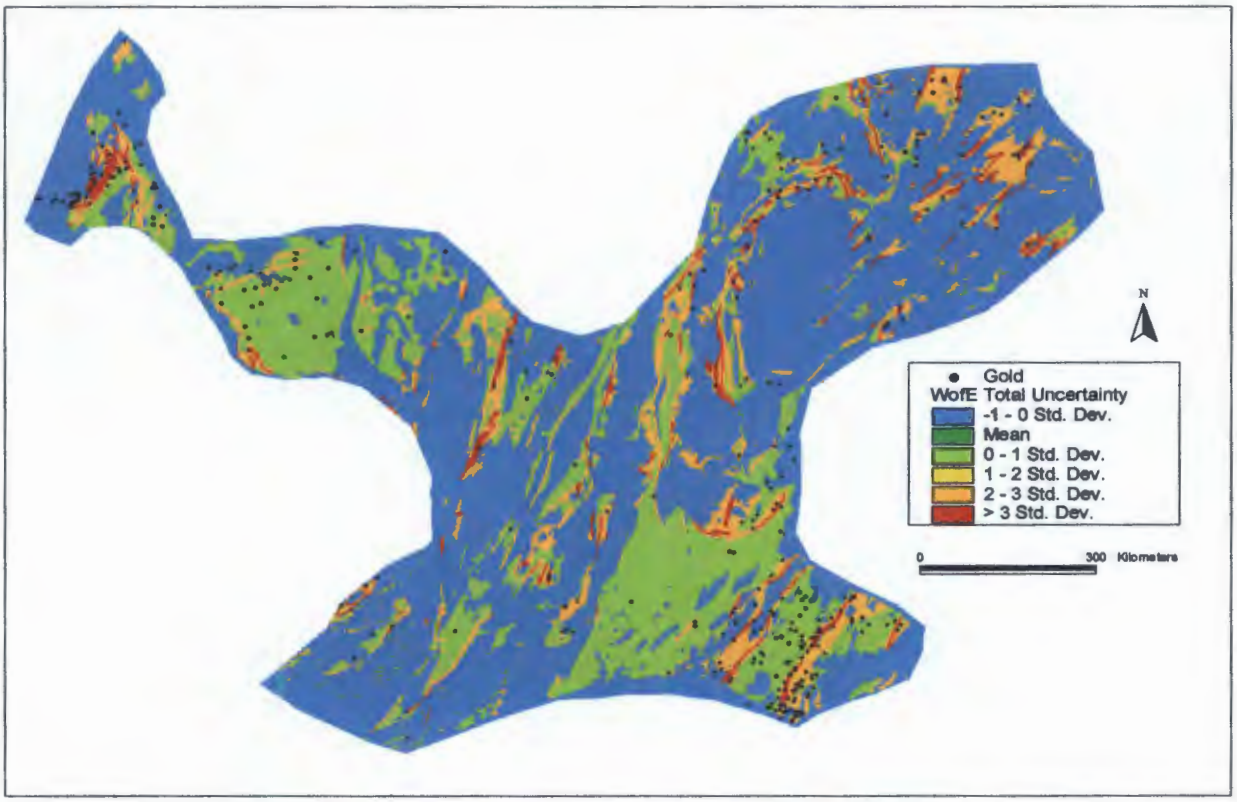

Figure 5.18b: Model B – Total uncertainty map of gold deposits, expressed in standard deviation units.

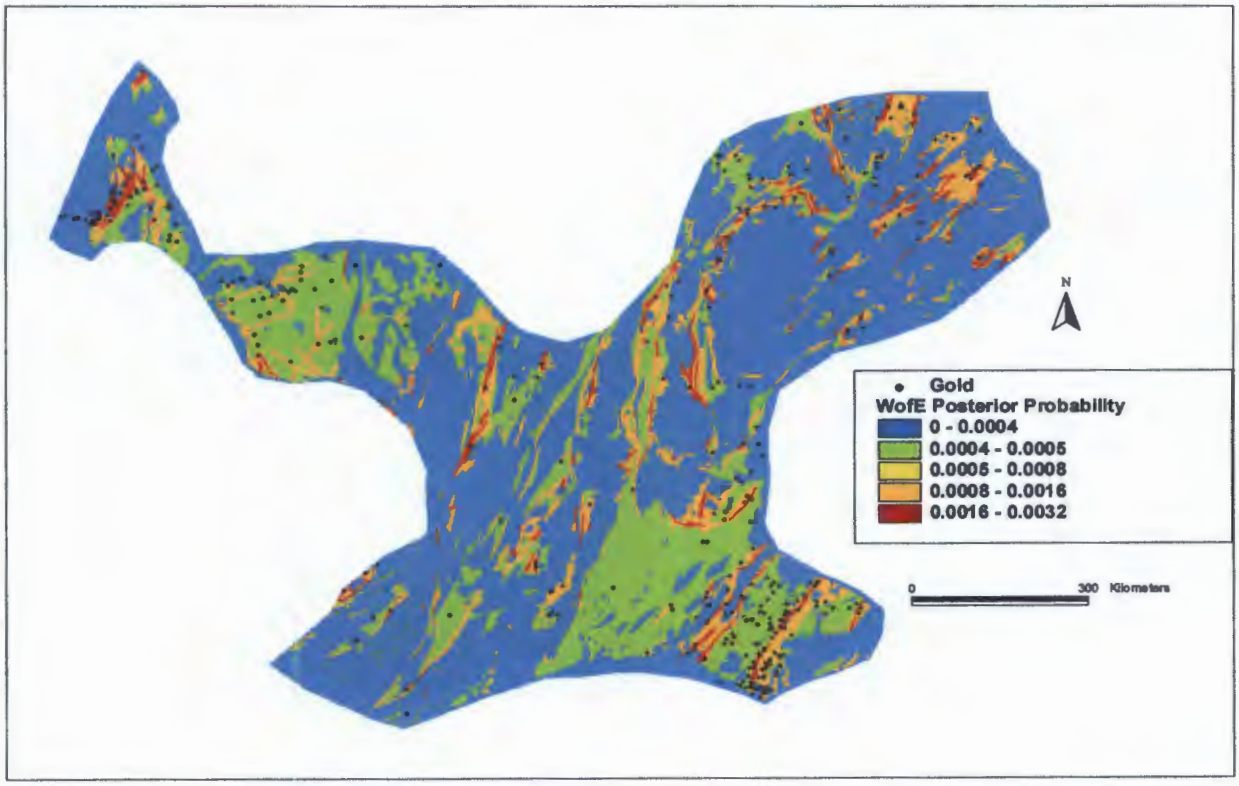

Figure 5.19a: Model C - Posterior probability map of gold deposits based on reclassified lithologies and merged (CGS and De Beers) brittle and ductile faults. [CI = 0.96].

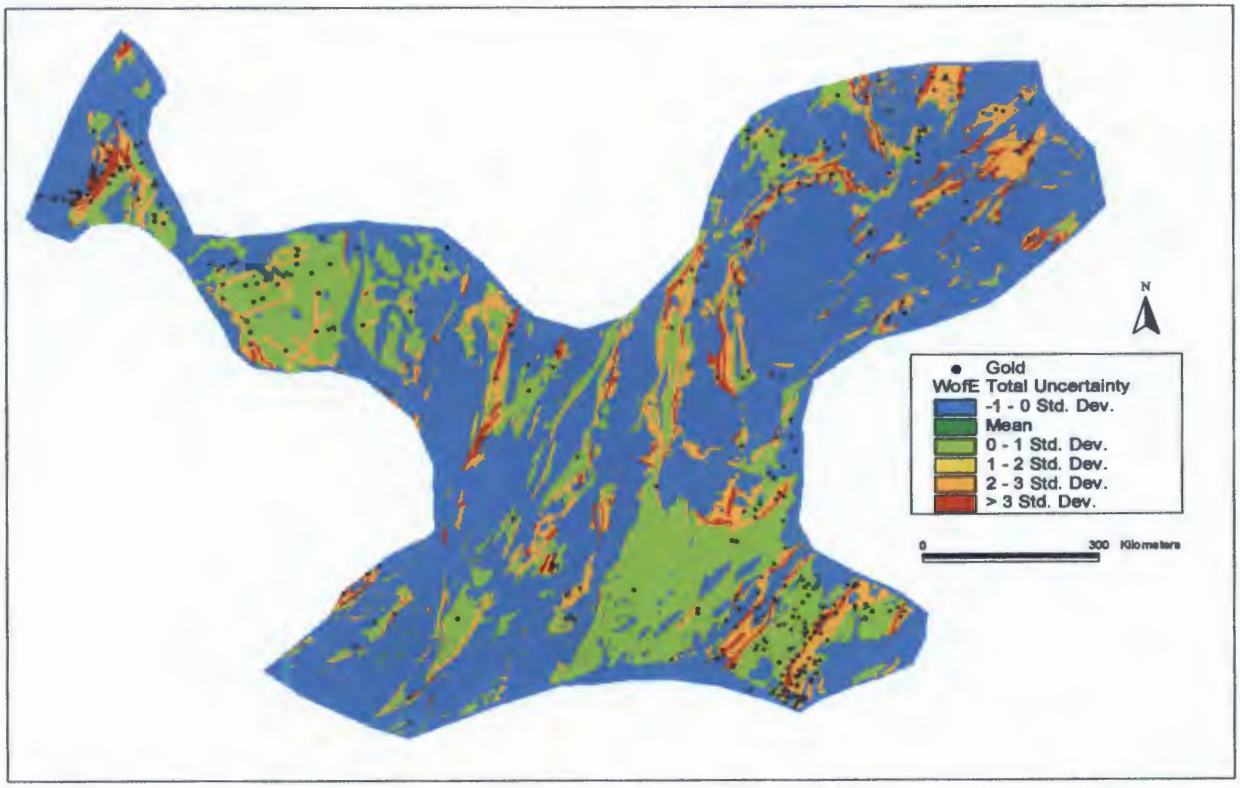

Figure 5.19b: Model C – Total uncertainty map of gold deposits, expressed in standard deviation units.

5.2.1.3 Validation of Results

The mineral potential map of model B is validated against a random set (88) of mineral deposits not used to generate the probabilistic model (Fig 5.20). In this map, 3% of validation deposits fall in very favourable area and 42% fall in favourable area of gold deposits. The results are not as encouraging as that of the Zimbabwe craton. Twenty three percent (23%) of the deposits fall in the "random area" (blue, < prior probability). This is probably because the brittle faults and ductile shears for the Birimian Shield are not differentiated and because such data is not available (lack of structural information). Also note that the Birimian Shield is large and the gold deposits are sparsely distributed over the area (which is reflected by poor probabilities; prior probability = 0.0004). Therefore, a smaller, enriched area is analysed (Ashanti Belt, section 5.2.1.4).

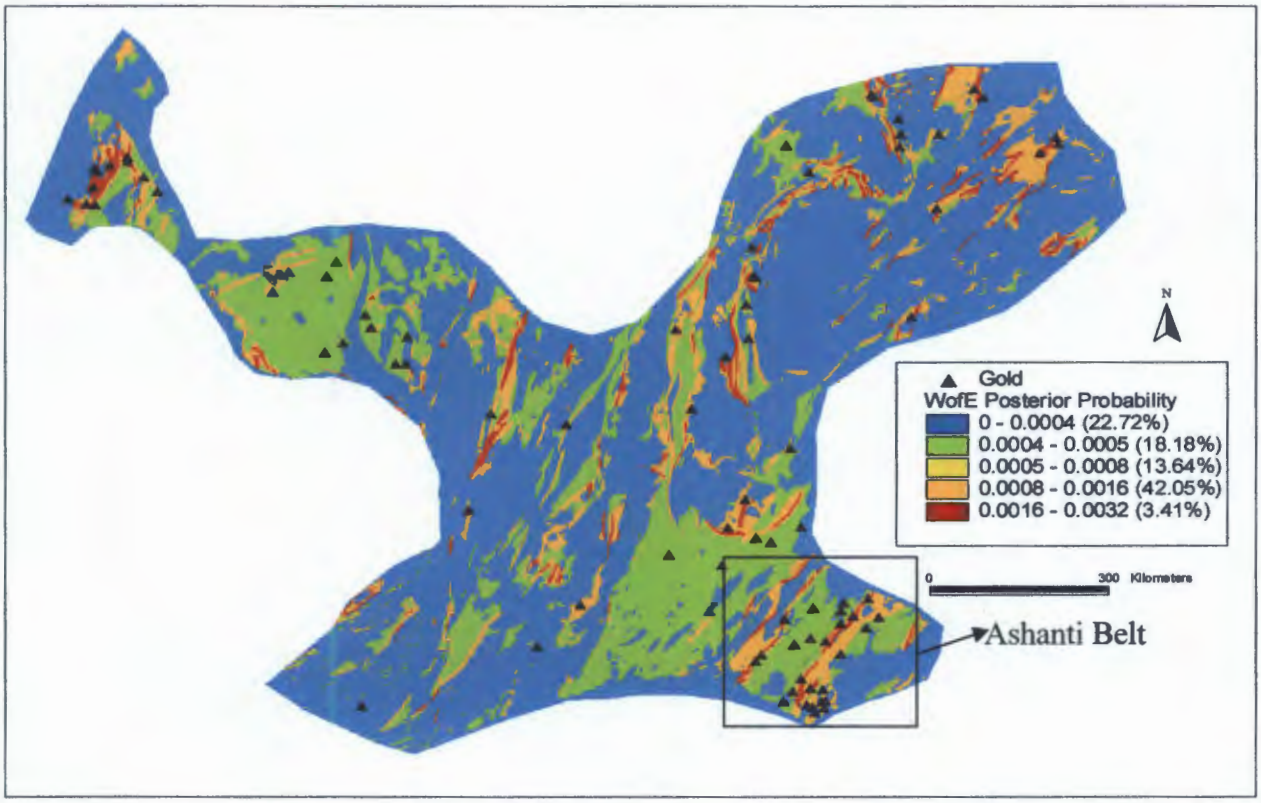

Figure 5.20: Model B –Posterior probability map for gold deposit with validation deposits superimposed. The percentage (%) of gold deposits that fall within each unit are indicated in the legend. 23% of the deposits fall in the "random area. Also note the Ashanti belt in the SE corner of the Birimian Shield (section 5.2.1.4).

5.2.1.4 Gold (Au) deposits in the Ashanti Belt

A block area "the Ashanti belt" (Fig. 5.21), subjectively chosen by visual observation of the deposits distribution, in the SE corner of the Birimian Shield, is considered to be well explored. The total training area is 70 595 km^2, and the unit area equal to 1 km^2. In the Ashanti area the total number of gold deposits is 121, and the prior probability is 0.0017. The weights results are shown in Table 5.11a. for the mapped lithologic units. Based on the contrast values, the number of points, area and weight values, the geology map (Fig. 3.2b) is reclassified into 3 classes (Table 5.11b). The greenstone belt-dominantly volcanics unit show a positive association with 53 known gold deposits (favourable, C_w = 1.046). The greenstone belt-dominantly sediments show a random association with 52 gold deposits. The third class is negative association, comprising of syn-to post-tectonic granitoids and younger cover units, and all the classes containing zero mineral points. The reclassified lithology of the Ashanti belt is similar to that of the Birimian Shield, except that greenstone belt dominantly sediments is now "random" before it was slightly "better" than random.

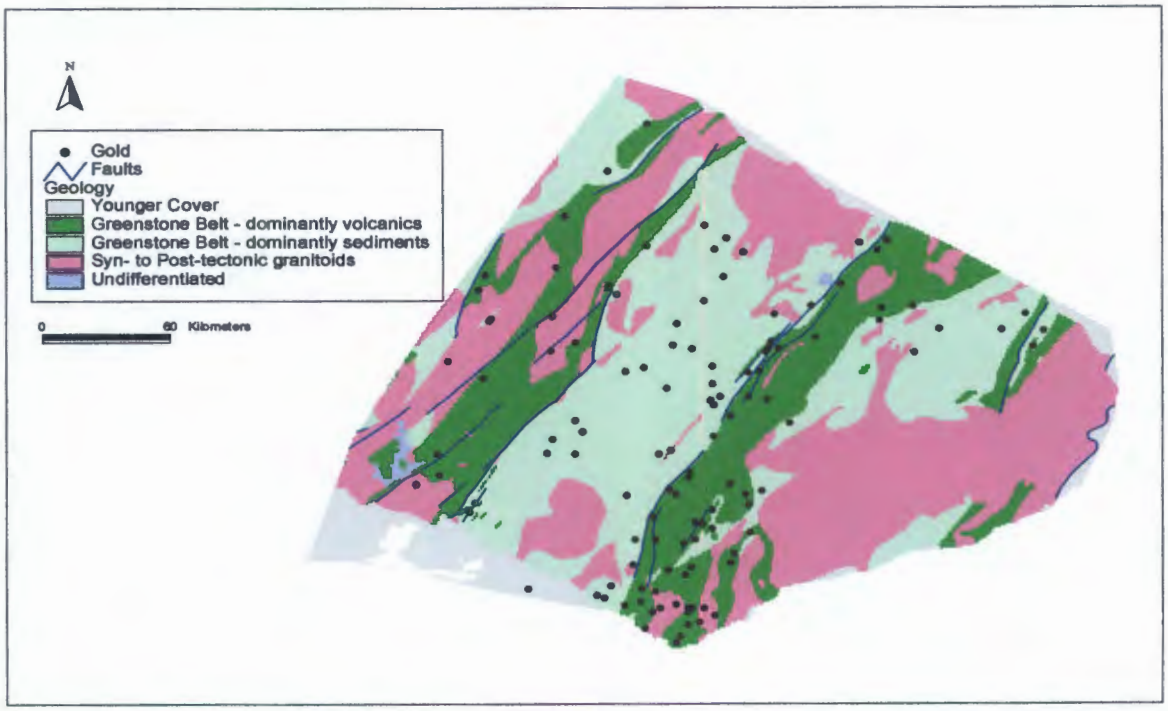

Figure 5.21. The geology and faults of the Ashanti Belt, extracted from the simplified geology of the Paleoproterozoic Birimian Shield, West Africa.

CLASS	S_VALUE	AREA_SQ_KM	NO_POINTS	WPLUS	S_WPLUS	WMINUS	S_WMINUS	CONTRAST	S_CONTRAST	STUD_CNT	
4	Greenstone Belt - dominantly volcanics	14650	53	0.7120	0.1376	-0.3343	0.1213	1.0463	0.1835	5.7028	1
2	Greenstone Belt - dominantly sediments	23466	52	0.2204	0.1388	-0.1390	0.1205	0.3594	0.1838	1.9551	2
3	Syn- to Post-tectonic granitoids	25580	15	-1.1107	0.2583	0.3399	0.0973	-1.4506	0.2760	-5.2561	
1	Younger Cover	4062	1	-1.9789	1.0001	0.0534	0.0914	-2.0323	1.0043	-2.0236	3
5	Undifferentiated	281	0								
-99	Missing Data	2556	0								
		70595	121								

Table 5.11a. Weights table for gold deposits from WofE applied to lithologic map of the Ashanti belt (Birimian Shield)

CLASS	DESCRIPTION	AREA_SQ_KM	NO_POINTS	WPLUS	S_WPLUS	WMINUS	S_WMINUS	CONTRAST	S_CONTRAST	STUD_CNT
1	Favourable	14650	53	0.7120	0.1376	-0.3343	0.1213	1.0463	0.1835	5.7028
2	Random	23466	52	0.2204	0.1388	-0.1390	0.1205	0.3594	0.1838	1.9551
3	Negative association	32479	16	-1.1936	0.2501	0.4312	0.0977	-1.6248	0.2685	-6.0517

Table 5.11b. Reclassified weights table for gold deposits (Ashanti belt, Birimian Shield)

The WofE method is applied to the faults of the Ashanti belt in order to find the buffer distance that maximizes the spatial association between gold deposits and the faults. WofE analysis shows a weak positive association with gold deposits (Fig. 5.22a). It is clear from Figure 5.22a that as the buffer area increase the contrast value decreases. This is also illustrated in figure 5.22b where the plotted percentage of gold deposits (points) against percentage of area, increases proportional with the area. The cut-off (optimal) distance is set at about 1 km (within which 14% of deposits are present in a total percentage area of 5%).

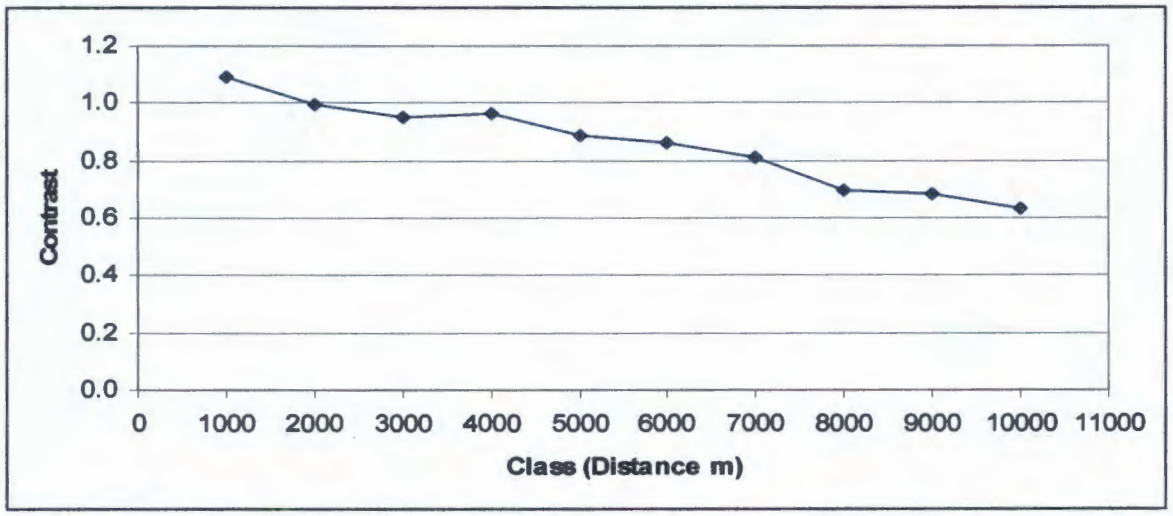

Figure 5.22a: Variation of gold contrast versus buffer distance away from the faults. The contrast reaches an apparent maximum at a distance of 4000 m, and decreases slightly as the distance away from the faults increases.

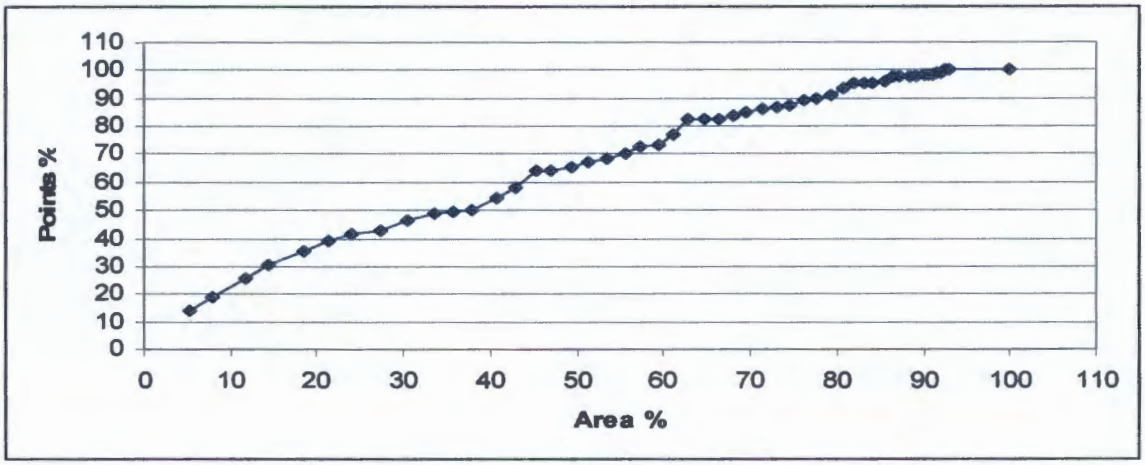

Figure 5.22b: Percentage of gold deposits (points) versus the total area (percentage) at successive distance away from the faults. Note that the number of deposit increases near-linearly with increasing total area.

By intergrating the evidential themes, a final posterior probability map is produced based on reclassified lithologies and binary faults (<1km). The predictive map shows similar variations in favourability area for gold deposits (Fig. 5.23a) as model B and C (Fig. 5.18a-5.19a). The posterior probability map indicates that the very favourable areas (highest probability) spatially coincide with the faults. Therefore, the Ashanti belt is strongly driven by the lithologies and faults. Although, there is a limited number of faults in the area, the predictive map still indicate the Ashanti belt as a good potential area for gold exploration.

The Ashanti block is therefore used as a testing block to quantify the spatial association between mineral deposits, faults and lithologies to compare against the Birimian Shield as a whole. The two areas (the Birimian Shield and Ashanti belt) studied here shows similar characteristics, based on the lithology and the faults. No obvious spatial association between the faults and the gold deposits. Therefore, probably the rest of Birimian Shield is not well enough mapped (it is generally flat and poorly outcropped), and the potential for finding gold deposits near shear zones (which might be located in future, using geophysics) would be a good indicator for future exploration.

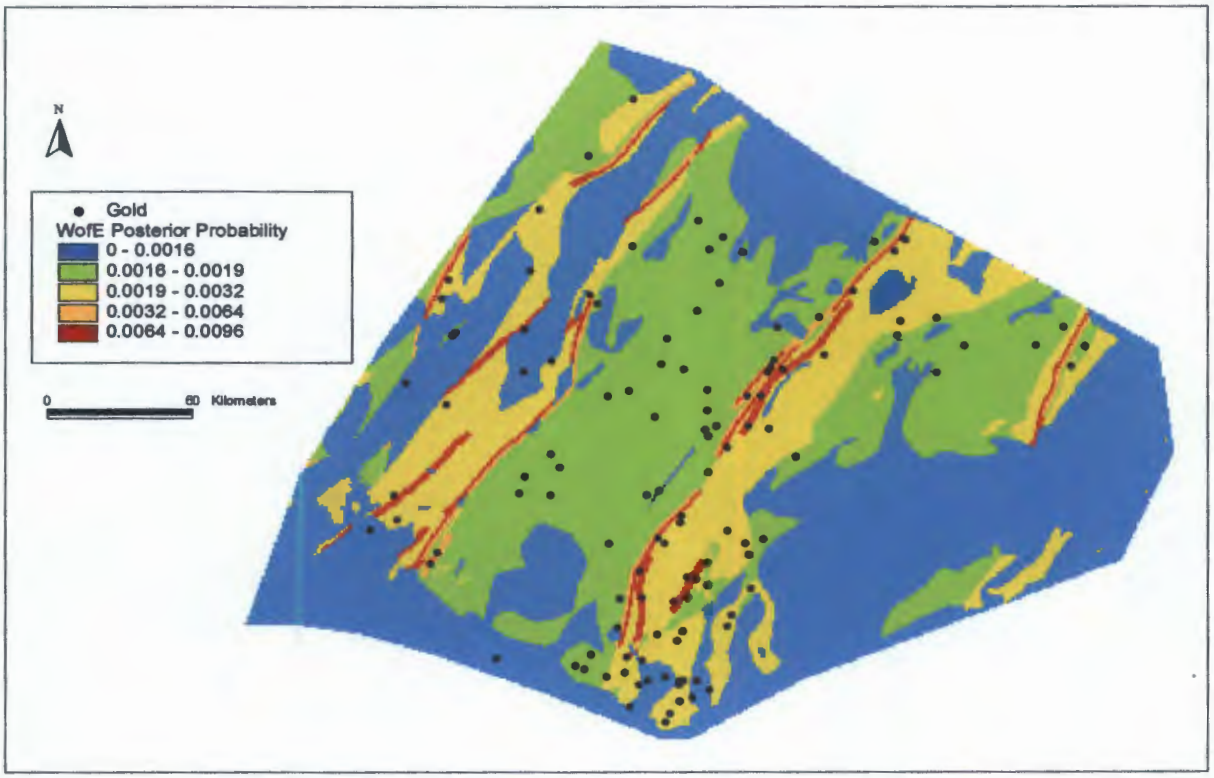

Figure 5.23a. Posterior probability map of gold deposits in the Ashanti belt based on reclassified lithology and faults. [CI = 0.97]

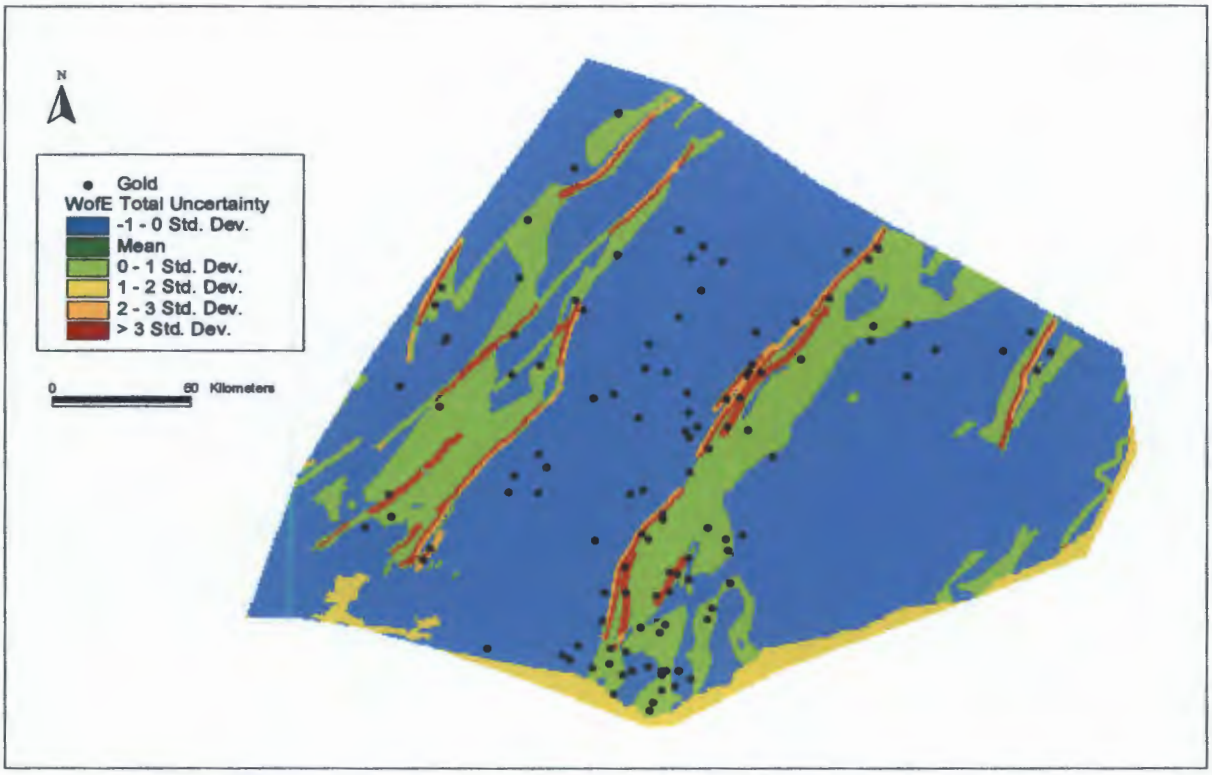

Figure 5.23b. Total uncertainty map of gold deposits, expressed in standard deviation units. Note that the high uncertainties in favourable areas (zones of highest posterior probability).

5.2.2 CuZnPbBa deposit model

In the training area the total number of CuZnPbBa deposits is 92, and the prior probability equals 0.0001.

5.2.2.1 Reclassification of evidential theme patterns

A simplified geology map is reclassified into lithological units in order to calculate the positive weights and negative weights of evidence (Table 5.12a). Based on contrast values of weights, the lithologic units were reclassified into two classes: favourable and negative association classes (Table 5.12b). The greenstone belt-dominantly volcanics areas are the only ones that show a positive association, with 18 known CuZnPbBa deposit.

Faults and ductile shears have no spatial association with the deposits, and therefore are not used as an evidence theme. Only lithology theme is used as a predictor theme.

5.2.2.2 Predictive mineral potential maps

A final posterior probability map is generated based only on the lithology theme (Figure 5.24a). The posterior probability map is classified by 2 breaks, showing favourable and unfavourable areas. The CuZnPbBa map is not well differentiated, the analysis indicates very low spatial associations. The predictive map is driven only by the lithologic theme, with very high uncertainty (Fig. 5.24b). This is probably related to the fact that the analysis is based on only a small number of deposits across a very large area.

CLASS	S_VALUE	AREA_SQ_KM	NO_POINTS	WPLUS	S_WPLUS	WMINUS	S_WMINUS	CONTRAST	S_CONTRAST	STUD_CNT	
2	Greenstone Belt - dominantly volcanics	86864	18	0.6832	0.2357	-0.1137	0.1163	0.7969	0.2628	3.0320	1
1	Younger Cover	78717	10	0.1938	0.3162	-0.0213	0.1104	0.2151	0.3350	0.6421	
3	Greenstone Belt - dominantly sediments	228406	24	0.0040	0.2041	-0.0014	0.1213	0.0054	0.2374	0.0229	
4	Syn- to Post-tectonic granitoids	295485	30	-0.0303	0.1826	0.0150	0.1270	-0.0454	0.2224	-0.2039	
6	Post-tectonic granitoids	164365	9	-0.6478	0.3333	0.1041	0.1098	-0.7519	0.3510	-2.1424	2
5	Pre- and Syn-tectonic granitoids	21275	1	-0.8005	1.0000	0.0136	0.1048	-0.8141	1.0055	-0.8096	
7	Undifferentiated	3965	0								
-99	Missing Data	5571	0								
		884648	92								

Table 5.12a. Weights table for CuZnPbBa deposits from WofE applied to lithologic map of the Birimian Shield

CLASS	DESCRIPTION	AREA_SQ_KM	NO_POINTS	WPLUS	S_WPLUS	WMINUS	S_WMINUS	CONTRAST	S_CONTRAST	STUD_CNT
1	Favourable	86864	18	0.6832	0.2357	-0.1137	0.1163	0.7969	0.2628	3.0320
2	Negative association	797784	74	-0.1137	0.1163	0.6832	0.2357	-0.7969	0.2628	-3.0320

Table 5.12b. Reclassified weights table for CuZnPbBa deposits (Birimian Shield)

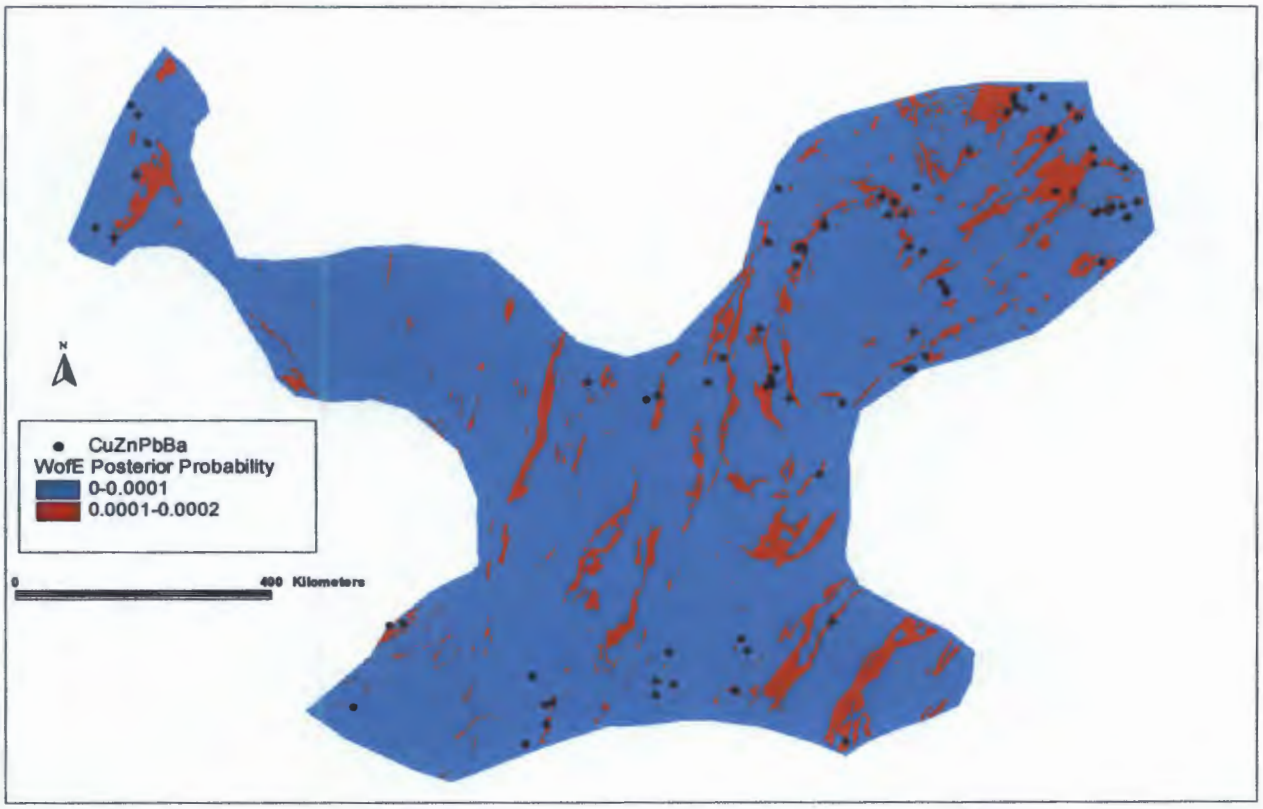

Figure 5.24a: Posterior probability map of CuZnPbBa deposit model.

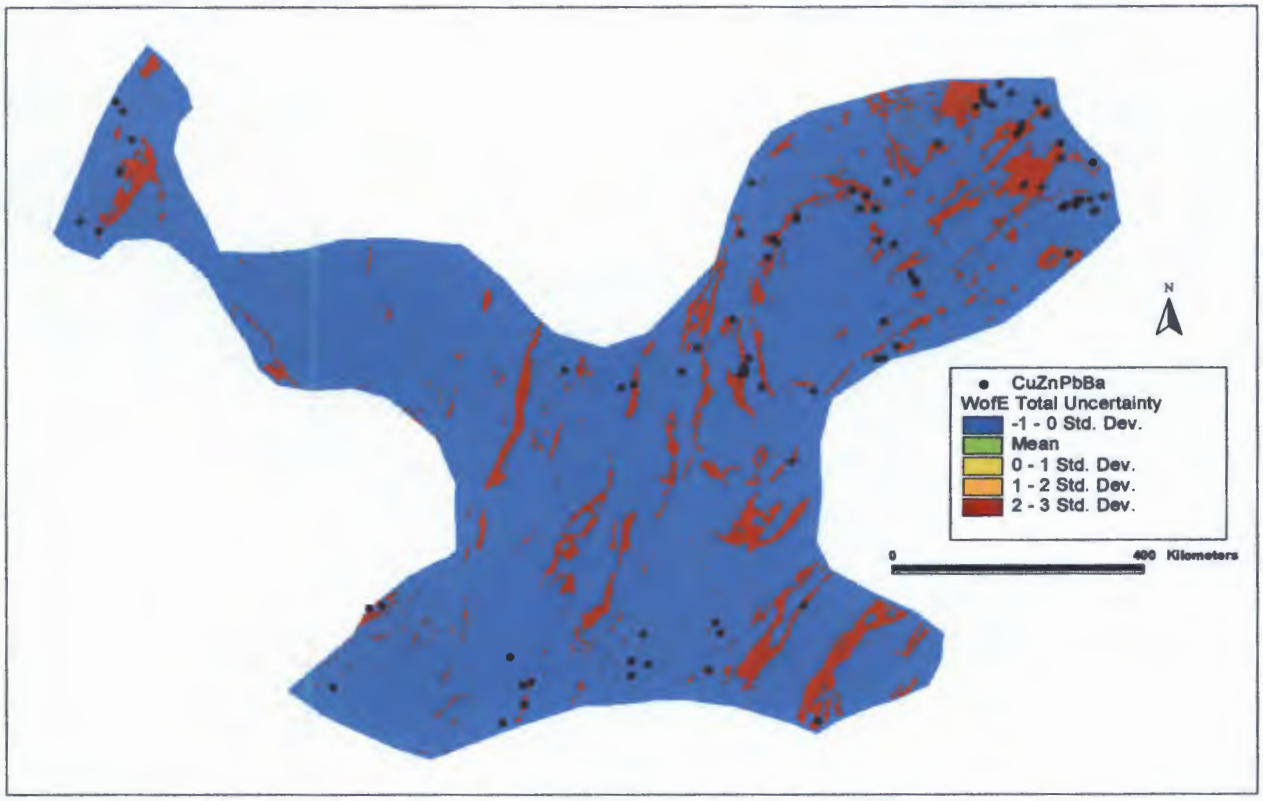

Figure 5.24b: Total uncertainty map of CuZnPbBa deposit expressed in one standard deviation units. Note the high uncertainty, which is probably because only one evidential theme is used.

5.3 The Neoproterozoic Arabian-Nubian Shield

The evidential themes used for the Arabian-Nubian Shield include its simplified geology and faults. The total training area is 2 823 485 km^2 [much larger than Birimian (884 648 km^2) and Zimbabwe (240 544 km^2) regions], and the unit area equals 1 km^2. For reliable analysis to be applied, WofE requires a significant number of training points per unit area, so the mineral deposits of CrNiPgeTi (90), SnSb (22) and W (11) and UThREE (47) are therefore not analysed in this region, because the total number of mineral deposits are too low relative to the size of the region (Table 3.2).

5.3.1 Gold deposit

In the training area the total number of known gold deposits tested is 516 and the prior probability is 0.0002. The mineral deposits are not divided into two subsets for probabilistic and validation models, because the prior probability is small.

5.3.1.1 Reclassification of evidential theme patterns

The weights results are shown in Table 5.13a. for the mapped lithologic units. Based on the contrast value, the number of points, area and weight values, the geology map (Fig. 3.2c) is reclassified into 5 classes (Table 5.13b). The greenstone belt-undifferentiated unit shows positive association with 93 known gold deposits (very favourable; C_W=2.73). The greenstone belt-dominantly volcanic and sediments are combined into one unit, and contrast values are positive. The third class is random, and the remaining two classes consist of all the classes with lower ranking contrast values as well as those containing zero mineral points.

CLASS	S_VALUE	AREA_SQ_KM	NO_POINTS	WPLUS	S_WPLUS	WMINUS	S_WMINUS	CONTRAST	S_CONTRAST	STUD_CNT	
5	Greenstone Belt-Undifferentiated	39767	93	2.5436	0.1038	-0.1845	0.0486	2.7281	0.1146	23.7969	1
4	Greenstone Belt-dominantly volcanics	137548	110	1.4690	0.0954	-0.1894	0.0496	1.6585	0.1075	15.4239	2
7	Greenstone Belt-dominantly sediments	21407	13	1.1935	0.2774	-0.0178	0.0446	1.2114	0.2810	4.3111	
3	Syn-to Post-tectonic granitoids	242594	77	0.5444	0.1140	-0.0711	0.0477	0.6155	0.1236	4.9809	3
6	Pre-tectonic granitoids	297251	85	0.4401	0.1085	-0.0679	0.0482	0.5079	0.1187	4.2792	
2	Undifferentiated	409252	63	-0.1793	0.1260	0.0277	0.0470	-0.2070	0.1345	-1.5396	4
1	Younger Cover	1645816	75	-1.3968	0.1155	0.7285	0.0476	-2.1252	0.1249	-17.0142	
8	Post-tectonic intrusives	8101	0								5
-99	Missing Data	21749	0								
		2823485	516								

Table 5.13a. Weights table for gold deposits from WofE applied to lithologic map of the Arabian-Nubian Shield

CLASS	DESCRIPTION	AREA_SQ_KM	NO_POINTS	WPLUS	S_WPLUS	WMINUS	S_WMINUS	CONTRAST	S_CONTRAST	STUD_CNT
1	Very Favourable	47868	93	2.3578	0.1038	-0.1815	0.0486	2.5393	0.1146	22.1541
2	Favourable	158955	123	1.4360	0.0902	-0.2139	0.0504	1.6500	0.1034	15.9648
3	Slightly favourable	539845	162	0.4883	0.0786	-0.1628	0.0532	0.6511	0.0949	6.8634
4	Random	409252	63	-0.1793	0.1260	0.0277	0.0470	-0.2070	0.1345	-1.5396
5	Negative association	1667565	75	-1.3968	0.1155	0.7285	0.0476	-2.1252	0.1249	-17.0142

Table 5.13b. Reclassified weights table for gold deposits (Arabian-Nubian Shield)

The WofE method is applied to the brittle faults/ductile shears in order to find the buffer distances that maximize the spatial association between the gold deposits and the faults. Results from analysis shows that no obvious spatial association between the brittle faults and gold deposits (Figure 5.25a). The contrast value is also very small (<0.6). This is also illustrated in figure 5.25b where the plotted percentage of gold deposits (points) against percentage of area, increases proportional with the area. The cut-off (optimal) distance is determined at 5 km (based on the more robust analyses of the ductile shears of the Zimbabwe Craton). Based on the optimum buffer distance of 5 km, the brittle faults are reclassified into binary pattern (near contact <5000m, and away contacts >5000m).

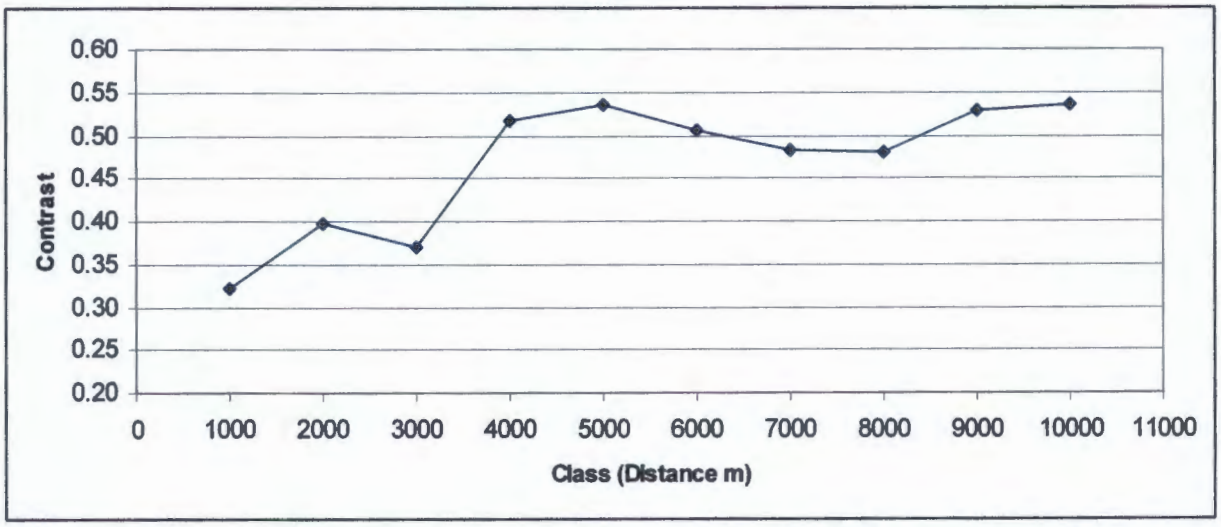

Figure 5.25a: Variation of contrast of gold deposits versus buffer distance away from the faults. Note that the contrast reaches a maximum at about 5000 m.

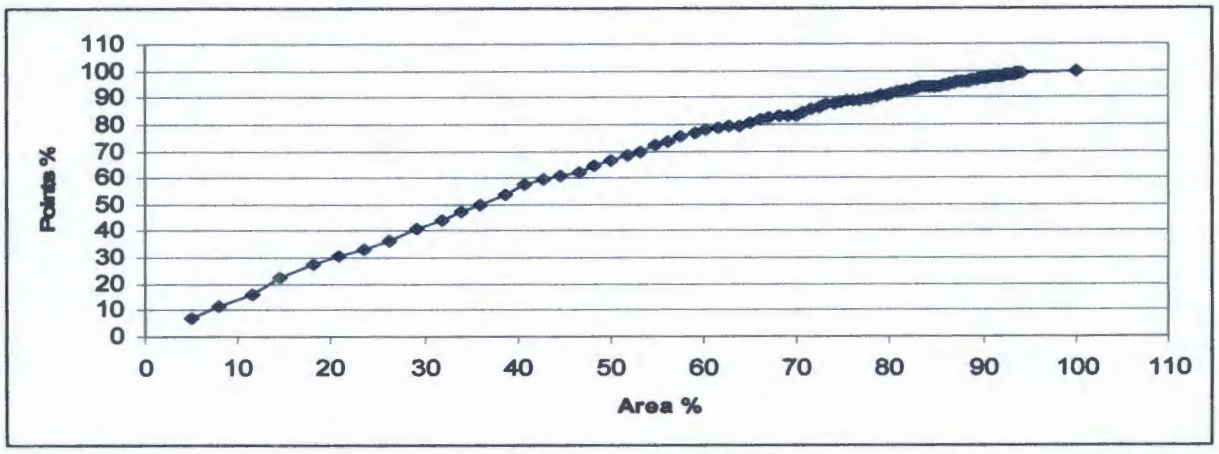

Figure 5.25b: Percentage of gold deposits (Points) versus the total area (percentage) at successive distance away from faults. Note that the number of deposit increases near-linearly with distance away from the faults.

5.3.1.2 Integration of evidential theme patterns

The evidential themes patterns (lithological units and binary map of faults) were combined to produce a mineral potential map. The posterior probability map is shown in Figure 5.26a. The map is symbolized by 6 breaks representing classes from lowest (blue) to highest (red) posterior probability. All areas that are greater than the prior probability are favourable, whereas values less than the prior probability are relatively unfavourable. An uncertainty map of the posterior probability based on one standard deviation breaks is presented in Figure 5.26b, showing high effects of uncertainty at highly favourable areas of posterior probability and at the edge of the study area where information is missing. This might be expected since the model is strongly driven by the lithology, as the faults show a random spatial association with gold deposits.

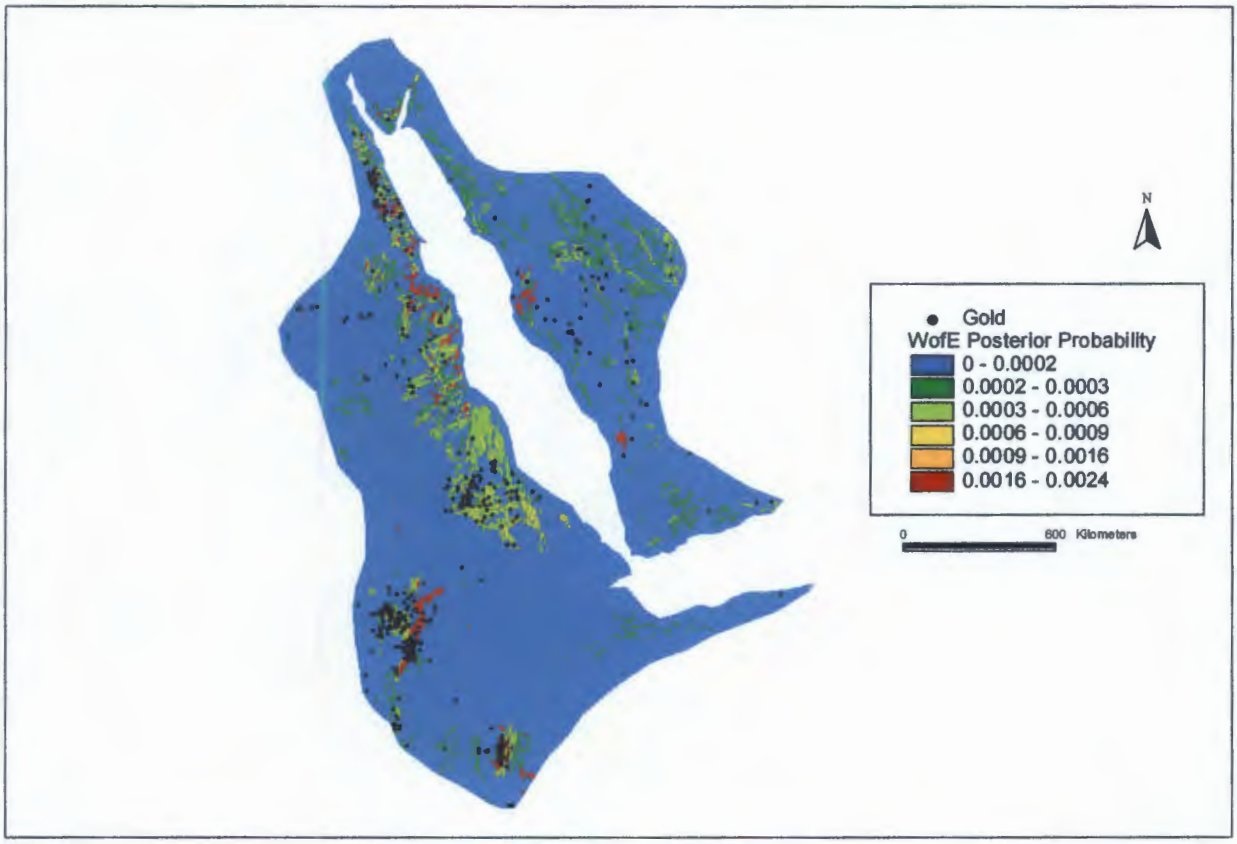

Figure 5.26a: Posterior probability map of gold deposits based on reclassified lithologies and brittle faults. [CI = 0.99]

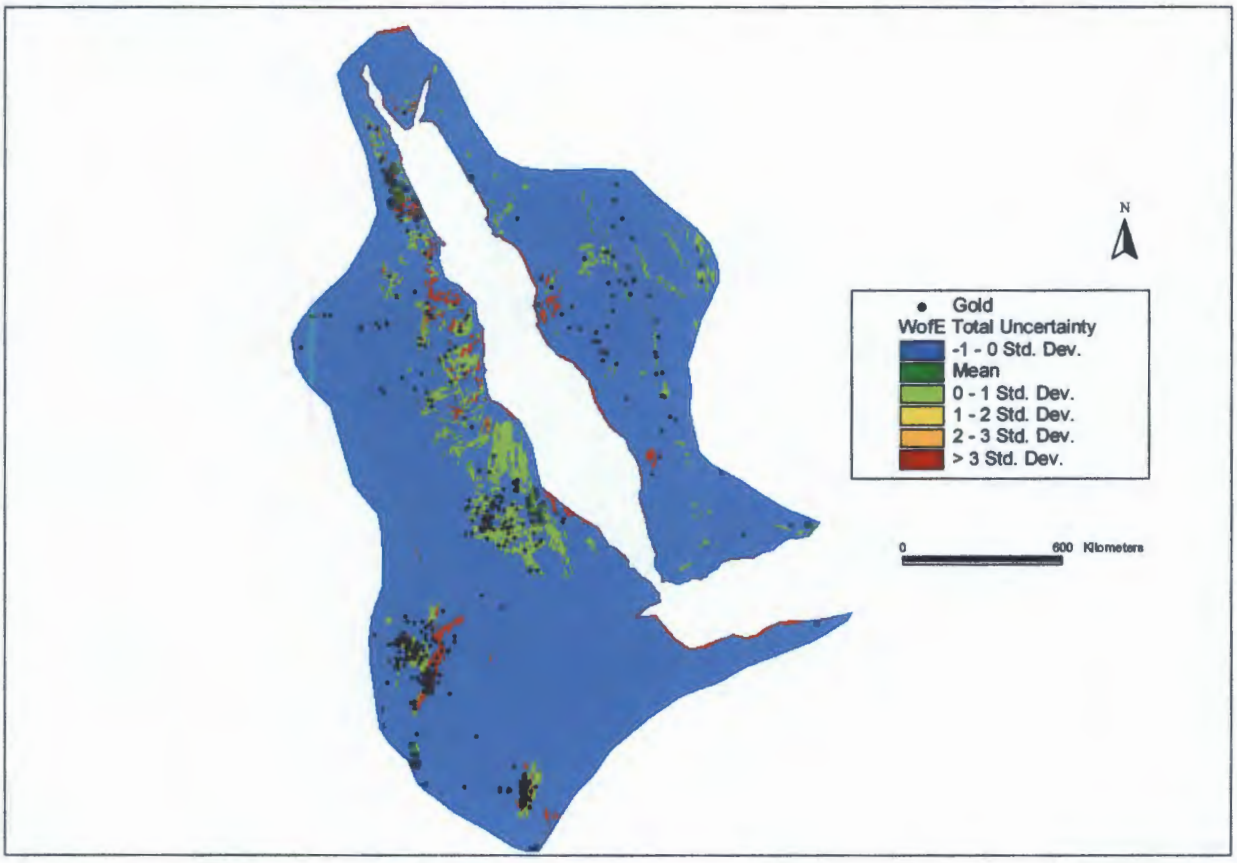

Figure 5.26b: Total uncertainty map of Gold deposit expressed in standard deviation units.

5.3.2 CuZnPbBa

In the training area the total number of CuZnPbBa deposits is 182, and the prior probability equals 0.0001.

5.3.2.1 Reclassification of evidential theme patterns

Based on the contrast value, number of points, area and weights values, post-tectonic intrusive unit shows highest positive association with 5 CuZnPbBa deposits (Table 5.14a). The greenstone belt–dominantly volcanic, sediments and undifferentiated are grouped together because they show a positive association, but contrast values are lower than for the post-tectonic intrusives. The third and fourth classes show contrast values of lower ranking. The new weights for the reclassified map are given in Table 5.14b. Only the lithologic map is used as evidential theme, the faults show no obvious spatial association.

5.3.2.2 Predictive mineral potential maps

The posterior probability map is generated based only on the lithology theme (Figure 5.27a). The posterior probabilities are classified by 3 breaks. The CuZnPbBa map is really not well differentiated, the analysis indicates very low spatial associations. The posterior probability map is driven only by the lithology. The uncertainty of posterior probability is generated using one standard deviation breaks (Fig. 5.27b), showing region of favourability (high posterior probability) estimates so relatively uncertain. Only post-tectonic intrusives is favourable zone (high posterior probability) which also reflects high uncertainty.

CLASS	S_VALUE	AREA_SQ_KM	NO_POINTS	WPLUS	S_WPLUS	WMINUS	S_WMINUS	CONTRAST	S_CONTRAST	STUD_CNT	
8	Post-tectonic intrusives	8101	5	2.2575	0.4474	-0.0251	0.0754	2.2826	0.4537	5.0316	1
4	Greenstone Belt-dominantly volcanics	137548	35	1.3711	0.1691	-0.1646	0.0828	1.5356	0.1882	8.1585	
7	Greenstone Belt-dominantly sediments	21407	6	1.4678	0.4083	-0.0260	0.0756	1.4938	0.4152	3.5974	2
5	Greenstone Belt-Undifferentiated	39767	8	1.1360	0.3536	-0.0309	0.0760	1.1670	0.3617	3.2266	
2	Undifferentiated	409252	37	0.3361	0.1644	-0.0708	0.0833	0.4069	0.1843	2.2075	
3	Syn-to Post-tectonic granitoids	242594	20	0.2439	0.2236	-0.0265	0.0788	0.2704	0.2371	1.1404	3
6	Pre-tectonic granitoids	297251	20	0.0407	0.2236	-0.0049	0.0788	0.0456	0.2371	0.1923	
1	Younger Cover	1645816	51	-0.7545	0.1414	0.5621	0.0874	-1.3166	0.1662	-7.9200	4
-99	Missing Data	21749	0								
		2823485	182								

Table 5.14a. Weights table for CuZnPbBa deposits from Wofe applied to lithologic map of the Arabian-Nubian Shield

CLASS	DESCRIPTION	AREA_SQ_KM	NO_POINTS	WPLUS	S_WPLUS	WMINUS	S_WMINUS	CONTRAST	S_CONTRAST	STUD_CNT
1	Very favourable	8101	5	2.2575	0.4474	-0.0251	0.0754	2.2826	0.4537	5.0316
2	Favourable	198722	49	1.3396	0.1429	-0.2421	0.0870	1.5817	0.1673	9.4545
3	Random	949097	77	0.2278	0.1140	-0.1405	0.0981	0.3683	0.1503	2.4496
4	Negative association	1667565	51	-0.7545	0.1414	0.5621	0.0874	-1.3166	0.1662	-7.9200

Table 5.14b. Reclassified weights table for CuZnPbBa deposits (Arabian-Nubian Shield)

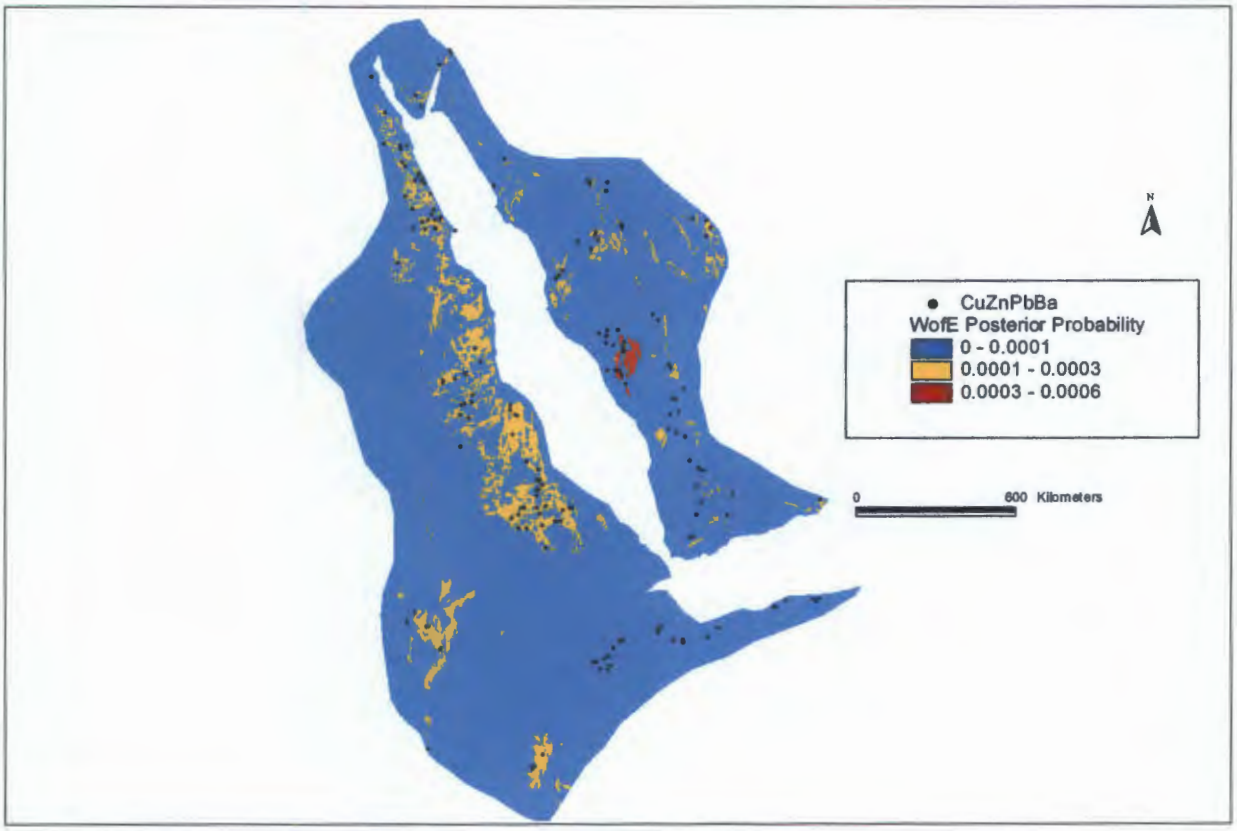

Figure 5.27a: Posterior probability map of CuZnPbBa deposits. [CI = 1]

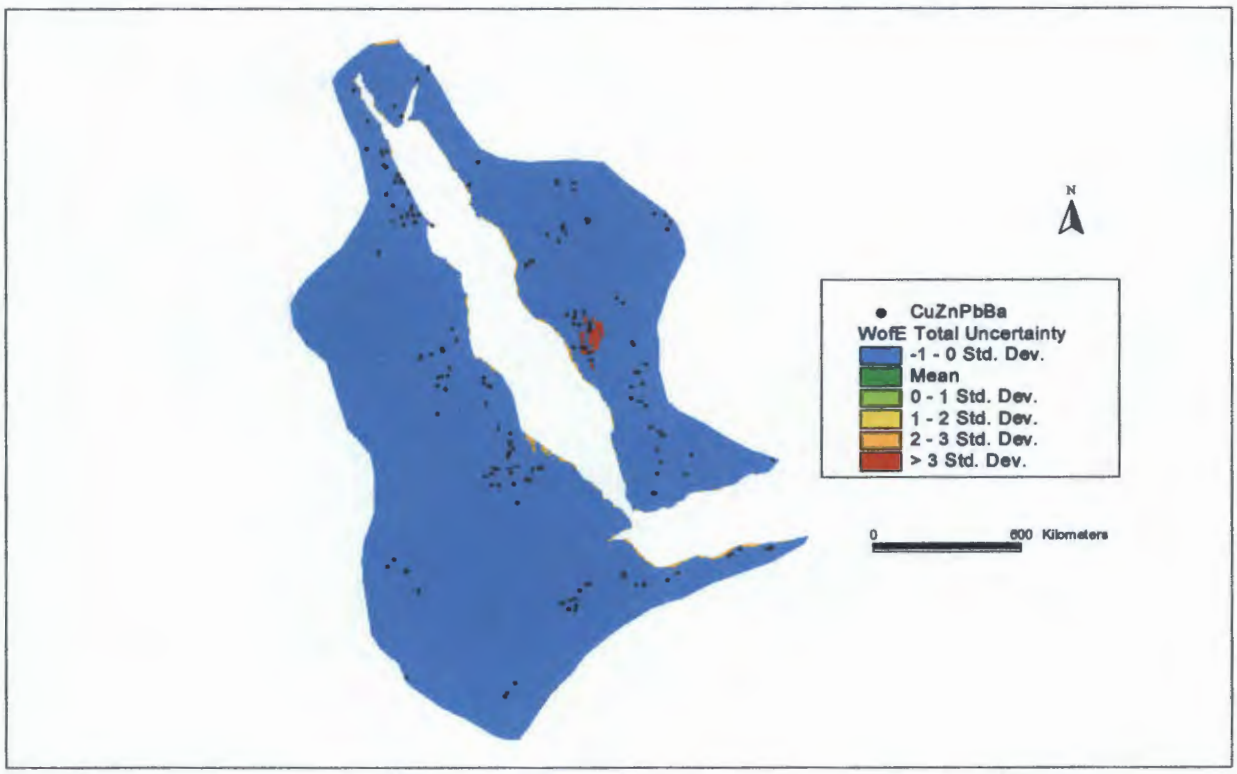

Figure 5.27b: Total uncertainty map of CuZnPbBa deposit expressed in standard deviation units.

5.4 Discussion

The results of WoFe modelling for gold deposits in all three regions show some similarity in terms of favourable and unfavourable sites for such mineralization. There is a strong host rock (lithology) control on mineralization in all regions with the greenstone belts and the granitoids rocks (pre- and syn-tectonic granitoids; post-tectonic granitoids), resulting in a significant spatial association. This is not unexpected because all regions are granite-greenstones terrains (Chapter 2) that, at least in the Archean, are generally known to be richly endowed in gold mineralization. For the Zimbabwe Craton, a set of ductile shear zones and brittle faults are differentiated whereas these structures on the Birimian and Arabian-Nubian Shields are not differentiated in this way (Figs. 3.4-3.5). Brittle faults in all regions were first tested independently for spatial association with gold deposit, and were found to show only a weak spatial association.

In contrast, ductile shears in the Zimbabwe Craton show a positive association with gold deposits. An optimal cut-off distance was found to be about 5 km for the Zimbabwe Craton. For the other two regions (Birimian and Arabian-Nubian Shield) there is a weak spatial association between shear zones/faults and gold deposits. In contrast, WofE applied to the well mapped Ashanti belt shows that the faults have a slightly higher spatial association (using a 1 km optimal cut-off distance) with gold deposits. These results, therefore, suggest that maybe there is a lack of structural information and mapping of ductile shear zones across the Birimian Shield as a whole, since this large area is generally poorly exposed.

In the next chapter, the mineral deposits of the three regions are now further evaluated in terms of mineralization per unit area, from which other fundamental information is derived about the metal endowments, in turn, this will help to evaluate the time integrated change of mineralization.

It should be pointed out that the weights of evidence method relies on "accurate" placing of deposits and evidential themes (e.g. lithology and faults) supplied in the databases used. It was previously mentioned (pg 3-10), for example, that faults and shears (tectonic themes) plotted from different sources, may give slightly different results. Although care has been taken in this investigation to be as precise as possible in locating deposits, the accuracy of this cannot be quantified.

Chapter 6

Diversity of mineral deposits across the three study regions of African crust

6.1 Introduction

This chapter deals principally with details of the general distribution of the identified mineral deposits across the three study regions. The various element groups comprising the mineral deposits are discussed in the order given in Table 6.1. The aim of this chapter is to derive fundamental information about the diversity of mineralization in the three studied regions, so that the metallogenic characters of these areas can be compared directly. Since the three areas formed at a different times (ranging from Archean to Neoproterozoic), any variations in the diversity of their mineralization may reveal important information about the evolution of mineralization in continental crust. In addition, variations in total concentration of these elements in the three areas are also used in the following chapter to test for secular changes in mineralization across Africa.

Selected regions	Au	CrNiPgeTi	CuZnPbBa	SnSb	W	UThREE	Total	Area in sq.km
Zimbabwe Craton	625	108	97	66	275	3	1174	240544
Birimian Shield	441	38	92	21	5	32	629	884648
Arabian-Nubian Shield	516	90	182	22	11	47	868	2823485
Overall Total	1582	236	371	109	291	82	2671	3948677

Table 6.1 Selected element groups of known mineral deposits ($j_{1\text{-}6}$) from the three studied regions ($i_{1\text{-}3}$).

6.2 Spatial coefficients of element groups

To directly compare the density of mineralization of different areas, Mihalasky and Bonham-Carter (2001), de Wit and Thiart (2005) and Thiart and de Wit (2006) use a measure of spatial association known as spatial coefficient, derived from the WofE

approach. Data per unit area of crust are normalized in order to derive this comparable measure of spatial association (spatial coefficient, ρ_{ij}) (e.g. Thiart and de Wit, 2006):

$$\rho_{ij} = \frac{N(C_i \cap D_j)/N(D_j)}{A(C_i)/A(C_\bullet)} \tag{6-1}$$

where $A(C_i)$ is the area of the i^{th} craton/shield (C_i), and $A(C_\bullet)$ is the total of all regions in the study $(A(C_\bullet) = \Sigma A(C_i))$. $N(D_j)$ is the total number of deposits in the j^{th} mineral group (D_j). $N(C_i \cap D_j)$ represents the number of deposits of element group (D_j) in craton/shield (C_i). This normalized spatial measure represents the proportion of deposits (j) of all the j^{th} deposits (in cratons/shields) that occur in the specified area (i) per unit area of all (three) selected regions of African crust combined. The spatial coefficients (ρ_{ij}) range in value from 0 to ∞ (infinity), and is equals to 1 if there is no spatial association between an area and an element group. For values of $\rho_{ij} > 1$, there is a positive association between mineral group (j) and craton (i); values between 0 and 1 indicates a negative association. Table 6.2 shows the spatial coefficient ρ_{ij} of element groups within the three selected regions of this study.

Selected regions	Au	CrNiPgeTi	CuZnPbBa	SnSb	W	UThREE	Total	Area in sq.km
Zimbabwe Craton	6.49	7.51	4.29	9.94	15.51	0.60	7.22	240544
Birimian Shield	1.24	0.72	1.11	0.86	0.08	1.74	1.05	884648
Arabian-Nubian Shield	0.46	0.53	0.69	0.28	0.05	0.80	0.45	2823485

Table 6.2 Spatial association (ρ_{ij}) between element groups and the three selected regions

The spatial coefficient values shown in Table 6.2 range from negative (<1) to positive (>10) values, creating great skewness in the data range. Using the natural log of ρ_{ij} eliminates this skewness in ρ_{ij} values (Table 6.3).

By taking the natural log (ln) of ρ_{ij}, the resulting measure is positive for a positive association, negative for a negative association, and equals to zero for no association. Mihalasky and Bonham-Carter (2001) show that an approximate measure of standard error of $\ln \rho_{ij}$ is:

$$s(\ln \rho_{ij}) = \sqrt{\frac{1}{N(C_i \cap D_j)}} \tag{6-2}$$

The log of the spatial coefficient and approximate standard errors are given in Table 6.3. The spatial coefficient and 2x standard deviation bars are given in Figure 6.1. The vertical error bars provide an approximate confidence interval to facilitate interpretations.

Selected regions	Au	CrNiPgeTi	CuZnPbBa	SnSb	W	UThREE	Total
Zimbabwe Craton	1.87 (0.0400)	2.02 (0.0962)	1.46 (0.1015)	2.30 (0.1231)	2.74 (0.0603)	-0.51 (0.5774)	1.98 (0.0292)
Birimian Shield	0.22 (0.0476)	-0.33 (0.1622)	0.10 (0.1043)	-0.15 (0.2182)	-2.57 (0.4472)	0.55 (0.1768)	0.05 (0.0399)
Arabian-Nubian Shield	-0.78 (0.0440)	-0.63 (0.1054)	-0.38 (0.0741)	-1.26 (0.2132)	-2.94 (0.3015)	-0.22 (0.1459)	-0.79 (0.0339)

Table 6.3 Natural log of the spatial coefficient ($\ln \rho_{ij}$) with the approximate standard error ($s(\ln \rho_{ij})$), below and in brackets of element groups of the three study regions.

Figure 6.1 expresses the diversity amongst the selected regions for each set of elements in the six element groups, and provides (natural log) spatial coefficient values for each set of elements. Figure 6.2 represents the natural log of the spatial coefficient for the total number of element groups (sum of all six groups) for each region.

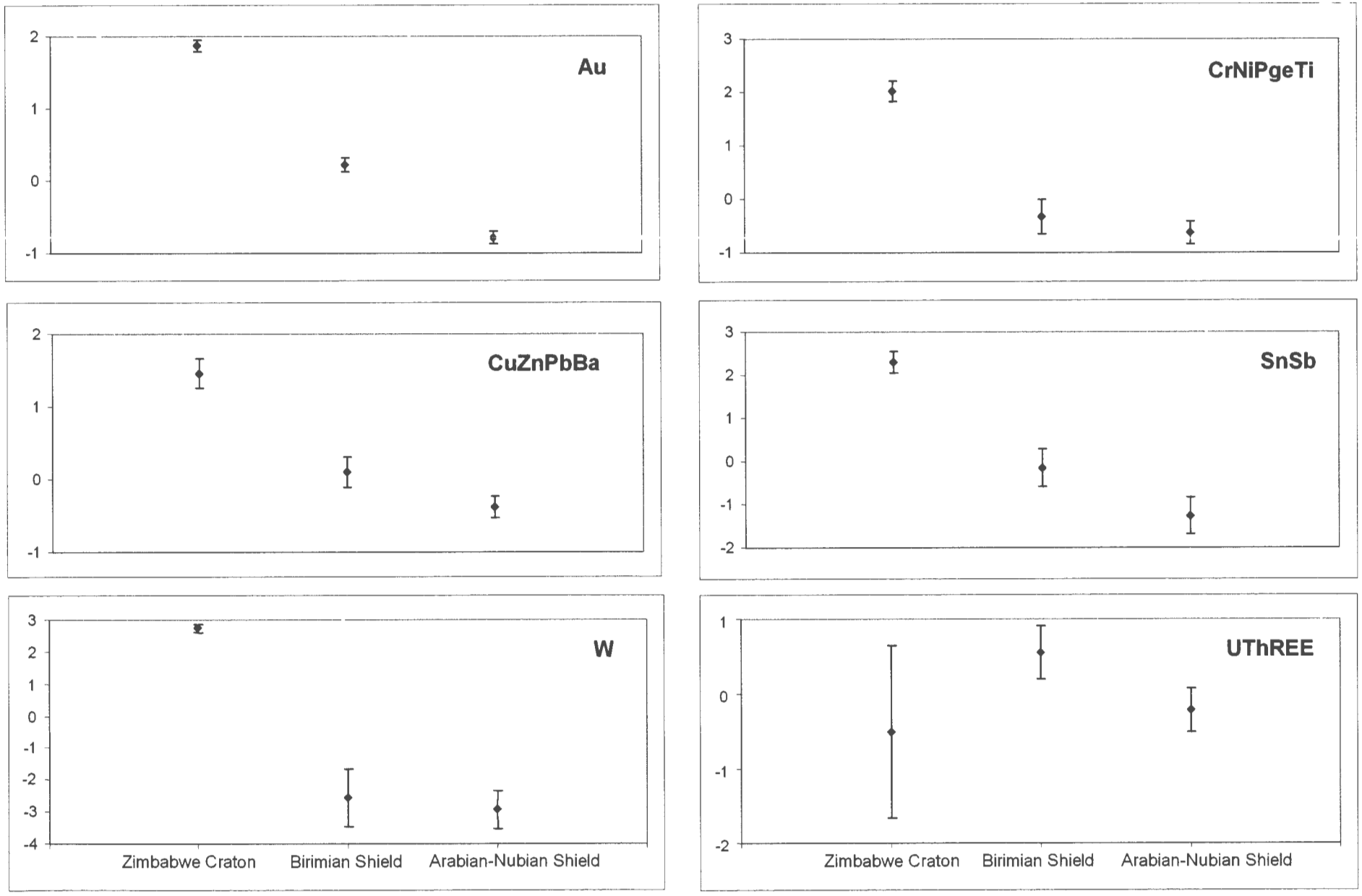

Figure 6.1 The mineral diversity of selected elements of three African crust, as shown by plotting the (natural log, Y-axis) spatial coefficient of the six element groups.

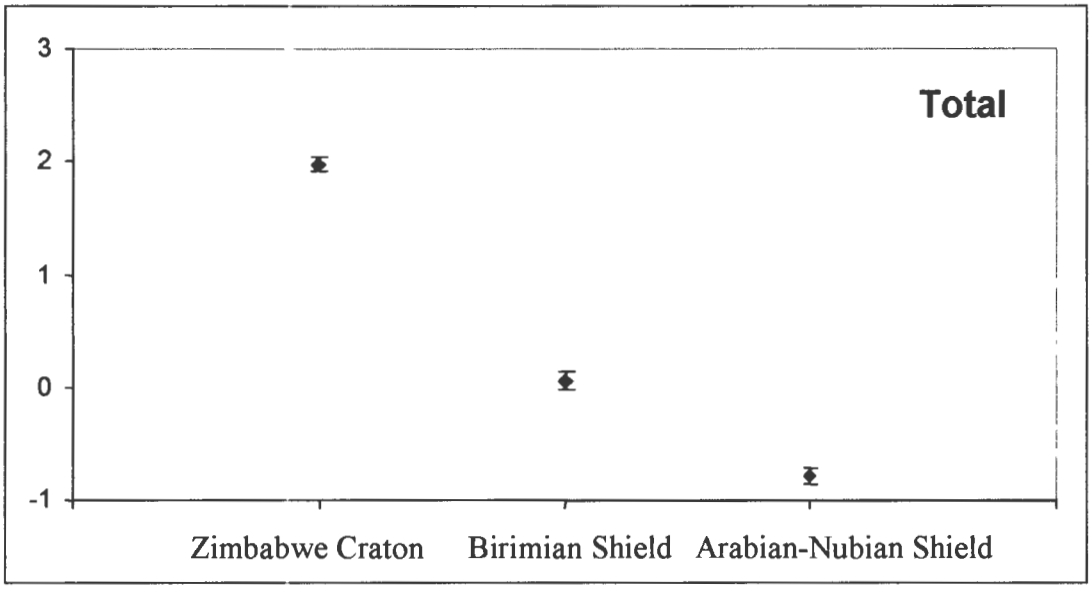

Figure 6.2 Mineral diversity of selected elements in the crust of the three study regions, derived by plotting the (natural log, Y-axis) spatial coefficient ($\ln \rho_{ij}$) of the total sum of six element groups in each region. Each region delineates a unique combination of elements. Confidence interval equals to 2x standard error.

Figure 6.1 displays a significant difference in mineral variation (diversity) for each region. The Arabian-Nubian Shield shows the lowest spatial coefficient for all six element groups. The Birimian Shield has an intermediate spatial coefficient for five element groups, but the highest coefficient for UThREE. The Zimbabwe craton displays the strongest spatial coefficient for five element groups, but the lowest coefficient for UThREE. Figure 6.2 shows clearly that there is a downwards trend with time from the Archean to the Neoproterozoic of the total sum of six element groups in representative juvenile crust during this time interval. This implies that mineralization during formation of the youngest juvenile crust, was of low diversity.

The above results are consistent with the analyses carried out by de Wit and Thiart, (2005), Thiart and de Wit (2006) on a near-global scale (Gondwana Continents) for Archean cratons (>2.5 Ga) compared to younger crust (<2.5 Ga). Their analysis shows that each craton appears to have a unique metallogenic fingerprint and that a significant mineral diversity exists in the crust of different cratons of similar ages, and that Archean crust has a

greater mineral diversity than that of younger crust. This study yields similar results in that all three regions formed over an approximately same length of geologic time, but at different times spanning nearly 2500 million years, and the oldest region has the greater diversity of mineral deposits.

In order to evaluate any secular change in mineralization, a final analysis to determine variations in the density of mineral deposits per unit area over time is given in the next chapter.

Chapter 7

Testing for secular change of mineralization in African crust

One of the main objectives of this study is to provide information about any variation in the total concentration of mineral deposit of the chozen elements across the three African crustal segments of different ages, and to use this information to test for secular change in mineralization over a period of about 2500 million years of Earth history (~500-3000 Ma). This chapter evaluates the results of the spatial analysis and treats the mineral deposits data further in an integrated time frame. As discussed in Chapter 2, the selected elements were chosen because of their range of behavioural characteristics within the earth and, in particular, for their concentration within mineral deposits throughout the three selected regions. The aim of this chapter is to summarize the overall distribution of the selected elements in each crustal segment in order to provide a quantitative insight into possible secular changes in mineralization of African crust, beyond that based purely on expert knowledge (e.g. Groves et al., 2005).

7.1 Variations in mineralization of three African crustal segments

First, the results described in Chapter 6 are replotted in this section by combining all the data of the three selected regions to create their respective metallogenic 'fingerprints' (e.g. de Wit and Thiart, 2005). These 'fingerprints' enable direct comparison of the metal endowment of old-crust (Zimbabwe craton) with mineralization in median-age crust (Birimian Shield) and with relatively young-crust (Arabian-Nubian Shield). On the basis of the distributions of mineral deposits throughout the three African crustal segments, it is possible to construct 'abundance/significance' mineral deposit signatures for each of the regions. These are given in Figure 7.1 and represent the spatial association between all element groups and the three African crustal segments.

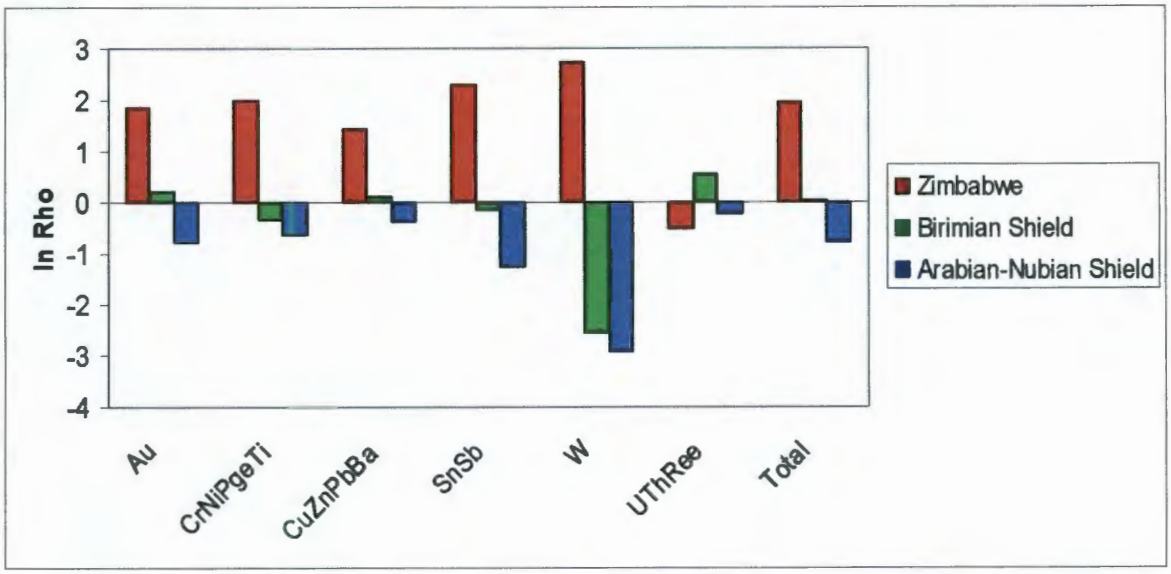

Figure 7.1. Spatial associations between all element groups and three selected regions of African crust.

The results emphasize the variations in mineralization between the three African crustal segments of different ages in Chapter 6. The Archean Zimbabwe craton (old-crust) forms a stronger association with five out of six element groups. Only the UThREE group is greater in the median-age crust (Birimian), and possibly in the younger crust (Arabian-Nubian Shield). The younger crust of the Arabian-Nubian Shield is the least well-endowed crustal segment for all the remaining five element groups. What is obvious from these results is that there is a distinct difference both in overall metal endowment between the six element groups for each African region, as well as the combined total element groups, which shows that the oldest crust is the most enriched in mineral deposits per unit area.

The implications of these differences would suggest that the various terrains were subjected either to fundamental different processes (for example, different tectonics or geodynamics in the Archean, e.g. Hamilton, 1998) or different rates of the same processes (e.g. different rates of geodynamic processes, e.g. de Wit, 1998), assuming similar states of preservation. The three regions were chosen because of the similarities of their geology (granite-greenstone terrain) and the juvenile nature of their crust at the time of their

formation. Thus, it can be assumed that they were not formed in vastly different tectonic environments. Alternatively, the oldest terrain, the Zimbabwe craton is composed of Archean greenstones belt that originated during a time of higher heat production and probably a higher mantle temperature (e.g. Pollack, 1997). Au, PGE and Ni concentrations are suggested to be higher in their mantle-derived Archean host rocks compared to those formed at younger times (e,g. de Wit and Ashwal, 1997 and Herrington et al., 1997; Groves et al., 2005). The high concentrations of Au, PGE and Ni in the Zimbabwe Archean terrains are consistent with these suggestions.

Therefore, the high concentration of five element groups in the Zimbabwe craton may be related to higher mantle temperatures in the Archean, and possibly reflect higher rates of geodynamics processes. Perhaps more deep mantle plumes 'ponded' at the base of the mantle (Pollack, 1997; Barley et al., 1998). Alternatively deep recycling of oceanic lithosphere (subduction) may have been more efficient in the Archean (e.g. de Wit, 1998; Hynes, 2001). Both processes would have resulted in the higher concentration of siderophile elements from near the core-mantle boundary into the overlying lithosphere. In similar way, gold may have been more effectively concentrated in syn-tectonic brittle-ductile faults tapping deeper mantle fluids (e.g. Groves et al., 2005 and references therein).

Wilsher (1995) also emphasized that cratonic stabilization is also considered to have been an important evolutionary stage of the continental crust. Stabilization of the cratons has important implications for the formation and preservation of mineral deposits. The Great Dyke (CrNiPgeTi group) is a product of this stabilization (e.g. Mukasa et al., 1998; Oberthür et al., 2002). Because deposits are unlikely to suffer major reworking when they are not located at the boundaries of tectonic domains.

7.2 Towards quantifying secular change in mineralization of Africa

To compare the spatial association between elements groups of three selected regions of African crust in a time-integrated manner, the total number of deposits per unit area is plotted against a time scale (Fig. 7.2).

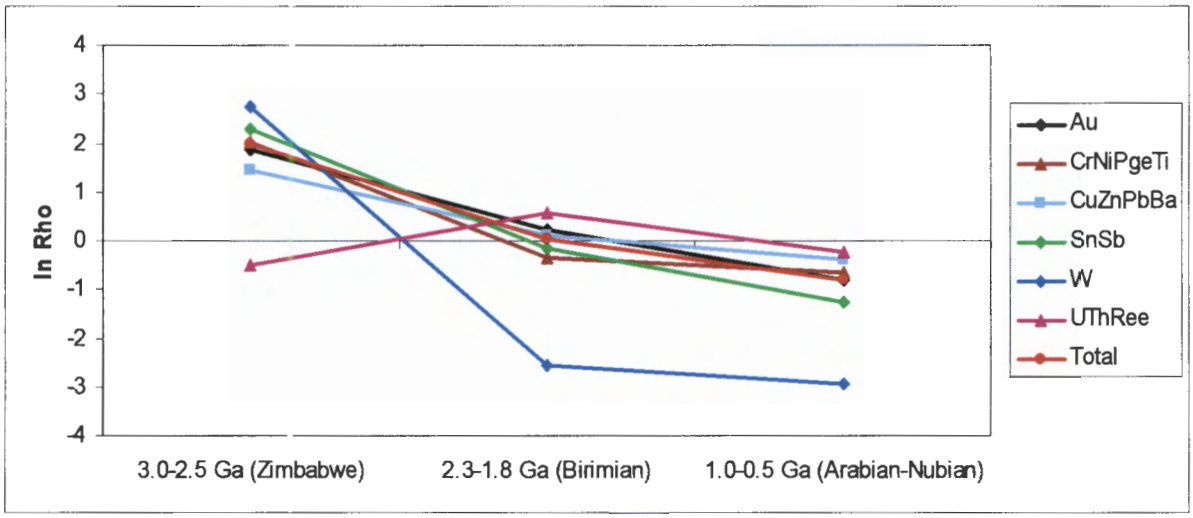

Figure 7.2. Relative concentration of mineral deposits of all six element groups in the three studied African regions. Five of the six element groups are concentrated to a greater degree in the Zimbabwe craton compared to that of younger crust.

This figure shows clearly the decrease in time in density of mineral deposits per unit area among the selected regions for each set of elements of the six mineral groups. Positive values indicate a measure of the spatial association between the area (selected region) and mineral deposits group (likelier to find a deposit: the greater the value, the greater the chance). Negative values indicate a measure of the negative association (less likely to find a deposit).

The results of this study support qualitative models that state mineral deposit density and diversity of Earth's continental lithosphere has decreased with time. It is possible, therefore that metallic elements in ore deposits were transferred more efficiently from the mantle to the continental lithosphere in the Archean. The detailed reasons for this are not well understood, but as mentioned in chapter 6 a greater Archean heat production is almost

universally accepted by earth scientists to have been the major cause for this, and other characteristics of Archean cratons (e.g. Pollack, 1997). This study therefore also corroborates conclusion of de Wit and Thiart (2005), and Thiart and de Wit (2006) that suggest old continental crust, globally, is more enriched in mineral deposits than younger crust (e.g. compare Fig 7.2 with Fig 7.3). These results are all consistent with a secular change in metallogenesis during the evolution of Earth's continental crust.

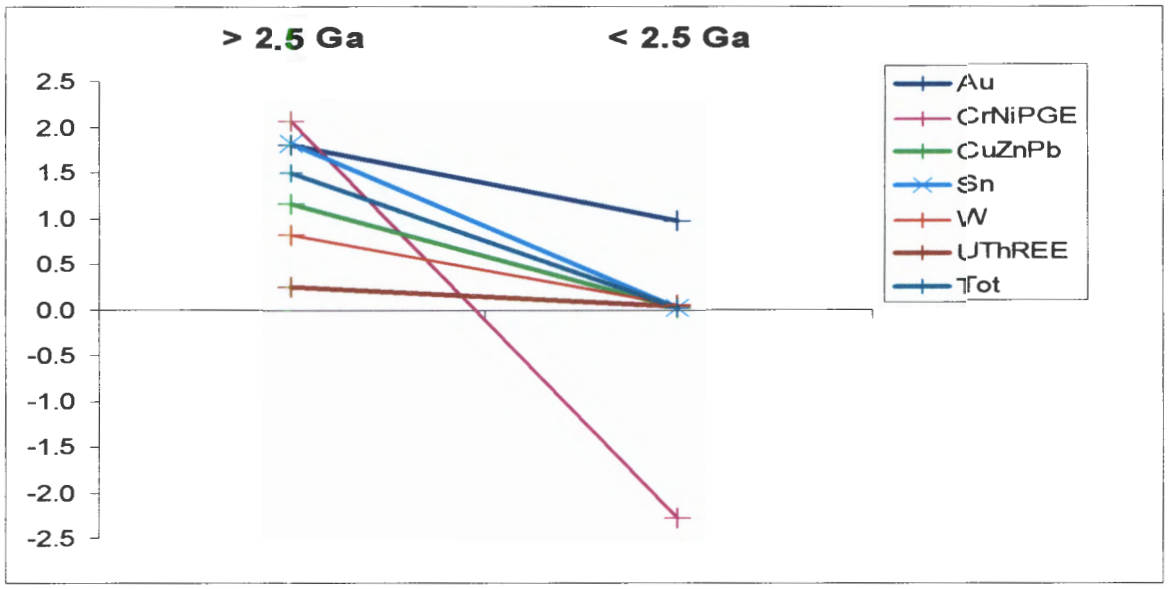

Figure 7.3. Concentration of mineral deposits of six element groups in the cratons (>2.5 Ga) and younger crust (<2.5 Ga) of the Gondwana continents, reproduced from de Wit and Thiart (2005) and Thiart and de Wit (2006). The results are similar to those found in this study on a smaller scale within one continent (e.g. Fig 7.2).

7.3 Discussion

De Wit and Thiart (2005) and Thiart and de Wit (2006) concluded that on a global scale Archean cratons are mineral-diversity hotspots that represent regional geochemical heterogeneities in the early Earth, and also that a significant mineral diversity exists amongst them. The results from this study show that a similar conclusion can be derived from the mineral deposits on a single continent, in this case, Africa. It is clear, therefore, that mineral endowment of the African crust has undergone major evolutionary changes from Archean to Neoproterozoic time.

Numerous other studies of mineral deposits over the past years have revealed distinctive differences through geological time. Such evolutionary changes in mineral deposits from Archean to Recent have been suggested to provide guides to the evolution of Earth's tectonic evolution and related processes (e.g. Hutchinson, 1981; Windley, 1993, 1995, Barley et al., 1998; Condie, 1998, 2000; Kerrich et al., 2000; Goldfarb et al., 2001; Groves et al., 2005). These changes are most likely in response to changes in the conditions of the earth's crust, mantle, hydrosphere, atmosphere, or biosphere under which these deposits were formed. Barley and Groves (1992) and Groves et al. (2005), for example, have qualitatively suggested that the distribution of mineralization through time is related to the following three major factors: the secular decrease in global heat flow in a cooling Earth; long-term changes in tectonic processes; and the evolution of the atmosphere-hydrosphere-biosphere system.

Groves et al. (2005) also suggest that mineral deposits show heterogeneous temporal distributions (e.g. punctuated at specific time) with each specific group of deposits having a distinctive, commonly unique, temporal pattern that they relate to the conjunction of formational and preservational processes on an evolving Earth. Barley and Groves (1992) and Barley et al. (1998) believe that some episodic changes in the temporal distribution of

specific mineral deposit types may be due to long-term episodic supercontinent formation and breakup. This conjecture is more difficult to test given the data in this study, and this needs further work on larger areas in Africa.

Groves et al. (2005) relates all the secular changes in tectonic processes to a change from strongly plume-influenced buoyant style plate tectonics in the Archean and Paleoproterozoic to modern-style plate tectonics from the Neoproterozoic to present. Similar studies by Griffin et al. (2003) suggests that there are progressive changes in mantle plume intensity and frequency with time that led to progressive evolution of thinner, less buoyant sub-continental lithospheric mantle. These might imply that crustal formation and preservation processes, and formation of mineral deposits were linked in the early Earth but became decoupled in the Proterozoic to recent. However, there is considerable controversy about the evolution of tectonic processes since the Archean (e.g. de Wit 1998; Hamilton, 1997), and all of this needs further robust analyses.

Finally it is sometimes argued that the higher concentration of Archean mineral deposits may represent a greater preservation potential of Archean Cratons relative to Proterozoic and younger Shields. Thus, greater mineral wealth of Archean cratons may be merely a consequence of greater rates of recycling (erosion) of young crust relative to that of Archean crust, perhaps due to the relatively stable deep lithospheric mantle keels that underlie cratons but not younger lithosphere (e.g. Fouch et al., 2004; de Wit and Thiart, 2005). However, in this study, the three areas studied comprise similar geology at similar low grade metamorphic assemblages, so that differential erosion is not likely. Therefore, in this African based study, the preservation potential for each of the three areas is likely to be similar.

Chapter 8

Conclusions and Recommendations

8.1 Conclusion

This project has focused on quantifying spatial associations between the mineral deposits and geology across three African crustal segments, to derive fundamental information with which to "fingerprint" the metal endowment in different regions of African continental crust.

The main objectives of this study were all accomplished to varying degrees, namely:

1. Upgrading the existing Gondwana-Geoscientific Indexing Database (GO-GEOID). The GO-GEOID is now updated to include over 17 000 mineral deposits across Gondwana (from 16 000 mineral deposits, 1995-2000). Just over 1061 new mineral deposits in the three selected regions were added to the African database that now hold information on more than 8000 mineral deposits.

2. Developing and demonstrating a method to quantify spatial associations between known mineral deposits and geological features as inputs to produce predictive mineral potential maps. This objective was achieved by using one of the established spatial modelling method based on Bayesian probability model (weights of evidence, WofE model). The WofE method was used to quantify spatial associations between the mineral deposits and geological features (lithology, contacts and brittle faults / ductile shears) of three studied regions of greatly different ages. The results show that in all three regions, there is a strong lithology controls on mineralization, as reflected by their positive spatial associations. In all three regions, gold deposits are associated with the greenstone belts and the granitoids rocks. In contrast, the SnSb and W deposits are distributed near or along

the contacts of granitoids and greenstone belts. In the Zimbabwe Craton, ductile shears show a positive spatial association with gold deposits but the brittle faults/ductile shears have no obvious spatial association in the other two regions although they were included in the analyses. The evidential themes of the Zimbabwe Craton have greater predictive values than those of the Birimian and the Arabian Shield. However, a main limitation of the WofE method is that there should be a fairly large number of mineral deposit points. Therefore the spatial association of many element groups could not be tested in the Birimian and Arabian-Nubian Shields.

3. Determining variations in the total concentration of mineral deposits in crust of different ages, and testing for secular changes in mineralization over a period of 2500 million years of Earth history in Africa, from the Archean to the Neoproterozoic. The patterns of the mineral distribution within the selected areas are observed by determining spatial coefficient between the mineral deposits and the selected region. Results show that there is a distinct difference in the total concentration of mineral deposits in African crust of different ages, and each region appears to have a unique metal endowment "fingerprint" (or metallogenic). It was concluded that there is a greater concentration of mineral deposits in Archean crust (Zimbabwe craton) compared to younger crust (Arabian-Nubian Shield).

These differences are consistent with a decrease of mineral mass in Africa's preserved continental crust over time and this reflects a possible secular change in crustal evolution and geodynamic processes driven by a decrease in Earth's heat production. Therefore, this study has quantified to some degree the established observations that old-crust is more enriched in mineral deposits than younger crust, and that Archean metallogenesis was more efficient than in subsequent times.

8.2 Recommendation for future work

Although this project of spatial analyses of mineral deposits and geology across three African crustal segments of different age has been useful, some words of caution are required in form of recommendations for further studies:

- No distinction was made in this study between large and small mineral deposits. The results are therefore expressed merely in terms of the number of mineral deposits, representing points rather than volumes per unit crust analysed. This is clearly a weakness of this study that now needs to be addressed further by incorporating tonnages and grades of the deposits.

- The regions studied are known to have been explored to different degrees. As a result in some areas of Africa, fewer deposits reflect to some degree the history/state of exploration. Less developed countries with poor infrastructure and political instability are less likely to have discovered its mineral deposits to the same degree as better developed countries (e.g compare DRC with South Africa). Thiart and de Wit (2006) attempted to introduce this in their analysis using an economic index. This also needs further analyses in the present study areas.

- The WofE method requires evidential themes. In this study, more data inputs (evidence maps) are needed. There is lack, for example, of structural (faults and/or ductile shears) information. In addition, increasing the number of other input maps (such as geochemistry and geophysics) will increase the confidence that mineralization may be present or absent in specified regions.

- Finally, no allowance has been made for the level of relative erosion. However, all the three areas studied in this project have rock sequences that are at similar greenschist-facies metamorphism and therefore likely display a similar depth-section through the crust. Elsewhere, however, such a distinction must be taken into account.

As discussed in this thesis, African crustal segments (regions) appear to have a unique metal endowment in regions of different ages. These differences indicate a total decrease of mineral mass in Africa's preserved continental crust over time. Therefore, the approach adopted in this project provides insights towards better understanding the long-term evolution in mineralization processes.

References

Abdelsalam, M.G., (1994). The Oko shear zone: post-accretionary deformation in the Arabian-Nubian Shield. Journal of the Geological Society. London, **151**, 767-776

Abdelsalam, M.G., Stern, R.J., (1996). *Sutures and shear-zones in the Arabian-Nubian Shield.* Journal of African Earth Sciences, **23**, 289-310

Abouchami, W., Boher, M., Michard, A., Albréde, F., (1990). *A major 2.1 Ga event of mafic magmatism in West-Africa: an early stage of crustal accretion.* Journal of Geophysical Research, **95** (B11), 17605-17629

Agar, R.A., (1992). *The tectono-metallogenic evolution of the Arabian Shield.* Precambrian Research, **58**, 169-194

Agterberg, F.P.,Cheng, Q., (2002). *Conditional independence test for weights of evidence modeling.* Natural Resources Research, **11** (4), 249-255

Agterberg, F.P., Bonham-Carter, G.F., Wright, D.F., (1990). Statistical Pattern Integration for Mineral Exploration. **In:** Gaal, G., and Merriam, D.F. (eds). *Computer Applications in Resource Estimation:* Pergamon Press, Oxford. 1-21

Agterberg, F.P., Bonham-Carter, G.F., Cheng, Q.,Wright, D.F., (1993). *Weights of evidence modelling and weighted logistic regression for mineral potential mapping.* **In:** Davis, J.C., Herzfeld, U.C. (eds). Computers in Geology, 25 Years of Progress: Oxford University Press, Oxford, England, 13-32

Armstrong, R.L., (1981). *Radiogenic isotopes: the case for crustal recycling on a near steady-state no-continental growth earth.* Philosophical Transactions of the Royal Society, London, **301**, 443-472

Armstrong, R.L., (1991). *The persistent myth of crustal growth.* Plilos. Australian Journal of Earth Sciences, **38**, 613-630

Asadi, H.H., Hale M., (2001). *A Predictive GIS model for mapping potential gold and base metal mineralization in Takab area, Iran.* Computers & Geosciences **27**, 901-912

Attoh, K., Ekwueme, B.N., (1997). The West African Shield. **In:** de Wit, M. and Ashwal, L.D. (eds.) *Greenstone Belts*. Clarendon Press. Oxford, 517-528

Barley, M.E., Groves, D.I., (1992). *Supercontinent cycles and the distribution of metal deposits through time.* Geology, **20**, 291-294

Barley, M.E., Krapez, B., Groves, D.I., Kerrich, R., (1998). *The Late Archean bonanza: metallogenic and environmental consequences of the interaction between mantle plumes, lithospheric tectonics and global cyclicity.* Precambrian Research **91**, 65-90

Bates, R.L., Jackson, J.A., (1987). *Glossary of Geology*. 3rd edition. American Geological Institute Alexandria, Virginia, 788

Berhe, S.M., (1990). *Ophiolites in northeast and east Africa: implications for Proterozoic crustal growth.* Journal of the Geological Society, London, **147**, 41-57

Berhe, S. M., (1997). The Arabian-Nubian Shield. **In:** De Wit, M. and Ashwal, L.D. (eds) *Greenstone Belts*. Clarendon Press, Oxford, 761-771

Béziat, D., Bourges, F., Debat, P., Lompo, M., Martin, F., Tollon, F., (2000). A Paleoproterozoic ultramafic-mafic assemblage and associated volcanic rocks of the Boromo greenstone belt: fractionates originating from island-arc volcanic activity in the West African craton. Precambrian Research, **101**, 25-47

Bickle, M.J., Nisbet, E.G., (eds) (1993). *The Geology of the Belingwe Greenstone Belt, Zimbabwe: A study of the evolution of Archean continental crust.* Geological Society of Zimbabwe, Special Publication **2**, A.A. Balkema, Rotterdam, 239

Billa, M., Cassard, D., Lips, A.L.W., Bouchot, V., Tourlière, B., Stein, G. ,Guillou-Frottier, L., (2004). *Predicting gold-rich epithermal and porphyry systems in the central Andes with a continental-scale metallogenic GIS.* Ore Geology Reviews, **25**, 39-67

Blasband, B., White, S., Brooijmans, P., DeBrooder, H., Visser, W., (2000). *Late Proterozoic extensional collapse in the Arabian-Nubian Shield.* Journal of the Geological Society. London, **157**, 615-628

Blenkinsop, T., Martin, A., Jelsma, H.A., Vinyu, M.L., (1997). The Zimbabwe craton. **In:** de Wit, M.J. and Ashwal, L.D. (eds.), *Greenstone Belts*. Clarendon Press, New York, 567-580

Boher, M., Abouchami, W., Michard, A., Albréde, F., Arnt, T.N., (1992). *Crustal growth in West Africa at 2.1 Ga*. Journal of Geophysical Research, **97** (B1), 345-369

Boleneus, D.E, Raines, G.L., Causey, J.D., Bookstrom, A.A., Frost, T.P., Hyndman, P.C., (2002). *Assessment Method for Epithermal Gold Deposits in Northeast Washington State using Weights of Evidence GIS Modelling*. U.S. Geological Survey Open File Report OF01-501, http://geopubs.wr.usgs.gov/open-file/of01-501/

Bonham-Carter, G. F., (1994). *Geographic Information System for Geoscientists: Modelling with GIS*, Computer Methods in the Geosciences **13**, Pergamon. 398

Bonham-Carter, G. F., Agterberg, F.P., (1999). *Arc-WofE: a GIS tool for statistical integration of mineral exploration datasets*. Proc.52nd Session of Intern. Statistical Inst. (Helsinki, Finland) Unpaginated, http://www.stats.fi/isi99/proceedings.html

Bonham-Carter, G.F., Agterberg, F.P., Wright, D.F., (1988). *Integration of geological datasets for gold exploration in Nova Scotia.* Photogrammetric Engineering and Remote Sensing, **54** (11), 1585-1592

Bonham-Carter, G.F., Agterberg, F.P., Wright, D.F., (1989). Weights of evidence modelling: a new approach to mapping mineral potential. **In:** Agterberg, F.P. and Bonham-Carter, G.F. (eds). *Statistical Applications in the Earth Sciences*. Geological Survey of Canada, Paper 89-9, 171-183

Bossiére, G., Bonkoungou, I., Peucat, J.-J., Pupin, J.-P., (1996). *Origin and age of Paleoproterozoic conglomerates and sandstones of the Tarkwaian Group in Burkina Faso, West Africa*. Precambrian Research, **80**, 153-172

Bourges, F., Debat, P., Tollon, F., Munoz, M., Ingles, J., (1998). *The geology of the Taparko gold deposit Birimian greenstone belt, Burkina Faso, West Africa*. Mineralium Deposita **33**, 591-605

Bowring, S.A., Grotzinger, J.P., Isachsen, C.E., Knoll, A.M., Pelachaty, S.M., Kolosov, P., (1993). *Calibrating rates of early Cambrian evolution.* Science, **261**, 1293-1298

Bowring, S.A., Housh, T., (1995). *The earth's early evolution.* Science, **269**, 1535 -1540

Burke, K., (1996). *The African Plate*. Alex L. du Toit Memorial Lectures No. 24. South African Journal Geology, **99**, 339-409

Burrough, P.A., McDonnell, R.A., (1998). *Principles of Geographical Information Systems.* (2nd edition), Oxford University Press. 333

Cahen, L., Snelling, N.J., Delhal, J., Vail, J.R., Bonhomme, M., Ledent, D., (1984). *The geochronology and evolution of Africa.* Clarendon Press. Oxford, 512

Campbell, S.D.G., Pitfield, P.E.J., (1994). *Structural controls of gold mineralization in the Zimbabwe craton-exploration guidelines.* Zimbabwe Geological Survey Bulletin **101**, 270

Carranza, E.J.M., (2002). *Geologically- Constrained Mineral Potential Mapping: examples from the Philippines*. PhD Thesis. ITC Publication No. **86**, 477

Carranza, E.J.M., Hale, M., (2000). *Geologically- Constrained Probabilistic Mapping of Gold Potential, Baguio District, Philippines*. Natural Resources Research, **9**, No.3, 238-253

Condie, K.C. (ed.), (1992). *Proterozoic Crustal Evolution*. Developments in Precambrian Geology **10**. Elsevier, Amsterdam, 537

Condie, K.C. (ed.), (1994). *Archean Crustal Evolution*. Developments in Precambrian Geology **11**. Elsevier, Amsterdam, 547

Condie, K.C., (1998). *Episodic continental growth and supercontinents: a mantle avalanche connection?* Earth and Planetary Science Letters, **163**, 97-108

Condie, K.C., (2000). *Episodic continental growth models: afterthoughts and extensions.* Tectonophysics, **322,** 153-162

Chen, Y., (2004). *MRPM: three visual basic programs for mineral resource potential mapping*. Computers and Geosciences, **30**, 969-983

Cheng, Q., (2004). *Application of Weights of Evidence Method for Assessment of Flowing Wells in the Greater Toronto Area, Canada.* Natural Resources Research, **13**(2), 77-86

Davis, D.W., Hirdes, W., Schalteg ger, Nunoo, E.A. (1994). *U-Pb age constraints on deposition and provenance of Birimian and gold-bearing Tarkwaian sediments in Ghana, West Africa.* Precambrian Research, **67**, 89-107

de Wit, M.J., (1998). *On Archean granites, greenstones, cratons and tectonics: does the evidence demand a verdict*? Precambrian Research, **91**, 181-226

de Wit, M.J., (2003). *Madagascar: Heads it's a continent, tails it's an island.* Annals Review of Earth Planetary Science, **31**, 213-248

de Wit, M.J., (2005). *Valuing copper mined from ore deposits.* Ecological Economics, **55**, 437-443

de Wit, M.J., Ashwal, L.D. (eds) (1997). Preface: Covergence Towards Divergent Models of Greenstone Belts. *Greenstone Belts*. Oxford University Press, Oxford, xvii

de Wit, M.J., Berg, R., (1981). Platinum. **In:** Chewaka and de Wit (eds.). *Plate Tectonics and Metallogenesis: Some Guidelines to Ethiopian Mineral Deposits*. Ministry of Mines, Energy and Water Resources. Bulletin **2**. Ethiopian Institute of Geological Surveys. 83-88

de Wit, M.J., Jeffery, M., Bergh, H., Nicolaysen, L., (1988). *Geological map of sectors of Gondwana reconstructed to their disposition ~150 Ma, scale 1: 10 000 000.* American Association petroleum Geologists, Tulsa, Oklahoma.

de Wit, M., Thiart, C., (2005). *Metallogenic fingerprints of Archean cratons.* **In:** McDonald, I., Boyce, A.J., Butler, I.B., Herrington, R.J. and Polya, D.A. (eds). *Mineral Deposits and Earth Evolution*. Geological Society, London, Special Publications, **248**, 59-70

de Wit, M.J., Thiart, C., Doucoure, C.M., Wilsher, W., (1999). *Scent of a supercontinent: Gondwana's ores as chemical tracers – tin, tungsten and the Neoproterozoic Laurentia-Gondwana connection.* Journal of African Earth Sciences, **28**, 35-51

Debat, P., Nikiéma, S., Mercier, A., Lompo, M., Béziat, D., Bourges, F., Roddaz, M., Salvi, S., Tollon, F., Wenmenga, U., (2003). *A new metamorphic constraint for the Eburnean orogeny from Paleoproterozoic formations of the Man shield (Aribinda and Tampelga countries, Burkina Faso).* Precambrian Research, **123**, 47-65

Dilek, Y., Ahmed, Z., (2003). Proterozoic ophiolites of the Arabian Shield and their significance in Precambrian tectonics. **In:** Dilek, Y. and Robinson, P. T. (eds). *Ophiolites in Earth History.* Geological Society, London, Special Publications, **218**, 685-700

Dirks, P.H.G.M., Jelsma, H.A., (1998a). *Horizontal accretion and stabilization of the Zimbabwe Craton.* Geology, **26**, 11-14

Dirks, P.H.G.M., Jelsma, H.A., (1998b). *Silicic layer-parallel shear zones in a Zimbabwe Greenstone sequence: horizontal accretion preceding doming.* Gondwana Research, **1**, 177-194

Dirks, P.H.G.M., Jelsma, H.A., (2002). *Crust-mantle decoupling and the growth of the Archean Zimbabwe Craton.* Journal of African Earth Science, **34**, 157-166

Dirks, P.H.G.M., Jelsma, H.A., Hofmann, A., (2002). *Thrust-related accretion of an Archean greenstone belt in the Midlands of Zimbabwe.* Journal of Structural Geology, **24**, 1707-1727

Dirks, P.H.G.M., Jelsma, H.A., Mikhailov, A., Barber, B., (2002). *Lithospheric lineaments and their controls on the distribution of Archean gold deposits.* Geology (submitted)

Dirks, P.H.G.M., van der Merwe, J., (1997). *Early duplexing in an Archean greenstone sequence and its control on gold mineralization.* Journal of African Earth Sciences, **24**, 603-620

Dixon, C.J., (1979). *Atlas of Economic Mineral Deposits.* Chapman & Hall, London, 143

Doumbia, S., Pouclet, A., Kouamelan, A., Peucat, J.J., Vidal, M., Delor, C., (1998). *Petrogenesis of juvenile-type Birimian (Paleoproterozoic) granitoids in Central Côte-d'Ivoire, West Africa: geochemistry and geochronology.* Precambrian Research, **87**, 33-63

Egal, E., Thiéblemont, D., Lahondére, D., Guerrot, C., Costea, C.A., Iliescu, D., Delor, C., Goujou, J.-C., Lafon, J.M., Tegyey, M., Diaby, S., Kolié, P., (2002). *Late Eburnean granitization and tectonics along the western and northwestern margin of the Archean Kénéma-Man domain (Guinea, West African Craton).* Precambrian Research, **117**, 57-84

Eyal, M., Litvinovsky, B.A., Katzir, Y., Zanvilevich, A. N., (2004). *The Pan-African high-K calc-alkaline peraluminous Elat granite from southern Israel: geology, geochemistry and petrogenesis.* Journal of African Earth Sciences, **40**, 115-136

Feybesse, J.L., Milési, J.P., (1994). *The Archean/Proterozoic contact zone in West Africa: a mountain belt of decollement thrustingand folding on a continental margin related to 2.1 Ga convergence of Archean cratons*? Precambrian Research, **69**,199-227

Fouch, M.J., James, D.E., VanDecar, J.C., van der Lee, S., Kaapvaal Seismic Group, (2004). Mantle seismic structure beneath the Kaapvaal and Zimbabwe Cratons. South African Journal of Geology, **107**, 33-44

Frost-Killian, S., (2003). *International Metallogenic Map of Africa, at a scale of 1:5 000 000.* Commission for the Metallogenic Map of the World (CGMW). Council for Geoscience. Pretoria, South Africa

Fyfe, W.S., (1978). *The evolution of the earth's crust: modern plate tectonics to ancient hot spot tectonics?* Chemical Geology, **23**, 89-114

Genna, A., Nehlig, P., Le Goff, E., Gguerrot, Cc., Shanti, M., (2002). *Proterozoic tectonism of the Arabian Shield.* Precambrian Research, **117**, 21–40

Ghosh, J.G., de Wit, M.J, Zartman, R.E., (2004). *Age and tectonic evolution of Neoproterozoic ductile shear zones in the Southern Granulites Terrain of India, with implications for Gondwana Studies.* Tectonics, **3**, 1-38

Goldfarb, R.J., Groves, D.I., Gardoll, S., (2001). *Orogenic gold and geologic time: a global synthesis.* Ore Geology Reviews, **18,** 1–75

Goossens, P.J., (1983). *Precambrian Mineral Deposits and their Metallogeny.* Annale-Serie In 8°-Sciences Geologiques - n° 89, 97

Grenne T., Pedersen, R.B., Bjerkgard, T., Braathen, A., Selassie, M.G., Worku, T., (2003). *Neoproterozoic evolution of Western Ethiopia: igneous geochemistry, isotope systematics and U-Pb ages*. Geological Magazine, **140** (4), 373-395

Griffin, W.L., O'Reilly, S.Y., Abe, N., Aulbach, S., Davies, R.M., Pearson, N.J., Doyle, B.J., Kivi, K., (2003). *The origin and evolution of Archean lithospheric mantle.* Precambrian Research, **127**, 19-41

Groves, D.I., Goldfarb R.J., Gebre-Mariam, M, Hagemann, S.G., Robert, F., (1997). *Orogenic gold deposits: A proposed classification in the context of their crustal distribution and relationship to other gold deposit types.* Ore Geology Reviews, **13**, 7-27

Groves, D.I., Ridley, J.R., Bloem, E.M.J., Gebre-Mariam, M, Hagemann, S.G., Hronsky, J.M.A., Knight, J.T., McNaughton, N.J., Ojala, J., Vielreicher, R.M., McCuaig, T.C., Holyland, P.W., (1995). Lode-gold deposits of the Yilgarn block: products of Late Archean crustal-scale overpressured hydrothermalsystems. **In:** Coward, M.P. and Rice, A.C. (eds.), *Early Precambrian Processes*. Geological Society, London Special Publications, **95**, 155-172

Groves, D.I., Vielreicher, R.M., Goldfarb R.J., Condie, K.C., (2005). Controls on the heterogeneous distribution of mineral deposits through time. **In:** McDonald, I., Boyce, A.J., Butler, I.B., Herrington, R.J. and Polya, D.A. (eds.). *Mineral Deposits and Earth Evolution*. Geological Society, London, Special Publications, **248**, 71-101

Hamilton, W.B., (1998). *Archean magmatism and deformation were not products of plate tectonics.* Precambrian Research, **19**, 143-179

Hansen, D.T., (2000). *Describing GIS Application: Spatial statistics and Weights of Evidence Extension to Arcview in the Analysis of the Distribution of Archaeology Sites in the Landscape.* **In:** Proceedings of the Twentienth Annual ESRI International User Conference,SanDiego,CA.http://www.esri.com/library/userconf/proc00/professional/papers/PAP174/P174.htm

Harris J.R., Wilkinson, L., Grunsky, E.C., (2000). Effective use and interpretation of lithogeochemical data in regional mineral exploration programs: application of Geographic Information Systems(GIS)technology. Ore Geology Reviews, **16**, 107-143

Herrington, R.J., Evans, D.M., Buchanan, D.L., (1997). Metallogenic Aspects. **In:** de Wit, M. and Ashwal, L.D. (eds.), *Greenstone Belts*. Clarendon Press, New York, 176-219

Hirdes, W., Davis, D.W., (1998). *U-Pb zircon age of extrusive volcanism in the Birimian Supergroup of Ghana/West Africa*. Journal of African Earth Sciences, **27** (2), 291-294

Hirdes, W., Davis, D.W., (2002). *U-Pb geochronology of Paleoproterozoic rocks in the southern part of the Kedougou-Kéniéba inlier, Senegal, West Africa: evidence for dichronous accretionary development of the Eburnean province*. Precambrian Research, **118**, 83-99

Hirdes W., Davis D.W., Eisenlohr B.N. (1992). *Reassessment of Proterozoic granitoid ages in Ghana on the basis of U/Pb zircon and monazite dating*. Precambrian Research, **56**, 89-96

Hirdes, W., Davis, D.W., Lüdtke, G., Konan, G., (1996). *Two generations of Birimian (paleoproterozoic) volcanic belts in northeastern Côte-d'Ivoire: consequences for the 'Birimian controversy'*. Precambrian Research, **80**, 173-191

Hofmann, A., Kusky, T., (2004). The Belingwe Greenstone Belt: Ensialic or Oceanic? **In:** Kusky, T.M. (ed). *Precambrian Ophiolites and Related Rocks*. Elsevier, Amsterdam, 487-538

Hofmann, A., Dirks, P.H.G.M., Jelsma, H.A., Matura, N., (2003). *A tectonic origin for ironstone horizons in the Zimbabwe craton and their significance for greenstone belt geology.* Journal of the Geological Society, London, **160**, 83-97

Holland, H.D., Trendall, A.F. (eds.) (1984). *Patterns of Change in Earth Evolution.* Physical, Chemical, and Earth Sciences Research Report **5**. Dahlem Konferenzen. Springer-Verlag, Berlın. 431

Horstwood, M.S.A., Nesbitt, R.W., Noble, S.R., Wilson, J.F, (1999). *U-Pb zircon evidence for an extensive early Archean craton in Zimbabwe: a reassessment of the timing of craton formation, stabilization and growth.* Geology, **27**, 707-710

Hunter, G.J., (1999). Managing uncertainty in GIS. **In:** Longley, P.A., Goodchild, M.F., Manguire, D.J. and Rhind, D.W. (eds). *Geographical Information Systems*, **II**. John Wiley & Sons, 1101

Hunter, D.R., Stowe, C.W., (1997). *A* historial review of the origin, composition, and setting of Archean greenstone belts (pre-1980). **In:** de Wit, M.J. and Ashwal, L.D. (eds). *Greenstone Belts*. Oxford University Press, Oxford, 5-29

Hutchinson R.W., (1981). Mineral Deposits as guides to supracrustal evolution. **In:** O'Connell, R.J., and Fyfe, W.S. (eds), *Evolution of the earth: Geodynamics series*, **5**, American Geophysical Union, Washington DC, 120-140

Hutchinson R.W., (1992). Mineral Deposits and Metallogeny: indicators of Earth's Evolution. **In:** Schidlowski, M., Golubic, S. and Kimberley, M.M. (eds). *Early Organic Evolution: Implications for Mineral and Energy Resources*. Springer-Verlag Berlin Heidelberg, 522-545

Hynes, A., (2001). *Freeboard revisited: continental growth, crustal thickness change and Earth's thermal efficiency*. Earth and Planetary Sciences Letters, **185**, 161-172

Jelsma, H.A., (1993). *Granites and greenstones in northern Zimbabwe, tectono-thermal evolution and source regions*. PhD thesis, Free University of Amsterdam

Jelsma, H.A., (2003-2004). *Outline of the Southern Africa Craton*. De Beers Geoscience Centre, Exploration Division. South Africa

Jelsma, H.A., Dirks, P.H.G.M., (2000). *Tectonic evolution of a green-stone sequence in the northern Zimbabwe: sequential early stacking and pluton diapirism.* Tectonics **19**, 135-152

Jelsma, H.A., Dirks, P.H.G.M., (2002). Neoarchean tectonic evolution of the Zimbabwe craton. **In:** Fowler, C.M.R, Ebinger, C.J. and Hawkesworth, C.J. (eds.). *The Early Earth: Physical, chemical and biological development*. Geological Society of London, Special Publications, **199**, 183-211

Jelsma, H.A., Kroner, A., Bozhko, N., Stowe, C., (2004). *Single zircon ages for two Archean banded migmatitic gneises from central Zimbabwe.* South African Journal of Geology (Submitted)

Jelsma, H.A., Thiart. C., (2002). *Digital geological map for southern Africa.* Internal publication, Centre for Interactive Graphical Computing of Earth Systems, University of Cape Town

Jelsma, H.A., Vinyu, M.L., Valbracht, P.J., Davies, G.R., Wijbrans, J.R., Verdurmen, E.A.T., (1996). *Constraints on Archean Crustal evolution of the Zimbabwe craton: a U-Pb zircon, Sm-Nd and Pb-Pb whole rock isotope study.* Contribution of Mineral Petroleum, **124**, 55-70

Johnson, P.R., Woldehaimanot, B., (2003). Development of the Arabian-Nubian Shield: perspectives on accretion and deformation in the northern East Africa Orogen and the assembly of Gondwana. **In:** Yoshida, M., Windley, B.F. and Dasgupta, S. (eds.) *Proterozoic East Gondwana: Supercontinent Assembly and Breakup.* Geological Society, London, Special Publications, **206**, 289-325

Kemp, L.D., Bonham-Carter, G.F., Raines, G.L., (1999). *Arc-WofE: Arcview extension for weights of evidence mapping.* Ottawa, Canada. . http://ntserv.gis.nrcan.gc.ca/

Kemp, L.D., Bonham-Carter, G.F., Raines, G.L., Looney, C.G., (2001). *Arc-SDM: Arcview extension for spatial data modelling using weights of evidence, logistic regression, fuzzy logic and neural network analysis.* Ottawa, Canada. http://ntserv.gis.nrcan.gc.ca/sdm/

Kerrich, R., Goldfarb, R.J., Groves, D.I., Garwin, S., (2000). The geodynamics of world class gold deposits: characteristics, space-time distribution and origins. **In**: Hagemann, S.G. and Brown, P.E. (eds.). *Gold in 2000.* Reviews in Economic Geology, **13**, 501-551

Kouamelan, A.N., Delor, C., Peucat, J.J., (1997). *Geochronological evidence for reworking of Archean terrains during the Early Proterozoic (2.1 Ga) in the western Côte d'Ivoire (Man Rise-West African Craton).* Precambrian Research, **86**, 177-199

Kröner, A., Linnebacher, P., Stern, R.J., Reischmann, T., Manton, W., Hussen, I. M., (1991). *Evolution of Pan-African island-arc assemblages in the southern Red-Sea Hills, Sudan, and in southwestern Arabia as exemplified by geochemistry and geochronology.* Precambrian Research, **53**, 99-118

Kusky, T.M., (1998). *Tectonic setting and terrane accretion of the Archean craton.* Geology, **26**, 163-166

Kusky, T.M., (ed.) (2004). *Introduction - Precambrian Ophiolites and Related Rocks.* Developments in Precambrian Geology **13**. Elsevier, Amsterdam, 1-34

Kusky, T.M., Abdelsalam, M., Tucker, R., Stern, R., (2003). *Evolution of the East African and Related Orogens, and the Assembly of Gondwana*. Special Issue of Precambrian Research, **123** (1-4), 81-85

Kusky, T.M., Kidd, W.S.F., (1992). *Remnants of an Archean oceanic plateau, Belingwe greenstone belt, Zimbabwe*. Geology, **20**, 43-46

Kusky, T.M., Polat, A., (1999). *Growth of greenstone terranes at convergent margins, and stabilization of Archean cratons.* Tectonophysics, **305**, 43-77

Kusky, T.M., Vearncombe, J.R., (1997). Structural Aspects. In: de Wit, M. and Ashwal, L.D (eds.). *Greenstone Belts.* Clarendon Press, Oxford, 91-124

Ledru, P., Johan, V., Milési, J. P., Tegyey, M., (1994). *Markers of the last stages of the Paleoproterozoic collision: evidence for a 2 Ga continent involving circum-South Atlantic provinces*. Precambrian Research, **69**, 169-191

Ledru, P., Pons, J., Milési, J.P., Feybesse, J.L., Johan, V., (1991). *Transcurrent tectonics and polycyclic evolution in the Lower Proterozoic of Senegal-Mali.* Precambrian Research, **50**, 337-354

Leube, A., Hirdes, W., Mauer, R., Kesse, G.O., (1990). *The early Proterozoic Birimian Supergroup of Ghana and some aspects of its associated gold mineralization.* Precambrian Research, **46**, 139-165

Liégeois, J.P., Black, R., Navez, J., Latouche, L., 1994. Early and late Pan-African orogenies in the Aïr assembly of terranes (Tuareg shield, Niger). Precambrian Research, **67**, 59-88.

Liégeois, J.P., Claessens, W., Camara, D., Klerkx, J., (1991). *Short lived Eburnean orogeny in southern Mali.Geology, Tectonics, U-Pb and Rb-Sr geochronology.* Precambrian Research, **50**, 111-136

Macgregor, A.M., (1951). *Some Milestons in the Precambrian of Southern Rhodesia.* Presidential Address, Proceedings of the Geological Society of South Africa, **54**, 27-71

Marcoux, E., Milési, J.P., (1993). *Lead isotopes geochemistry and geochronology of Birimian ore deposits (West Africa).* Economic Geology, **88**, 1862-1879

Master, S., (1990). The "Ubendian" cycle in Equatorial and Southern Africa: Accretionary tectonics and continental growth. **In:** Rocci, G. and Deschamps, M. (eds), *New Data in African Earth Sciences.* CIFEG Occ. Publ. 1990/22, Orleans, 41-44

Meert, J.G., (2003). *A synopsis of events related to the assembly of eastern Gondwana.* Tectonophysics, **362**, 1-40

Mihalasky, M.J., Bonham-Carter, G.F., (2001). *Lithodiversity and its spatial association with metallic mineral sites, Nevada great basin.* Natural Resources Research, **10** (3), 209-226

Milési, J.P., Ledru, P., Feybesse, J.L., Dommanget, A., Marcoux, E., (1992). *Early Proterozoic ore deposits and tectonics of the Birimian orogenic belt, West Africa.* Precambrian Research, **58**, 305-344

Milési, J.P., Ledru, P., Feybesse, J.L., Dommanget, A., Ouedraogo, M., Marcoux, E., Prost, A., Vinchon, C., Sylvain, J., Johan, V., Tegyey, M., Calvez, J., Langny, P., (1989). *West African Gold Deposits: in their lower Proterozoic lithostructural setting, 1: 2 000 000.* BRGM (Bureau de Recherches Géologiques et Minières)

Mukasa, S.B., Wilson, A.H., Carlson, R.W., (1998). *A multielement geochronologic study of the Great Dyke, Zimbabwe: significance of the robust and reset ages.* Earth and Planetary Science Letters, **164**, 353-369

Mumm, S. A., Oberthür T., Vetter, U., Blenkinsop T.G., (1997). *High CO_2 content of fluid inclusions in gold mineralizations in the Ashanti belt, Ghana: a new category of ore forming fluids*? Mineralium Deposita, **32**, 107-118

Oberthür, T., Davis, D.W., Blenkinsop, T.G., Höhndorf, A., (2002). *Precise U-Pb mineral ages, Rb-Sr and Sm-Nd systematics for the Great Dyke, Zimbabwe-constraints on the late Archean events in the Zimbabwe craton and Limpopo belt.* Precambrian Research, **113,** 293-305

Oberthür, T., Vetter, U., Davis, D.W., Amanor, J.A., (1998). *Age constraints on gold mineralization and Paleoproterozoic crustal evolution in the Ashanti belt.* Precambrian Research, **89**, 129-143

Pan, G., Harris, D.P., (2000). *Information Synthesis for Mineral Exploration.* Oxford University Press, Inc. 461

Partington, G.A., Williams, P.J., (2000). Proterozoic Lode Gold and (Iron)-Copper-Gold Deposits: A Comparison of Australian and Global Examples. **In:** Hagemann, S.G. and Brown, P.E. (eds), *Gold in 2000.* Reviews in Economic Geology, **13,** Society of Economic Geologists, Inc. 69-97

Petters, S.W., (1991). *Regional Geology of Africa.* Springer-Verlag Berlin Heidelberg, Germany. 722

Pollack, H.N., (1997). Thermal characteristics of the Archean. **In:** de Wit, M. and Ashwal, L.D. (eds.) *Greenstone Belts*. Clarendon Press. Oxford, 223-232

Pons, J., Barbery, P., Dupius, D., Léger, J.M., (1995). *Mechanism of pluton emplacement and structural evolution of 2.1 Ga juvenile continental crust: the Birimian of southwestern Niger*. Precambrian Research, **70**, 281-301

Raines, G.L., (1999). Evaluation of weights of evidence to predict epithermal-gold deposits in the Great Basin of the Western United States. Natural Resources Research, **8** (4), 257-276

Raines, G.L., (2001). *Resources materials for a GIS spatial analysis course.* USGS Open-file Report 01-221, Version 1.0 http://geopubs.wr.usgs.gov/open-file/of01-221

Raines, G.L., Bonham-Carter, G.F., (2004). *Exploratory Spatial Modeling Demonstration for Carlin-type Deposis, Central Nevada, USA, using Arc-SDM.* Special volume of the Geological Association of Canada. http://ntserv.gis.nrcan.gc.ca/sdm/

Raines, G.L., Bonham-Carter, G.F., Kemp, L., (2000). *Predictive Probabilistic Modeling Using Arcview GIS.* ArcUser **3** (2), 45-48. http://ntserv.gis.nrcan.gc.ca/

Rambeloson, R.A., (1997). The Magalasy Shield. **In:** de Wit, M. and Ashwal, L.D. (eds.) *Greenstone Belts*. Clarendon Press. Oxford, 636-239

Sawkins, F.J., (1990). *Mineral deposits in relation to Plate tectonics*. 2nd Ed. Springer-Verlag, Berlin Heidelberg, 461

Scott, M., (2000). *GIS, Modern Mineral Potential Modelling and Quantitative Resource Assessment: Implications for the Geological Survey of Queensland.* AIG Journal – Applied geoscientific research and practice in Australia. Paper 2000-02, 1-16

Shackleton, R.M., (1996). *The final collision zone between East and West Gondwana: where is it?* Journal of African Earth Sciences, **23**, 271-287

Spiegelhalter, D.J., (1986). *Uncertainty in expert systems: In Artificial Intelligence and Statistics*. Gale, W.A. (ed.). Addison-Wesley, Reading, Massachusets, 17-55

Stein, M., (2003). *Tracing the plume material in the Arabian-Nubian Shield.* Precambrian Research, **123**, 223-234

Stern, R.J., (1994). *Arc assembly and continental collisions in the Neoproterozoic East African Orogen: Implication for the consideration of Gondwanaland.* Annals Review of Earth Planetary Science, **23**, 319-351

Stern, R.J., (2002). *Crustal evolution in the East Africa Orogen: a neodymium isotopic perspective*. Journal of African Earth Sciences, **34**, 109-117

Stern, R.J., Abdelsalam, M.G. (1998). *Formation of juvenile continental crust in the Arabian-Nubian Shield: evidence from granitic rocks of the Nakasib suture, NE Sudan.* Geologische Rundschau, Springer-Verlag GmbH, **87** (1), 150-160

Stern, R.J., Johnson, P.R., Kröner, A., Yibas, B., (2004). Neoproterozoic Ophiolites of the Arabian-Nubian Shield. **In:** Kusky, T.M. (ed), *Precambrian Ophiolites and Related Rocks.* Developments in Precambrian Geology, **13**. Elsevier, Amsterdam, 95-128

Tadesse, G., Allen, A., (2004). *Geochemistry of metavolcanics from the Neoproterozoic Tuludimtu orogenic belt, western Ethiopia.* Journal of African Earth Sciences, **39,**177-185

Tadesse, G., Allen, A., (2005). *Geology and geochemistry of the Neoproterozoic Tuludimtu Ophiolite suites, western Ethiopia.* Journal of African Earth Sciences, **41**, 192-211

Tadesse, S., Milési, J.P., Deschamps, Y., (2003). *Geology and mineral potential of Ethiopia: a note on geology and mineral map of Ethiopia.* Journal of African Earth Sciences, **36**, 273-313

Taylor, P.N., (1979). *Geology of Tin Deposits.* Developments in Economic Geology **11**, Elsevier, Amsterdam, 543.

Taylor, P.N., Kramers, J.D., Moorbath, S., Wilson, J.F., Orpen, J.L., Martin, A., (1991). *Pb/Pb, Sm-Nd and Rb-Sr geochronology in the Archean craton of Zimbabwe.* Chemical Geology (Isotope Geosciences Section), **87**, 175-196

Thiart, C, Bonham-Carter, G.F., Agterberg, F.P., Cheng, Q., Panahi, A., (2006). An application of the New Omnibus Test for conditional Independence in Weights-of-evidence Modelling. **In:** Harris, J. (ed.). *GIS Applications in Earth Sciences*, Geological Association of Canada Special Book, 131-142

Thiart, C., de Wit, M.J., (2000). *Linking Spatial Statistics to GIS: exploring potential gold and tin models of Africa.* South African Journal of Geology, **103**, 215-230

Thiart, C., de Wit, M.J., (2006). Fingerprinting the metal endowment of early continental crust to test secular changes in global mineralization. **In:** Kesler, S.E., ohmoto, H., (eds). *Evolution of Early Earth's Atmosphere, Hydrosphere, and Biosphere-Constraints from Ore Deposits*. Geological Society of America, Memoir **198**, 53-66

Thompson, A.B., Richter, F.M., Ahrendt, H., Bickle, M.J., Burke, K.C., Dymek, R.F., Frisch, W., Gee, R.D., Kröner, A., O'Nions, R.K., Oxburgh, E.R., Weber, K., (1984). The Long-term Evolution of the Crust and Mantle. **In:** Holland, H.D. and Trendall, A.F. (eds.) (1984). *Patterns of Change in Earth Evolution.* Physical, Chemical, and Earth Sciences Research Report **5**. Dahlem Konferenzen. Springer-Verlag, Berlin. 389-406

Triboulet, C., Feybesse, J.-L., (1998). *The Birrimian and Archean metabasic rocks of Toulepleu-Ity (Ivory Coast): rocks subjected to 8 kbar ([ap] 24 km) and 14 kbar ([ap] 42 km) during Palaeoproterozoic*. Earth and Planetary Science, **327**(1), 61-66

Vidal, M., Alric, G., (1994). *The Paleoproterozoic (Birimian) of Haute-Comoé, in the West African Craton in Côte-d'Ivoire: a transtensional back-arc basin.* Precambrian Research, **65**, 207-229

Vinyu, M.L., Frei, R., Jelsma, H.A., (1996). Timing between granitoid emplacement and associated gold mineralisation: examples from the ca. 2.7 Ga Harare_ Shamva greenstone belt, northern Zimbabwe. Canadian Journal Earth Sciences, **33**, 981-992

Wilsher, W., (1995). *Distribution of selected elements within mineral deposits throughout Gondwana, with geodynamics implications.* PhD thesis, University of Cape Town, South Africa

Wilsher, W.A., Herbert, R., Wullschleger, N., Naicker, I., Vitali, E., de Wit, M.J., (1993). *Towards intelligent spatial computing for the computing for the Earth Sciences in South Africa.* South African Journal of Sciences, **89**, 315-32

Wilson, J.F, Nesbitt, R.W., Fanning, C.M., (1995). Zircon geochronology of Archean felsic sequences in the Zimbabwe craton: a revision of greenstone stratigraphy and a model for Crustal growth. **In:** Coward, M.P. and Ries, A.C., (eds.), *Early Precambrian Processes.* Geological Society, London, Special Publication, **95**, 109-126

Windley, B.F., (1993). *Uniformitarianism today: plate tectonics is the key to the past.* Journal of the Geological Society, London, **150**, 7-19

Windley, B.F., (1995). *The Evolving Continents*. 3rd Ed. John Wiley & Sons, New York, 526

Windley, B.F., (2003). Continental growth in the Proterozoic: a global perspective. **In:** Yoshida, M., Windley, B.F. and Dasgupta, S. (eds). *Proterozoic East Gondwana: Supercontinent Assembly and Breakup.* Geological Society, London, Special Publications, **206**, 23-33

Windley, B.F, Whitehouse, M.J., Ba-Bttat, M.A.O., (1996). *Early Precambrian gneiss terranes and Pan-African island arcs in Yemen: crustal accretion of the eastern Arabian shield.* Geology, **24**, 131-134

Worku, H., Schandelmeier, H., (1996). *Tectonic evolution of the Neoproterozoic Adola Belt of southern Ethiopia: evidence for a Wilson Cycle process and implications for oblique plate collision.* Precambrian Research, **77**,179-210

Wright, D.F., Bonham-Carter, G.F., (1996). VHMS favourability mapping with GIS-based intergration models, Chisel Lake-Anderson Lake area. **In:** Bonham-Carter, G.F., Galley, A.G., and Hall, G.E.M., (eds), *EXTECH I: A Multidisciplinary Approach to Massive Sulphide Research in the Rusty Lake-Snow Lake Greenstone Belts, Manitoba*: Bulletin, **426**. Geological Survey of Canada, 339-376, 387-401

Yibas, B., (2000). *The Precambrian geology, tectonic evolution and controls of gold mineralization in southern Ethiopia.* PhD thesis, University of Witwatersrand, South Africa

Yihunie, T., (2002). *Pan-African deformations in the basement of the Negele area, southern Ethiopia.* International Journal of Earth Sciences (Geologische Rundschau), **91**: 922-933

Yihunie, T., Tesfaye, M., (2002). Structural *evidence for the allochthonous nature of the Bulbul terrane in southern Ethiopia: A west-verging thrust nappe*. Journal of African Earth Sciences, **34**, 85-93

Zimmer, M., Kröner, A., Jochum, K.P., (1995). *The Gabal Gerf complex, Nubian Shield, northeast Africa: geochemistry, petrology, isotope systematic and tectonic setting of a large, late Proterozoic, N-MORB-like ophiolite*. Chemical Geology, **123**, 29-51

Appendix

Appendix A1: Glossary

A glossary of terms relating to WofE modelling as described in the thesis

WPLUS	- Positive weight (W^+)
S_WPLUS	- Standard deviation of positive weight
WMINUS	- Negative weight (W^-)
S_WMINUS	- Standard deviation of negative weight
CONTRAST	- Positive weight minus negative weight
S_CONTRAST	- Standard deviation of the contrast
STUD_CNT	- Studentised Contrast: the contrast divided by its standard deviation
Buffer	- A polygon enclosing an area within specified distance from a point, line or polygon.
CI	- conditional independence of evidential themes with respect to the mineral deposits.
Evidence theme	- A spatial data set used as evidence for prediction of mineral deposits/occurrences.
Model	- The associations of mineral deposits to evidential themes
Missing Data	- Values of an evidential theme within the study area that are unknown.
Prior probability	- Total number of mineral deposits divided by total study area in a unit cells.
Posterior probability	- The probability that a unit cell contains mineral deposits after consideration of the evidential themes.
Study Area	- A grid theme that acts as a mask to define the area where the model is developed and applied.
Training Points (mineral deposits)	- The known mineral deposits predicted.
Unit Cell	- A conceptual area used for representing the area of training point, so that probabilities can be calculated.

Appendix A2: Evidential theme patterns for Zimbabwe Craton

CLASS	AREA_SQ_KM	AREA %	NO_POINTS	NO_POINTS %	WPLUS	S_WPLUS	WMINUS	S_WMINUS	CONTRAST	S_CONTRAST	STUD_CNT
1000	16191	7	42	8	0.2200	0.1545	-0.0179	0.0467	0.2379	0.1614	1.4741
2000	25290	11	62	12	0.1634	0.1272	-0.0211	0.0478	0.1845	0.1358	1.3580
3000	35392	15	77	15	0.0437	0.1141	-0.0077	0.0486	0.0514	0.1240	0.4149
4000	43985	18	87	17	-0.0517	0.1073	0.0112	0.0492	-0.0630	0.1181	-0.5334
5000	**54208**	**23**	**105**	**21**	**-0.0727**	**0.0977**	**0.0202**	**0.0503**	**-0.0929**	**0.1099**	**-0.8457**
6000	62028	26	118	24	-0.0908	0.0921	0.0297	0.0512	-0 1205	0.1054	-1.1434
7000	69380	29	128	26	-0.1215	0.0885	0.0453	0.0518	-0.1669	0.1025	-1.6273
8000	77367	32	145	29	-0.1057	0.0831	0.0465	0.0531	-0.1522	0.0986	-1.5437
9000	84907	35	160	32	-0.1003	0.0791	0.0508	0.0542	-0.1510	0.0959	-1.5747
10000	91671	38	171	34	-0.1105	0.0765	0.0624	0.0551	-0.1729	0.0943	-1.8331
67000	223393	93	501	100							

Table 1a. Weights table for proximity to brittle faults (Zimbabwe Craton). The class column is the distance from the faults in metres.

CLASS	DESCRIPTION	NO_POINTS	WPLUS	S_WPLUS	WMINUS	S_WMINUS	CONTRAST	S_CONTRAST	STUD_CNT
1	inside	105	-0.0727	0.0977	0.0202	0.0503	-0.0929	0.1099	-0.8457
2	outside	396	0.0202	0.0503	-0.0727	0.0977	0.0929	0.1099	0.8457

Table 1b. Reclassified weights table of the brittle faults (Zimbabwe Craton)

CLASS	AREA_SQ_KM	AREA %	NO_POINTS	NO_POINTS %	WPLUS	S_WPLUS	WMINUS	S_WMINUS	CONTRAST	S_CONTRAST	STUD_CNT
1000	27138	11	278	55	1.6012	0.0603	-0.6908	0.0670	2.2920	0.0901	25.4296
2000	40130	17	346	69	1.4272	0.0540	-0.9920	0.0804	2.4192	0.0968	24.9891
3000	53398	22	396	79	1.2753	0.0504	-1.3132	0.0976	2.5885	0.1099	23.5574
4000	63895	27	426	85	1.1681	0.0486	-1.5920	0.1155	2.7601	0.1253	22.0268
5000	**76179**	**32**	**446**	**89**	**1.0373**	**0.0475**	**-1.8302**	**0.1349**	**2.8675**	**0.1430**	**20.0554**
6000	84986	35	451	90	0.9385	0.0472	-1.8705	0.1414	2.8090	0.1491	18.8375
7000	93278	39	458	91	0.8604	0.0468	-1.9665	0.1525	2.8270	0.1596	17.7181
8000	102433	43	463	92	0.7773	0.0466	-2.0260	0.1622	2.8032	0.1688	16.6071
9000	111328	46	467	93	0.7023	0.0464	-2.0706	0.1715	2.7729	0.1777	15.6063
10000	119702	50	472	94	0.6401	0.0461	-2.1627	0.1857	2.8029	0.1914	14.6472

Table 2a. Weights table for proximity to ductile shears (Zimbabwe Craton).

CLASS	DESCRIPTION	NO_POINTS	WPLUS	S_WPLUS	WMINUS	S_WMINUS	CONTRAST	S_CONTRAST	STUD_CNT
1	inside	446	1.0373	0.0475	-1.8302	0.1349	2.8675	0.1430	20.0554
2	outside	55	-1.8302	0.1349	1.0373	0.0475	-2.8675	0.1430	-20.0554

Table 2b. Reclassified weights table of the ductile shears (Zimbabwe Craton)

CLASS	AREA_SQ_KM	AREA %	NO_POINTS	NO_POINTS %	WPLUS	S_WPLUS	WMINUS	S_WMINUS	CONTRAST	S_CONTRAST	STUD_CNT
1000	41263	17	297	59	1.2452	0.0582	-0.7114	0.0700	1 9566	0.0911	21.4781
2000	60930	25	370	74	1.0741	0.0521	-1.0507	0.0874	2.1248	0.1018	20.8767
3000	80534	33	415	83	0.9090	0.0492	-1.3561	0.1079	2.2651	0.1186	19.1054
4000	95653	40	439	88	0.7926	0.0478	-1.5842	0.1270	2.3768	0.1357	17.5104
5000	**112570**	**47**	**459**	**92**	**0.6738**	**0.0468**	**-1.8496**	**0.1543**	**2.5234**	**0.1613**	**15.6479**
6000	124331	52	464	93	0.5849	0.0465	-1.8800	0.1644	2.4649	0.1709	14.4248
7000	134986	56	470	94	0.5153	0.0462	-1.9608	0.1796	2.4760	0.1855	13.3493
8000	146279	61	475	95	0.4453	0.0460	-2.0235	0.1961	2.4688	0.2015	12.2548
9000	156745	65	479	96	0.3844	0.0458	-2.0729	0.2132	2.4573	0.2181	11.2675
10000	165878	69	483	96	0.3359	0.0456	-2.1582	0.2357	2.4941	0.2401	10.3880

Table 3a. Weights table for proximity to combined brittle faults and ductile shears (Zimbabwe Craton).

CLASS	DESCRIPTION	NO_POINTS	WPLUS	S_WPLUS	WMINUS	S_WMINUS	CONTRAST	S_CONTRAST	STUD_CNT
1	inside	459	0.6738	0.0468	-1.8496	0.1543	2.5234	0.1613	15.6479
2	outside	42	-1.8496	0.1543	0.6738	0.0468	-2.5234	0.1613	-15.6479

Table 3b. Reclassified weights table of the combined brittle faults and ductile shears (Zimbabwe Craton)

VALUE	COUNT	ROCKTYPES	FAULTS	AREA_SQM	TRNGPOINTS	POST_PROB	PSTPRBNRM	POST_LOGIT	SUM_WEIGHT	UNCERTAINT	MSNG_DATA	TOT_UNCRTY
7	317	0	2	317000000	0	0.00002430	0.00002428	-10.62516725	-4.45320000	0.00024296	0.00000000	0.00024296
10	89	0	1	89000000	0	0.00002558	0.00002556	-10.57376725	-4.40180000	0.00025579	0.00000000	0.00025579
1	165304	4	2	165304000000	92	0.00059416	0.00059366	-7.42776725	-1.25580000	0.00006770	0.00000000	0.00006770
2	27281	4	1	27281000000	24	0.00062548	0.00062496	-7.37636725	-1.20440000	0.00009603	0.00000000	0.00009603
3	10880	3	2	10880000000	17	0.00174098	0.00173952	-6.35156725	-0.17960000	0.00037315	0.00000000	0.00037315
4	2719	3	1	2719000000	7	0.00183263	0.00183109	-6.30016725	-0.12820000	0.00043558	0.00000000	0.00043558
11	3733	99	2	3733000000	5	0.00206684	0.00206511	-6.17966725	-0.00770000	0.00013682	0.00376205	0.00376454
12	74	-99	1	74000000	0	0.00217561	0.00217378	-6.12826725	0.04370000	0.00026588	0.00395775	0.00396667
5	4050	2	2	4050000000	25	0.00660982	0.00660427	-5.01256725	1.15940000	0.00119641	0.00000000	0.00119641
6	1174	2	1	1174000000	10	0.00695602	0.00695018	-4.96116725	1.21080000	0.00144566	0.00000000	0.00144566
9	20868	1	2	20868000000	285	0.01270758	0.01269692	-4.35276725	1.81920000	0.00109376	0.00000000	0.00109376
8	4055	1	1	4055000000	36	0.01336887	0.01335765	-4.30136725	1.87060000	0.00177946	0.00000000	0.00177946

Table 4a. Unique condition of gold deposit of Model A (brittle faults; Zimbabwe Craton)

VALUE	COUNT	ROCKTYPES	DUCTILEBUF	AREA_SQM	TRNGPOINTS	POST_PROB	PSTPRBNRM	POST_LOGIT	SUM_WEIGHT	UNCERTAINT	MSNG_DATA	TOT_UNCRTY
4	406	0	2	406000000	0	0.00000659	0.00000327	-11.93066725	-5.75870000	0.00006586	0.00000000	0.00006586
1	163209	4	2	163209000000	43	0.00016111	0.00007997	-8.73326725	-2.56130000	0.00002284	0.00000000	0.00002284
2	10907	3	2	10907000000	6	0.00047247	0.00023452	-7.65706725	-1.48510000	0.00010892	0.00000000	0.00010892
11	2945	-99	2	2945000000	1	0.00056103	0.00027848	-7.48516725	-1.31320000	0.00006013	0.00102945	0.00103121
3	2992	2	2	2992000000	6	0.00180018	0.00089357	-6.31806725	-0.14610000	0.00036073	0.00000000	0.00036073
6	29376	4	1	29376000000	73	0.00214009	0.00106230	-6.14476725	0.02720000	0.00024442	0.00000000	0.00024442
5	6687	1	2	6687000000	49	0.00347643	0.00172563	-5.65826725	0.51370000	0.00042003	0.00000000	0.00042003
8	2692	3	1	2692000000	18	0.00625209	0.00310341	-5.06856725	1.10340000	0.00133544	0.00000000	0.00133544
10	862	-99	1	862000000	4	0.00741603	0.00368117	-4.89666725	1.27530000	0.00049380	0.01312478	0.01313406
9	2232	2	1	2232000000	29	0.02344057	0.01163542	-3.72956725	2.44240000	0.00417725	0.00000000	0.00417725
7	18236	1	1	18236000000	272	0.04437170	0.02202521	-3.06976725	3.10220000	0.00372088	0.00000000	0.00372088

Table 4b. Unique condition of gold deposit of Model B (ductile shears; Zimbabwe Craton)

VALUE	COUNT	ROCKTYPES	COMBINEBUF	AREA_SQM	TRNGPOINTS	POST_PROB	PSTPRBNRM	POST_LOGIT	SUM_WEIGHT	UNCERTAINT	MSNG_DATA	TOT_UNCRTY
7	317	0	2	317000000	0	0.00000631	0.00000395	-11.97356725	-5.80160000	0.00006309	0.00000000	0.00006309
10	89	0	1	89000000	0	0.00006076	0.00003806	-9.70846725	-3.53650000	0.00060761	0.00000000	0.00060761
1	139936	4	2	139936000000	31	0.00015434	0.00009669	-8.77616725	-2.60420000	0.00002299	0.00000000	0.00002299
3	8759	3	2	8759000000	4	0.00045264	0.00028357	-7.69996725	-1.52800000	0.00010639	0.00000000	0.00010639
12	2882	-99	2	2882000000	1	0.00053749	0.00033672	-7.52806725	-1.35610000	0.00006265	0.00098637	0.00098836
2	52649	4	1	52649000000	85	0.00148468	0.00093012	-6.51106725	-0.33910000	0.00016903	0.00000000	0.00016903
5	2417	2	2	2417000000	5	0.00172472	0.00108050	-6.36096725	-0.18900000	0.00035453	0.00000000	0.00035453
9	5699	1	2	5699000000	45	0.00333093	0.00208675	-5.70116725	0.47080000	0.00043030	0.00000000	0.00043030
4	4840	3	1	4840000000	20	0.00434287	0.00272070	-5.43486725	0.73710000	0.00092841	0.00000000	0.00092841
11	925	-99	1	925000000	4	0.00515322	0.00322837	-5.26296725	0.90900000	0.00034007	0.00922817	0.00923443
6	2807	2	1	2807000000	30	0.01636891	0.01025472	-4.09586725	2.07610000	0.00293374	0.00000000	0.00293374
8	19224	1	1	19224000000	276	0.03118709	0.01953795	-3.43606725	2.73590000	0.00263407	0.00000000	0.00263407

Table 4c. Unique condition of gold deposit of Model C (combine brittle faults and ductile shears; Zimbabwe Craton)

VALUE	COUNT	ROCKTYPES	AREA_SQM	TRNGPOINTS	POST_PROB	PSTPRBNRM	POST_LOGIT	SUM_WEIGHT	UNCERTAINT	MSNG_DATA	TOT_UNCRTY
1	92735	3	92735000000	33	0.00035023	0.00035020	-7.95657799	-0.24850000	0.00006964	0.00000000	0.00006964
2	115763	4	115763000000	10	0.00008502	0.00008501	-9.37257799	-1.66450000	0.00002810	0.00000000	0.00002810
3	3316	1	3316000000	39	0.01157714	0.01157626	-4.44707799	3.26100000	0.00214580	0.00000000	0.00214580
4	24923	2	24923000000	26	0.00102670	0.00102662	-6.88037799	0.82770000	0.00022415	0.00000000	0.00022415
5	3807	-99	3807000000	0	0.00044898	0.00044895	-7.70807799	0.00000000	0.00004319	0.00135585	0.00135653

Table 5. Unique condition of the CrNiPgeTi deposits (Zimbabwe Craton)

VALUE	COUNT	ROCKTYPES	AREA_SQM	TRNGPOINTS	POST_PROB	PSTPRBNRM	POST_LOGIT	SUM_WEIGHT	UNCERTAINT	MSNG_DATA	TOT_UNCRTY
1	148880	4	148880000000	25	0.00016875	0.00016875	-8.68694399	-0.87140000	0.00003784	0.00000000	0.00003784
2	49801	3	49801000000	23	0.00046410	0.00046410	-7.67494399	0.14060000	0.00010761	0.00000000	0.00010761
3	13133	2	13133000000	14	0.00107126	0.00107125	-6.83784399	0.97770000	0.00030609	0.00000000	0.00030609
4	24923	1	24923000000	33	0.00133053	0.00133052	-6.62084399	1.19470000	0.00026778	0.00000000	0.00026778
5	3807	-99	3807000000	2	0.00040325	0.00040325	-7.81554399	0.00000000	0.00004094	0.00038812	0.00039028

Table 6. Unique condition of the CuZnPbBa deposits (Zimbabwe Craton)

VALUE	COUNT	ROCKTYPES	CONTACTS	AREA_SQM	TRNGPOINTS	POST_PROB	PSTPRBNRM	POST_LOGIT	SUM_WEIGHT	UNCERTAINT	MSNG_DATA	TOT_UNCRTY
1	549272	4	1	137318000000	7	0.00005132	0.00005096	-9.87742915	-1.67670000	0.00002145	0.00000000	0.00002145
2	111164	3	1	27791000000	6	0.00022302	0.00022144	-8.40802915	-0.20730000	0.00007812	0.00000000	0.00007812
3	108276	3	2	27069000000	5	0.00009171	0.00009106	-9.29682915	-1.09610000	0.00004789	0.00000000	0.00004789
4	57648	4	2	14412000000	0	0.00002110	0.00002095	-10.76622915	-2.56550000	0.00001202	0.00000000	0.00001202
5	17068	2	1	4267000000	2	0.00063870	0.00063417	-7.35542915	0.84530000	0.00038582	0.00000000	0.00038582
6	88000	1	1	22000000000	45	0.00200795	0.00199371	-6.20862915	1.99210000	0.00046634	0.00000000	0.00046634
7	3828	2	2	957000000	1	0.00026270	0.00026084	-8.24422915	-0.04350000	0.00018854	0.00000000	0.00018854
8	11692	1	2	2923000000	0	0.00082655	0.00082069	-7.09742915	1.10330000	0.00037315	0.00000000	0.00037315
9	8468	-99	1	2117000000	0	0.00031009	0.00030789	-8.07832915	0.12240000	0.00005533	0.00059207	0.00059465
10	6760	-99	2	1690000000	0	0.00012752	0.00012662	-8.96712915	-0.76640000	0.00005437	0.00024372	0.00024972

Table 7. Unique condition of the SnSb deposits (Zimbabwe Craton)

VALUE	COUNT	ROCKTYPES	CONTACTS	AREA_SQM	TRNGPOINTS	POST_PROB	PSTPRBNRM	POST_LOGIT	SUM_WEIGHT	UNCERTAINT	MSNG_DATA	TOT_UNCRTY
1	152274	4	1	152274000000	60	0.00046036	0.00044844	-7.68304331	-0.91030000	0.00006530	0.00000000	0.00006530
2	16636	3	1	16636000000	24	0.00149051	0.00145190	-6.50714331	0.26560000	0.00032553	0.00000000	0.00032553
3	40311	4	2	40311000000	21	0.00022308	0.00021730	-8.40774331	-1.63500000	0.00005014	0.00000000	0.00005014
4	1721	3	2	1721000000	1	0.00072266	0.00070394	-7.23184331	-0.45910000	0.00020199	0.00000000	0.00020199
5	406	2	2	406000000	1	0.00130774	0.00127387	-6.63814331	0.13460000	0.00133231	0.00000000	0.00133231
6	22466	1	1	22466000000	162	0.00723874	0.00705125	-4.92104331	1.85170000	0.00084238	0.00000000	0.00084238
7	2923	1	2	2923000000	6	0.00352009	0.00342892	-5.64574331	1.12700000	0.00073695	0.00000000	0.00073695
8	2117	-99	1	2117000000	0	0.00127143	0.00123850	-6.66634331	0.10640000	0.00011172	0.00208836	0.00209134
9	1690	-99	2	1690000000	0	0.00061637	0.00060041	-7.39104331	-0.61830000	0.00012030	0.00101576	0.00102286

Table 8. Unique condition of the W deposits (Zimbabwe Craton)

Appendix A3: Evidential theme patterns for the Birimian Shield

CLASS	AREA_SQ_KM	AREA %	NO_POINTS	NO_POINTS	WPLUS	S_WPLUS	WMINUS	S_WMINUS	CONTRAST	S_CONTRAST	STUD_CNT
1000	26710	3	19	4	0.5784	0.2295	-0.0247	0.0547	0.6031	0.2359	2.5563
2000	42338	5	27	5	0.4691	0.1925	-0.0305	0.0554	0.4997	0.2003	2.4942
3000	61394	7	34	7	0.3279	0.1715	-0.0294	0.0560	0.3573	0.1805	1.9799
4000	77299	9	39	8	0.2347	0.1602	-0.0257	0.0564	0.2604	0.1698	1.5331
5000	**98474**	**11**	**49**	**10**	**0.2208**	**0.1429**	**-0.0314**	**0.0574**	**0.2523**	**0.1540**	**1.6385**
6000	114067	13	57	11	0.2251	0.1325	-0.0381	0.0581	0.2632	0.1447	1.8190
7000	129432	15	58	12	0.1161	0.1313	-0.0213	0.0582	0.1374	0.1437	0.9562
8000	147570	17	65	13	0.0988	0.1241	-0.0210	0.0589	0.1199	0.1373	0.8727
9000	165144	19	68	14	0.0314	0.1213	-0.0074	0.0592	0.0388	0.1350	0.2873
10000	182569	21	72	14	-0.0117	0.1179	0.0030	0.0597	-0.0148	0.1321	-0.1118

Table 9a. Weights table for proximity to CGS brittle faults (Birimian Shield). The class column is the distance from the faults in metres.

CLASS	DESCRIPTION	AREA_UNITS	NO_POINTS	WPLUS	S_WPLUS	WMINUS	S_WMINUS	CONTRAST	S_CONTRAST	STUD_CNT
1	inside	98474	49	0.2208	0.1429	-0.0314	0.0574	0.2523	0.1540	1.6385
2	outside	786174	304	-0.0314	0.0574	0.2208	0.1429	-0.2523	0.1540	-1.6385

Table 9b. Reclassified weights table of the CGS brittle faults (Birimian Shield)

CLASS	AREA_SQ_KM	AREA %	NO_POINTS	NO_POINTS	WPLUS	S_WPLUS	WMINUS	S_WMINUS	CONTRAST	S_CONTRAST	STUD_CNT
1000	53812	6	49	14	0.8256	0.1429	-0.0867	0.0574	0.9123	0.1540	5.9237
2000	83752	9	71	20	0.7540	0.1187	-0.1251	0.0596	0.8791	0.1328	6.6185
3000	118233	13	93	26	0.6791	0.1037	-0.1624	0.0620	0.8414	0.1209	6.9617
4000	145740	16	115	33	0.6822	0.0933	-0.2143	0.0648	0.8965	0.1136	7.8913
5000	**180637**	**20**	**130**	**37**	**0.5901**	**0.0877**	**-0.2310**	**0.0670**	**0.8211**	**0.1104**	**7.4386**
6000	205616	23	144	41	0.5628	0.0834	-0.2597	0.0692	0.8225	0.1083	7.5928
7000	229573	26	153	43	0.5132	0.0809	-0.2678	0.0707	0.7810	0.1074	7.2698
8000	257214	29	162	46	0.4566	0.0786	-0.2707	0.0724	0.7274	0.1068	6.8084
9000	283550	32	171	48	0.4132	0.0765	-0.2761	0.0741	0.6893	0.1065	6.4710
10000	308899	35	184	52	0.4008	0.0737	-0.3072	0.0769	0.7080	0.1066	6.6436

Table 10a. Weights table for proximity to De Beers brittle faults (Birimian Shield).

CLASS	DESCRIPTION	AREA_UNITS	NO_POINTS	WPLUS	S_WPLUS	WMINUS	S_WMINUS	CONTRAST	S_CONTRAST	STUD_CNT
1	inside	180637	130	0.5901	0.0877	-0.2310	0.0670	0.8211	0.1104	7.4386
2	outside	704011	223	-0.2310	0.0670	0.5901	0.0877	-0.8211	0.1104	-7.4386

Table 10b. Reclassified weights table of the De Beers brittle faults (Birimian Shield)

CLASS	AREA_SQ_KM	AREA %	NO_POINTS	NO_POINTS	WPLUS	S_WPLUS	WMINUS	S_WMINUS	CONTRAST	S_CONTRAST	STUD_CNT
1000	61202	7	56	16	0.8304	0.1337	-0.1011	0.0580	0.9315	0.1457	6.3912
2000	95219	11	79	22	0.7324	0.1126	-0.1395	0.0604	0.8719	0.1277	6.8254
3000	134174	15	102	29	0.6449	0.0991	-0.1766	0.0631	0.8215	0.1175	6.9940
4000	164897	19	127	36	0.6580	0.0888	-0.2397	0.0665	0.8977	0.1109	8.0922
5000	**203886**	**23**	**145**	**41**	**0.5782**	**0.0831**	**-0.2670**	**0.0693**	**0.8453**	**0.1082**	**7.8108**
6000	231622	26	159	45	0.5428	0.0793	-0.2951	0.0718	0.8379	0.1070	7.8310
7000	258180	29	167	47	0.4833	0.0774	-0.2957	0.0733	0.7790	0.1066	7.3060
8000	288788	33	176	50	0.4237	0.0754	-0.2952	0.0752	0.7190	0.1065	6.7525
9000	317658	36	183	52	0.3674	0.0739	-0.2859	0.0767	0.6533	0.1065	6.1320
10000	345238	39	196	56	0.3528	0.0714	-0.3156	0.0798	0.6684	0.1071	6.2392

Table 11a. Weights table for proximity to combined CGS and De Beers brittle faults (Birimian Shield).

CLASS	DESCRIPTION	NO_POINTS	WPLUS	WMINUS	S_WPLUS	WMINUS	S_WMINUS	CONTRAST	S_CONTRAST	STUD_CNT
1	inside	145	0.5782	-0.2670	0.0831	-0.2670	0.0693	0.8453	0.1082	7.8108
2	outside	208	-0.2670	0.5782	0.0693	0.5782	0.0831	-0.8453	0.1082	-7.8108

Table 11b: Reclassified weights table of the combined CGS and De Beers brittle faults (Birimian Shield)

VALUE	COUNT	ROCKTYPES	CGS	AREA_SQM	TRNGPOINTS	POST_PROB	PSTPRBNRM	POST_LOGIT	SUM_WEIGHT	UNCERTAINT	MSNG_DATA	TOT_UNCRTY
11	2509	0	2	2509000000	0	0.00000310	0.00000309	-12.68367794	-4.85760000	0.00003101	0.00000000	0.00003101
10	617	0	1	617000000	0	0.00000443	0.00000441	-12.32637794	-4.50030000	0.00004434	0.00000000	0.00004434
7	156301	4	2	156301000000	6	0.00004129	0.00004115	-10.09487794	-2.26880000	0.00001593	0.00000000	0.00001593
6	8064	4	1	8064000000	1	0.00005902	0.00005882	-9.73757794	-1.91150000	0.00002470	0.00000000	0.00002470
1	370678	3	2	370678000000	71	0.00020591	0.00020521	-8.48787794	-0.66180000	0.00002749	0.00000000	0.00002749
2	24823	3	1	24823000000	13	0.00029431	0.00029331	-8.13057794	-0.30450000	0.00006181	0.00000000	0.00006181
9	6325	-99	2	6325000000	2	0.00038747	0.00038615	-7.85547794	-0.02940000	0.00002984	0.00038367	0.00038483
12	61	-99	1	61000000	0	0.00055379	0.00055191	-7.49817794	0.32790000	0.00009937	0.00054812	0.00055705
5	206887	2	2	206887000000	124	0.00057304	0.00057109	-7.46397794	0.36210000	0.00006613	0.00000000	0.00006613
8	21519	2	1	21519000000	11	0.00081894	0.00081615	-7.10667794	0.71940000	0.00016290	0.00000000	0.00016290
4	80554	1	2	80554000000	116	0.00139526	0.00139051	-6.57327794	1.25280000	0.00016447	0.00000000	0.00016447
3	6310	1	1	6310000000	9	0.00199328	0.00198650	-6.21597794	1.61010000	0.00039902	0.00000000	0.00039902

Table 12a. Unique condition of gold deposit of Model A (CGS brittle faults; Birimian Shield)

VALUE	COUNT	ROCKTYPES	DEBEERS	AREA_SQM	TRNGPOINTS	POST_PROB	PSTPRBNRM	POST_LOGIT	SUM_WEIGHT	UNCERTAINT	MSNG_DATA	TOT_UNCRTY
12	1973	0	2	1973000000	0	0.00000272	0.00000257	-12.81667794	-4.99060000	0.00002715	0.00000000	0.00002715
11	1153	0	1	1153000000	0	0.00000630	0.00000596	-11.97517794	-4.14910000	0.00006299	0.00000000	0.00006299
6	146864	4	2	146864000000	5	0.00003615	0.00003419	-10.22787794	-2.40180000	0.00001398	0.00000000	0.00001398
7	17501	4	1	17501000000	2	0.00008385	0.00007931	-9.38637794	-1.56030000	0.00003317	0.00000000	0.00003317
1	355211	3	2	355211000000	73	0.00018027	0.00017052	-8.62087794	-0.79480000	0.00002454	0.00000000	0.00002454
9	6312	-99	2	6312000000	2	0.00033924	0.00032089	-7.98847794	-0.16240000	0.00002762	0.00033595	0.00033709
3	40290	3	1	40290000000	11	0.00041810	0.00039548	-7.77937794	0.04670000	0.00006678	0.00000000	0.00006678
4	193956	2	2	193956000000	102	0.00050171	0.00047457	-7.59697794	0.22910000	0.00005941	0.00000000	0.00005941
10	74	-99	1	74000000	0	0.00078662	0.00074406	-7.14697794	0.67910000	0.00009178	0.00077810	0.00078349
8	34450	2	1	34450000000	33	0.00116313	0.00110020	-6.75547794	1.07060000	0.00016849	0.00000000	0.00016849
2	62099	1	2	62099000000	78	0.00122171	0.00115561	-6.70627794	1.11980000	0.00014761	0.00000000	0.00014761
5	24765	1	1	24765000000	47	0.00282962	0.00267654	-5.86477794	1.96130000	0.00041502	0.00000000	0.00041502

Table 12b. Unique condition of gold deposit of Model B (De Beers; Birimian Shield)

VALUE	COUNT	ROCKTYPES	COMBINE	AREA_SQM	TRNGPOINTS	POST_PROB	PSTPRBNRM	POST_LOGIT	SUM_WEIGHT	UNCERTAINT	MSNG_DATA	TOT_UNCRTY
12	1956	0	2	1956000000	0	0.00000268	0.00000253	-12.83087794	-5.00480000	0.00002677	0.00000000	0.00002677
11	1170	0	1	1170000000	0	0.00000609	0.00000574	-12.00937794	-4.18330000	0.00006087	0.00000000	0.00006087
6	145624	4	2	145624000000	5	0.00003564	0.00003361	-10.24207794	-2.41600000	0.00001379	0.00000000	0.00001379
7	18741	4	1	18741000000	2	0.00008103	0.00007642	-9.42057794	-1.59450000	0.00003195	0.00000000	0.00003195
1	349884	3	2	349884000000	68	0.00017773	0.00016763	-8.63507794	-0.80900000	0.00002432	0.00000000	0.00002432
9	6284	-99	2	6284000000	2	0.00033445	0.00031544	-8.00267794	0.17660000	0.00002764	0.00033122	0.00033237
2	45617	3	1	45617000000	16	0.00040405	0.00038109	-7.81357794	0.01250000	0.00006326	0.00000000	0.00006326
5	186510	2	2	186510000000	99	0.00049464	0.00046653	-7.61117794	0.21490000	0.00005898	0.00000000	0.00005898
10	102	-99	1	102000000	0	0.00076019	0.00071698	-7.18117794	0.64490000	0.00008538	0.00075201	0.00075684
8	41896	2	1	41896000000	36	0.00112407	0.00106018	-6.78967794	1.03640000	0.00015892	0.00000000	0.00015892
4	60216	1	2	60216000000	77	0.00120451	0.00113605	-6.72047794	1.10560000	0.00014653	0.00000000	0.00014653
3	26648	1	1	26648000000	48	0.00273475	0.00257932	-5.89897794	1.92710000	0.00039176	0.00000000	0.00039176

Table 12c. Unique condition of gold deposit of Model C (merged; Birimian Shield)

CLASS	AREA_SQ_KM	AREA %	NO_POINTS	NO_POINTS%	WPLUS	S_WPLUS	WMINUS	S_WMINUS	CONTRAST	S_CONTRAST	STUD_CNT
1000	3676	5	17	14	0.9955	0.2431	-0.0981	0.0981	1.0936	0.2622	4.1714
2000	5649	8	23	19	0.8675	0.2089	-0.1276	0.1011	0.9952	0.2321	4.2875
3000	8297	12	31	26	0.7813	0.1799	-0.1712	0.1055	0.9525	0.2086	4.5666
4000	10166	14	37	31	0.7550	0.1647	-0.2098	0.1092	0.9648	0.1976	4.8824
5000	13082	19	43	36	0.6527	0.1527	-0.2345	0.1133	0.8872	0.1902	4.6649
6000	14978	21	47	39	0.6062	0.1461	-0.2536	0.1163	0.8598	0.1867	4.6040
7000	16834	24	50	41	0.5511	0.1416	-0.2611	0.1188	0.8121	0.1848	4.3940
8000	19323	27	52	43	0.4521	0.1389	-0.2422	0.1205	0.6943	0.1838	3.7770
9000	21433	30	56	46	0.4225	0.1338	-0.2600	0.1241	0.6824	0.1825	3.7393
10000	23701	34	59	49	0.3740	0.1304	-0.2600	0.1271	0.6339	0.1820	3.4823

Table 13a. Weights table for proximity to brittle faults (Ashanti belt, Birimian Shield). Cut-off distance at 1000 m.

CLASS	DESCRIPTION	AREA_SQ_KM	NO_POINTS	WPLUS	S_WPLUS	WMINUS	S_WMINUS	CONTRAST	S_CONTRAST	STUD_CNT
1	inside	3676	17	0.9955	0.2431	-0.0981	0.0981	1.0936	0.2622	4.1714
2	outside	66919	104	-0.0981	0.0981	0.9955	0.2431	-1.0936	0.2622	-4.1714

Table 13b. Reclassified weights table of the brittle faults (Ashanti belt)

VALUE	COUNT	BFAULT	ROCKTYPES	AREA_SQM	TRNGPOINTS	POST_PROB	PSTPRBNRM	POST_LOGIT	SUM_WEIGHT	UNCERTAINT	MSNG_DATA	TOT_UNCRTY
8	277	1	4	277000000	0	0.00003109	0.00003014	-10.37850858	-4.01130000	0.00031095	0.00000000	0.00031095
9	4	1	4	4000000	0	0.00009281	0.00008998	-9.28490858	-2.91770000	0.00092830	0.00000000	0.00092830
2	28621	1	3	28621000000	14	0.00047160	0.00045722	-7.65890858	-1.29170000	0.00013364	0.00000000	0.00013364
5	1021	2	3	1021000000	2	0.00140641	0.00136354	-6.56530858	-0.19810000	0.00050614	0.00000000	0.00050614
7	2550	2	-99	2550000000	0	0.00155409	0.00150672	-6.46530858	-0.09810000	0.00020748	0.00106178	0.00108186
1	22487	2	2	22487000000	46	0.00193655	0.00187752	-6.24490858	0.12230000	0.00037268	0.00000000	0.00037268
3	12984	2	1	12984000000	44	0.00316224	0.00306585	-5.75330858	0.61390000	0.00060453	0.00000000	0.00060453
10	6	1	-99	6000000	0	0.00462470	0.00448373	-5.37170858	0.99550000	0.00119490	0.00314805	0.00336720
4	979	1	2	979000000	6	0.00575847	0.00558294	-5.15130858	1.21590000	0.00168560	0.00000000	0.00168560
6	1666	2	1	1666000000	9	0.00938040	0.00909447	-4.65970858	1.70750000	0.00272948	0.00000000	0.00272948

Table 13c. Unique condition of the Gold deposits (Ashanti belt)

VALUE	COUNT	ROCKTYPE	AREA_SQM	POST_PROB	TRNGPOINTS	POST_PROB	PSTPRBNRM	POST_LOGIT	SUM_WEIGHT	UNCERTAINT	MSNG_DATA	TOT_UNCRTY
5	3965	4	3965000000	0.00000251	0	0.00000251	0.00000251	-12.89675253	-3.72570000	0.00002506	0.00000000	0.00002506
3	185640	3	185640000000	0.00005353	10	0.00005353	0.00005352	-9.83525253	-0.66420000	0.00001782	0.00000000	0.00001782
4	5571	-99	5571000000	0.00010400	0	0.00010400	0.00010399	-9.17105253	0.00000000	0.00001084	0.00004015	0.00004159
1	602608	2	602608000000	0.00010554	64	0.00010554	0.00010553	-9.15635253	0.01470000	0.00001717	0.00000000	0.00001717
2	86864	1	86864000000	0.00020591	18	0.00020591	0.00020588	-8.48785253	0.68320000	0.00005308	0.00000000	0.00005308

Table 14. Unique condition of CuZnPbBa deposit (Birimian Shield)

Appendix A4: Evidential theme patterns of the Arabian-Nubian Shield

CLASS	AREA%	NO_POINTS	NO_POINTS%	WPLUS	S_WPLUS	WMINUS	S_WMINUS	CONTRAST	S_CONTRAST	STUD_CNT
1000	5	35	7	0.3035	0.1691	-0.0189	0.0456	0.3223	0.1751	1.8410
2000	8	59	11	0.3592	0.1302	-0.0382	0.0468	0.3974	0.1384	2.8721
3000	12	82	16	0.3199	0.1104	-0.0504	0.0480	0.3703	0.1204	3.0751
4000	14	114	22	0.4238	0.0937	-0.0934	0.0499	0.5172	0.1061	4.8736
5000	**18**	**142**	**28**	**0.4148**	**0.0839**	**-0.1212**	**0.0517**	**0.5360**	**0.0986**	**5.4374**
6000	21	157	30	0.3773	0.0798	-0.1288	0.0528	0.5061	0.0957	5.2892
7000	23	171	33	0.3467	0.0765	-0.1356	0.0538	0.4823	0.0935	5.1564
8000	26	189	37	0.3298	0.0727	-0.1505	0.0553	0.4803	0.0914	5.2558
9000	29	212	41	0.3437	0.0687	-0.1847	0.0574	0.5283	0.0895	5.9038
10000	32	229	44	0.3329	0.0661	-0.2037	0.0590	0.5365	0.0886	6.0546

Table 15a. Weights table for proximity to brittle faults (Arabian-Nubian Shield).

CLASS	DESCRIPTION	NO_POINTS	WPLUS	S_WPLUS	WMINUS	S_WMINUS	CONTRAST	S_CONTRAST	STUD_CNT
1	inside	142	0.4148	0.0839	-0.1212	0.0517	0.5360	0.0986	5.4374
2	outside	374	-0.1212	0.0517	0.4148	0.0839	-0.5360	0.0986	-5.4374

Table 15b. Weights table for the binary reclassification of brittle faults (Arabian-Nubian Shield)

VALUE	COUNT	GEOLOGY	BFAULTS	AREA_SQM	TRNGPOINTS	POST_PROB	PSTPRBNRM	POST_LOGIT	SUM_WEIGHT	UNCERTAINT	MSNG_DATA	TOT_UNCRTY
11	7724	-99	2	21564000000	0	0.00014013	0.00013832	-8.87278862	-0.04290000	0.00001022	0.00023383	0.00023406
12	377	4	2	1489663000000	56	0.00003292	0.00003249	-10.32128862	-1.49140000	0.00000497	0.00000000	0.00000497
2	1489663	3	2	818228000000	154	0.00018230	0.00017995	-8.60968862	0.22020000	0.00001896	0.00000000	0.00001896
4	156153	4	1	156153000000	1	0.00004542	0.00004483	-9.99948862	-1.16960000	0.00000860	0.00000000	0.00000860
1	21564	-99	1	185000000	0	0.00019332	0.00019082	-8.55098862	0.27890000	0.00002616	0.00032243	0.00032349
3	818228	3	1	130869000000	28	0.00025148	0.00024823	-8.28788862	0.54200000	0.00003880	0.00000000	0.00003880
5	185	2	2	127415000000	86	0.00061604	0.00060808	-7.39158862	1.43830000	0.00007546	0.00000000	0.00007546
6	130869	2	1	31540000000	17	0.00084969	0.00083871	-7.06978862	1.76010000	0.00014211	0.00000000	0.00014211
7	127415	1	1	6753000000	17	0.00234017	0.00230994	-6.05518862	2.77470000	0.00042039	0.00000000	0.00042039
8	31540	1	2	33014000000	54	0.00169735	0.00167542	-6.37698862	2.45290000	0.00023614	0.00000000	0.00023614
10	33014	0	2	7724000000	0	0.00000117	0.00000115	-13.65558862	-4.82570000	0.00001173	0.00000000	0.00001173
9	6753	0	1	377000000	0	0.00000162	0.00000160	-13.33378862	-4.50390000	0.00001619	0.00000000	0.00001619

Table 15c. Unique condition of gold deposit (Arabian-Nubian Shield)

VALUE	COUNT	GEOLOGY	AREA_SQM	TRNGPOINTS	POST_PROB	PSTPRBNRM	POST_LOGIT	SUM_WEIGHT	UNCERTAINT	MSNG_DATA	TOT_UNCRTY
2	1645816	-99	21749000000	50	0.00003031	0.00003031	-10.40391135	-0.75450000	0.00000484	0.00000000	0.00000484
1	21749	4	1645816000000	0	0.00006446	0.00006446	-9.64941135	0.00000000	0.00000478	0.00006320	0.00006338
3	949097	3	949097000000	77	0.00008095	0.00008095	-9.42161135	0.22780000	0.00001101	0.00000000	0.00001101
4	198722	2	198722000000	49	0.00024603	0.00024603	-8.30981135	1.33960000	0.00003958	0.00000000	0.00003958
5	8101	1	8101000000	5	0.00061584	0.00061585	-7.39191135	2.25750000	0.00027906	0.00000000	0.00027906

Table 16. Unique condition of CuZnPbBa deposit (Arabian-Nubian Shield)